LUMINOUS BLUE COMPACT GALAXIES: PROBES OF GALAXY ASSEMBLY

by

Cassidy Louann Newton

Bachelor of Science, 2007

Angelo State University

San Angelo, Texas

Submitted to the Graduate Faculty of the

College of Science and Engineering

Texas Christian University

in partial fulfillment of the requirements

for the degree of

Doctor of Philosophy

December 2012

Acknowledgments

I foremost want to thank my advisors, Dr. Pamela Marcum and Dr. Michael Fanelli. They have really stuck behind me and supported me. If I had to start over, I would pick them as advisors again. I would also like to thank Dr. Peter Frinchaboy for being there when I needed someone to help with an immediate question, and always being willing to help. Even though he will not see this I would like to thank Dr. Zerda for letting me "live" in his lab the past year, he was fun to pick on (someone should tell him I said that). The entire TCU Physics faculty and staff have been great in seeing me through not only the Physics PhD, but also the partial MBA. This department has been a wonderful home for a very long time. I have appreciated the help and support from my fellow grad students, many of whom have moved on to wonderful things. I am especially indebted to Dr. Christopher Fuse, who did not stop being a mentor and friend even all the way from Florida. I want to thank the support of the NASA ADP Grant NNX11AF75G, the Texas Space Grant Consortium, the Texas Christian University Fellowship, and McDonald Observatory. Finally, I would like to thank my parents, my sister and her husband, and my amazing husband JD. One could never have asked for a better support group.

Table of Contents

List of Figures

List of Tables

Chapter 1

Introduction

The life cycles of galaxies over cosmic time are yet to be fully understood. How did galaxies evolve from their formative stages to the structures we observe today? This dissertation details the identification and analysis of a sample of Luminous Blue Compact Galaxies (LBCGs), a class of galaxy in the local ($z < 0.05$) universe exhibiting blue colors, high surface brightness, and high star formation rates. These systems appear to be very similar in their global properties to the early evolutionary phases of most galaxies, however their locality permits detailed investigation over a broad range of the electromagnetic spectrum in contrast to the smaller angular sizes and extreme faintness of distant galaxies. We use a combination of optical, ultraviolet, and infrared data to investigate a sample of LBCGs utilizing space and ground-based data.

1.1 Luminous Blue Compact Galaxies

Blue compact galaxies continually receive attention since they were first identified as starburst systems (e.g., Loose & Thuan 1985, Fanelli, O'Connell, &Thuan 1988, Kong 2004, Gil de Paz, Madore, Pevunova 2003, Cairos 2003, Hopkins et al. 2002). The majority of the effort at this point has been directed toward blue compact dwarf

systems (e.g. Thuan & Martin 1981, Cairos et al. 2001, Noeske et al. 2005). Over the 40 years since their initial identification, most investigations of blue compact systems have considered dwarf and low-luminosity objects, $-14 > M_B > -18$, and have not concentrated on the more extreme luminous compacts with $M_B \leq -19$. Gallagher (1990) showed the significance of luminous blue galaxies some time ago, however little attention has been specifically directed at the bright end of the blue compact luminosity distribution. Previously LBCGs have been classified as faint blue galaxies, compact narrow emission line galaxies (Guzman et al. 1996), luminous compact galaxies (Hammer et al. 2001), and blue compact galaxies (Pisano et al. 2001; Kong, & Cheng 2002), with varying selection criteria that can overlap our own. To begin the project we define our selection criteria for LBCGs.

A luminous galaxy is defined as having an absolute magnitude that exceeds $M_B < -19$. The most luminous blue compacts are comparable in total luminosity to large spirals, yet display remarkably blue optical colors: $[+0.3 \approx (B-V) \approx +0.6]$, which are amongst the bluest optical colors found for the integrated colors of any galactic system. Figure 1.1 shows the distribution of the absolute magnitudes for our LBCG optical sample.

A blue galaxy is defined as having a $(B-V) < 0.6$, where B−V is one of the color indices in the UBV photometric system. For comparison keep in mind that the majority of regular type galaxies have a B−V between 0.5 and 1 (Prugniel,& Heraudeau 1998). Young star forming regions are typically blue because the most

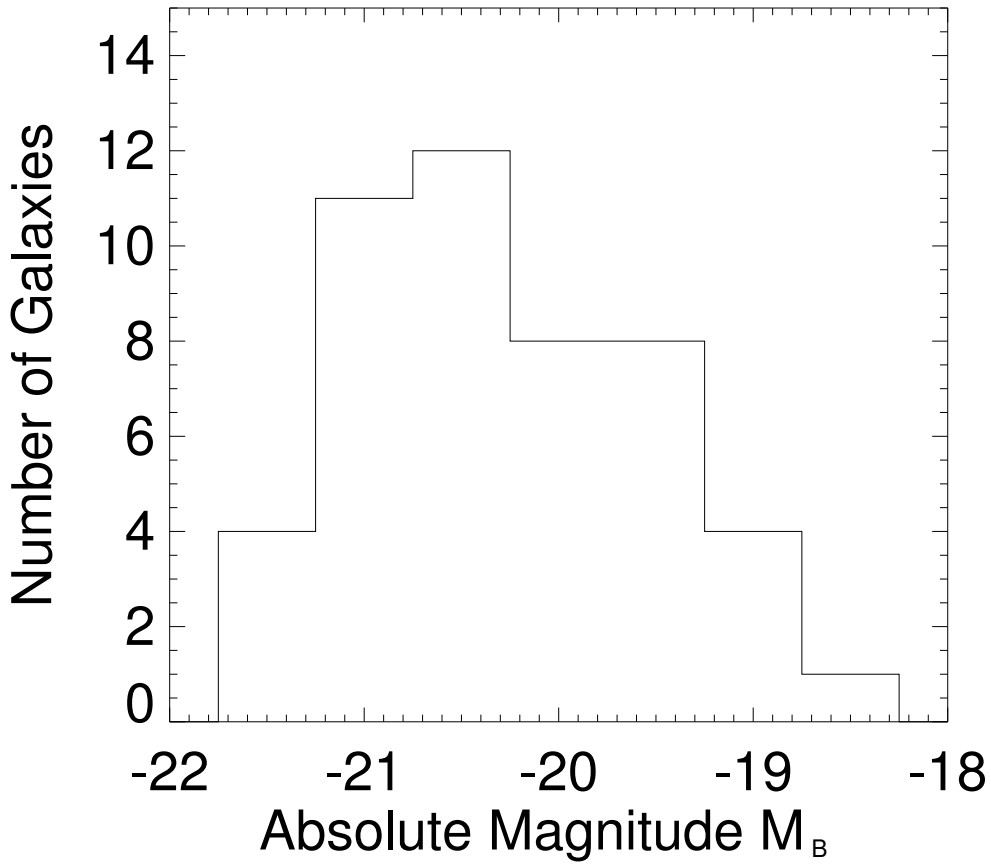

Figure 1.1: Distribution of absolute magnitudes of the LBCG optical sample

massive stars, such as O's and B's, are blue. Main sequence stars that are the most luminous put out energy at a higher rate, therefore their "fuel" is used up faster. The hottest stars, like the O and B stars, will live for about 10 million years or less. A lifetime of a few million years is short compared to the life of a low mass star, such as a red dwarf, that will burn fuel slowly and last tens to hundreds of billions of years.

An excess of blue light signifies that all the O and B stars have not had time to reach the end of their life cycle, which for the ones massive enough will be a supernova.

Morphologically, the young population 1 stellar component produces one or more regions of high surface brightness, inducing the "compact" appearance on survey images with small dynamic ranges. Compact galaxies were initially identified by Zwicky and others as unusual high surface brightness ("compact") systems seen in the Palomar Sky Survey images (Zwicky 1964).

For comparison, Kong & Cheng (2002), defined a blue compact galaxy as having a $M_B < -21$, (B-V) < 0.45, compact morphology, a saturated region surrounded by small amounts of nebulosity, and no regular structures, like spiral arms. However, they may have irregular features, like bridges. Note that there is some overlap in the definition of the samples.

1.2 LBCGs as the Missing Puzzle Piece in Galaxy Evolution

Before the astrophysical significance of LBCGs can be understood, a familiarity with the classification of galaxies and theories of evolution should be reached. As O'Connell (1997) states, morphology is a means of inferring the evolutionary state and history of galaxies. The most accepted classification scheme is the Hubble-Sandage, which used the criteria of brightness, openness of arms, disk-bulge ratios, and degree

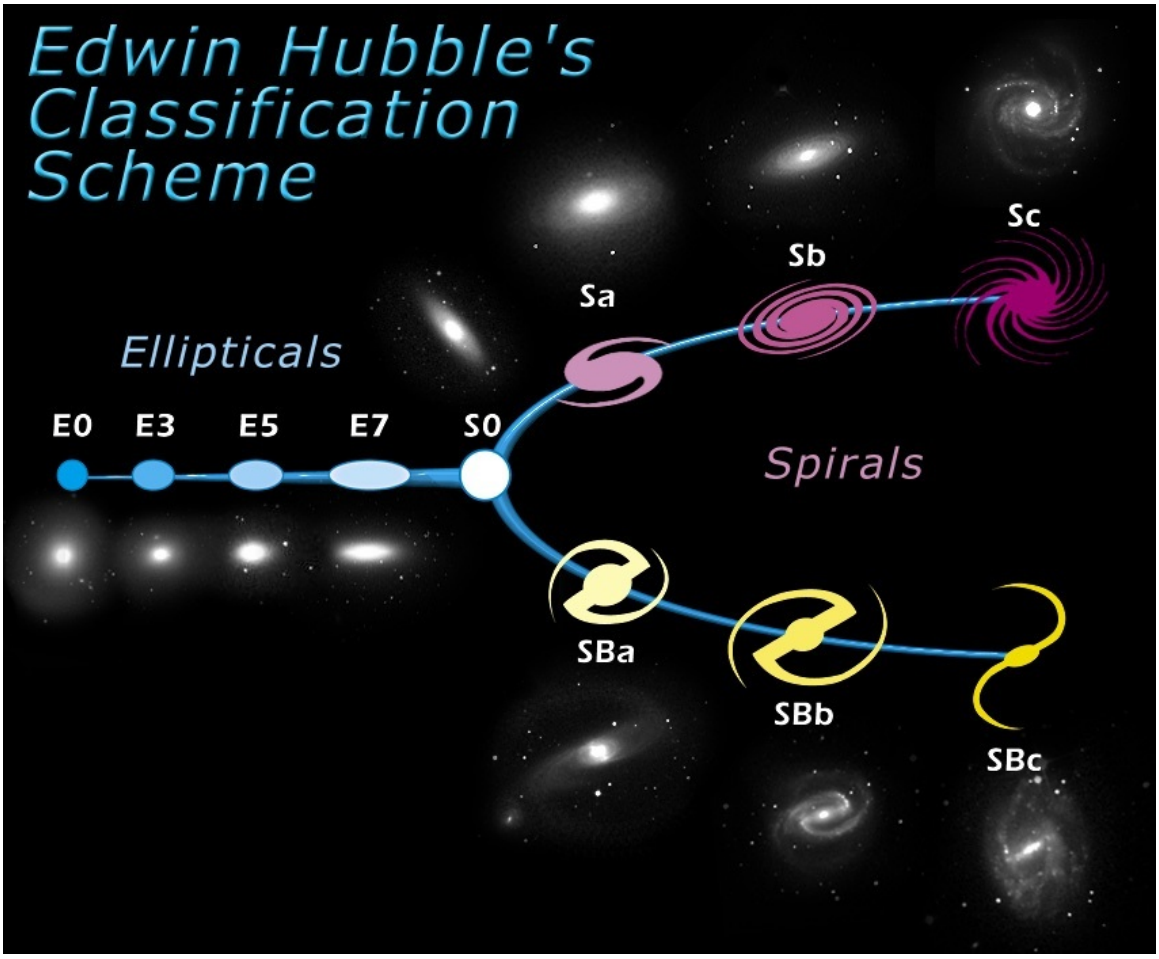

Figure 1.2: Hubble's Tuning Fork

of resolution of arms into stars. The Hubble classification scheme shown in Figure 1.2 separates ellipticals by axial ratio, and organizes spiral galaxies by disk-to-bulge ratio and the winding of arm structure.

Examining the Hubble fork one sees late-type galaxies on the right-hand side and early-type galaxies on the left-hand side. The lay-out of the Hubble fork stems from the thought that galaxies evolve from the left-hand to right-hand side. However, Eggen, Lynden-Bell, & Sandage (1962) showed that evolution from ellipticals

to spirals was unlikely. Later simulations suggest evolution occurs from right to left along the Hubble diagram (Toomre & Toomre 1972). Spirals can interact and merge, eventually developing into elliptical galaxies (Barnes 1985). However, this theory has not been accepted either, which leads to the question, how did galaxies evolve? No diagram exists by which structure, formation, and evolution of galaxies can be interpreted on a physical basis similar to the Hertzprung-Russel diagram for stars (Okamura 1988). A great need exists for an objective quantitative classification system.

We believe LBCGs will provide fundamental insights into the galaxy assembly process, through both large sample surveys and deep, high-resolution, pan-chromatic observations of small, carefully selected "best-case" samples. The data compiled here, along with spectrophometric and dynamical modeling, will provide the local calibrators for interpreting galaxy evolution at intermediate and high redshifts. Perez-Gallego et al. (2005) reached the same conclusion as us with regard to the significance of LBCGs for exploring galaxy evolution; they also noted the lack of statistical properties for LBCGs. LBCGs are likely to be the best analogs in the nearby universe to the early evolutionary phases of most galaxies, and therefore act as probes of galaxy evolution since a locally defined sample can be studied across the electromagnetic spectrum with high spatial and spectral resolution. Luminous compact star-forming galaxies appear to represent a prominent phase in the early history of galaxy formation. Important findings that have led to this belief include the fact that the number

density of luminous compact star-forming galaxies rises significantly out to z $\sim$ 1 (Koo et al. 1994; Guzman et al. 1997; Phillips et al. 1997; Lilly 1998; Mallen-Ornelas et al. 1999). At z $\sim$ 1 there is an era of transition; massive galaxies shut off their star formation and their mass is mostly already in place (Twite et al. 2012; Glazebrook et al. 2004; Bundy et al. 2006; Conselice et al. 2007; Perez-Gonzalez et al. 2008a; Ilbert et al. 2010).The number of LBCGs decline with redshift, therefore evolution into some other galaxy type is the only solution if LBCGs were rampant at higher z (Garland et al. 2004).

As the Madau plot in Figure 1.3 shows, the universal star formation rate (SFR) has declined steadily from $z = 1$, when the universe was 40% of its current age, to the present day. Of very distant galaxies at z $\sim$ 2-4, half are compact, meaning half of the total star formation rate in the early universe were produced by these objects (Smail et al. 1998). Because of their substantial angular extent (0.5 $<D_{25}<$ 1.5 arcminutes), LBCGs in the nearby universe can be examined with sufficient spatial resolution to determine the starburst life cycles and potential triggering mechanisms. Comparison to young galaxies in the distant universe detected in deep ground and space-based surveys, such as the Hubble Deep Fields, would be a natural follow up step. High-redshift systems are extremely faint and subtend only a few arcseconds. Galaxies at a redshift of $2 < z < 6$ require long interactions with the largest telescopes just to obtain minimal signal. Multiwavelength observations of samples of local ($z < 0.05$) luminous blue compacts provide crucial data on the process of galaxy assembly.

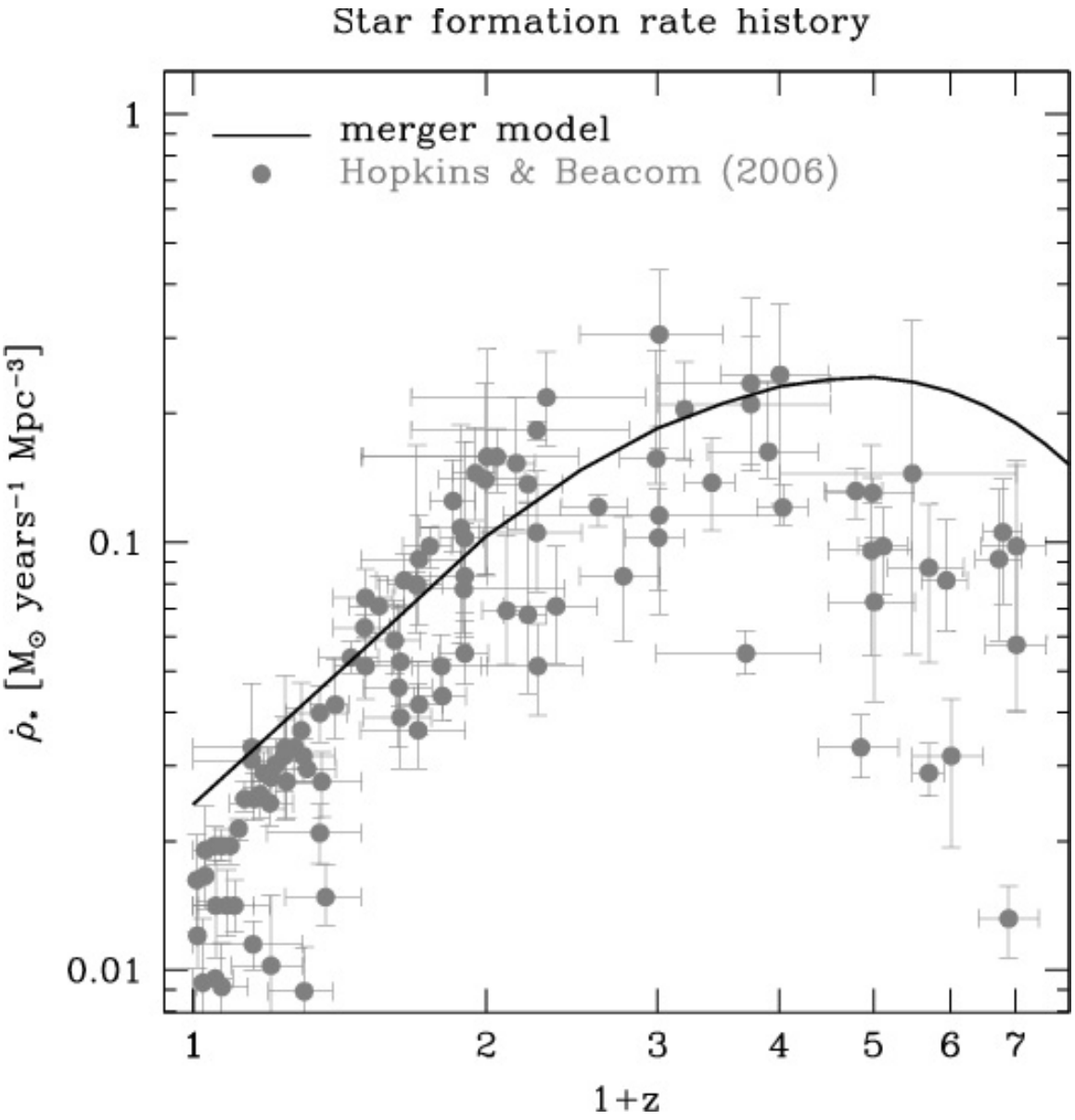

Figure 1.3: The Madau diagram, showing the volume-averaged total star formation rate as a function of redshift. The diagram quantifies the rate of star formation over the history of the universe.

One of the most promising results we have seen is the possibility of LBCGs being evolved ultraluminous infrared galaxies (ULIRGs). ULIRGs are more than likely an evolutionary stage of normal galaxies in which a large amount of dense gas, that has been driven to the nucleus, is feeding a black hole and fueling high star formation (Norman & Scoville 1988). Dust engulfing the ULIRGs absorbs the UV light being produced by the high star formation and reradiates that light in the infrared part of the spectrum. A significant portion of the bolometric luminosity of a galaxy is absorbed by interstellar dust and re-emitted in the thermal IR, at wavelengths of roughly 10-300μm (Kennicutt 1998). The total bolometric luminosity of these galaxies exceeds $10^{12}L_{\odot}$ (Sanders & Mirabel 1996). With continuous star formation in a ULIRG, supernovae could eventually blow away enough dust that UV light could begin to escape, creating the UV bright LBCGs described in this paper. Only in cases where dust layers are disturbed does the dust appear to be a major factor in UV morphologies of LBCGs (Marcum et al. 2001).

Some groups have postulated theories over the evolutionary stage of LBCGs other than evolved ULIRGS, and it is important to evaluate all possibilities. Previous papers have led to the belief that LBCGs are progenitors of different intermediate and low mass galaxies in the local universe, they are just brightened by intense star formation (Koo et al. 1995; Guzman et al. 1997). A subset of LBCGs at intermediate redshift may be the progenitors of local low-mass dwarf elliptical galaxies (Koo et al. 1994; Guzman et al. 1996). Werk, Jangren, & Salzer (2004) finds this theory

unlikely because it requires that the gas present in the LBCG be removed, possibly by supernovae driven outflows. Outflow should not occur but for the least massive systems according to hydrodynamical models (Mac Low &Ferrara 1999).

Other LBCGs might be disk galaxies in the process of building a bulge to become local luminous spiral galaxies (Phillips et al. 1997; Hammer et al. 2001). To constrain this scenario (Noeske et al. 2006) completed a structural study of the extended components in intermediate redshift LBCGs using the Hubble Space Telescope Ultra Deep Field to search for extended disk components in 26 LBCGs defined the same as by Garland and Werk. The Noeske group found that approximately 90% of the LBCGs at a redshift between 0.2 and 1.3 were truly small galaxies. The remaining 10% that are large, disk-like galaxies with bright nuclei, support the scenario that some LBCGs at higher z could be a bulge in a large disk.

Lowenthal et al. (1997) suggested that Lyman break galaxies at $z = 3$, because of the compact cores and high surface brightness, may be high-redshift counterparts of intermediate redshift LBCGs. A drop in density of LBCGs may link to the fall in the star formation rate density between $z = 1$ and the present (Madau et al. 1996). The LBCGs may still exist, they are just in a less active state.

Blue Compact Dwarfs (BCDs) have low luminosities, compact optical size, and spectra similar to HII regions. BCDs are theoretically dwarf irregulars (dIs) during their quit phases of low star formation, and they turn into dwarf ellipticals (dEs) during their final evolutionary stage (Thuan 1985; Davies & Phillips 1988).

Aloisi et al. (1999), Crone et al. (2002), Papaderos et al. (2002), and Ostlin et al. (1998), performed studies on BCGs using single-star photometry to identify stars in different evolutionary phases using the color-magnitude diagram. The consensus was that BCGs are evolved stellar populations, and their star forming histories are discontinuous. Kong et al. (2003) used a population synthesis model approach to BCGs and found a variety of star formation histories. Three main stellar components were found including a current burst, an underlying older population, and some intermediate age populations. The nuclei are mostly dominated by young components, and the star formation there is ongoing. Overall, Kong et al. (2003) found that the stellar populations hint that BCGs are old galaxies undergoing intermittent star formation periods. A typical BCG was not found with its first generation of stars.

The presence of a bar can have profound effects on the internal dynamics of a LBCG that is also a spiral. Torque from a bar causes gases to fall inward (Schwarz 1984, Wada & Habe 1992, Friedle & Benz 1993). Contini et al. (1998) showed that fueling driven from the bar produces the activity seen at the core of barred spiral galaxies. The effects that a bar has on a starburst is still controversial (Hawarden et al. 1998). Chapelon et al. (1999) found that normal (non-starburst) late-type galaxies are the first stage of galaxy evolution, and bars in early-type galaxies do not have the same properties.

Blue compact dwarf galaxies (BCDGs) are less massive than normal galaxies, and cannot sustain a spiral density wave. Therefore, they so do not suffer disk instabilities.

The star formation is forced to burst activity (Casini & Heidman 1976, Boesfaard, Edwards, & Heidmann 1982). Mueller & Arnet (1976) believed the SF process in later type spirals were produced by shock waves from SN winds. Gerola & Seidan (1978) expanded on this theory to include "self-propogating stochastic SF". Brinks (1990), Taylor, Brinks, & Skillman (1993), Taylor et al. (1995, 1996) have proposed that SF could be induced by tidal interactions with HI companions, which is the running theory for Mrk 1094.

1.3 A Multiwavelength Diagnostic Approach

The question that is the umbrella to all others in this dissertation is: what are the steps in galaxy evolution? Are mergers and interactions the main proponents of star formation? How much of a role does early-type galaxies play in star formation compared to interacting galaxies?

Chapter II details the study of luminous blue compact galaxies in the optical wavelength range. The optical light from galaxies is a mixture of warm and cool stellar components, in which older populations have significant influence (Marcum et al. 2001). An optical study aids in the analysis of morphology and structure. Surface brightness profiles and growth curves identify different stellar components and distinguish the young star-forming regions from a possible underlying older population. The profiles can further be used to find magnitudes and colors of the galaxy

sample, many of which have never been cataloged. Optical imaging can analyze the star formation process: how star formation proceeds and how it is triggered.

We present ultraviolet and far-infrared star formation rates for a sample of 188 luminous blue compact galaxies (LBCGs) in chapter III. The star formation rates (SFRs) are calculated using archival far-ultraviolet data obtained from the *Galaxy Evolution Explorer (GALEX)*, and the *Infrared Astronomical Satellite (IRAS)*. A comparison of the ultraviolet (UV) and far-infrared (FIR) star formation rates will show if the FIR or UV is a more dominant factor. Since LBCGs are possible decedents of ultra luminous infrared galaxies (ULIRGs), the far-infrared star formation rates are expected to be high. However, since the LBCG galaxy sample was largely selected for being UV luminous, the UV star formation rates could have taken a dominant role. The ratio of FIR to UV SFRs is compared to the far-infrared luminosities. Studies have used this relation to find a dust attenuation correction for the ultraviolet SFR based on a far-infrared luminosity dependence. A similar comparison of the FIR(SFR)/UV(SFR) ratio to the ultraviolet luminosity does show a correlation, showing the emergence of ultraviolet in galaxies with continuous star formation. Finding a pattern that hints at an evolution of FIR dominated to UV dominated will help address the ULIRG to LBCG theory. Viewing a comparison of the UV SFR to B−V we will find if galaxies in our sample with the strongest ultraviolet are also the bluest, also lending to the theory that with continued star formation ULIRGS can evolve into LBCGs. The role of environment on star formation is investigated to find

if interactions and mergers are the main trigger to high star formation. A correlation between global stellar spatial distribution and SFRs is investigated to find if galaxies with high SFRs have formed stars in large discrete knots over their disks, or just just in their cores. Finally, K band data from the *Two-micron All Sky Survey (2MASS)* is used to test the relation of high SFRs to galaxy mass. The lack of a correlation between the K-band data and FIR star formation rates would mean the variation of SFRs in our sample is due to factors other than mass, such as interactions, an internal trigger, or just young star formation.

Massive young stars emit most of their energy in the ultraviolet part of the spectrum, and at least in star forming galaxies, they outshine the emission from any other evolutionary stage of a composite stellar population (Bruzual &Charlot 2003). Stars that have surface temperatures above 10,000K are brighter in the UV than at longer wavelengths (Fanelli et al. 1992). The observation of nearby galaxies in the UV, chapter IV, is important in order to understand the evolution of galaxies from the high-redshift universe (where their properties are commonly derived from rest-frame UV observations) to the present. The analysis of the UV morphology of nearby galaxies as a local benchmark for studies in the optical at high redshift have been carried out by several authors including Kuchinski et al. (2000, 2001), Marcum et al. (2001), Windhorst et al. (2002), and Lauger et al. (2005). UV data can address fundamental questions such as the relation between the qualitative (optical) morphology of these galaxies and more quantitative properties such as colors, luminosities, total-infrared-

to-UV ratios, etc. (Gil De Paz et al. 2007). The entire star formation rate of a galaxy could not be found without observing the contribution of the UV. Up to 30% of the early type galaxies imaged in the UV show rejuvination signatures (e.g. Yi et al. 2005, Donas et al. 2007, Schawinski et al. 2007, Jeong et al. 2005). Comparing UV and optical colors to evolutionary tracks of instantaneous burst models can help us find the age range, and extinction values for the LBCG sample.

The combination of the optical, infrared, and ultraviolet wavelengths will give us a better picture of luminous blue compact galaxies than if we used one band on its own. To understand the entire story of a galaxy, each wavelength will need to be studied.

Chapter 2

Optical Structure and Environment

2.1 Optical Sample Selection

The candidate LBCG list was constructed in 2000 from the galaxy catalogs produced by Haro (1956), Markarian (1967) and Zwicky (1964), using the subset of objects observed in HI reported by Gordon & Gottesman (1981) and Thuan & Martin (1980). The Haro and Mrk surveys attempted to identify galaxies with a "UV" excess, where UV means the ground-based near-ultraviolet wavelength domain (3300-4300 $\mathring{A}$) and "excess" means an observed flux larger than the typical near-UV flux observed from normal galaxies. Zwicky surveyed large sections of the sky for compact galaxies; he defined a compact galaxy as one that can just be distinguished from stars on plates obtained with the Palomar 48 inch Schmidt telescope (Zwicky 1964).

Only galaxies with known redshifts were considered. A distance was required in order to derive the object's luminosity, one of the primary criteria. Most of the redshift data came from HI or optical spectroscopy. A Hubble constant, Ho = 73 km/sec, was used to assign a distance, and correct the measured recessional velocities for motion of the galaxy within the Local Group and infall into the Virgo Cluster.

Dwarf galaxies (MB ¡ -18.5) were excluded, based on extant photometry at the time the sample was constructed, which almost completely consisted of photographic

photometry measured from the original Palomar Sky Survey. Photographic blue magnitudes from the POSS, mpg, were assumed to be approximately equivalent to a "B" magnitude in the Johnson system. The magnitudes have errors of $\pm$ 0.4 mag. More accurate photometry is a goal of this project.

AGN were excluded where spectrophotometry indicated that the source of the UV excess was radiation from an accretion disk surrounding a nuclear supermassive black hole. The spectroscopic markers for an AGN are either broad emission lines or specific emission line ratios which are interpreted as gas illuminated by an accretion disk. Since many objects lacked high-quality optical spectra, it was expected that some leakage of active galaxies into the sample might occur.

Global colors for most of the sample were not known at the time the sample was first constructed; a primary motivation for this program was to obtain that data. The candidates were assumed to be generally bluer than normal galaxies because they had been selected by Haro and Markarian for an observed UV excess. Some objects were expected to be blue-core galaxies, the property responsible for their inclusion in the Haro and Mrk surveys, but that the global colors of such systems might cause them to be redder than the cutoff in our LBCG criterion.

Morphological class was not a discriminant in the sample selection; the galaxy type, or its environment, were not considered. Star formation rates inferred using any technique were also not a discriminant in the sample selection. Blue galaxies could be actively forming O, B, or A stars or be in a "post-burst" phase, in which

the blue light arises from an aging population of B and A stars formed 107 to a few 108 years ago.

The input sample list was substantially larger than the data reported here - we were constrained by weather and the need to observe objects across the full range of right ascension, to maximize observing efficiency. The optical data sample is in Table 2.1. The final sample of galaxies includes 49 galaxies. Only one galaxy, Mrk 33, did not meet the magnitude cut-off, but it was included on purpose for comparative purposes against published data. Thirteen galaxies were redder than our B−V max limit by more than .09.

Table 2.1. Properties of the Optical Sample

Name	2nd Name	R.A. (J2000.0)	Dec (J2000.0)	V (km s^{-1})	D (Mpc)	a x b (′)	a x b (Kpc)
(1)	(2)	(3)	(4)	(5)	(6)	(7)	(8)
Mrk 342	···	00 38 18.9	+13 32 01	11139	152.6	···	···
Haro 15	Mrk 960	00 48 35.9	-12 43 07	6324	86.6	0.9 x 0.6	22.7 x 15.1
Mrk 360	VV 790a	01 43 56.5	+17 03 43	8058	110.4	0.4 x 0.4	12.8 x 12.8
Mrk 364	V Zw 155	01 57 49.4	+27 51 56	8172	112.0	0.3 x 0.3	9.8 x 9.8
Mrk 366	III Zw 042	02 11 33.5	+13 55 02	7962	109.1	0.6 x 0.6	19.0 x 19.0
Mrk 367	CGCG 461-063	02 13 37.1	+17 05 08	11042	151.3	0.5 x 0.4	22.0 x 17.6
Mrk 589	UGC 1716	02 13 45.0	+04 06 08	3403	46.6	0.5 x 0.5	6.8 x 6.8
Mrk 1184	···	02 45 54.8	-05 38 26	8686	119.0	0.7 x 0.3	24.2 x 10.4
Mrk 1404	KUG 310-077	03 12 37.1	-07 34 22	10657	146.0	0.5 x 0.5	21.2 x 21.7
Mrk 1079	NGC 1509	04 03 55.2	-11 10 45	8426	115.4	0.8 x 0.6	26.9 x 20.1
Mrk 1094	UGCA 102	05 10 48.1	-02 40 54	2728	37.4	0.7 x 0.6	7.6 x 6.5
Mrk 8	IC 2184	07 29 25.4	+72 07 44	3578	53.1	0.8	12.4
Haro 1	NGC 2415	07 36 56.7	+35 14 31	3892	53.3	0.9 x 0.9	14.0 x 14.0
Mrk 385	IRAS 8004+2514	08 03 28.0	+25 06 10	8335	114.2	0.7 x 0.5	23.3 x 15.6
Mrk 1211	PGC 22728	08 05 45.7	+07 35 27	15892	217.7	0.4	25.3
Mrk 390	KUG 832+307	08 35 33.0	+30 32 03	7718	105.7	0.5 x 0.4	15.4 x 12.3
Mrk 18	UGC 04730	09 01 58.4	60 09 06	3324	49.0	0.9 x 0.3	12.8 x 4.3

Table 2.1 (continued)

Name	2nd Name	R.A. (J2000.0)	Dec (J2000.0)	V (km s^{-1})	D (Mpc)	a x b (′)	a x b (Kpc)
(1)	(2)	(3)	(4)	(5)	(6)	(7)	(8)
Mrk 402	KUG 932+306	09 35 19.2	+30 24 32	7522	103.0	0.5 x 0.4	15.0 x 12.0
II Zw 44	CGCG 123-030	10 15 14.6	+21 06 34	6244	85.5	0.5 x 0.4	12.4 x 9.9
Mrk 139	CGCG 211-034	10 15 49.1	+43 47 17	5373	73.6	0.7 x 0.5	15.0 x 10.7
Mrk 144	KUG 1023+442	10 26 54.0	+44 00 24	8440	115.6	0.5 x 0.5	16.8 x 16.8
Mrk 33	UGC 5720	10 32 31.9	+54 24 04	1764	24.2	1.1 x 0.8	7.7 x 5.6
Mrk 148	UGC 5747	10 35 34.8	+44 18 57	7408	101.5	0.8 x 0.4	23.6 x 11.8
Haro 25	Mrk 727	10 48 44.2	+26 03 13	7755	106.2	0.3 x 0.3	9.3 x 9.3
Mrk 154	CGCG 241-021	10 50 47.3	+50 10 09	12770	174.9	0.5 x 0.4	25.4 x 20.4
Mrk 171	NGC 3690	11 28 32.2	+58 33 44	3424	46.9	2.9	39.6
Mrk 181	UGC 6583	11 36 54.4	+19 58 15	6325	86.6	0.7 x 0.4	17.6 x 10.1
Haro 34	IC 3730	12 45 06.5	+21 10 10s	6874	94.2	0.3 x 0.3	8.2 x 8.2
Mrk 54	CGCG 188-030	12 56 55.6	+32 26 51	13659	187.1	0.7 x 0.4	38.1 x 21.8
Mrk 238	VV 605	13 01 16.6	+65 00 04	15171	207.8	0.4 x 0.3	24.2 x 18.1
Mrk 248	UGC 8327	13 15 17.2	+44 24 26	11216	153.6	0.8 x 0.5	35.7 x 22.3
Mrk 255	SBS 1320+532	13 22 59.7	+52 58 10	9376	128.4	0.5 x 0.5	18.7 x 18.7
Mrk 271	ARP 239	13 41 41.7	+55 40 20	7763	106.3	···	···
Haro 42	Mrk 685	14 31 08.9	+27 14 12	4734	64.8	0.6 x 0.4	11.3 x 7.5

Table 2.1 (continued)

Name	2nd Name	R.A. (J2000.0)	Dec (J2000.0)	V (km s^{-1})	D (Mpc)	a x b (′)	a x b (Kpc)
(1)	(2)	(3)	(4)	(5)	(6)	(7)	(8)
I Zw 101	ARK 467	15 03 45.8	+42 41 59	5239	71.8	0.7 x 0.5	14.6 x 10.4
Mrk 492	KUG 1556+269	15 58 43.7	+26 49 05	4562	62.5	0.9 x 0.6	16.4 x 10.9
Mrk 297	NGC 6052	16 05 12.9	+20 32 32	5009	68.6	0.9	18.0
Mrk 300	IC 1189	16 06 14.8	+18 10 58	11896	163.0	0.7 x 0.4	33.2 x 19.0
Mrk 697	PGC 57470	16 12 18.1	+29 04 46	9986	136.8	0.7 x 0.5	27.9 x 19.9
Mrk 499	UGC 10565	16 48 24.1	+48 42 33	8117	111.2	0.5 x 0.4	16.2 x 12.9
I Zw 191	PGC 60671	17 40 24.8	+47 43 59	6149	84.2	0.2 x 0.2	4.9 x 4.9
II Zw 82	IC 1317	20 23 15.6	+00 39 53	3955	54.2	0.7 x 0.6	11.0 x 9.5
Mrk 512	IRAS 21091-134	21 11 45.6	-01 22 19	9772	133.9	···	···
Mrk 518	UGC 11865	21 58 36.0	+12 02 20	9464	129.6	0.6 x 0.5	22.6 x 20.0
Mrk 303	NGC 7244	22 16 26.8	+16 28 17	7711	105.6	0.7 x 0.3	21.5 x 9.2
Mrk 306	UGC12066	22 31 51.2	+19 41 29	5763	78.9	1.1 x 0.7	25.2 x 16.1
II Zw 185	IC 5243	22 41 24.5	+23 22 32	7307	100.1	0.7 x 0.6	20.4 x 17.5
Mrk 531	NGC 7648	23 23 54.0	+09 40 03	3652	50.0	1.6 x 1.0	23.3 x 14.5
Mrk 325	NGC 7673	23 27 41.0	+23 35 20	3564	48.8	1.3 x 1.2	18.5 x 17.0

Col. (1) Primary galaxy name. Col. (2) Alternate name. Most galaxies in this sample have multiple alternate designations, reflecting their inclusion in a number of catalogs. Cols. (3)-(4) Right Ascension and Declination, obtained from NASA's Extragalactic Database (NED). The coordinates are from the J2000 epoch. Col. (5) Recessional velocity, corrected for Galactic motion and Virgo infall, obtained from NED. Col. (6) Distance in megaparsecs, derived using Col. (5) and $H_0 = 73$ km s^{-1} Mpc^{-1}. Col. (7) Angular diameter of the major and minor axes, expressed in arcminutes. Col. (8) Corresponding physical diameter expressed in kiloparsecs derived using the distances in Col. (6).

2.2 McDonald Observatory

2.2.1 Observations

Although all-sky surveys are slowly changing astronomy to a field of online data mining, being awarded time at McDonald Observatory gave us the opportunity to obtain deeper images. While all-sky surveys such as the Sloan Digital Sky Survey (SDSS) do provide extensive sky coverage, deeper imaging helps detect even the faintest signs of mergers and interactions. Table 2.2 shows the 5 observing runs used for this project. The SDSS exposure times in each of the five bands are only 54 seconds. Even coadding the gri bands in SDSS will provide a short exposure time of 162 seconds. To not miss out on low surface brightness characteristics, long exposure times, on the order of ∼60-900 seconds, were used while at McDonald. The 2.1 meter Otto Struve telescope was used along with the WHT guider and the 1024 x 1024 TK4 CCD chip. We used a process called dithering in which a guide star was moved between successive exposures, causing the result images to be on different pixels. The dithering process minimized chip artifacts when exposures are combined. The WHT guider was used to manually reposition the guide star, and to keep the guide star in the correct location throughout the extent of the exposure. After 2 × 2 on-chip binning the TK4 has a pixel scale of 0.348" pix^{-1} and an angular field-of-view of 2.97' × 2.97'. A section of the observation log is shown in Table 2.3. The observing log lists galaxies, filters, dates of observation, and exposure times.

The wide-band filters used included the U, B, V, R, and I filters. The U filter stands for ultraviolet, and it allows light of wavelengths between about 320 nanometers (nm) and 400 nm to pass through. The B filter is for blue, and it filters light of wavelengths between about 400 nm and 500 nm. Likewise, the V, R, and I filters stand for visible, red, and infrared respectively, and their respective wavelength ranges are approximately 500 nm to 700 nm, 550 nm to 800 nm , and 700 nm to 900 nm. As for narrow-band filters, we used Hα which has an effective wavelength at 6562Å. However, due to redshift, the observed wavelength to the Hα lies between 6601 and 6895 $\mathring{A}$. A set of narrow-band interference filters were used which are designed to be transparent over a small wavelength range, 50-100 A; each filter is described by a central wavelength and this wavelength range. The central wavelengths are different - designed to capture redshifted Hα emission.

Table 2.2. Observing Runs

Starting Date	Number of Nights
(1)	(2)
July 3, 2002	3
December 27, 2002	6
April 24, 2003	5
August 1, 2003	5
October 31, 2008	5

Table 2.3. Observing Log

Name	Date of Observation	U	B	V	R	I	Hα
(1)	(2)	(3)	(4)	(5)	(6)	(7)	(8)
Mrk 518	2008 Oct	60	60	60	570	···	1200
...	2003 Aug	900	540	720	···	···	···
Mrk 1404	2008 Oct	120	960	60	1140	···	5400
Mrk 367	2008 Oct	···	600	···	···	···	···
Mrk 385	2008 Oct	120	60	60	2280	···	4500
...	2002 Dec	600	600	600	480	600	···

Col. (1) Primary galaxy name. Col. (2) Date of Observation. Cols. (3)-(8) The exposure times that are total on-object exposures and generally the sum of 3 dithered exposures for each respective filter.

2.2.2 Data Reduction

An extensive, custom, user-built reduction package coded in idl was used to flat field and bias-subtract individual frames. A bias, taken with the shutter closed, removes the camera system noise from an image. A flat-field, taken with shutter open, and dome open at sunrise or sunset, removes gradients across the detector where sensitivity drops off.

There are many components that contribute to night-sky light; the most powerful is moonlight. Others include: airglow from collisions of atoms and molecules in the upper atmosphere with charged particles and x-rays from the sun and outer space, zodiacal light which is sunlight scattered by interplanetary dust, unresolved faint stars and galaxies, galactic extinction due to absorption patches, and emission and/or reflection nebulosities (Okamura 1988). To account for the extra light we perform a sky subtraction on each image. To perform a sky-subtraction, I would hand draw a region in the sky on each image individually that did not include any of the galaxy, stars, light excess around the rim of the image, or image defect. Any flux in the hand drawn region should be pure noise. Once the noise was found in the area selected, a calculation could be made of the noise/area, and subtracted from the entire image.

For each galaxy in each filter the best image is chosen and labeled as the reference image. Every other image is then aligned with this reference image, and scaled to match the flux. To align an image to its reference, I would change the image contrast until I could see the cores of the stars in both images. I would then zoom in on the

same stars in the reference and non-reference image and hand select the cores. The alignment program records the cores of the stars in the images, and will decide how much, and in which direction to shift an image for it to be aligned to the reference image. In order to scale the flux I would zoom in on every flux point individually in each reference image, including stars and the very center of the galaxy. However, this time I was zooming in on the entire flux of the object, not just the core. In order to accurately find the borders for each object, I would have to manipulate the contrast in the image to find exactly where the light would fall off. Once I was zoomed in on a flux point, I would select the lower left and upper right bounds and calculate the flux within those bounds. After applying the boundaries and calculating flux, the non-reference images were scaled to the reference images using the boundaries and fluxes previously decided upon.

Every image is also masked to remove defects, and clip off the edges where light could have leaked in. A defect could be a piece of dust that had fallen on the lens, or a streak from a meteor or airplane. After fixing defects the images are coadded, or stacked, in order to eliminate cosmic rays and detector artifacts. When taking repetitive images of a galaxy, a cosmic ray will not hit the same place twice. Therefore, when a coadd is applied, if there is point saturated in one image but not the others, the program knows that this area must be a cosmic ray, and takes it out. It is also nice to align the coadded images for each galaxy in the different filters.

Before photometry, we mask out every object in the image that is not the galaxy itself, including stars and other galaxies. Only the UBVRI bands were masked for stars and galaxies. First, the non-target objects must have the star mask defined by zooming in on the object and changing the contrast until the border of where the light completely falls off is visible. The selected regions were completely cut from the images. For galaxies with Hα images, I looked at the Hα continuum subtracted image in order to tell what objects were foreground stars, and what objects were parts of the galaxy. If an object is bright in the continuum subtracted Hα image, then it is more than likely part of the galaxy. If Hα was not available to decipher if an object was part of a galaxy or not, I would look at NED, look at SDSS true color images, or do literature searches, to discern the difference. Once a masking border was decided on, the masking hole had to be filled in order to perform accurate photometry later on. Contours were applied to the image at intervals of my discretion. If a foreground star directly in front of a galaxy was masked, then I must apply contours thickly in that area because the surface brightness changes very quickly, much like sitting on top of a mountain. For masked stars out in the background area, the contours do not have to be as thick because the surface brightness does not change as quickly. Once contours were applied to an image, I would zoom in one by one on the masked regions. I hand repaired the contours through the masked regions. If I felt that the masked region was too large and I was having to guess the shape of the contours, I would leave the region as masked, but this occurrence was rare. The images were

then produced filling in the masked holes according to the new contour lines that I had drawn. The process of actually masking and filling in regions where non-target objects are is extremely rare, and makes our final data more accurate.

2.2.3 Calibration

We calibrated with two different methods. The first, and more standard method, used for 20 of the galaxies involves the use of standard stars. Photometric standard stars are stars whose light in multiple bands have been measured very carefully. When observing, it is important to occasionally take images of star fields with standard stars to compare their instrumental magnitude to that in catalogs. A correction can then be calculated for the evening. Landolt (1992) cataloged 257 standard stars in 156 fields, each having a 6.8' x 6.8' field of view. We could only use this method on some of the galaxies because not all of the them had enough standard star images taken on photometric nights. During the second night of the October 2008 run we had extremely photometric conditions, so we used the opportunity to rotate between short image exposures of as many galaxies in our sample as possible, and standard stars. The more standard stars that can be viewed in a night, the more accurate the correction will be. The standard star calibration method begins with the equation

$$m(calibrated) = m(instrumental) + z + kX \tag{2.1}$$

where m(calibration) is the standard star apparent magnitude from the Landolt Catalog, m(instrumental) is the measured magnitude from the telescope, X is the airmass

recorded during observations in the log, z is the photometric zero point between standard and instrumental systems, and k is the atmospheric extinction coefficient. The z and k constants are what need to be solved for; to do this we can rearrange the above equation to look like

$$(m(calibrated) - m(instrumental)) = kX + z \tag{2.2}$$

which is just the familiar

$$y = mx + b. \tag{2.3}$$

To solve for the variables a linear least squares fits is performed. Once z and k are known, we can return to equation 2.1, except now m(instrumental) is the magnitude of the target galaxies, not the standard stars. I can solve for the calibrated magnitudes of the galaxies since m(instrumental), X, k, and z are all known.

The second more uncommon method of calibration we undertook photometrically calibrates by "bootstrapping" to Sloan Digital Sky Survey (SDSS) magnitudes. Between three and four stars in the fields of the LBCGs had photometry calculated from the Sloan pipeline. I used the SDSS data release 8 finding chart tool. Once the coordinates of a galaxy are entered, the finding chart tool will provide a galaxy centered image where each object in the field can be selected individually. Using the navigation tool I was able to select the surrounding stars in the SDSS images that matched the surrounding stars in my McDonald images and read off their ugriz magnitudes from a provided table. The SDSS magnitudes were then converted to the

Johnson system U,B,V,R,I magnitudes using conversions from Jester et al. (2005).

$$B = g + 0.39(g - r) + 0.21 \tag{2.4}$$

$$V = g - 0.59(g - r) - 0.01 \tag{2.5}$$

$$R - I = 1.00(r - i) + 0.21 \tag{2.6}$$

$$V - R = 1.09(r - i) + 0.22 \tag{2.7}$$

$$U - B = 0.78(u - g) - 0.88 \tag{2.8}$$

Magnitudes of the same stars in the McDonald U,B,V,R,I bands were also measured in the Johnson system. In order to find the fluxes of the stars in the McDonald images, I used a similar process to finding the flux in the reference images for flux scaling. I would zoom in on individual stars, select the lower left and upper right boundary, and see what the flux was inside the hand selected boundary. The flux was then converted to a magnitude scale using a random zero point since we were about to calibrate. The difference between the McDonald U,B,V,R,I magnitudes and the SDSS u,g,r,i,z magnitudes constitute a bootstrap calibration. Since we used 3 to 4 stars per image, an average was taken of the calculated bootstrap values to achieve the most accurate calibration we could. Table 7.1 shows the Sloan coordinates of the stars used in the bootstrap calibration method.

Mrk 171 required a different kind of bootstrap calibration. I was not able to successfully use Sloan values to calibrate this galaxy because the star field was very thick. The light from various stars overlapped so I could not get good readings on

individual stars. However, Mrk 171 has been studied enough that there are trusted values in the literature. For the V band magnitude I used a value of 12.65 (Huchra, 1977), and for the B magnitude I used a value 12.31 (Hibbard & Yum 1999). First, the point on the growth curve (plot of increasing galaxy surface brightness versus radius) where the curve starts to flatten must be identified, i.e. the galaxy does not get significantly brighter as r continues to increase. Once I had a radius defined for the galaxy, the bootstrap process was not that different from before, except for the use of the galaxy itself instead of stars. I calculated what change I needed to make in the magnitude to get my instrumental magnitude for the whole galaxy to match what was in the literature.

2.3 Morphology

In Figure 2.1 we present the reduced and foreground star-subtracted images for the optical sample. Each image has a dynamic color table wrapped twice to show the detailed structure, and Gaussian smoothing. The top scale bar represents 5 arcseconds, and the bottom scale bar represents 5 kpc. Multiple morphology types can be seen in our sample. Loose & Thuan (1985) created a system to classify blue compact dwarfs, and we applied this classification scheme to our data. The three major categories are based on the morphology of the starburst and the shape of the external envelope. The three main categories are: the IE galaxies which have complex inner structure with several star-forming regions on top of a regular external envelope,

the NE galaxies which have a clearly defined nucleus and regular isophotes at all intensity levels, and the iI galaxies which have irregular outer and inner isophotes. Table 2.4 shows the Loose & Thuan classifications for our sample of galaxies. After a classification of the LBCG sample, it was found that $\sim 31\%$ are iE, $\sim 29\%$ are nE, and $\sim 41\%$ are iI. For comparison, Cairos et al. (2001) used the same classification scheme on their BCDs and found $\sim 39\%$ were iE, $\sim 21\%$ were nE, and $\sim 32\%$ were iI. A higher percentage of our sample falls in the iI category, more than likely because we are not looking at dwarfs, so we see more large scale interactions. The iE category was a close second for our galaxy sample. The smallest portion of our sample has regular inner and outer structure.

Of our galaxy sample, 30 of 50 galaxies show either a sign of interaction (e.g. bridge, tail, extended loop) or a companion is present. Four out of nineteen interacting galaxies consisted of three or more galaxies rather than just two. The environment for a LBCG is definitely not the same across the board. Sometimes they will be found crowded and or in the process of a merger, other times they seem to be alone with no sign of an interaction.

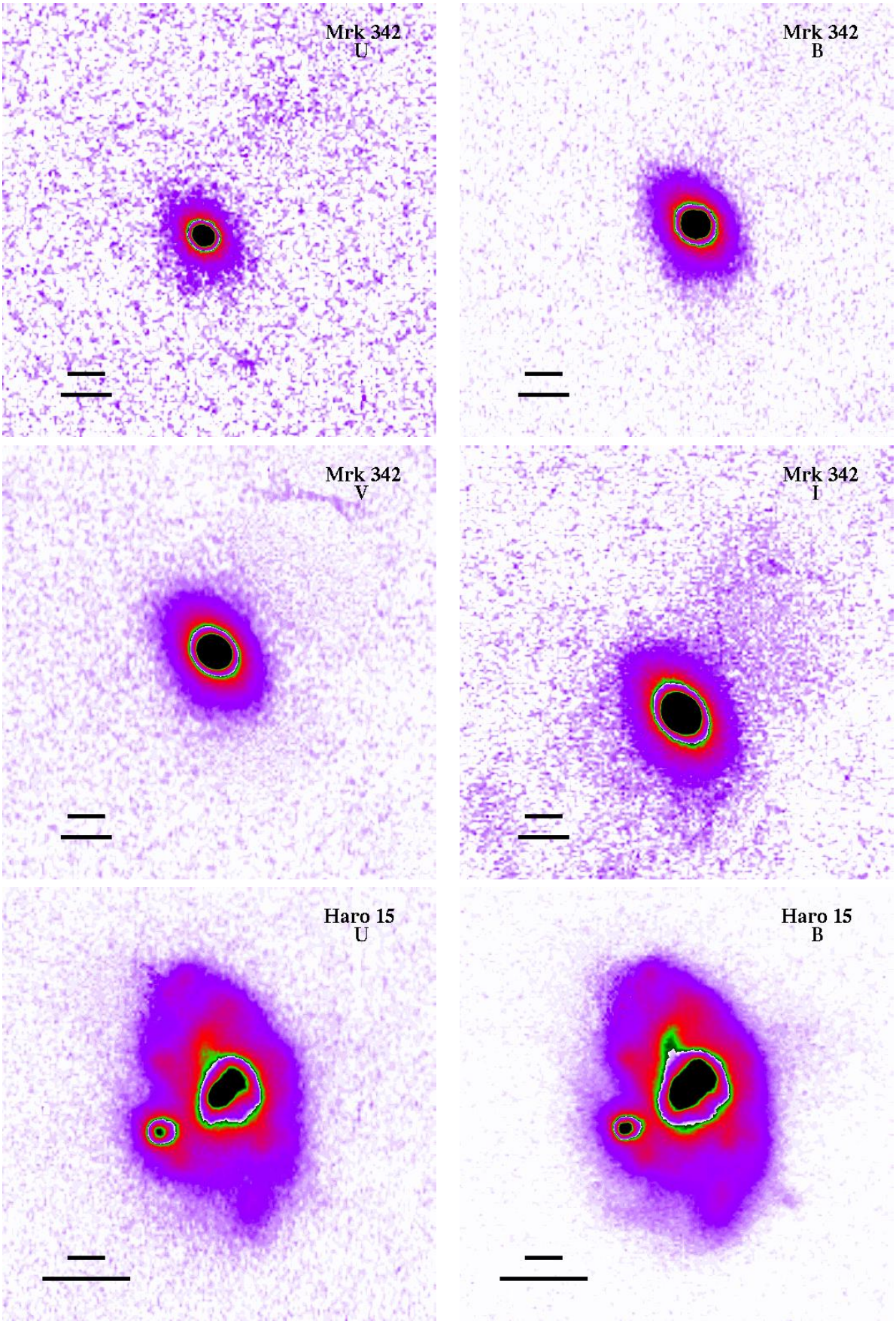
Mrk 342
U
Mrk 342
B
Mrk 342
V
Mrk 342
I
Haro 15
U
Haro 15
B

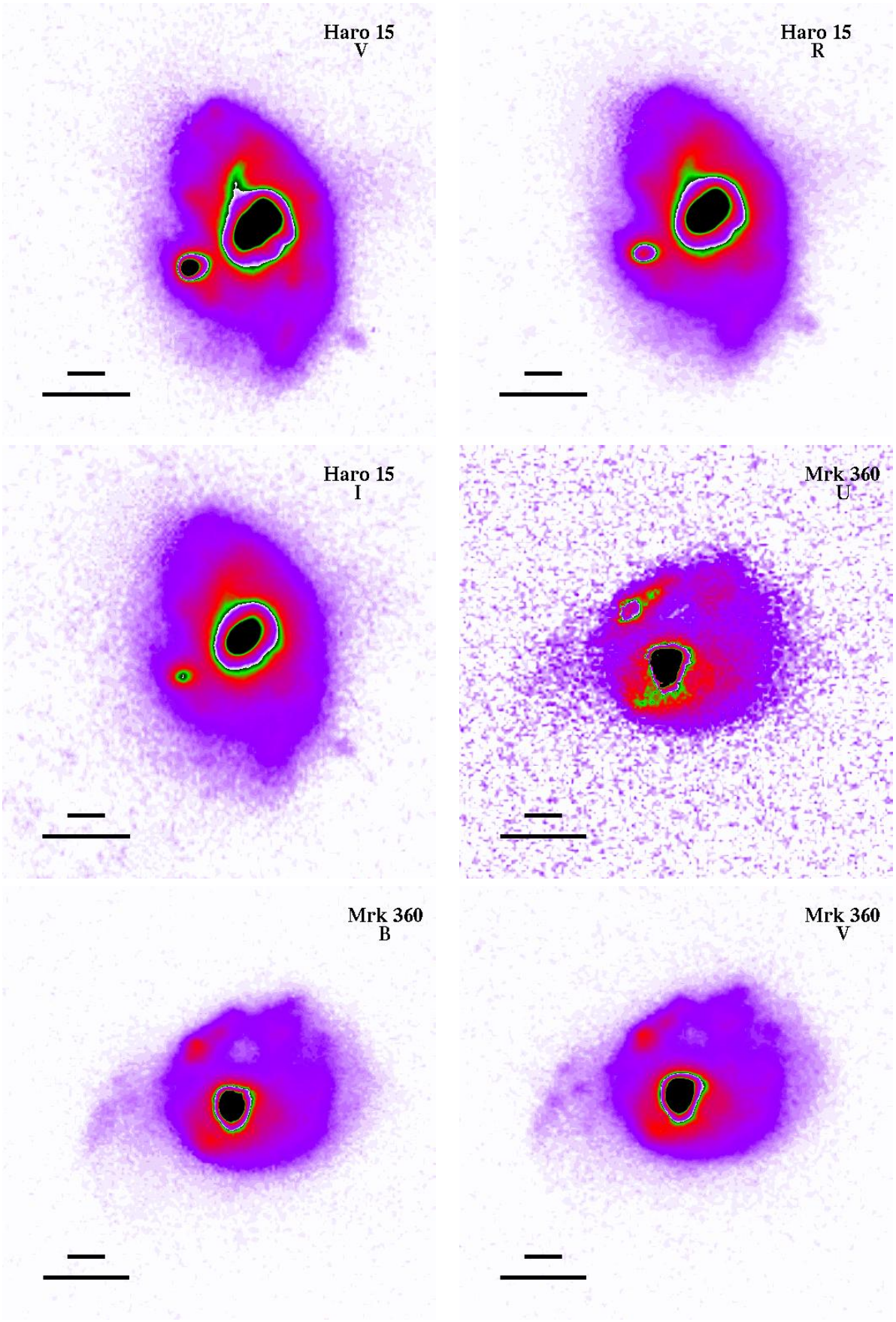
Haro 15
V
Haro 15
R
Haro 15
I
Mrk 360
U
Mrk 360
B
Mrk 360
V

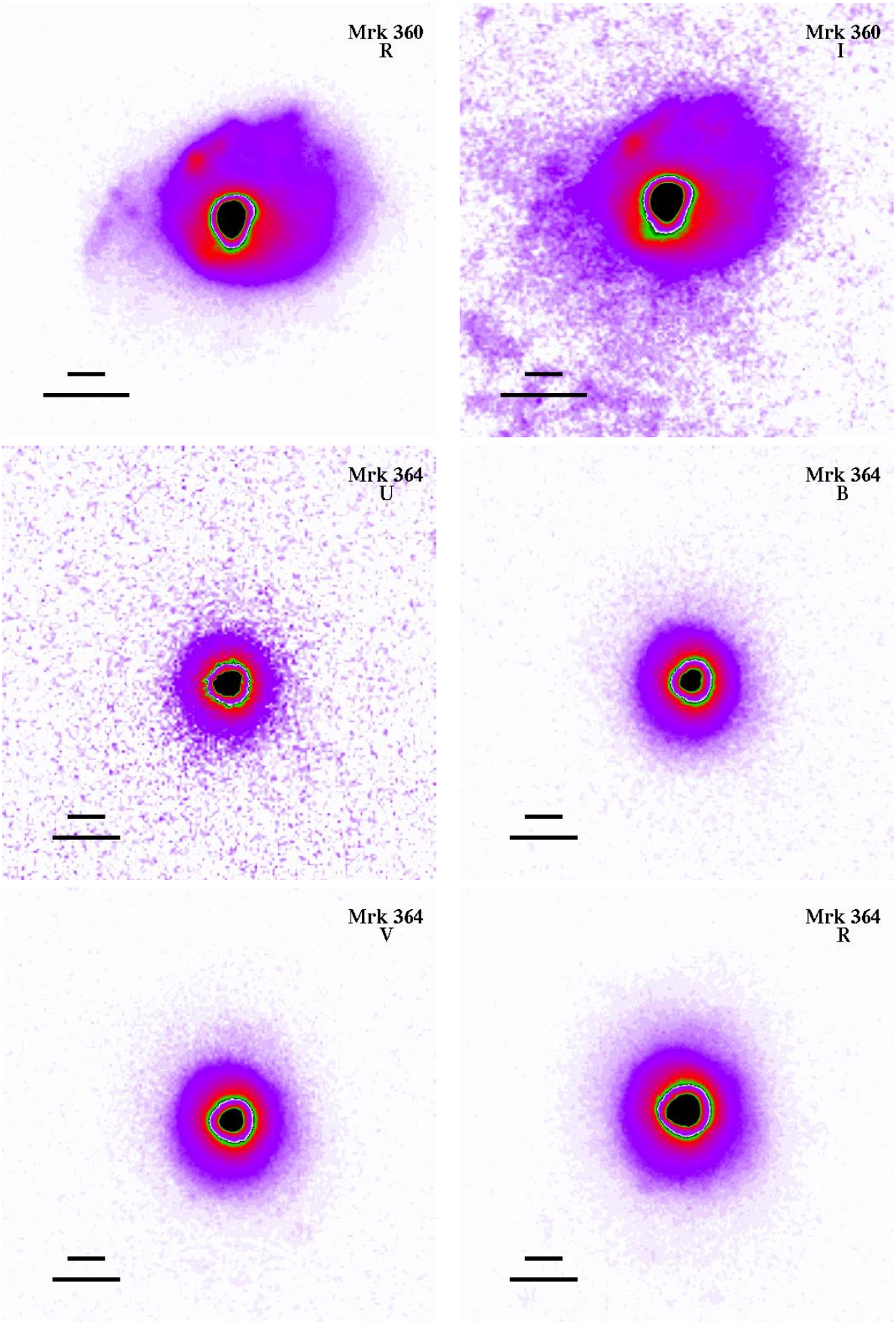
Mrk 360
R
Mrk 360
I
Mrk 364
U
Mrk 364
B
Mrk 364
V
Mrk 364
R

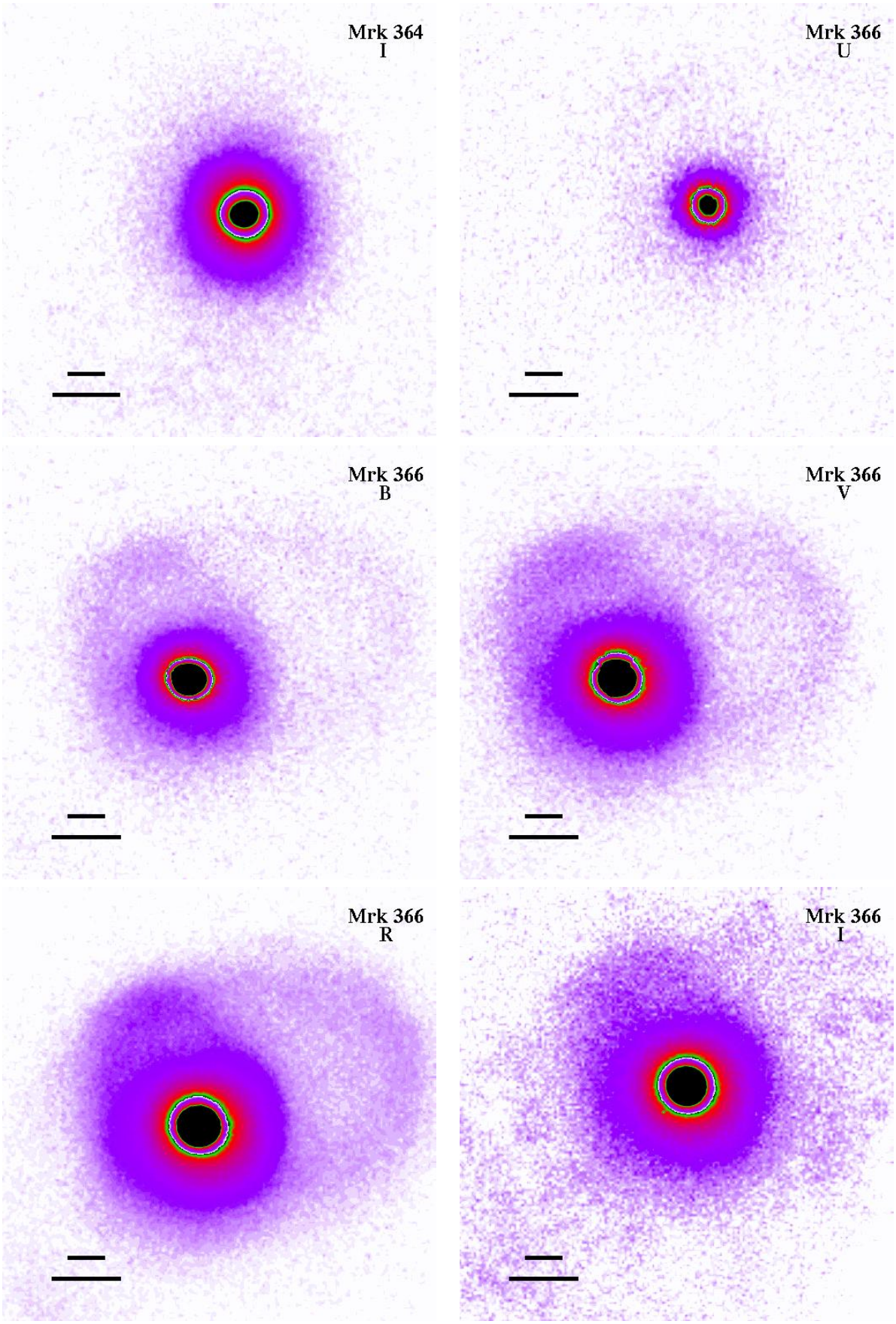
Mrk 364
I
Mrk 366
U
Mrk 366
B
Mrk 366
V
Mrk 366
R
Mrk 366
I

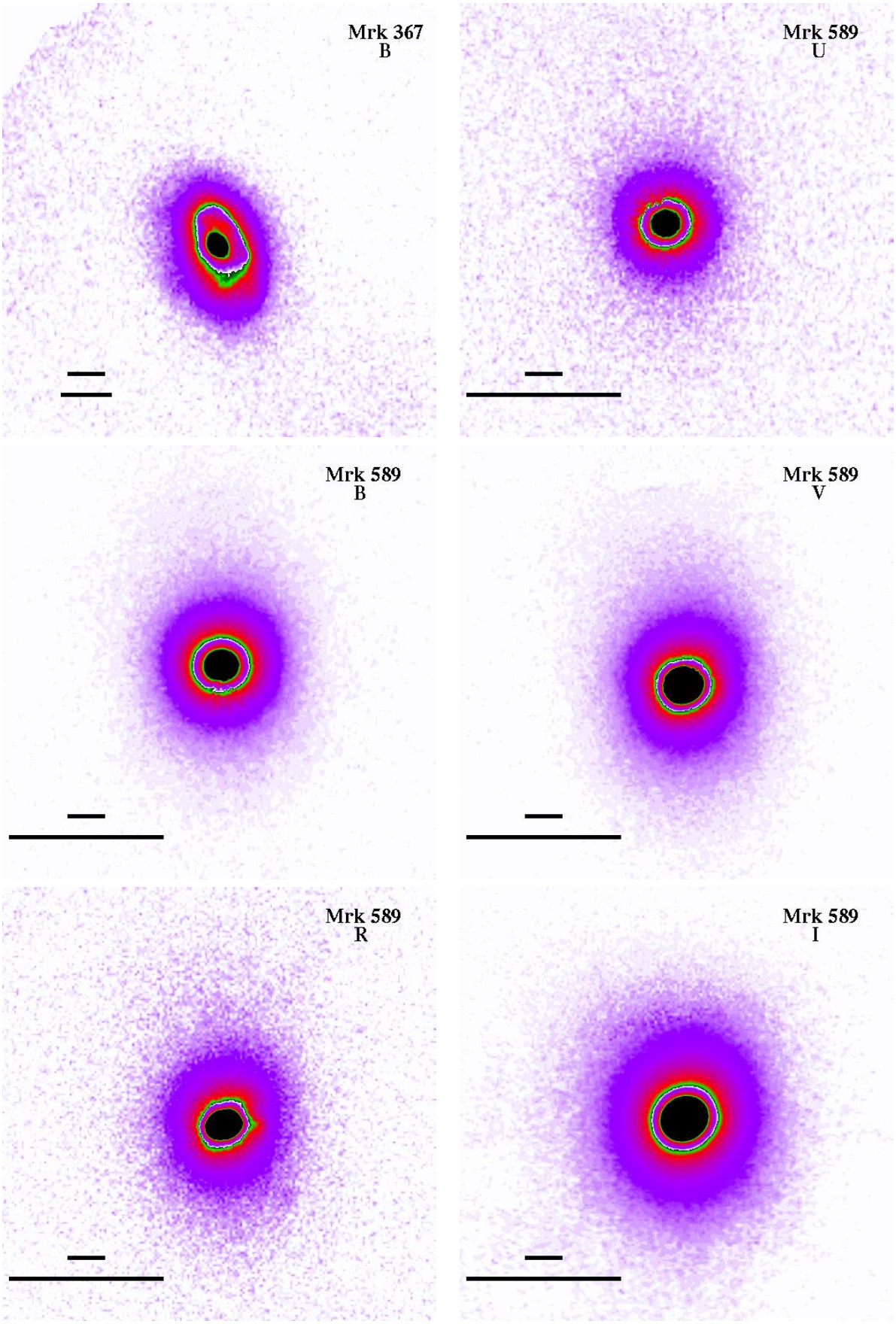
Mrk 367
B
Mrk 589
U
Mrk 589
B
Mrk 589
V
Mrk 589
R
Mrk 589
I

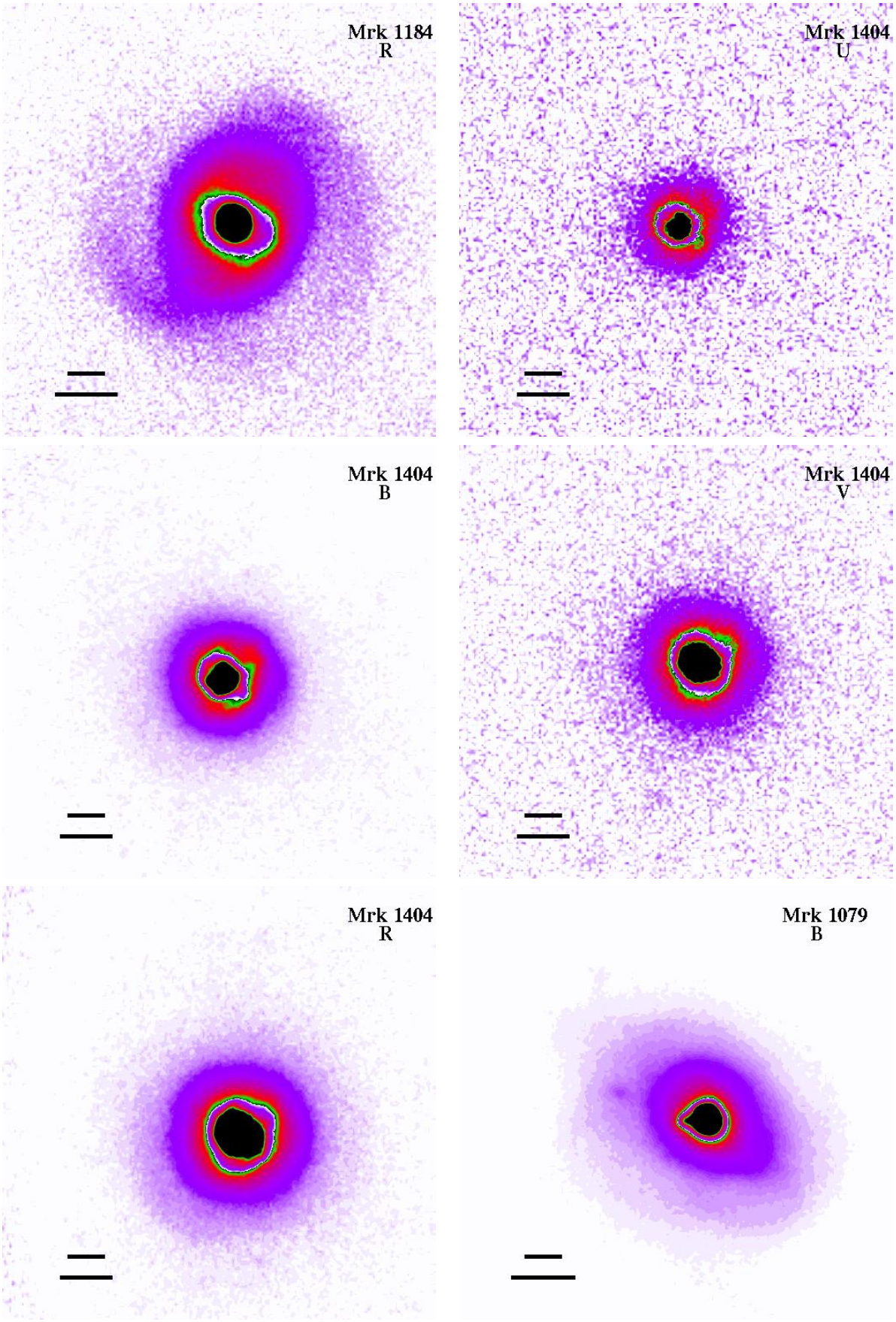
Mrk 1184
R
Mrk 1404
U
Mrk 1404
B
Mrk 1404
V
Mrk 1404
R
Mrk 1079
B

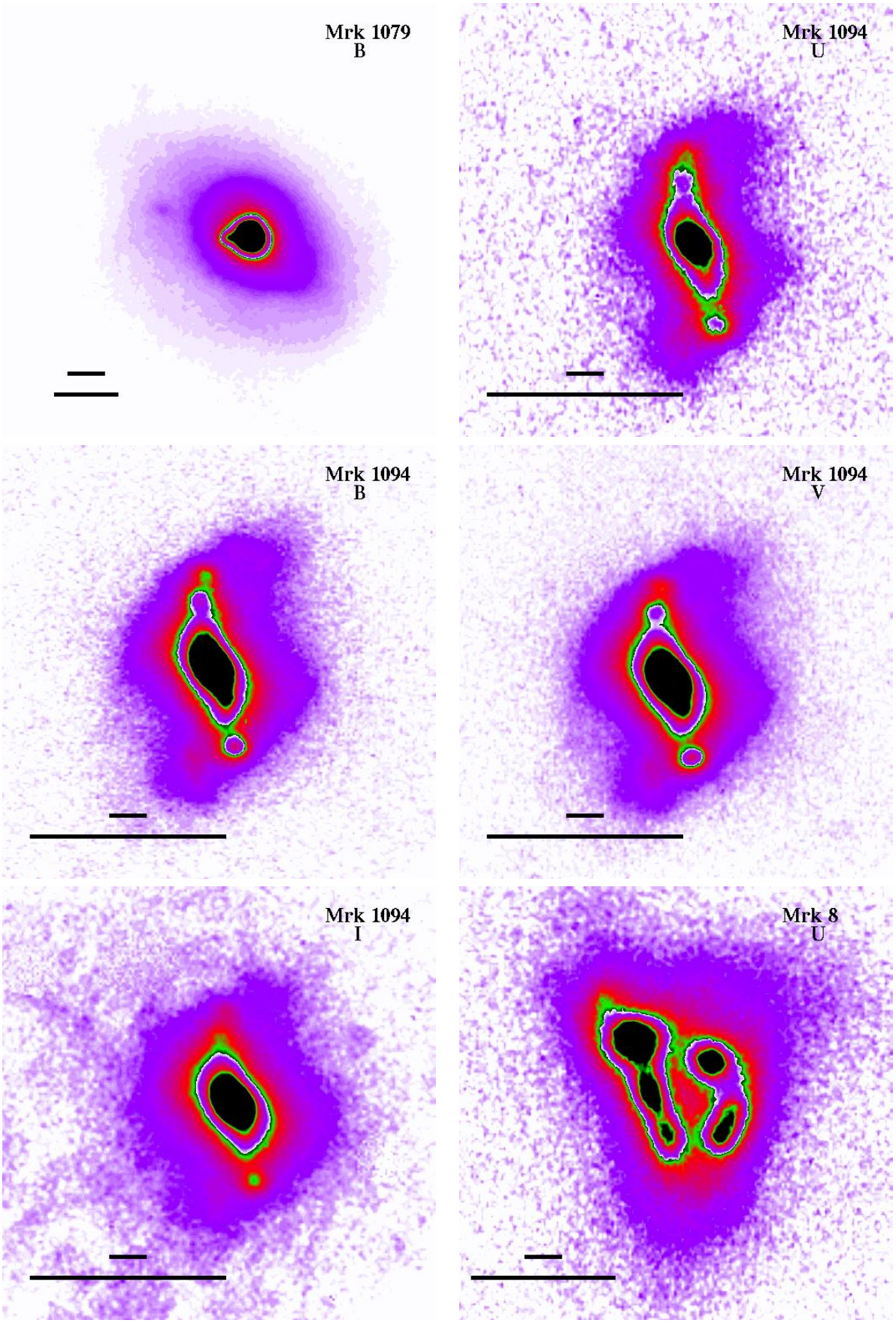
Mrk 1079
B
Mrk 1094
U
Mrk 1094
B
Mrk 1094
V
Mrk 1094
I
Mrk 8
U

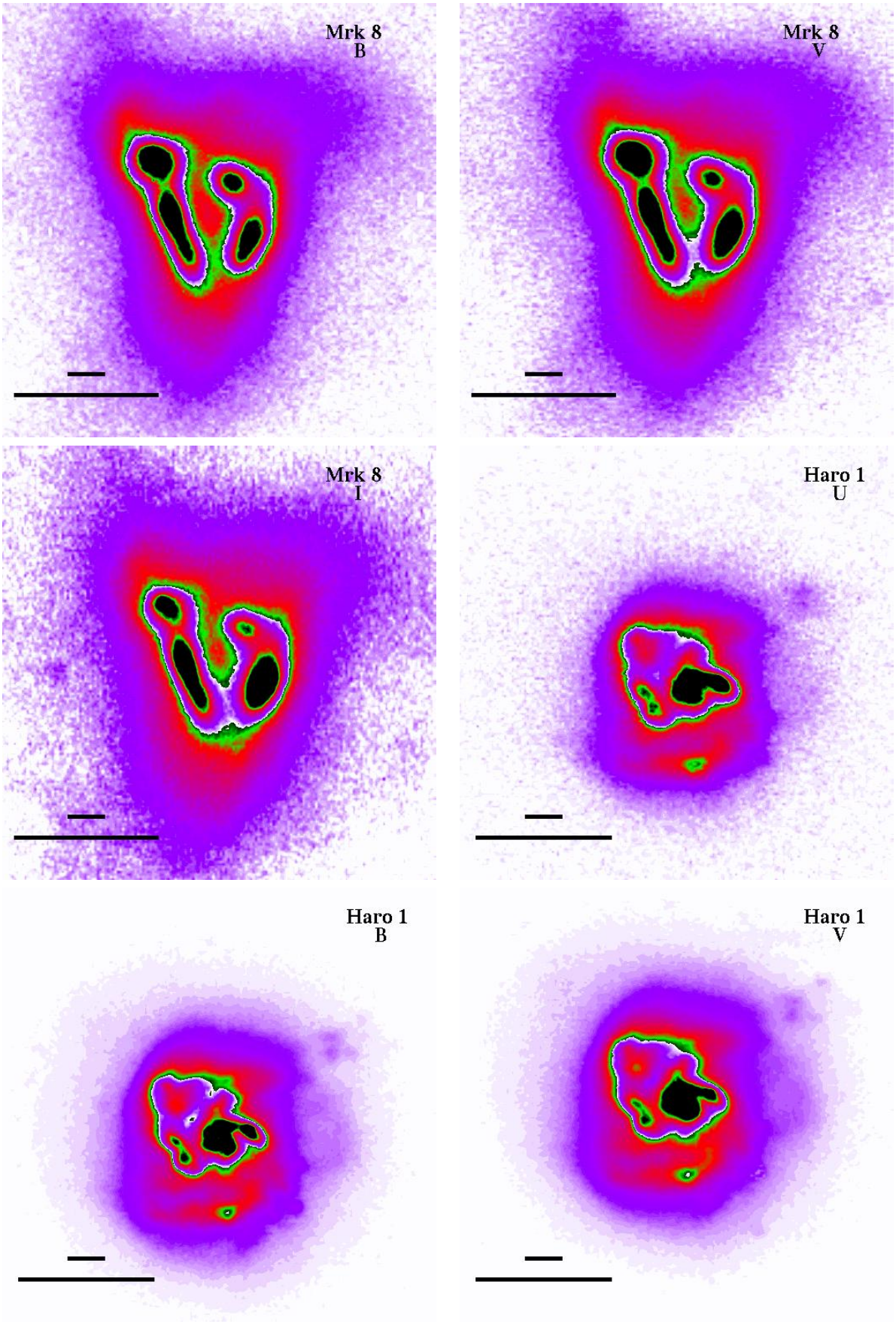
Mrk 8
B
Mrk 8
V
Mrk 8
I
Haro 1
U
Haro 1
B
Haro 1
V

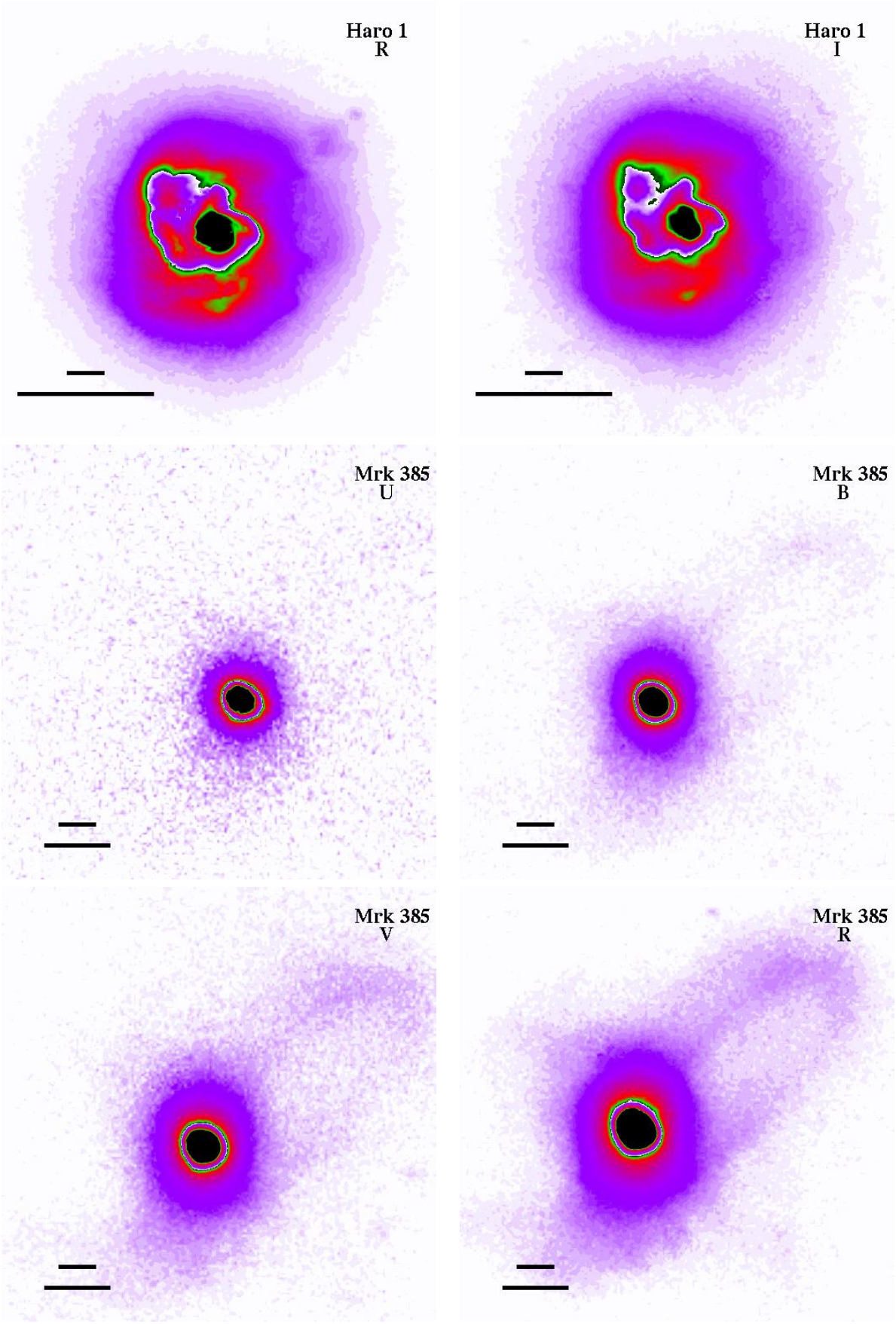
Haro 1
R
Haro 1
I
Mrk 385
U
Mrk 385
B
Mrk 385
V
Mrk 385
R

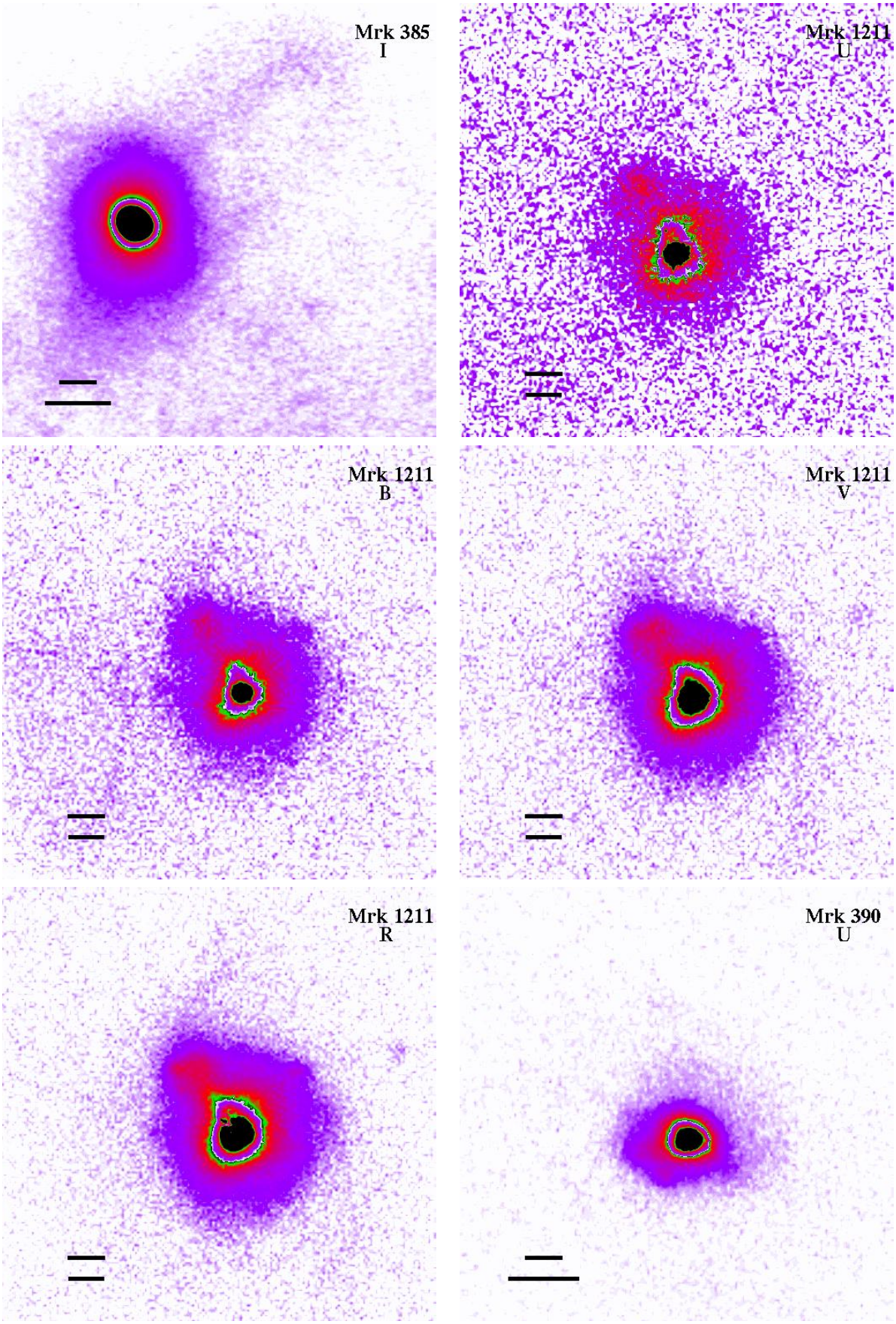
Mrk 385
I
Mrk 1211
U
Mrk 1211
B
Mrk 1211
V
Mrk 1211
R
Mrk 390
U

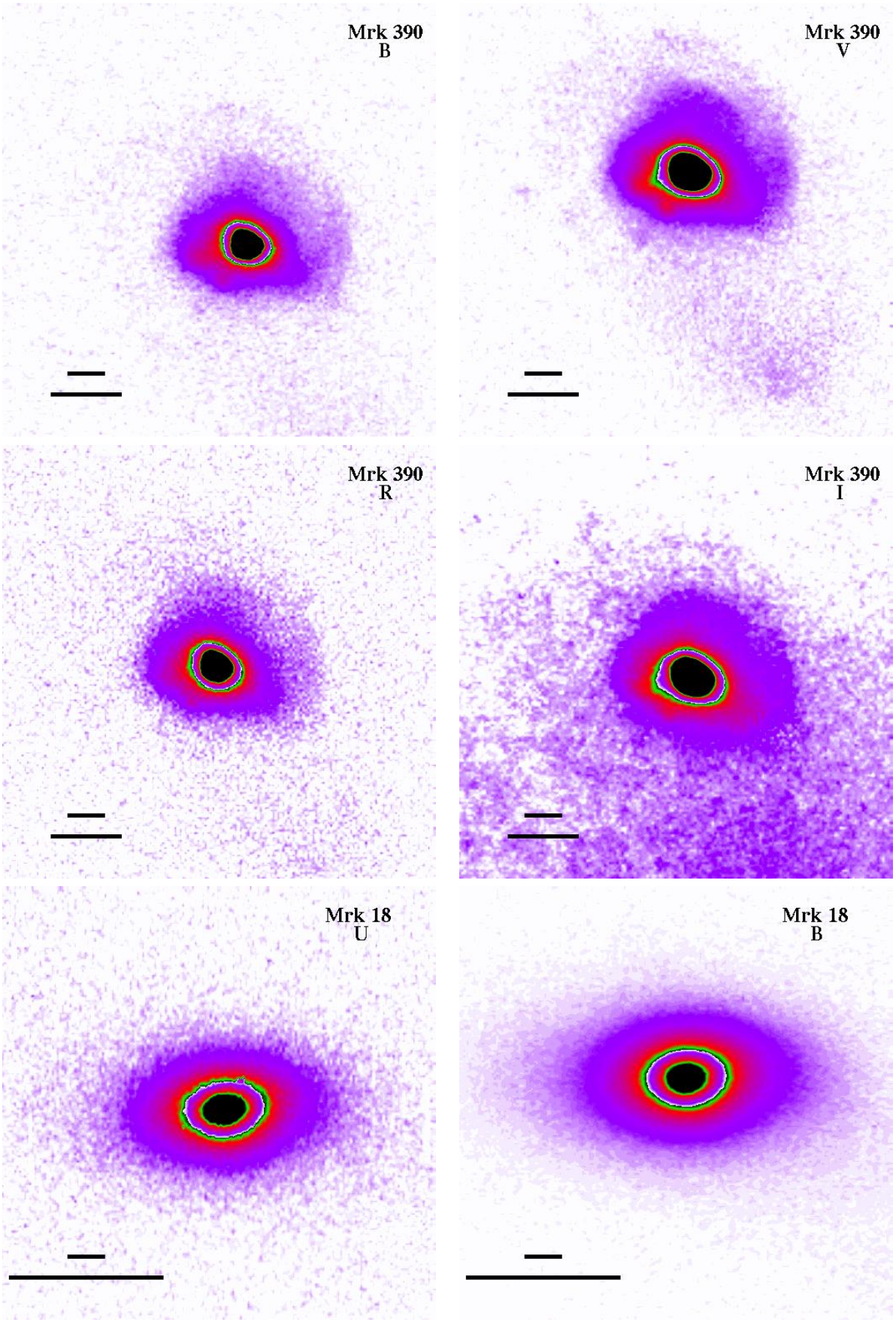
Mrk 390
B
Mrk 390
V
Mrk 390
R
Mrk 390
I
Mrk 18
U
Mrk 18
B

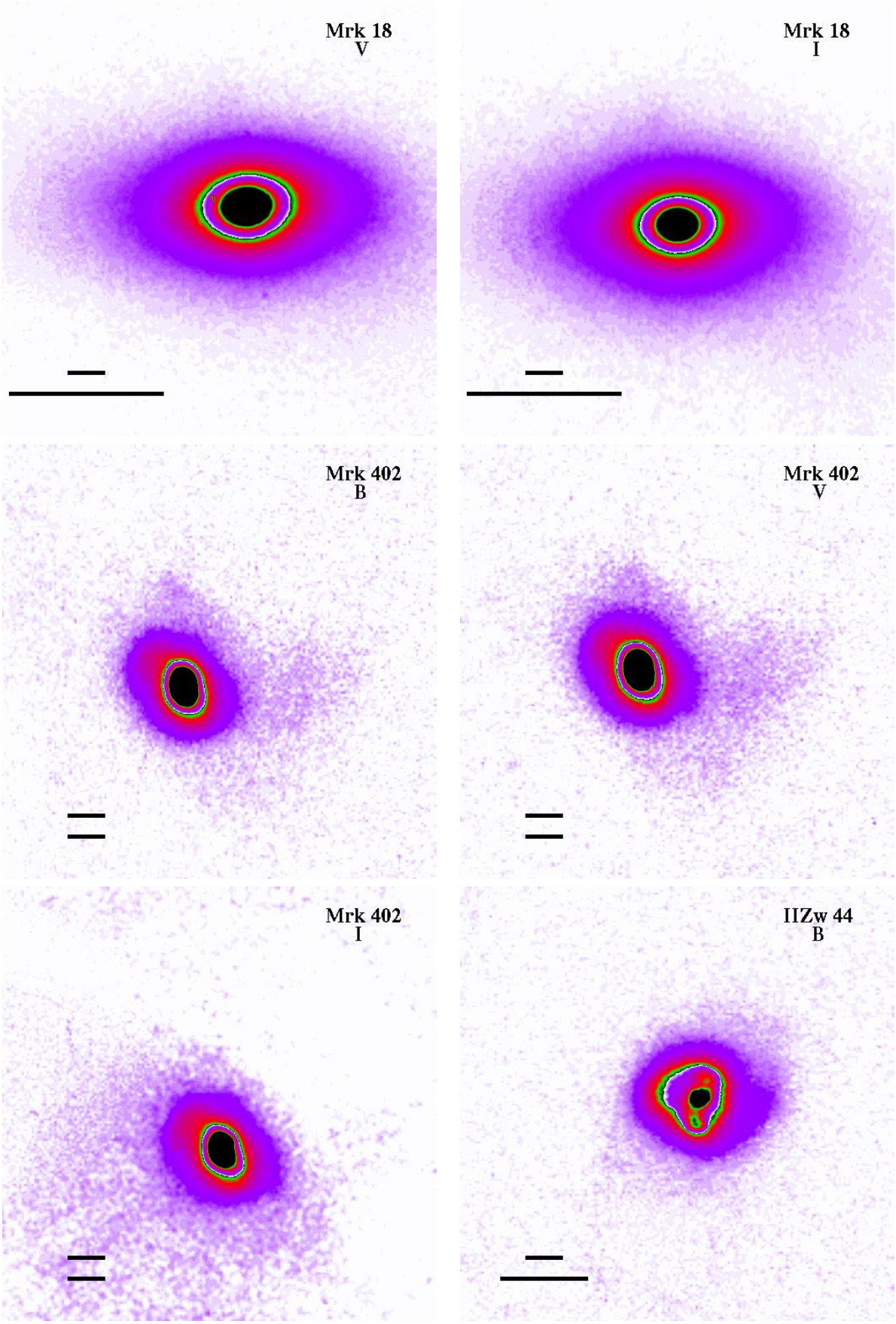
Mrk 18
V
Mrk 18
I
Mrk 402
B
Mrk 402
V
Mrk 402
I
IIZw 44
B

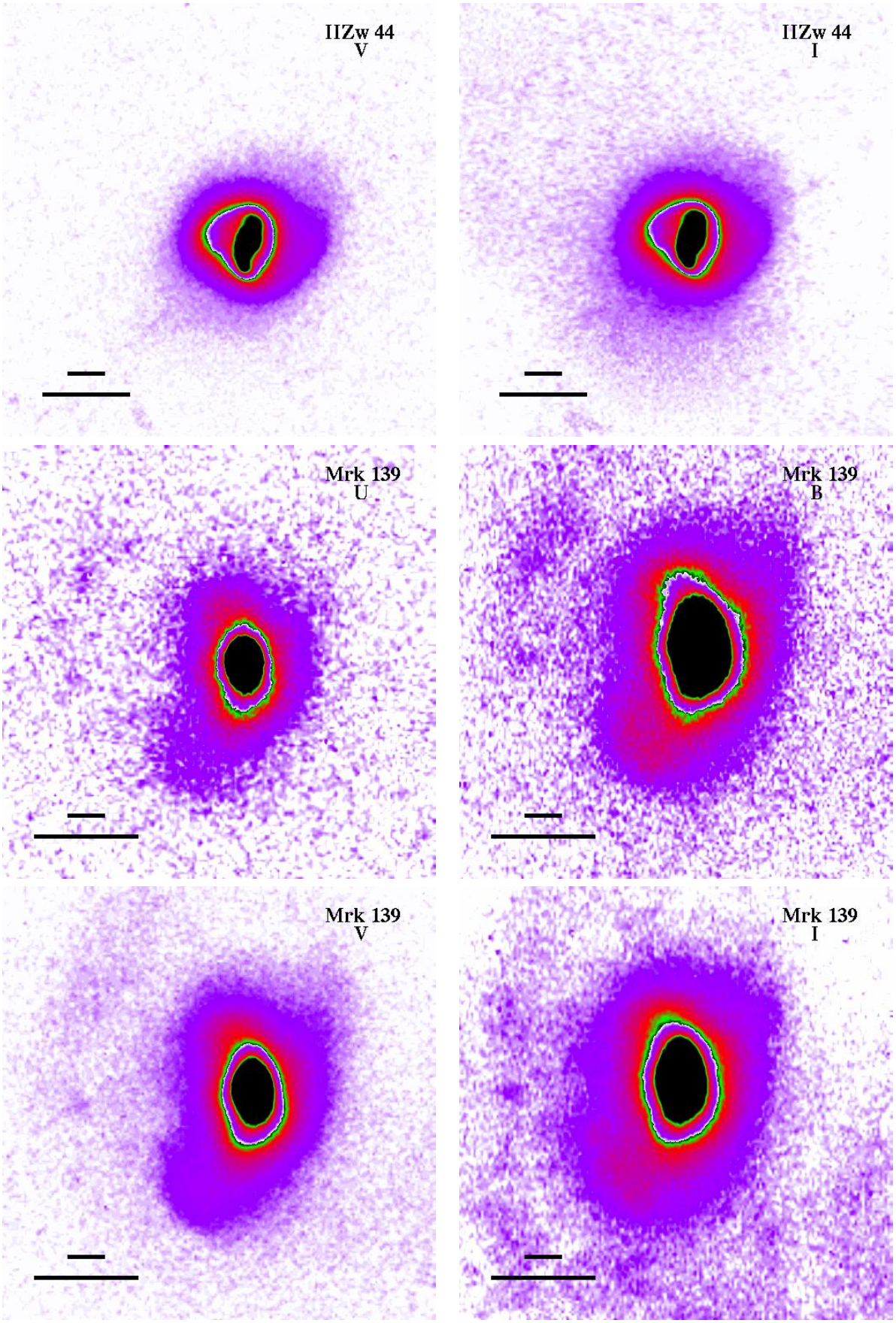
IIZw 44
V
IIZw 44
I
Mrk 139
U
Mrk 139
B
Mrk 139
V
Mrk 139
I

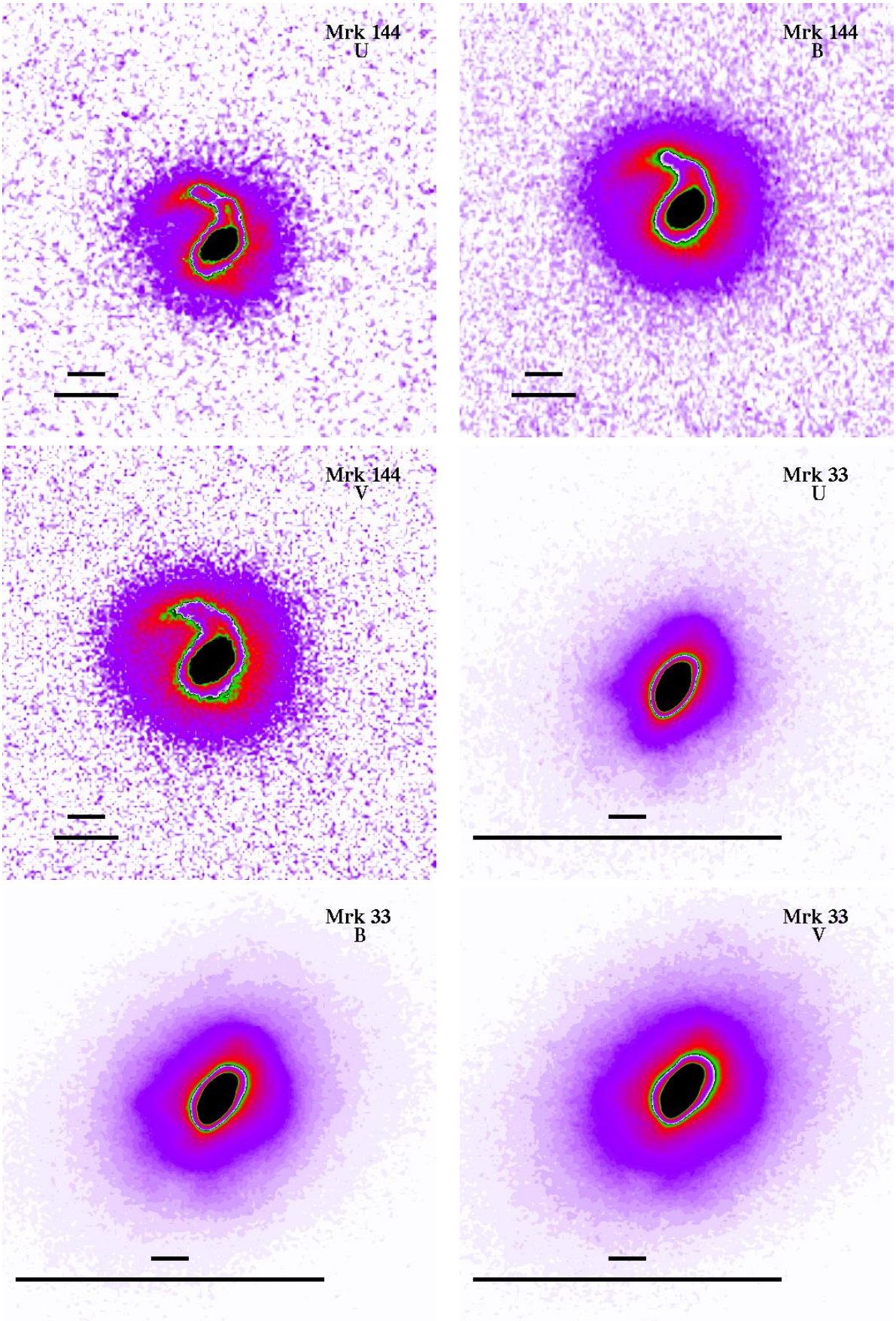
Mrk 144
U
Mrk 144
B
Mrk 144
V
Mrk 33
U
Mrk 33
B
Mrk 33
V

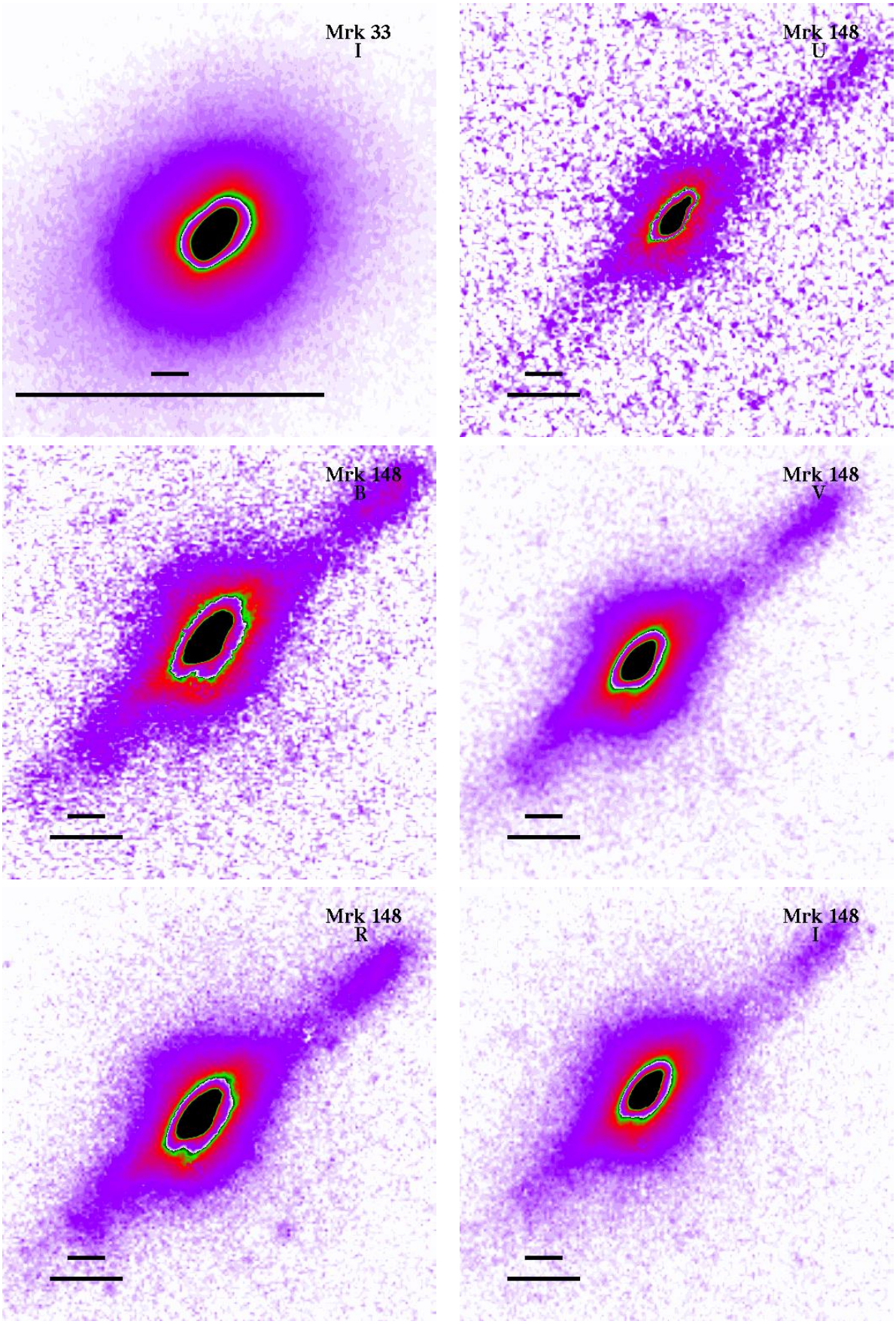
Mrk 33
I
Mrk 148
U
Mrk 148
B
Mrk 148
V
Mrk 148
R
Mrk 148
I

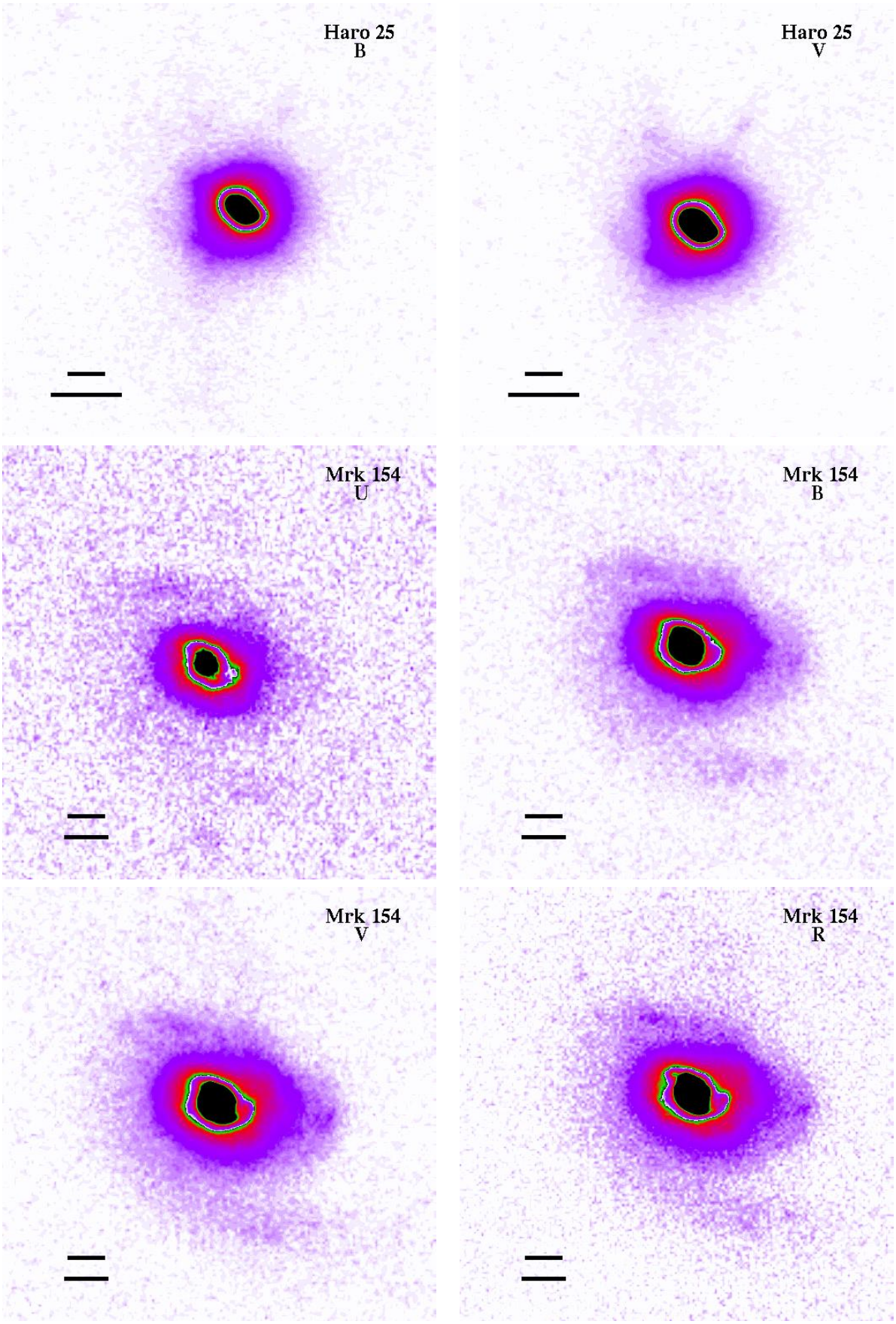
Haro 25
B
Haro 25
V
Mrk 154
U
Mrk 154
B
Mrk 154
V
Mrk 154
R

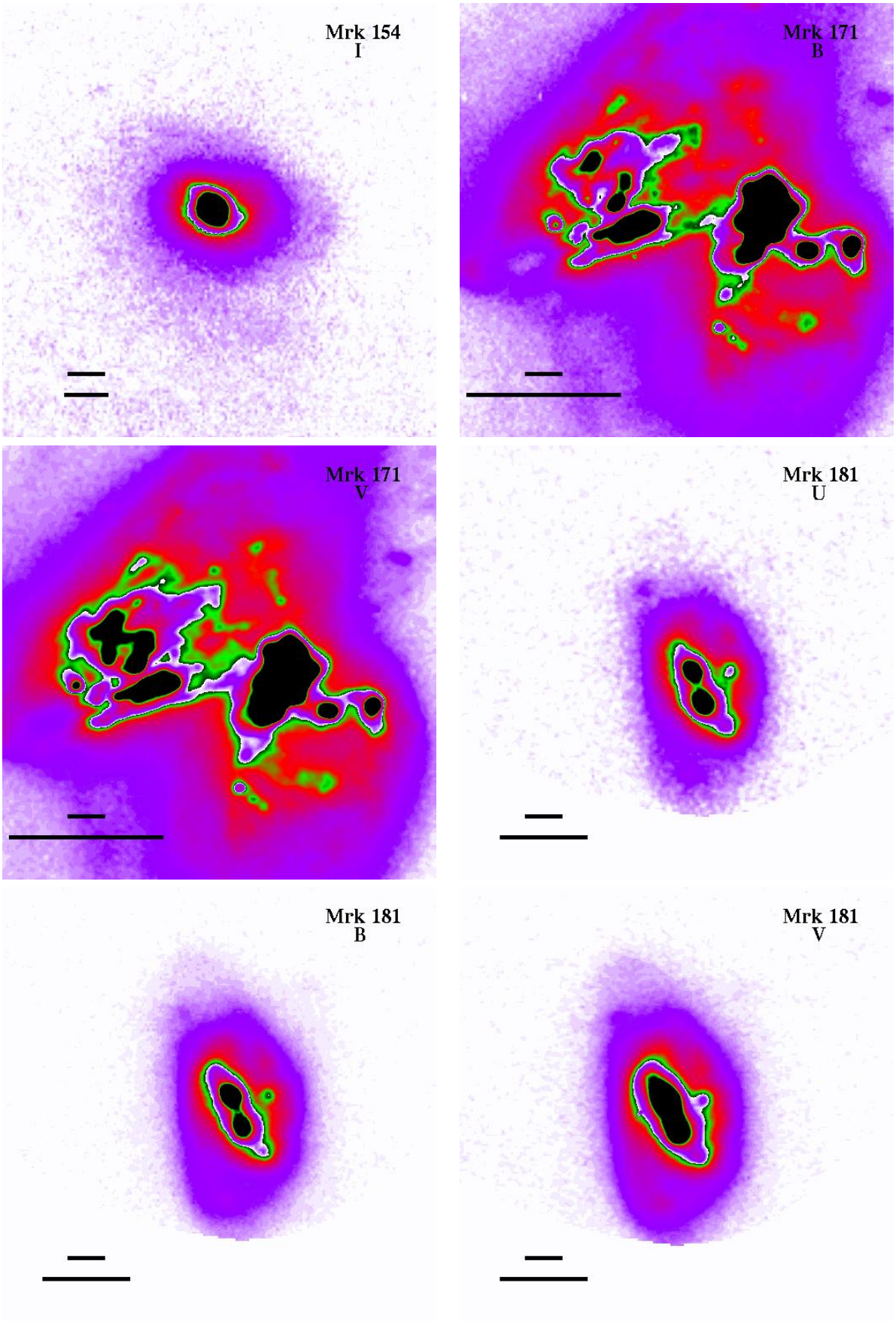
Mrk 154
I
Mrk 171
B
Mrk 171
V
Mrk 181
U
Mrk 181
B
Mrk 181
V

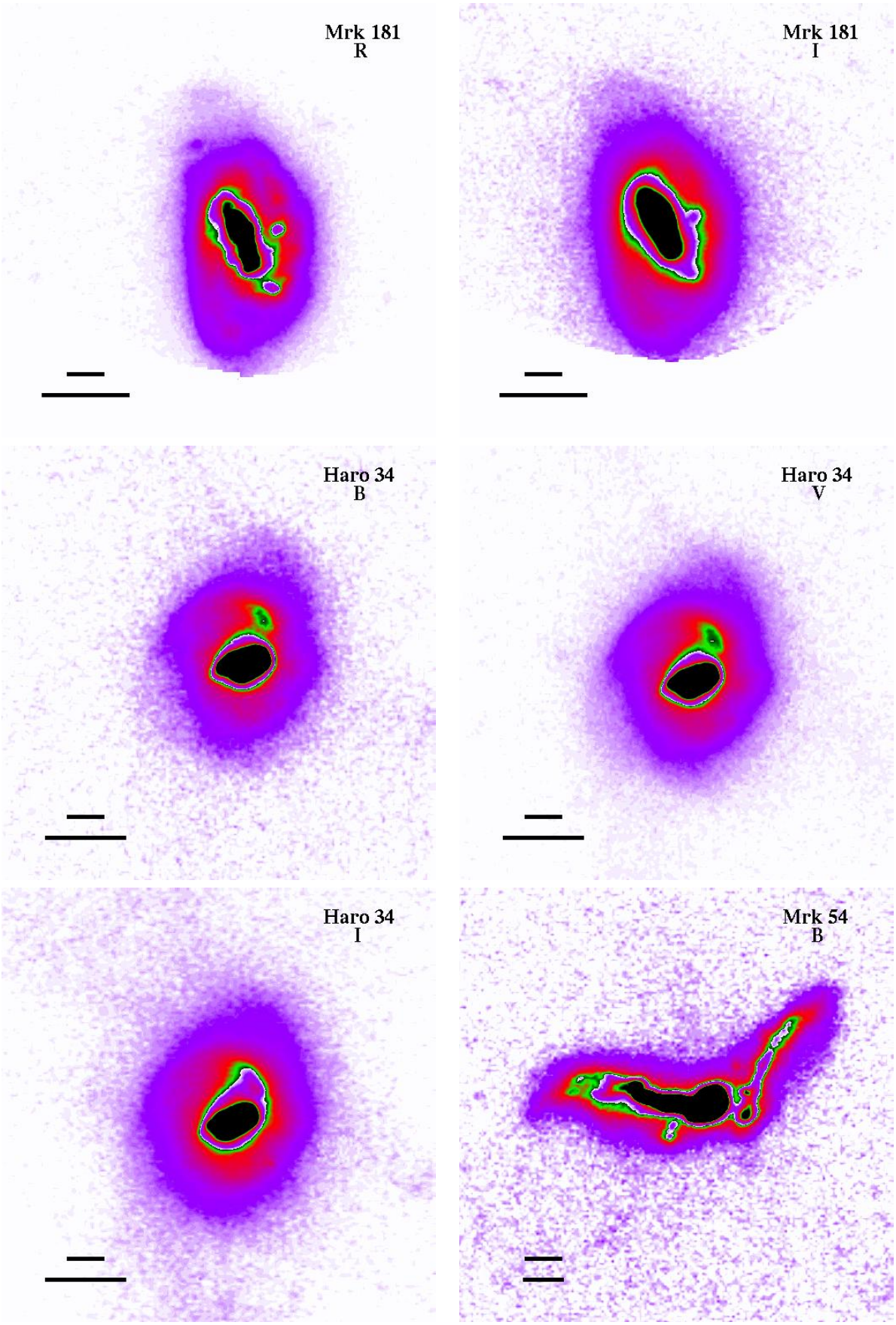
Mrk 181
R
Mrk 181
I
Haro 34
B
Haro 34
V
Haro 34
I
Mrk 54
B

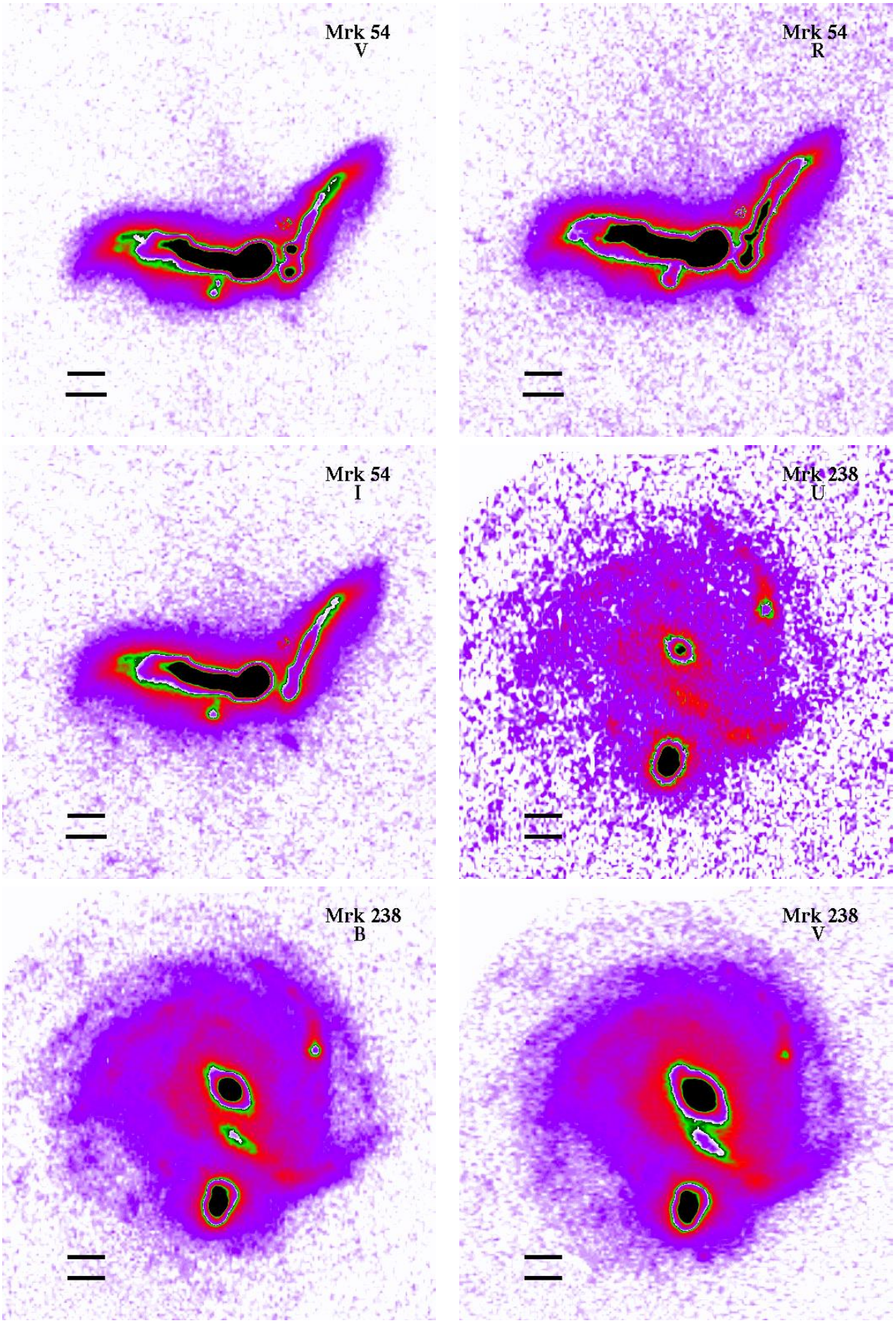
Mrk 54
V
Mrk 54
R
Mrk 54
I
Mrk 238
U
Mrk 238
B
Mrk 238
V

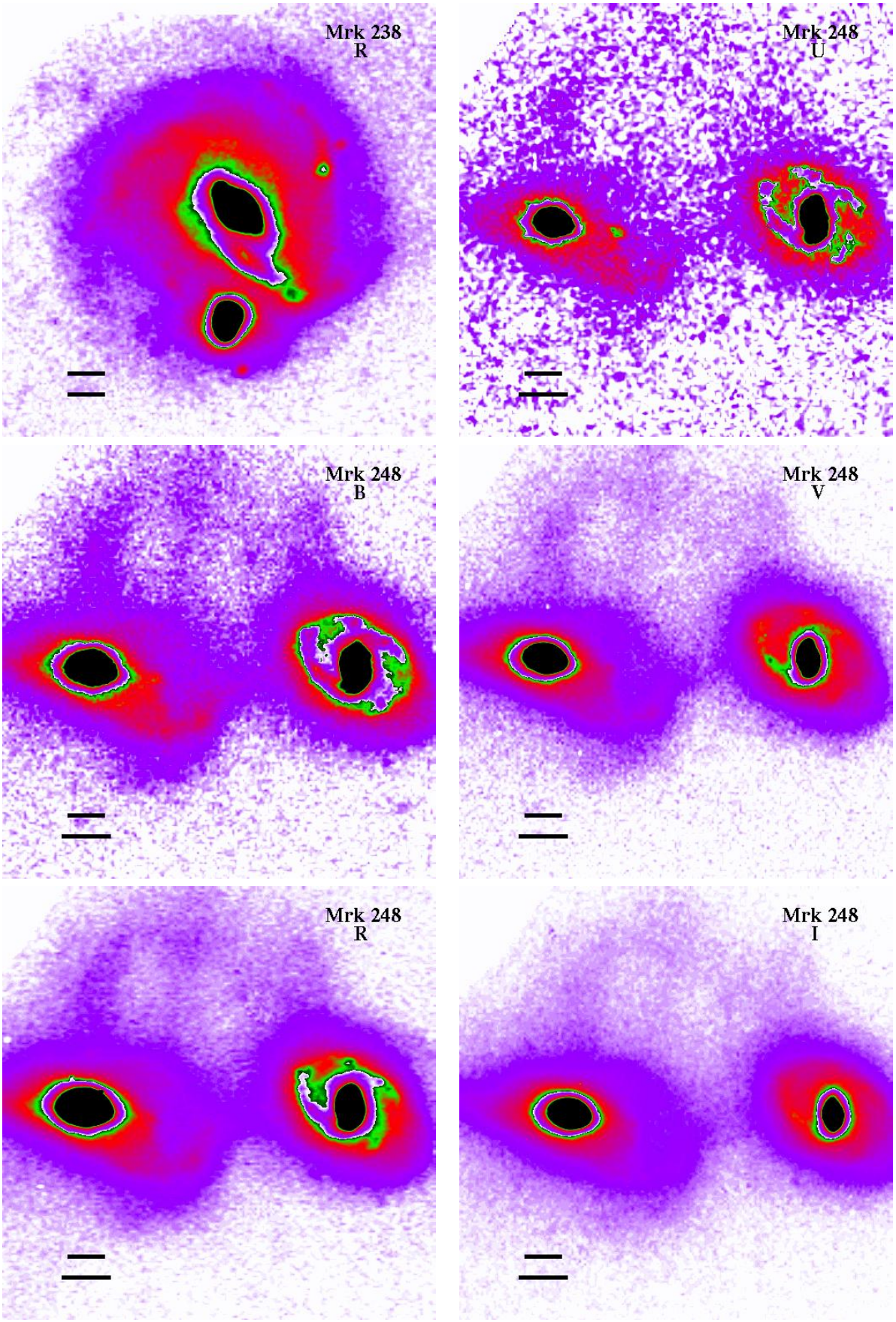
Mrk 238
R
Mrk 248
U
Mrk 248
B
Mrk 248
V
Mrk 248
R
Mrk 248
I

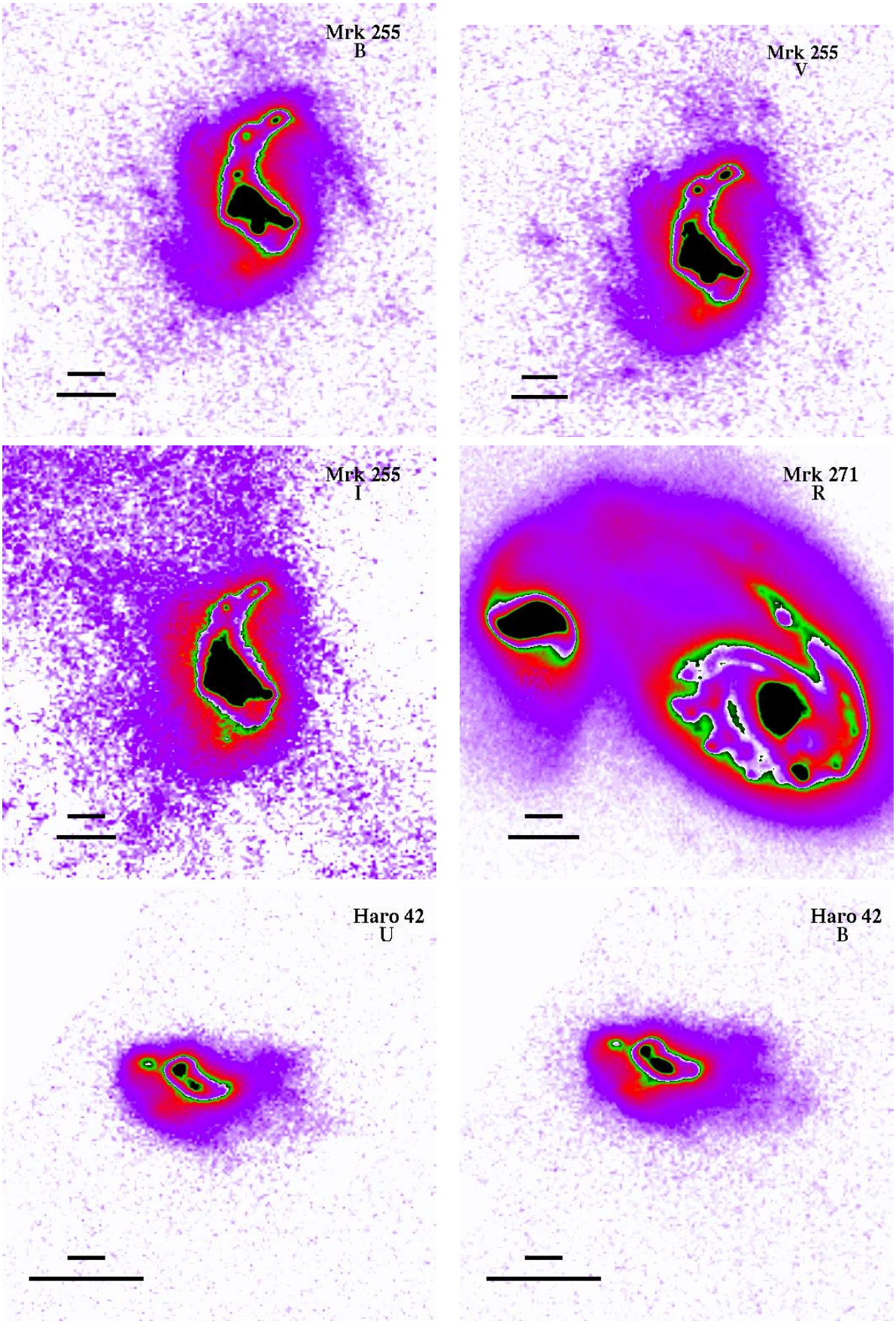
Mrk 255
B
Mrk 255
V
Mrk 255
I
Mrk 271
R
Haro 42
U
Haro 42
B

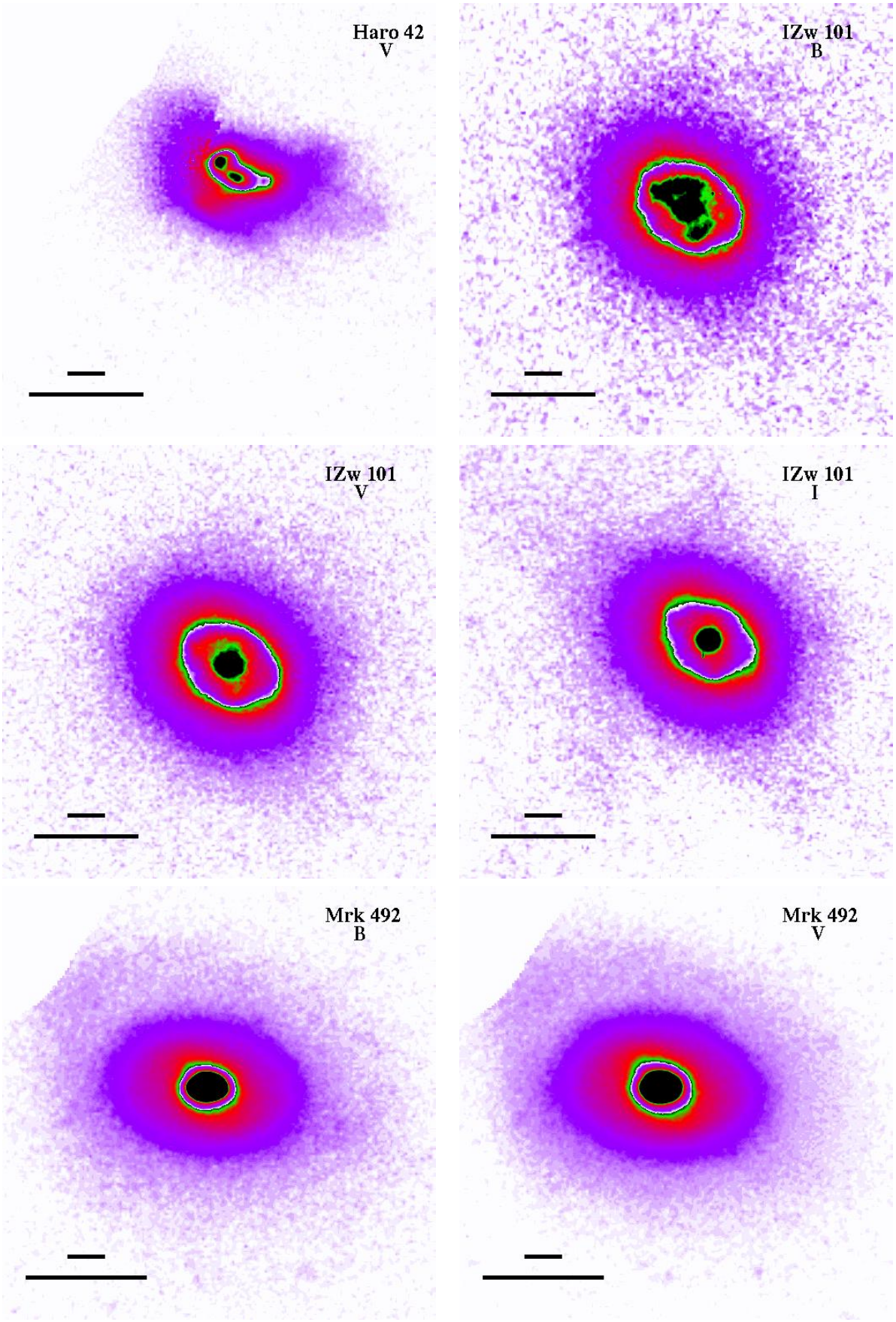
Haro 42
V
IZw 101
B
IZw 101
V
IZw 101
I
Mrk 492
B
Mrk 492
V

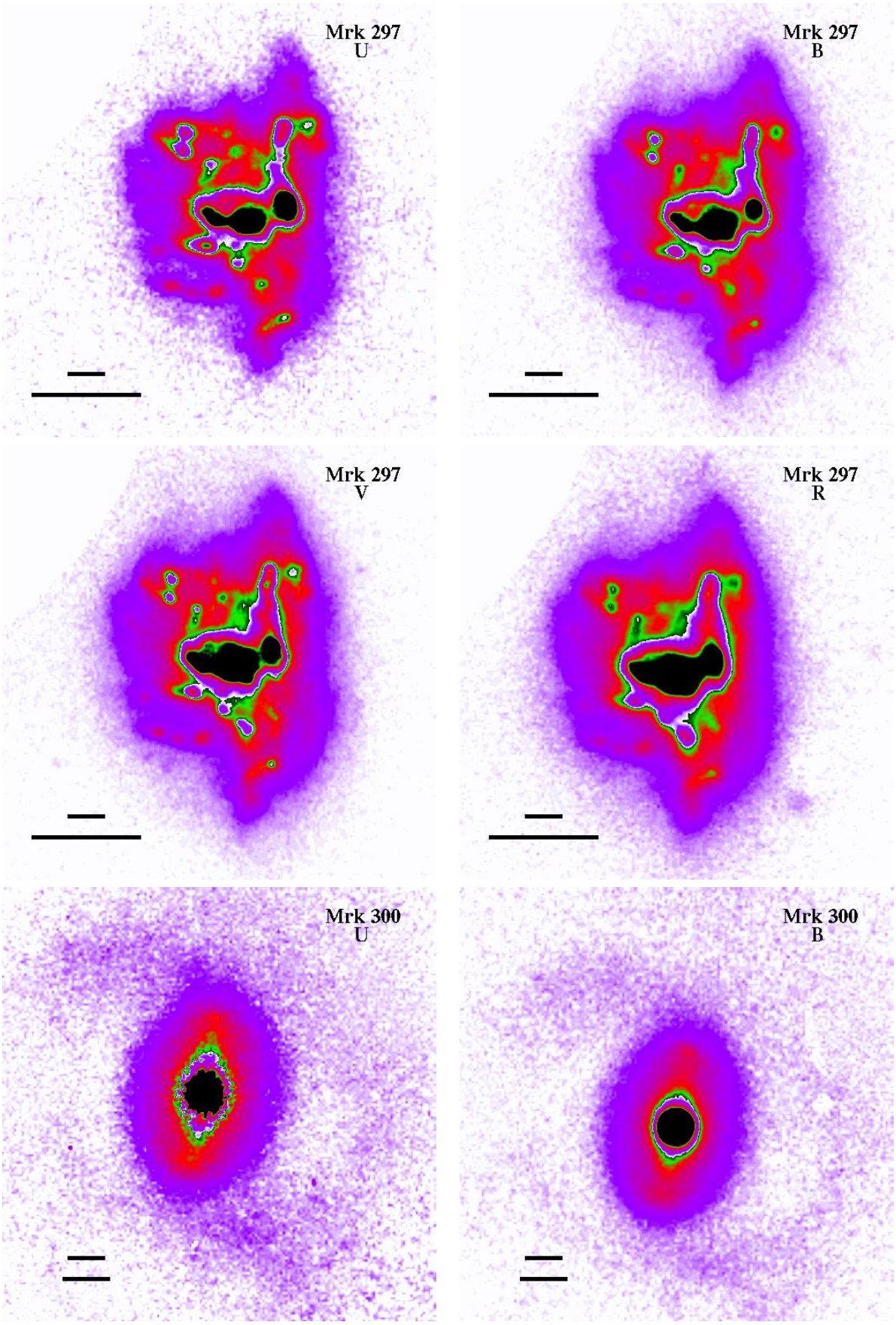
Mrk 297
U
Mrk 297
B
Mrk 297
V
Mrk 297
R
Mrk 300
U
Mrk 300
B

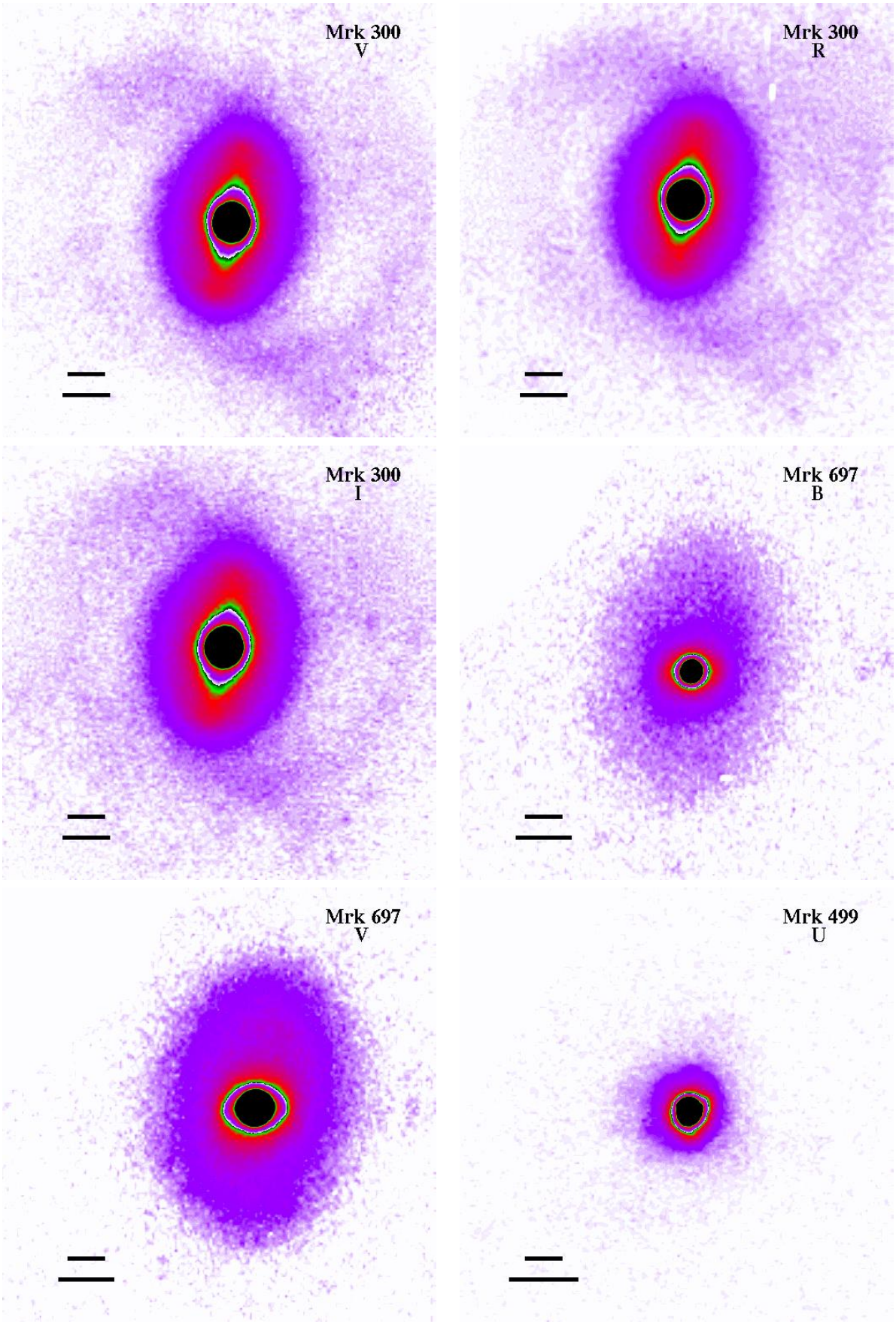
Mrk 300
V
Mrk 300
R
Mrk 300
I
Mrk 697
B
Mrk 697
V
Mrk 499
U

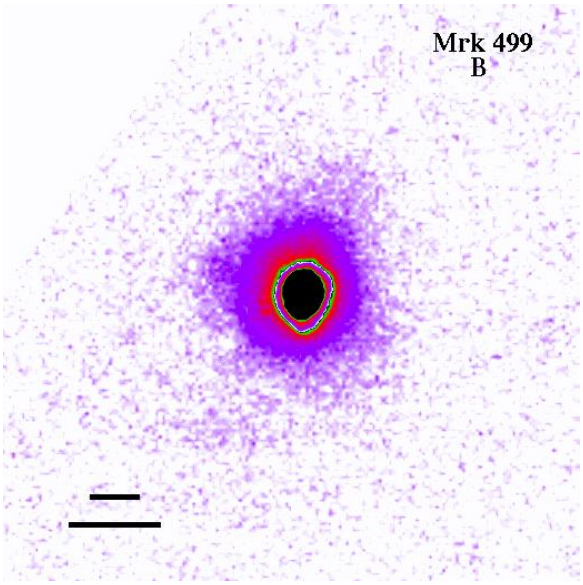
Mrk 499
B

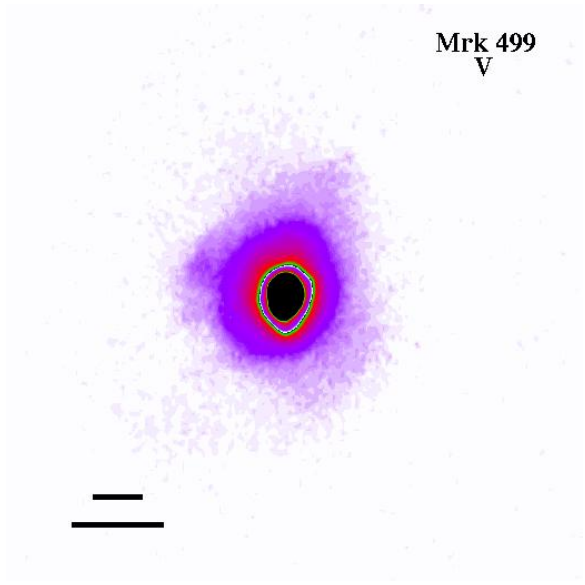
Mrk 499
V

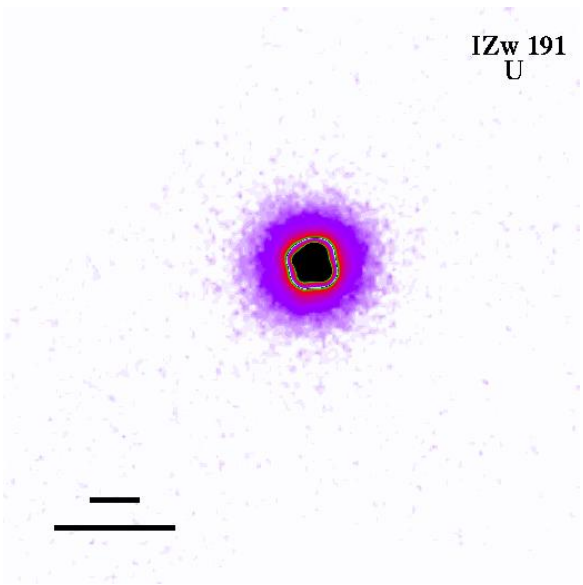
IZw 191
U

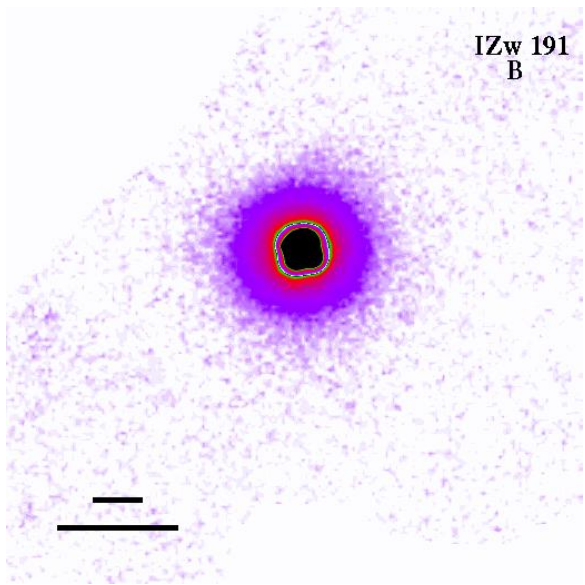
IZw 191
B

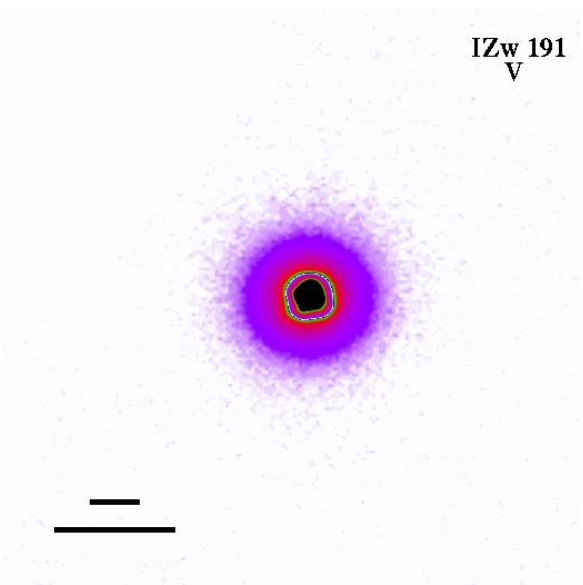
IZw 191
V

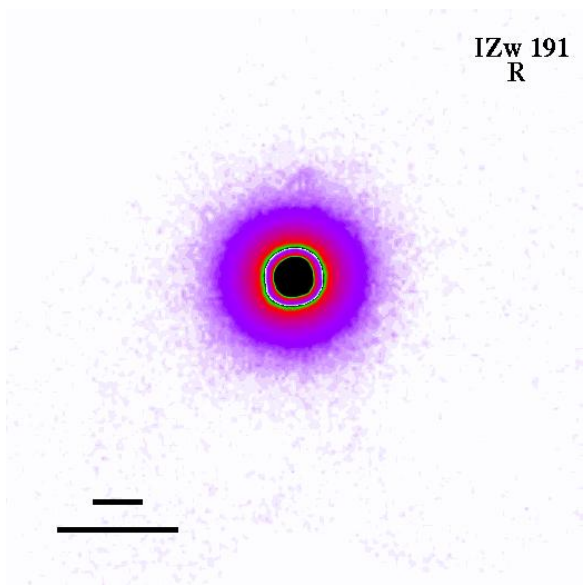
IZw 191
R

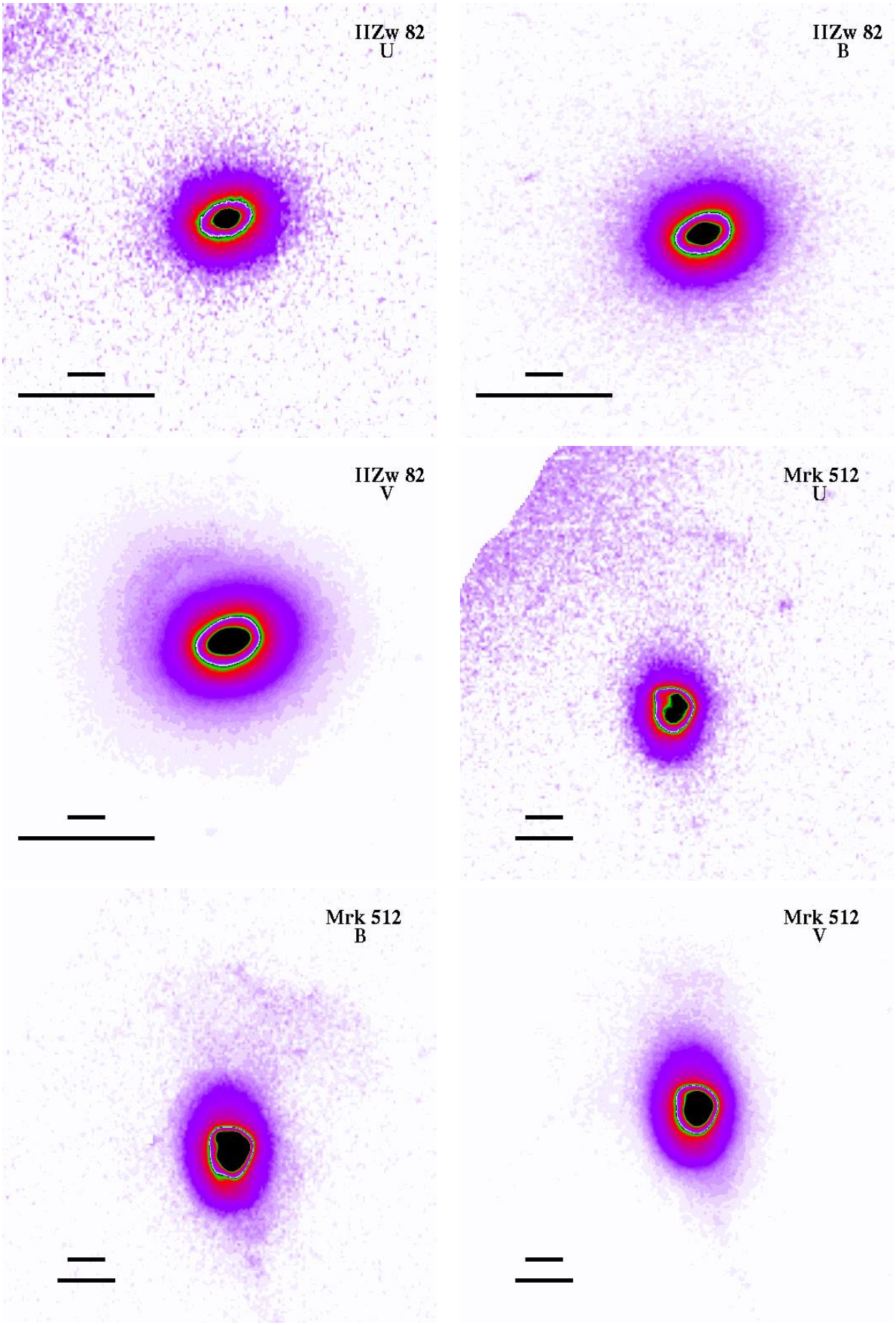
IIZw 82
U
IIZw 82
B
IIZw 82
V
Mrk 512
U
Mrk 512
B
Mrk 512
V

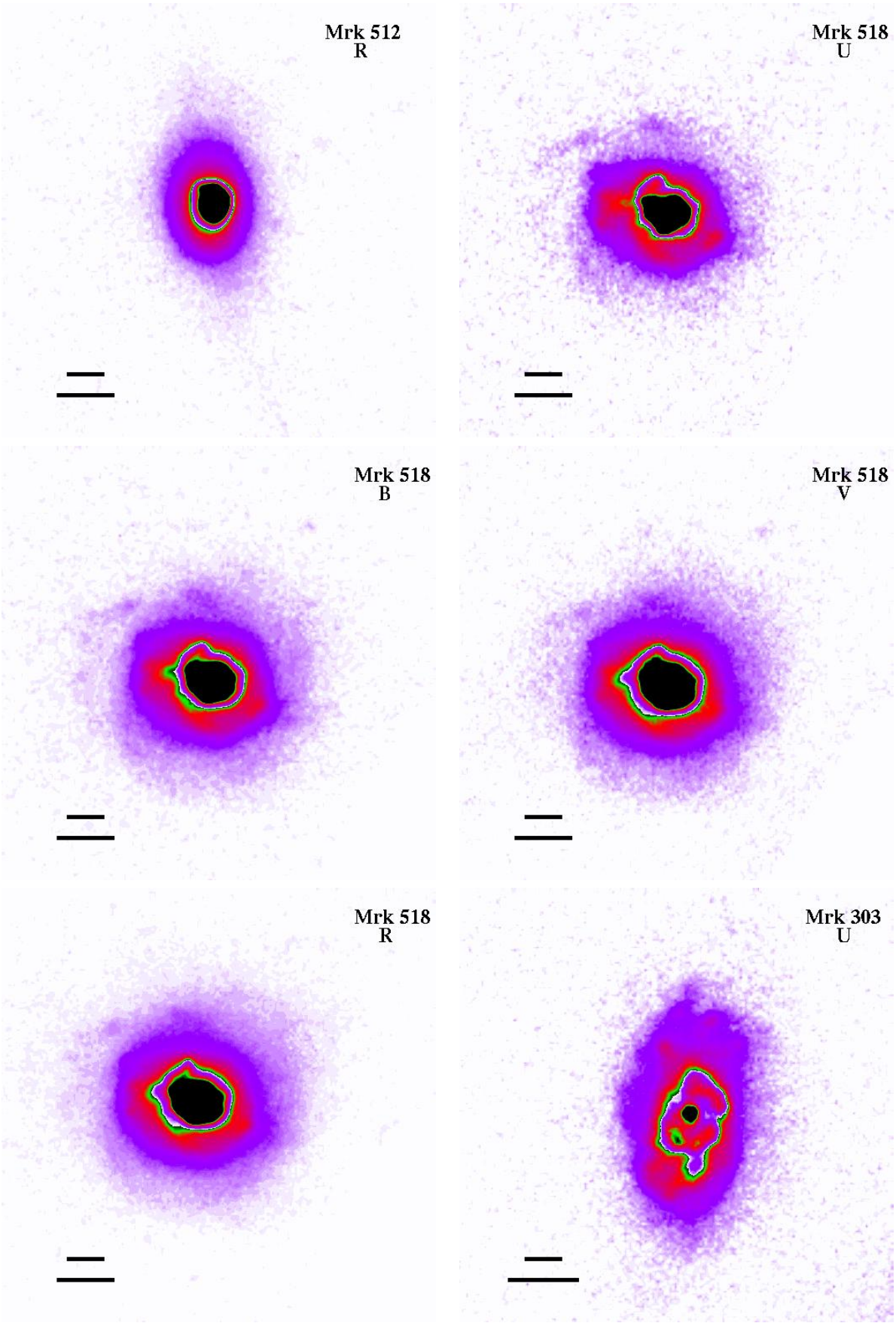
Mrk 512
R
Mrk 518
U
Mrk 518
B
Mrk 518
V
Mrk 518
R
Mrk 303
U

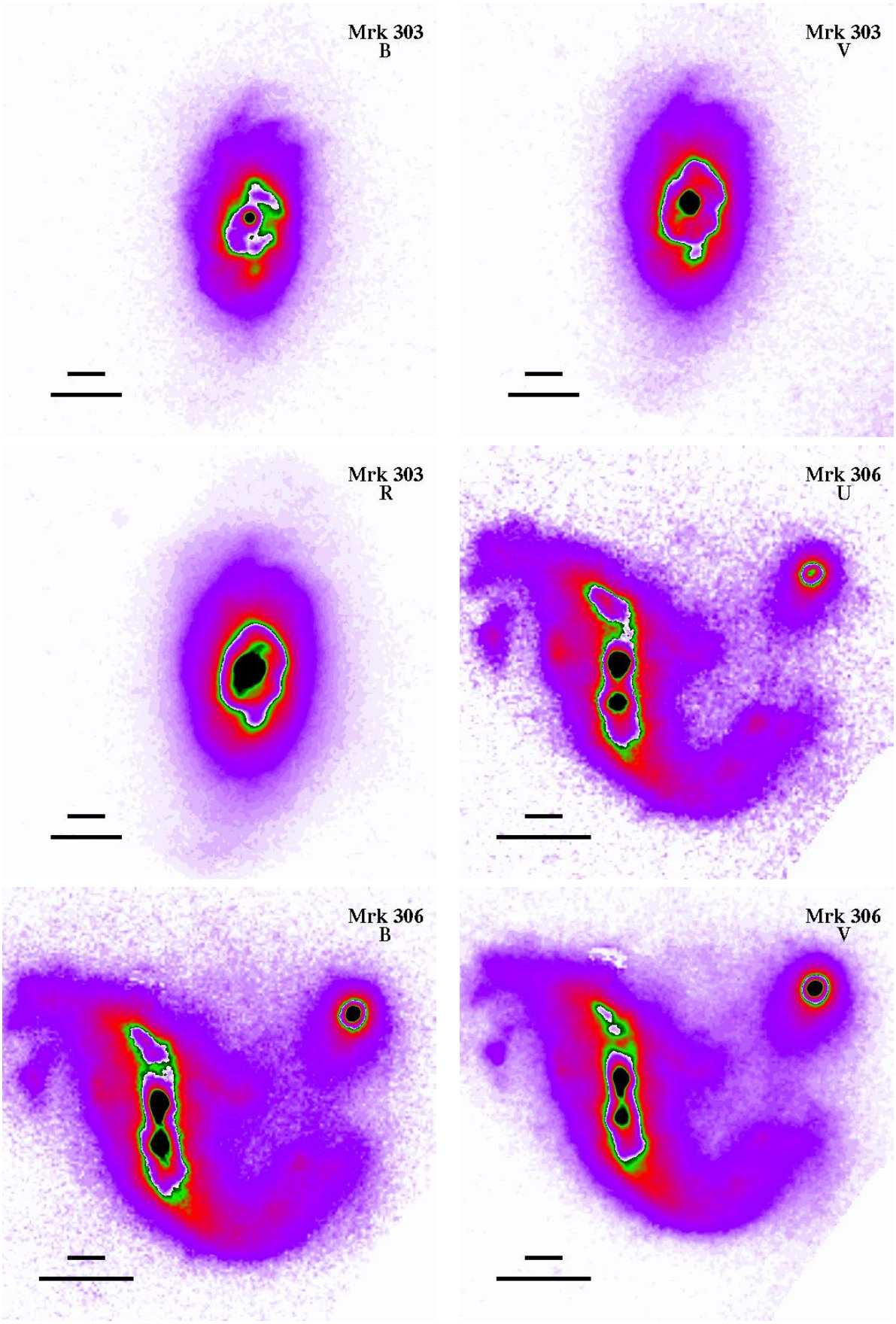
Mrk 303
B
Mrk 303
V
Mrk 303
R
Mrk 306
U
Mrk 306
B
Mrk 306
V

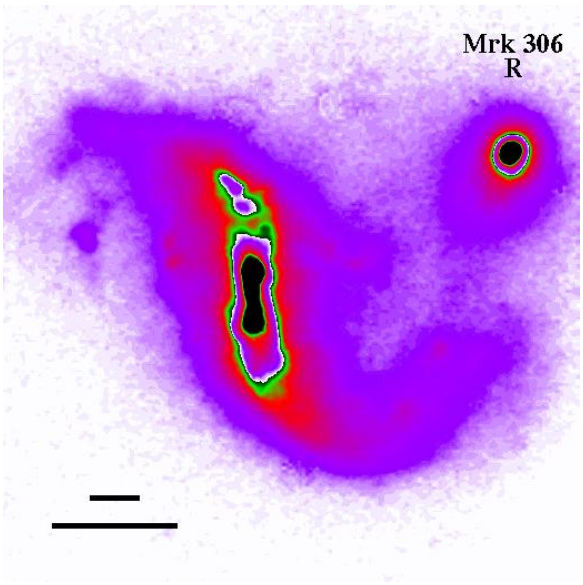
Mrk 306
R

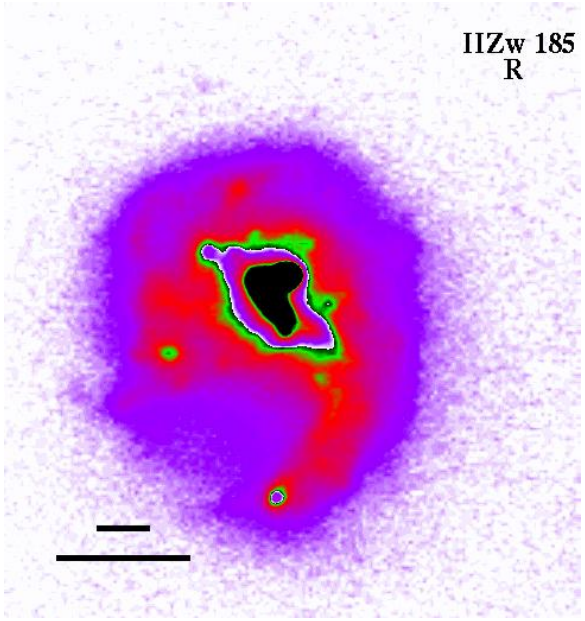
IIZw 185
R

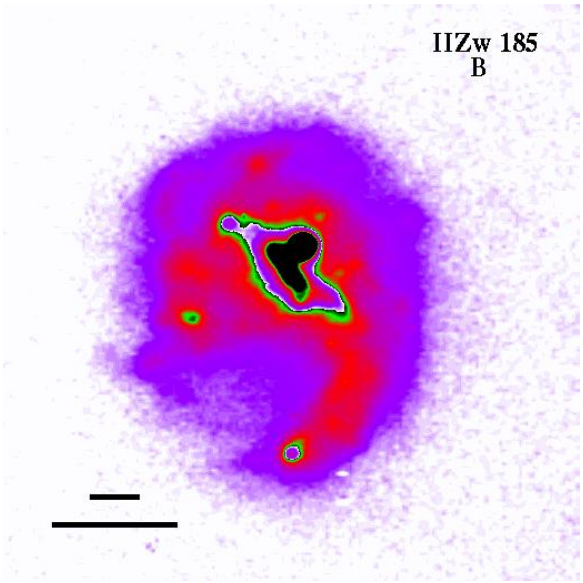
IIZw 185
B

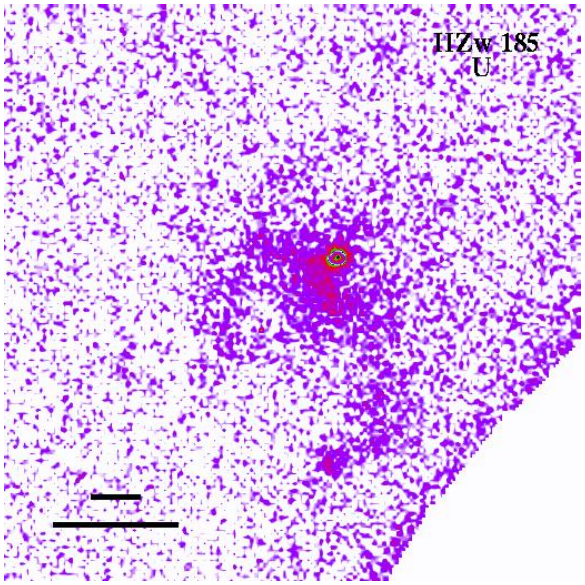
IIZw 185
U

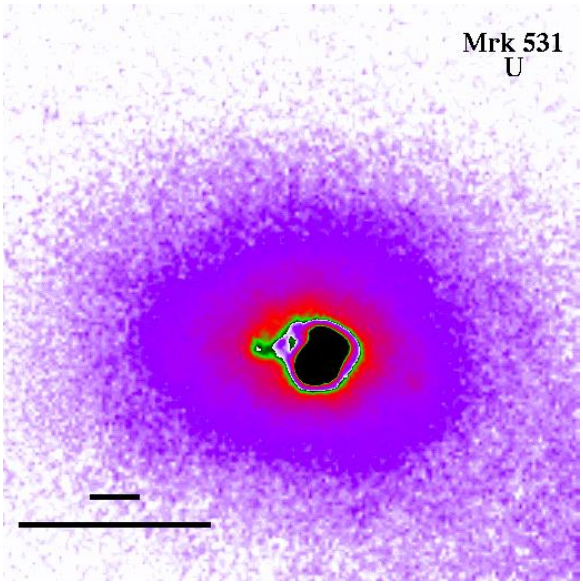
Mrk 531
U

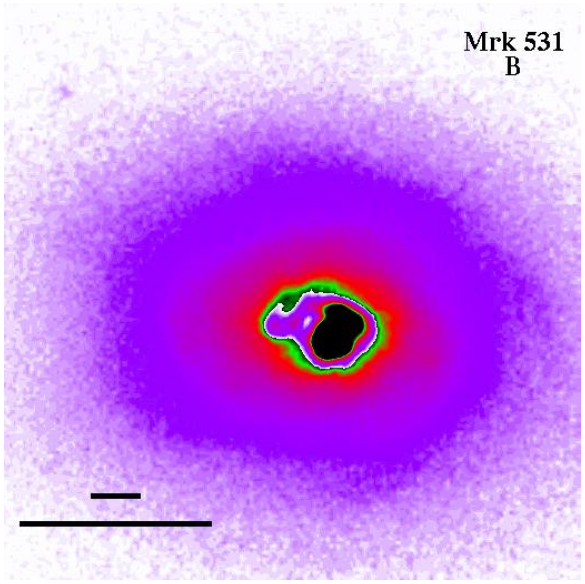
Mrk 531
B

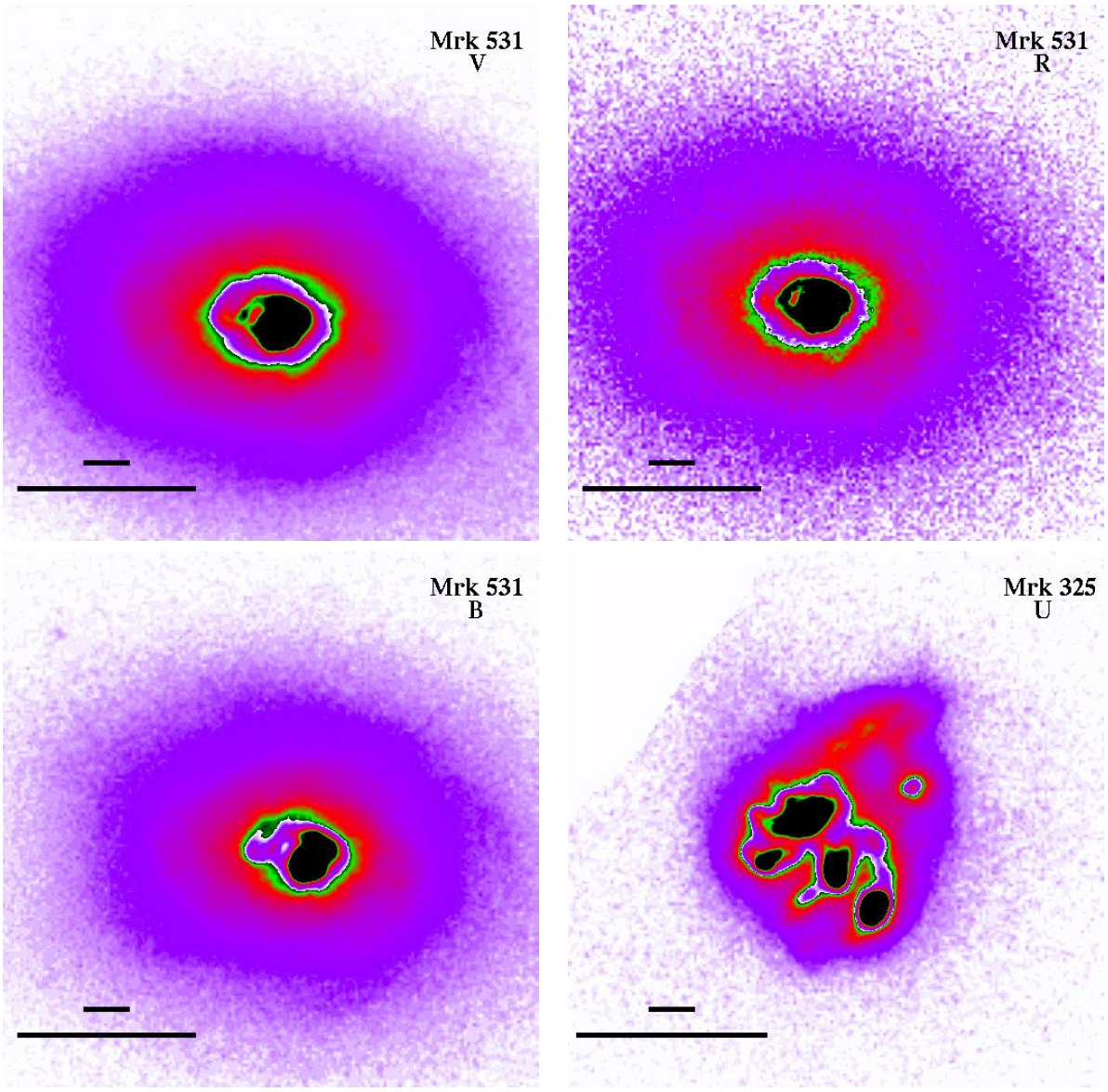
Mrk 531
V
Mrk 531
R
Mrk 531
B
Mrk 325
U

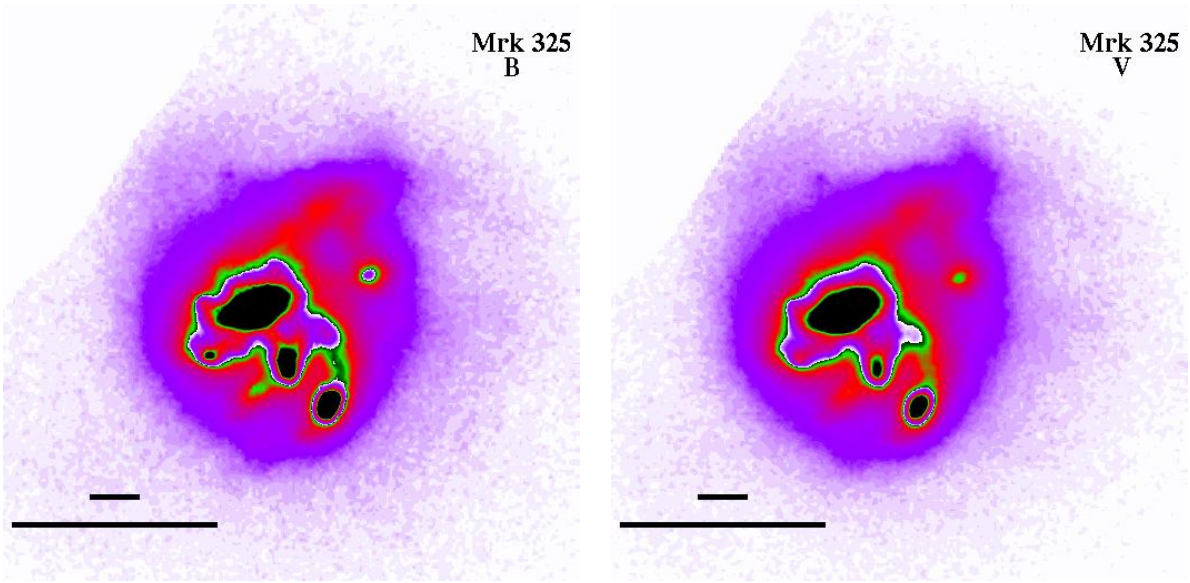

Figure 2.1: Optical-band (UBVRI) images for the McDonald sample: 1×1 arminute images with the top scale bar showing 5 arcseconds, and the bottom showing a physical scale of 5 kpc at the adopted distance (see Table 2.1). Darker to lighter colors (black, green, red, purple, white) show higher to lower intensity. The color table is wrapped once to show more detail in the galaxy. The images themselves are not calibrated. North is up, east is to the left. Images have been Gaussian smoothed, although some images show more noise than others because they were taken on less photometric nights, or at a higher airmass. Our images were taken under good seeing conditions, averaging in the range of $1.0''$ - $1.5''$. We used no images with a seeing greater than $2.0''$.

2.4 Light and Color Distributions

2.4.1 Derivation of the Brightness Profiles

Light distribution and color are powerful tools for the study and characterization of stellar populations of different structural components. The variation of optical light with radius is quantified with the use of surface brightness profiles (SBPs) and growth curves (GCs). To make the SBPs and GCs, a set of apertures were applied to the reference images. Apertures are placed around the core of a galaxy, found by changing the image contrast and zooming until only a pin-point of the core is visible on screen. The core is selected and the coordinates stored. In multi-galaxy systems a distinct core was not always visible. In these cases I would pick the galaxy under study and select its core. If the system was too complex, I simply could not select a core for aperture placement, and therefore could not make detailed light profiles. However, I was always at least able to place an aperture around the entire system in order to later calculate a magnitude from the flux within the entire object. Details of that process are described later. The apertures were placed more densely near the core of galaxies where the luminosity decline is more rapid. Once the center of the galaxy had been identified a 2 arcsecond rule was used. The innermost aperture could not be any larger than 2 arcseconds (and the 2 arcseconds is the diameter, so the radius, or semi-major axis, would be 1 arcsecond), but the annular apertures larger than that central one could be separated by as small of a distance as 2 pixels in

Table 2.4. Morphological Classification of the Optical Sample

Name	Morphology	Name	Morphology	Name	Morphology	Name	Morphology
(1)	(2)	(3)	(4)	(5)	(6)	(7)	(8)
Mrk 342	nE	Mrk 531	iE	Haro 1	iI	Mrk 492	nE
Haro 15	iI	Mrk 154	iE	Mrk 385	nE	Mrk 297	iI
Mrk 360	iE	Mrk 171	iI	Mrk 1211	iI	Mrk 300	iI
Mrk 364	nE	Mrk 181	iE	Mrk 390	iI	Mrk 697	nE
Mrk 366	nE	Haro 34	iE	Mrk 18	nE	Mrk 499	nE
Mrk 367	iE	Mrk 54	iI	Mrk 402	nE	I Zw 191	nE
Mrk 589	nE	Mrk 238	iI	II Zw 44	iE	II Zw 82	nE
Mrk 1184	iI	Mrk 248	iI	Mrk 139	iI	Mrk 512	iE
Mrk 1404	iE	Mrk 255	iI	Mrk 144	iE	Mrk 518	iE
Mrk 1079	iE	Mrk 271	iI	Mrk 33	nE	Mrk 303	iE
Mrk 1094	iI	Haro 42	iI	Mrk 148	iI	Mrk 306	iI
Mrk 8	iI	I Zw 101	iE	Haro 25	nE	II Zw 185	iI
Mrk 325	iE	...	...	...	...		

Cols. (1, 3, 5, & 7) Primary galaxy name. Cols. (2, 4, 6, & 8) The morphological classification of the optical sample using the Loose & Thuan (1985) schema, discussed at the start of section 2.3.

the brightest regions. The 2 arcsecond rule is due to 'seeing', or the blurring of images by the atmosphere. In the interior of the galaxies even small separations will provide sufficiently high flux. In the outermost diffuse regions, it is not helpful to have annuli that are much wider than about 4 arcseconds. Any larger and the resolution is just too low to really be useful to light profiles. The ellipticity was decided by us because the first aperture is hand drawn on by the selection of how long the major and minor axes should extend from the core of the galaxy. Here ellipticity is defined as $e = 1-[\frac{b}{a}]$ for an ellipse with semi-major and semi-minor aces of lengths a and b respectively. Once the apertures were created for the reference image, they were easily transferred to the other images since we had already aligned. Once the apertures were placed, the flux inside each consecutive aperture was calculated.

Next, a program was run that would correct for the area of the aperture, or normalize by the area, to give flux-per-area. The output files from this program had a separate file for each galaxy listing the values for a SBP and GC separately for each band. In the growth curve files, for each successive radius, the total surface brightness up to that point is listed. For the surface brightness profile files, for each successive radius, the surface brightness between the newest aperture and previous one is listed. These output files had the previously calculated calibration values applied to them, along with extinction. Internal extinction was not corrected for, but Galactic extinction was taken into account. Data from Burstein & Heiles (1984) was used to correct for the Galactic extension; they tabulated the extinction in the B

band, [$A_B = 4E(B - V)$]. Figure 2.2 shows all the SBPs, GCs, and color profiles for the galaxies in our optical sample where aperture placement was possible. Surface brightness has been plotted versus both the radius r and $r^{1/4}$ to allow a comparison with the most popular standard laws (exponential disk and de Vaucouleurs). Each galaxy gets its own page except the few that had irregular enough morphologies that a SBP was not possible; those galaxies have their GCs grouped together at the end of the figure.

Table 2.5 shows the ellipticity, position angle, and method of calibration for each galaxy in the reference filter. The position angles were originally measured northward from the west axis, but traditionally angles are measured eastward from the north axis, so we changed over to state our position angles in the traditional format. Each image was also aligned with an image from skyview to find the rotation angle to put true north in the image at the actual north position. Skyview is a virtual observatory which dynamically generates images of the sky in different wavelength regimes from a static image database. Both of the angle corrections discussed above have been corrected for in Table 2.5. The names of the galaxies have been changed to incorporate if a neighbor or interaction feature has been included in the apertures for a galaxy.

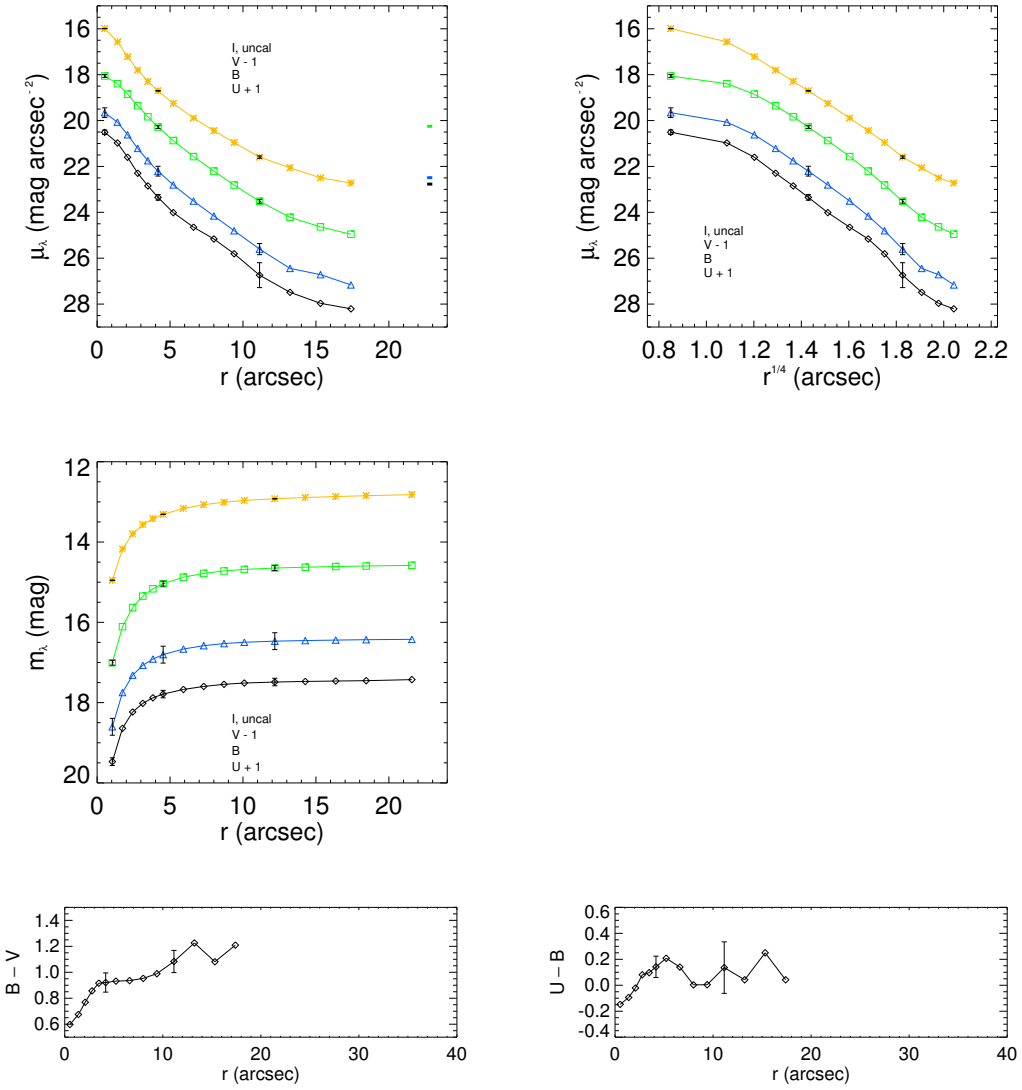

Figure 2.2: Surface brightness profiles, growth curves, and color profiles for a subset of the optical sample. Growth curves are the integrated brightness, expressed in magnitudes, as a function of radius. Surface brightness profiles measure the observed brightness per unit area in fixed radial annuli and are plotted versus radius and radius$^{1/4}$. Color profiles represent the difference, in magnitudes, between the surface brightness in two bands, as a function of radius. The U, B, V, R, and I bands are black diamonds, blue triangles, green squares, red crosses, and yellow asterisks, respectively. The offsets shown in the key are to exaggerate the space between the different bands so it will be easier to view. An uncal in the key is because that certain filter lacked data that could be calibrated. The error bars are calculated as explained in section 2.6. The SBPs and color profiles are truncated at a radius where the noise became as dominant of a factor as the galaxy light. The surface brightness profiles have color coded tick marks on the right margin which show the level of sky background that was removed. A handful of galaxies only have growth curves because the morphology was too asymmetrical to produce a surface brightness profile.
(1) Mrk 342

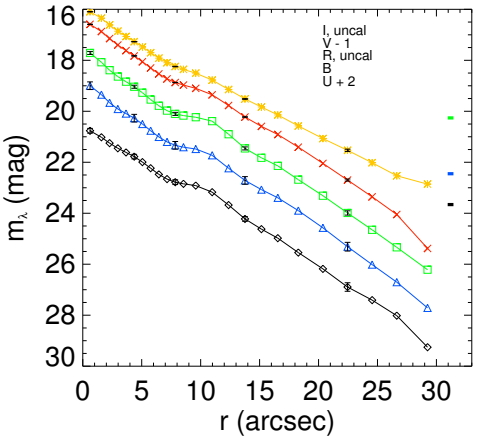
I, uncal
V - 1
R, uncal
B
U + 2
m$_\lambda$ (mag)
r (arcsec)

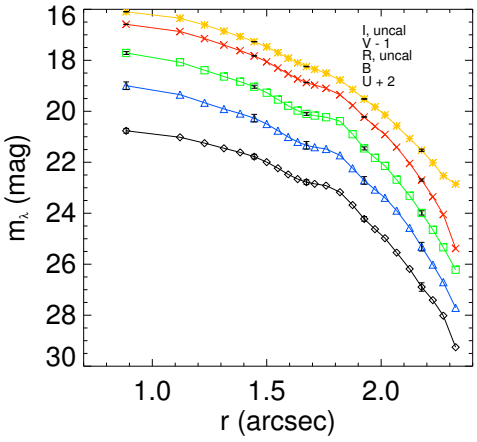
I, uncal
V - 1
R, uncal
B
U + 2
m$_\lambda$ (mag)
r (arcsec)

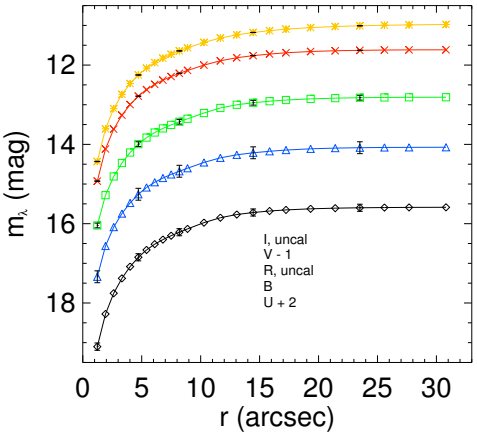
I, uncal
V - 1
R, uncal
B
U + 2
m$_\lambda$ (mag)
r (arcsec)

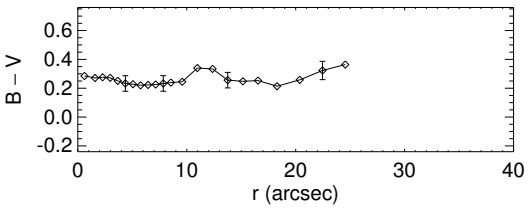
B – V
r (arcsec)

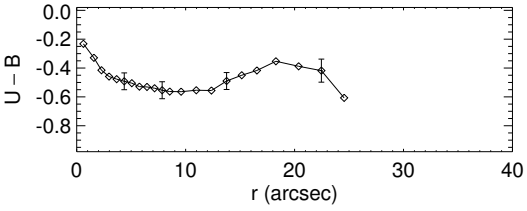
U – B
r (arcsec)

(2) Haro 15

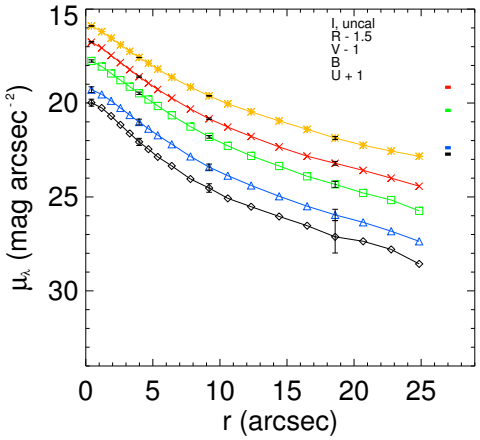
I, uncal
R - 1.5
V - 1
B
U + 1
μλ (mag arcsec-2)
r (arcsec)

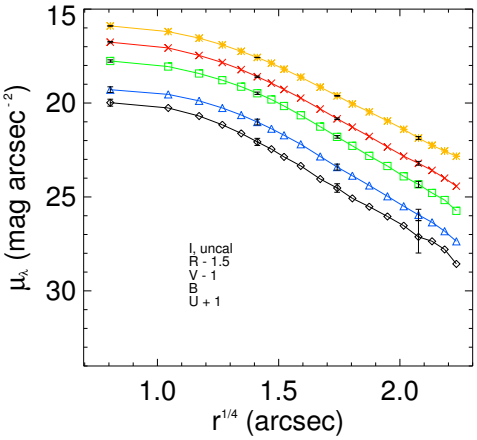
I, uncal
R - 1.5
V - 1
B
U + 1
μλ (mag arcsec-2)
r1/4 (arcsec)

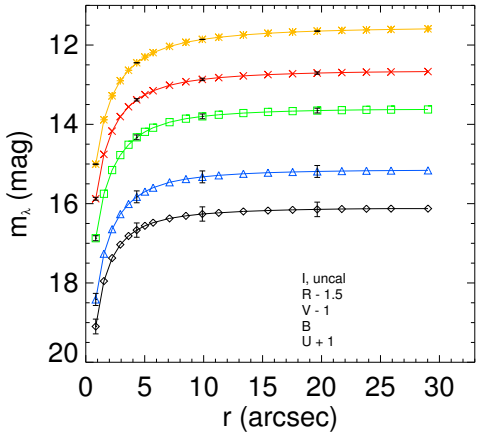
I, uncal
R - 1.5
V - 1
B
U + 1
mλ (mag)
r (arcsec)

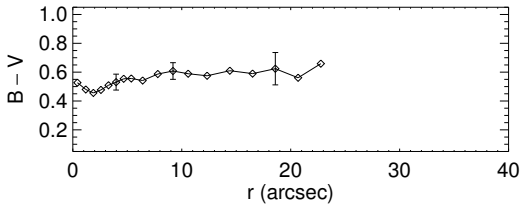
B – V
r (arcsec)

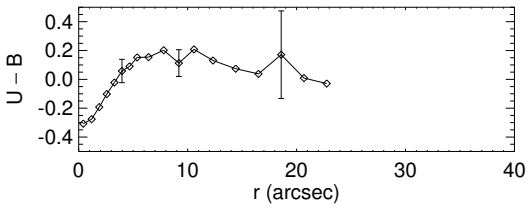
U – B
r (arcsec)

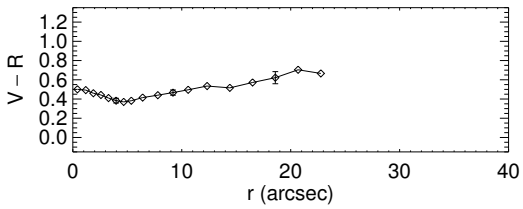
V – R
r (arcsec)

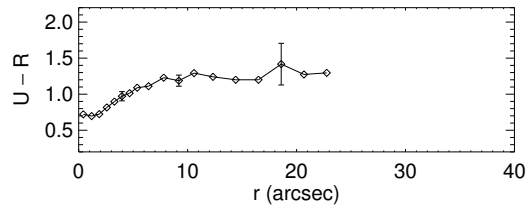
U – R
r (arcsec)

(3) Mrk 364

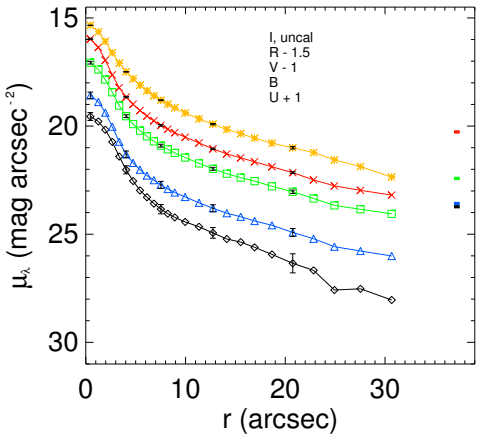
I, uncal
R - 1.5
V - 1
B
U + 1
μλ (mag arcsec-2)
r (arcsec)

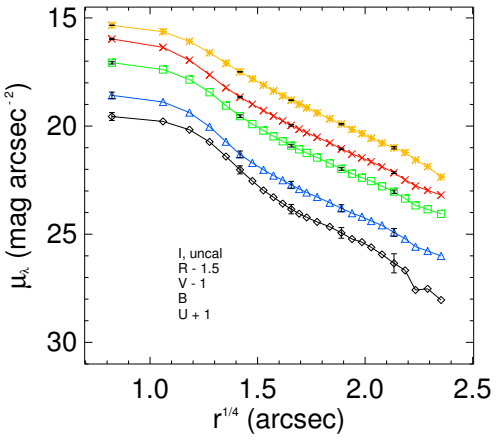
I, uncal
R - 1.5
V - 1
B
U + 1
μλ (mag arcsec-2)
r1/4 (arcsec)

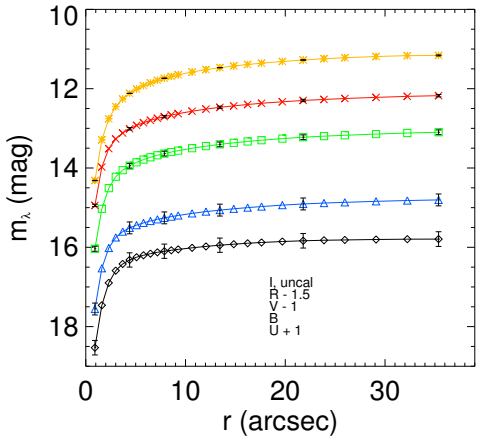
I, uncal
R - 1.5
V - 1
B
U + 1
mλ (mag)
r (arcsec)

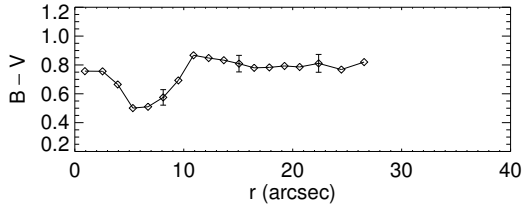
B – V
r (arcsec)

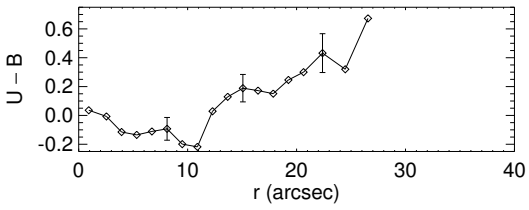
U – B
r (arcsec)

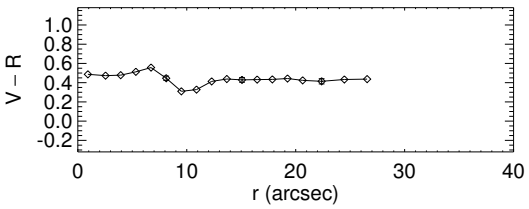
V – R
r (arcsec)

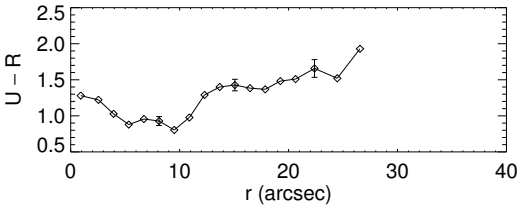
U – R
r (arcsec)

(4) Mrk 366

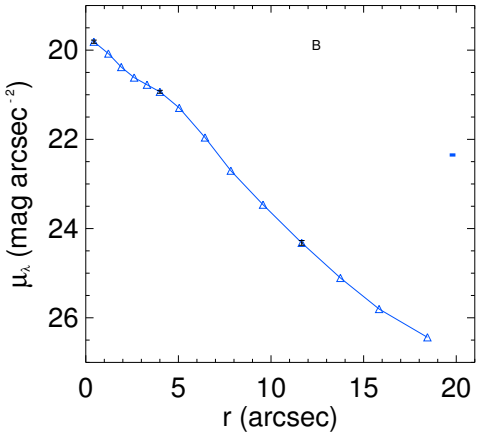
B
μλ (mag arcsec-2)
r (arcsec)

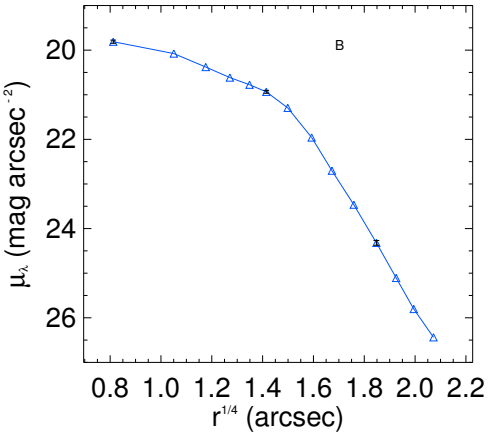
B
μλ (mag arcsec-2)
r1/4 (arcsec)

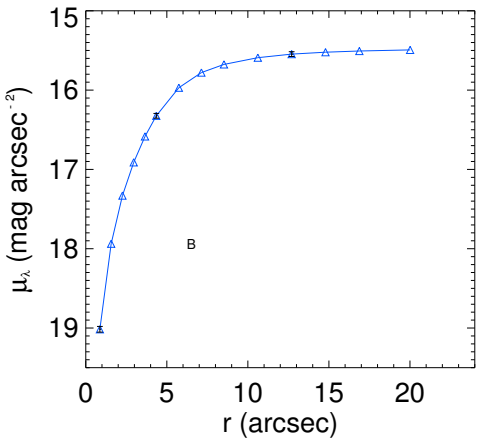
B
μλ (mag arcsec-2)
r (arcsec)

(5) Mrk 367

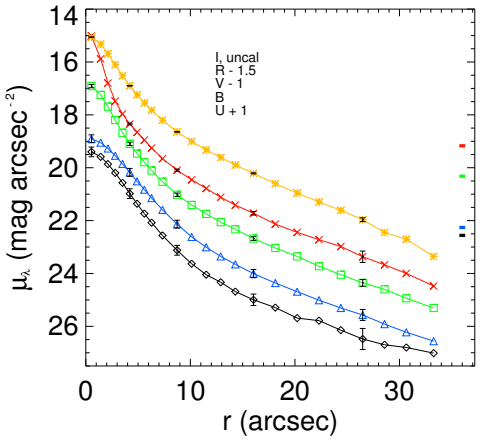
I, uncal
R - 1.5
V - 1
B
U + 1
μλ (mag arcsec-2)
r (arcsec)

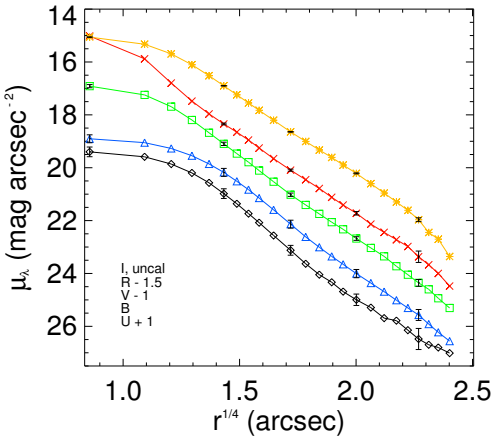
I, uncal
R - 1.5
V - 1
B
U + 1
μλ (mag arcsec-2)
r1/4 (arcsec)

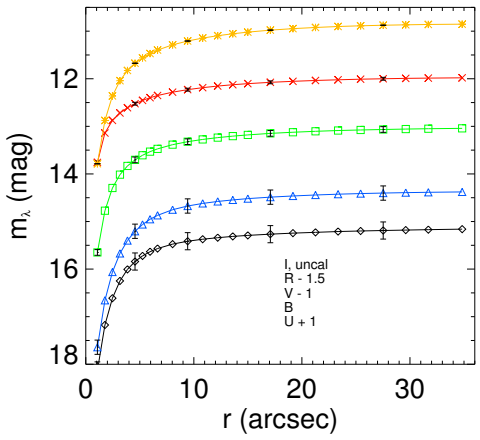
I, uncal
R - 1.5
V - 1
B
U + 1
mλ (mag)
r (arcsec)

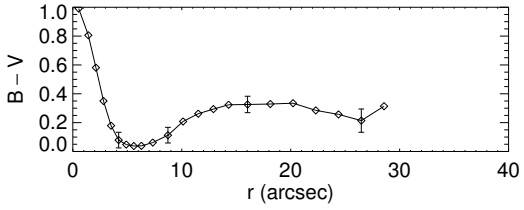
B – V
r (arcsec)

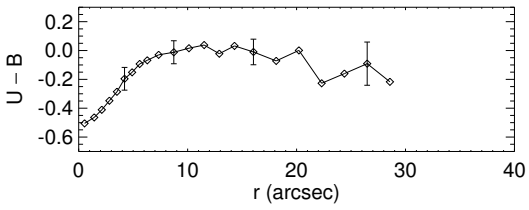
U – B
r (arcsec)

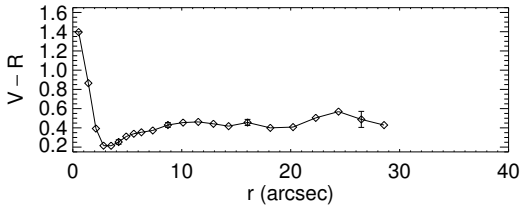
V – R
r (arcsec)

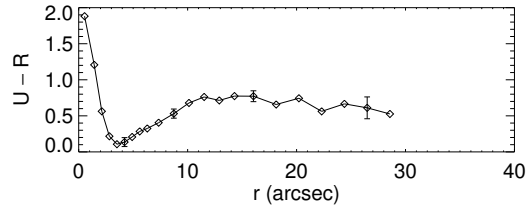
U – R
r (arcsec)

(6) Mrk 589

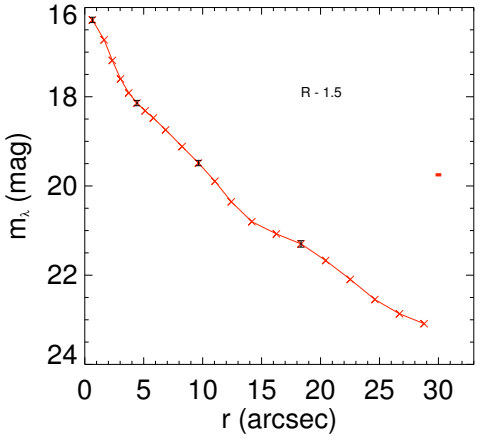
16
18
20
22
24
m_λ (mag)
R - 1.5
0
5
10
15
20
25
30
r (arcsec)

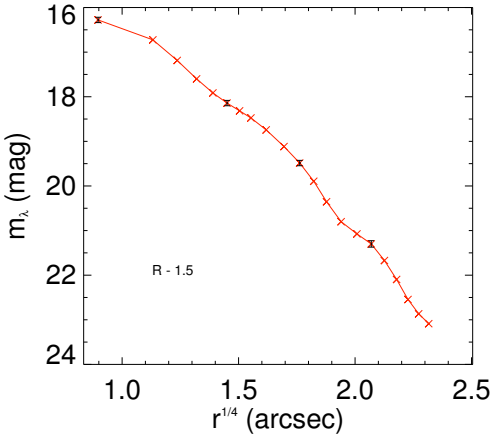
16
18
20
22
24
m_λ (mag)
R - 1.5
1.0
1.5
2.0
2.5
$r^{1/4}$ (arcsec)

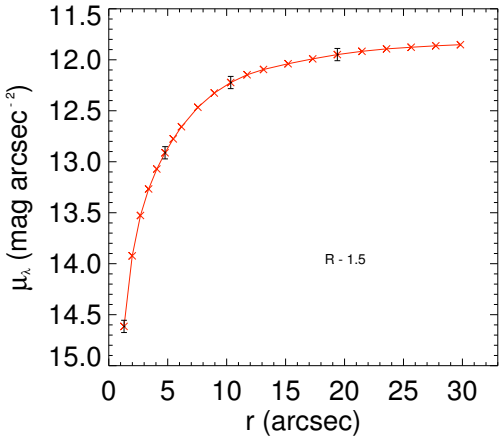
11.5
12.0
12.5
13.0
13.5
14.0
14.5
15.0
μ_λ (mag arcsec^{-2})
R - 1.5
0
5
10
15
20
25
30
r (arcsec)

(7) Mrk 1184

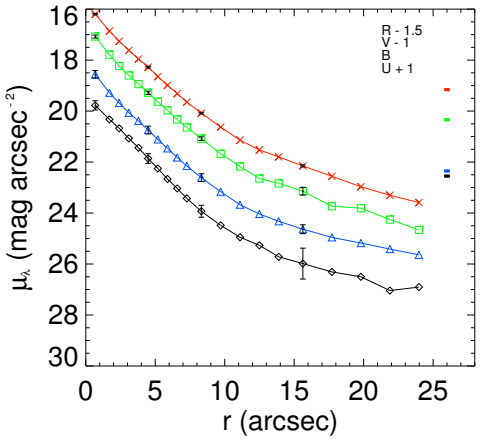
R - 1.5
V - 1
B
U + 1
μλ (mag arcsec-2)
r (arcsec)

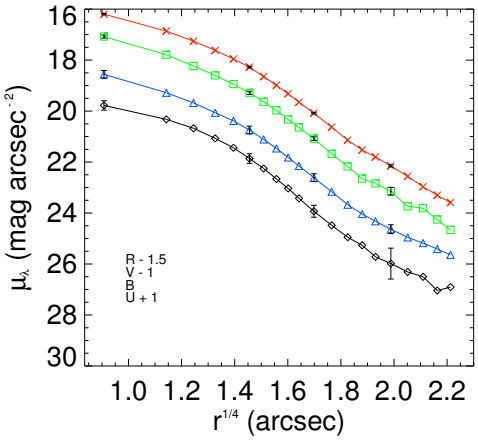
R - 1.5
V - 1
B
U + 1
μλ (mag arcsec-2)
r1/4 (arcsec)

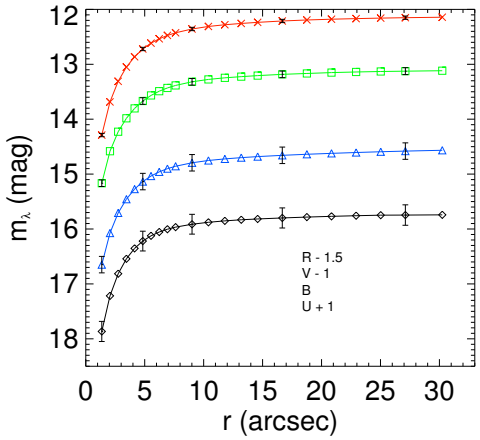
R - 1.5
V - 1
B
U + 1
mλ (mag)
r (arcsec)

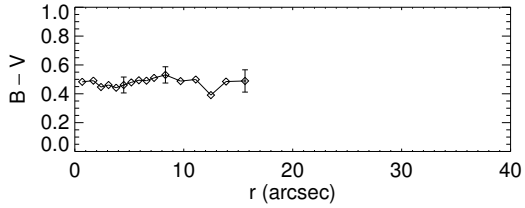
B – V
r (arcsec)

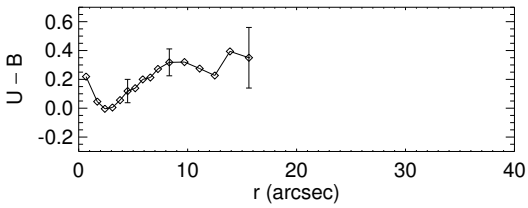
U – B
r (arcsec)

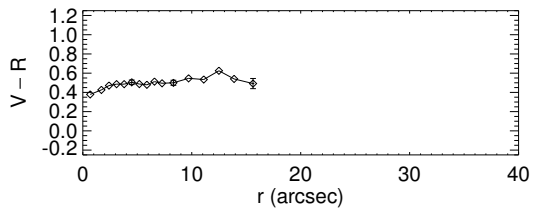
V – R
r (arcsec)

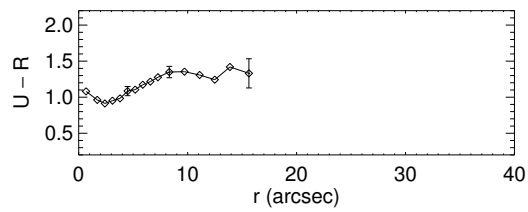
U – R
r (arcsec)

(8) Mrk 1404

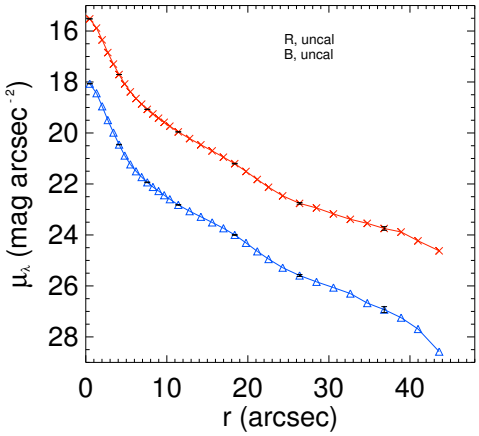
R, uncal
B, uncal
μλ (mag arcsec-2)
r (arcsec)

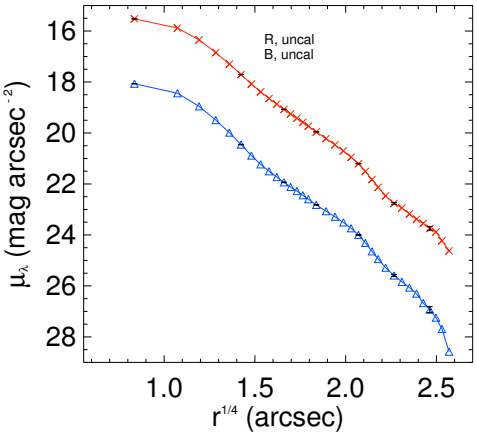
R, uncal
B, uncal
μλ (mag arcsec-2)
r1/4 (arcsec)

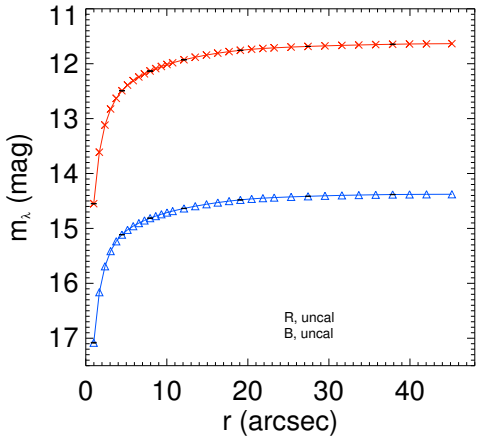
R, uncal
B, uncal
mλ (mag)
r (arcsec)

(9) Mrk 1079

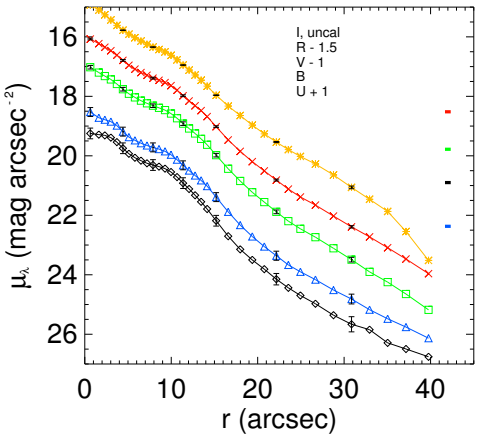
I, uncal
R - 1.5
V - 1
B
U + 1
μλ (mag arcsec-2)
r (arcsec)

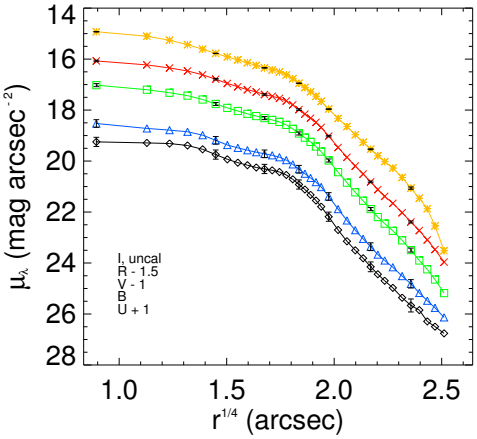
I, uncal
R - 1.5
V - 1
B
U + 1
μλ (mag arcsec-2)
r1/4 (arcsec)

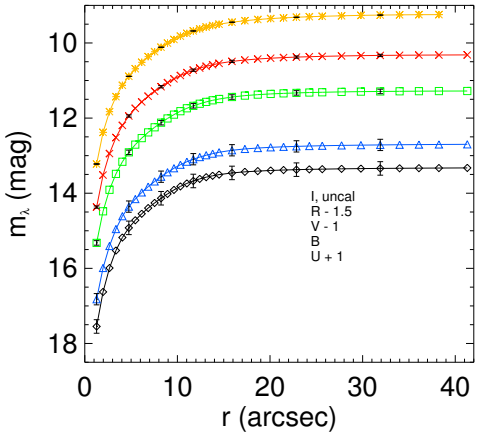
I, uncal
R - 1.5
V - 1
B
U + 1
mλ (mag)
r (arcsec)

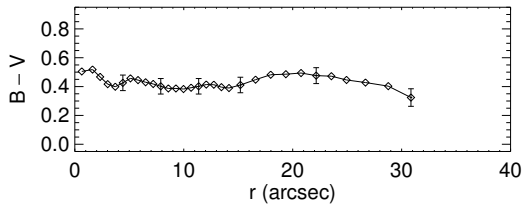
B – V
r (arcsec)

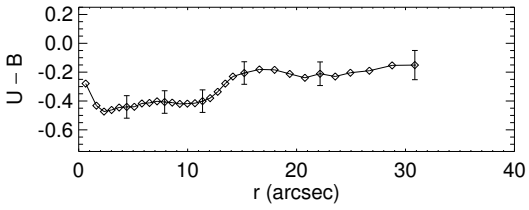
U – B
r (arcsec)

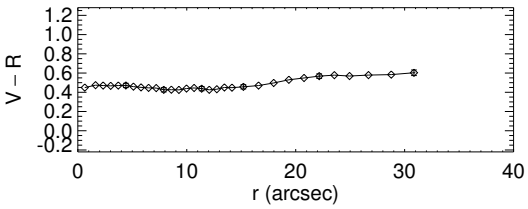
V – R
r (arcsec)

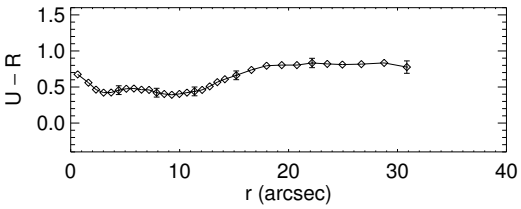
U – R
r (arcsec)

(10) Haro 1

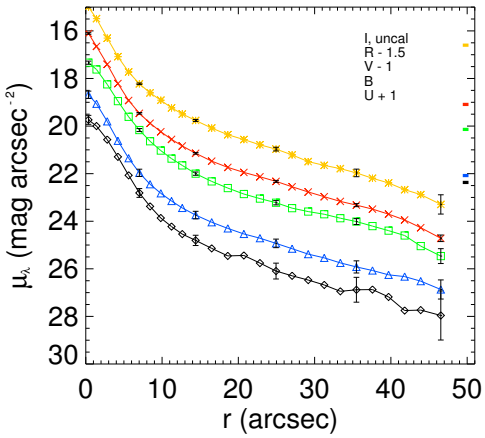
I, uncal
R - 1.5
V - 1
B
U + 1
μλ (mag arcsec-2)
r (arcsec)

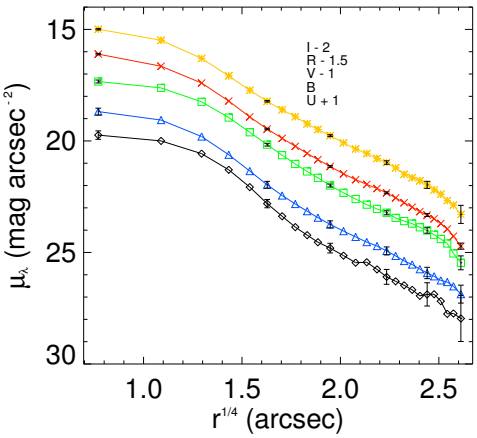
I - 2
R - 1.5
V - 1
B
U + 1
μλ (mag arcsec-2)
r1/4 (arcsec)

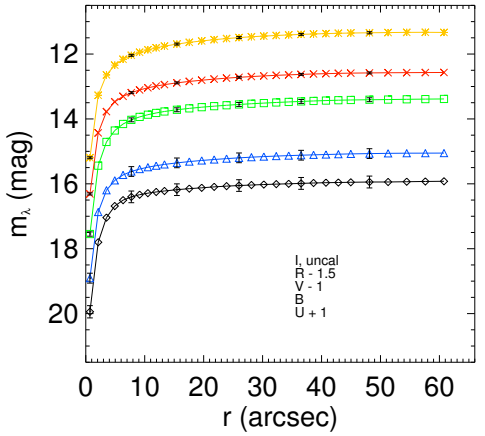
I, uncal
R - 1.5
V - 1
B
U + 1
mλ (mag)
r (arcsec)

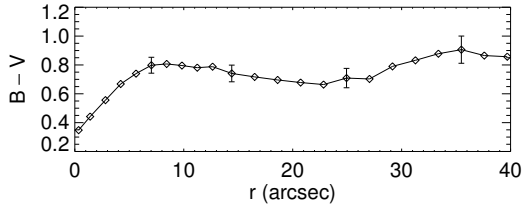
B – V
r (arcsec)

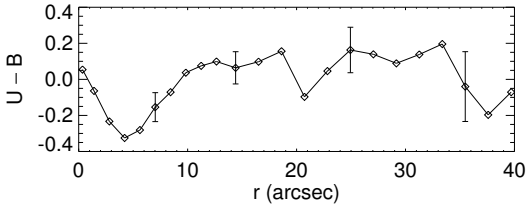
U – B
r (arcsec)

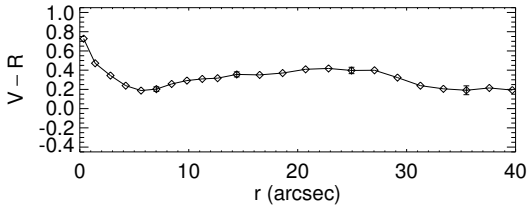
V – R
r (arcsec)

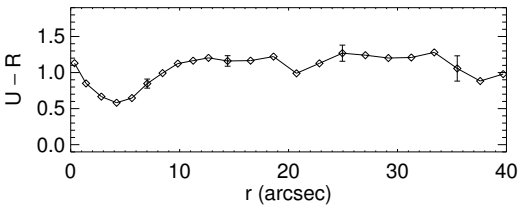
U – R
r (arcsec)

(11) Mrk 385

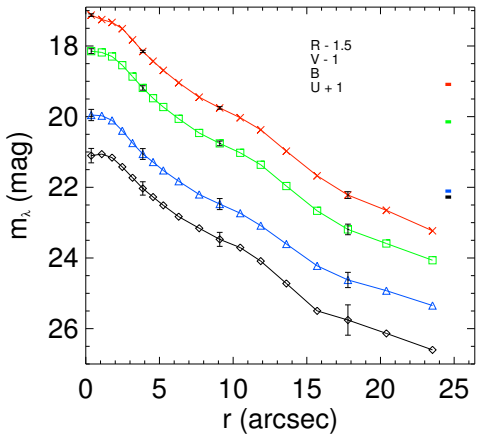
R - 1.5
V - 1
B
U + 1
m$_\lambda$ (mag)
r (arcsec)

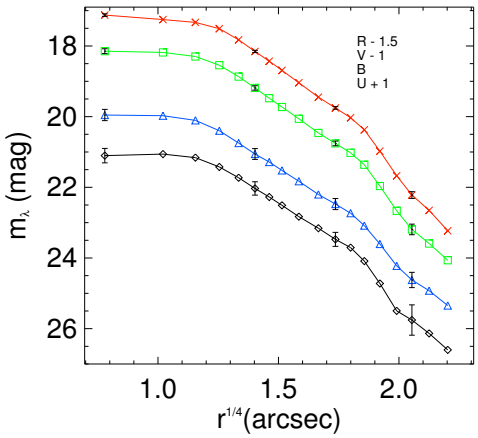
R - 1.5
V - 1
B
U + 1
m$_\lambda$ (mag)
r$^{1/4}$(arcsec)

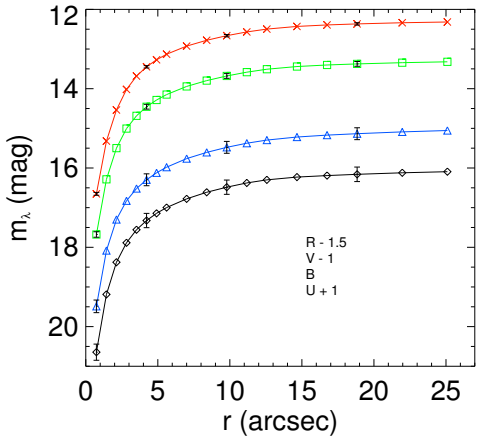
R - 1.5
V - 1
B
U + 1
m$_\lambda$ (mag)
r (arcsec)

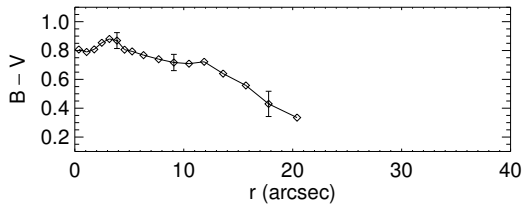
B – V
r (arcsec)

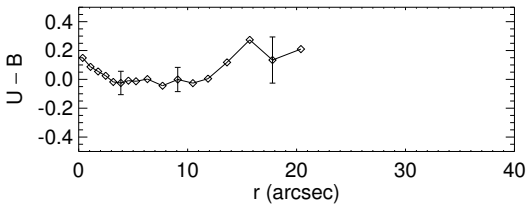
U – B
r (arcsec)

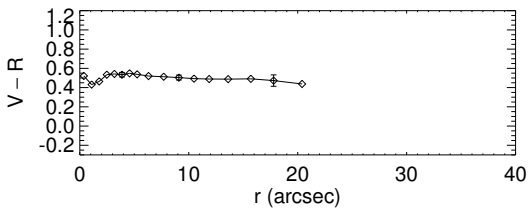
V – R
r (arcsec)

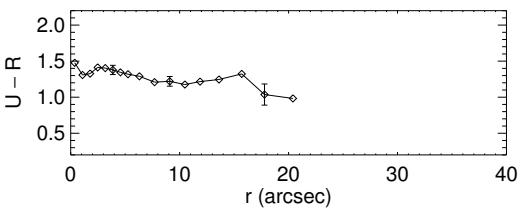
U – R
r (arcsec)

(12) Mrk 1211

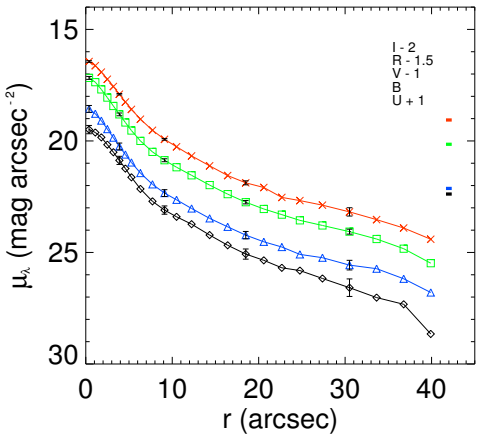
I - 2
R - 1.5
V - 1
B
U + 1
μλ (mag arcsec-2)
r (arcsec)

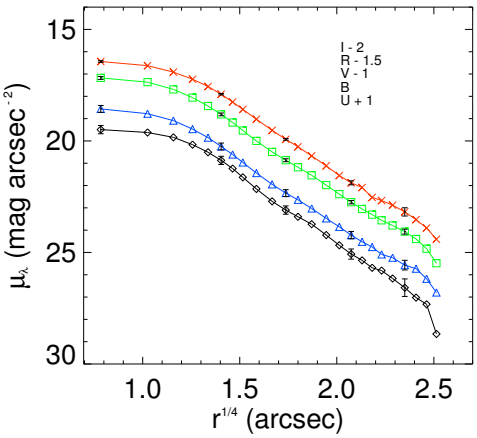
I - 2
R - 1.5
V - 1
B
U + 1
μλ (mag arcsec-2)
r1/4 (arcsec)

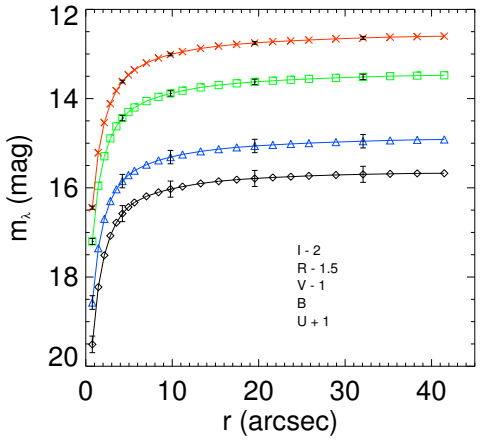
I - 2
R - 1.5
V - 1
B
U + 1
mλ (mag)
r (arcsec)

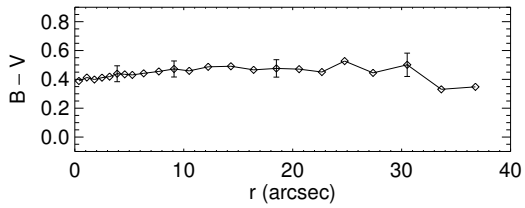
B – V
r (arcsec)

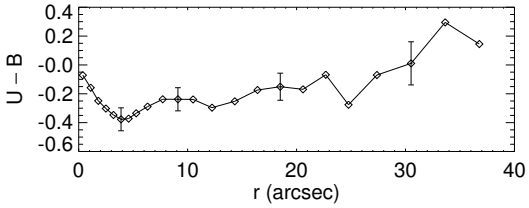
U – B
r (arcsec)

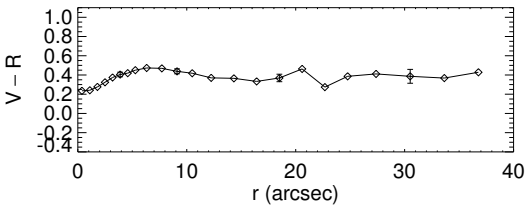
V – R
r (arcsec)

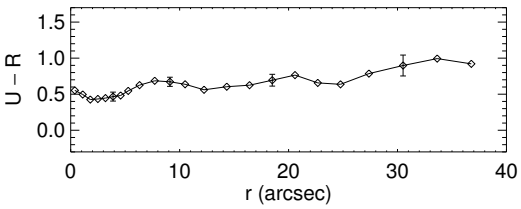
U – R
r (arcsec)

(13) Mrk 390

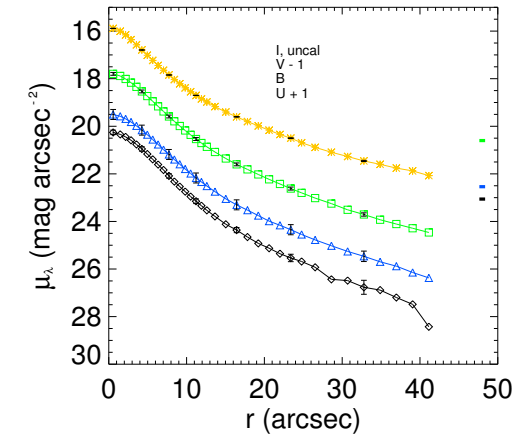
I, uncal
V - 1
B
U + 1
μλ (mag arcsec-2)
r (arcsec)

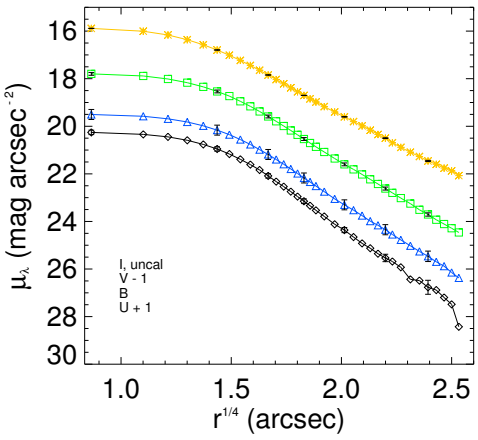
I, uncal
V - 1
B
U + 1
μλ (mag arcsec-2)
r1/4 (arcsec)

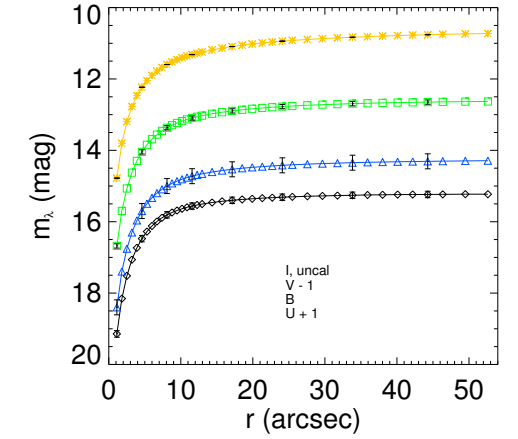
I, uncal
V - 1
B
U + 1
mλ (mag)
r (arcsec)

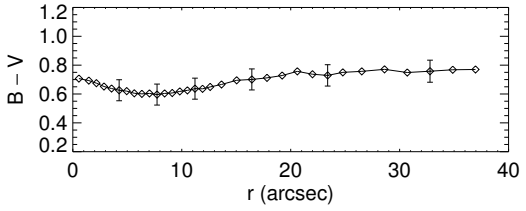
B – V
r (arcsec)

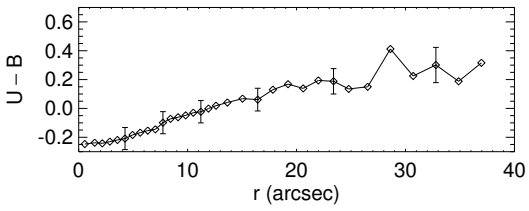
U – B
r (arcsec)

(14) Mrk 18

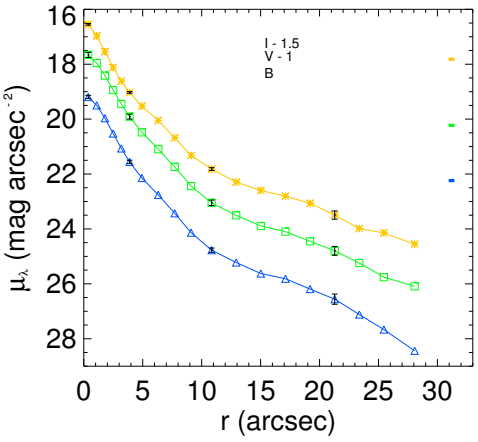
I - 1.5
V - 1
B
μλ (mag arcsec-2)
r (arcsec)

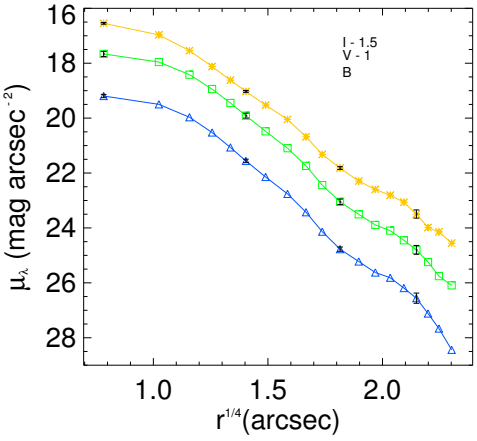
I - 1.5
V - 1
B
μλ (mag arcsec-2)
r1/4(arcsec)

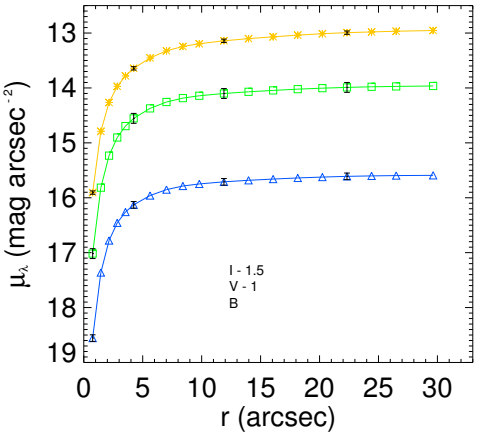
I - 1.5
V - 1
B
μλ (mag arcsec-2)
r (arcsec)

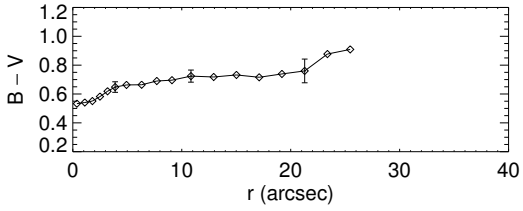
B – V
r (arcsec)

(15) Mrk 402

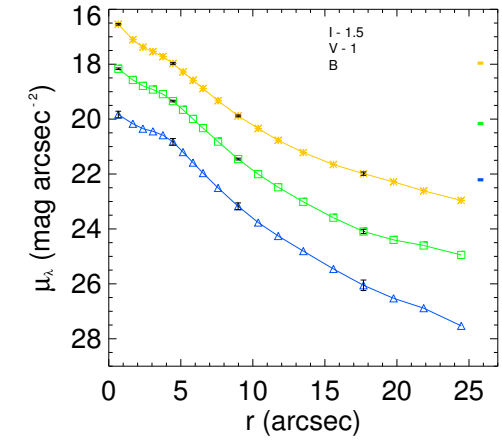
I - 1.5
V - 1
B
μλ (mag arcsec-2)
r (arcsec)

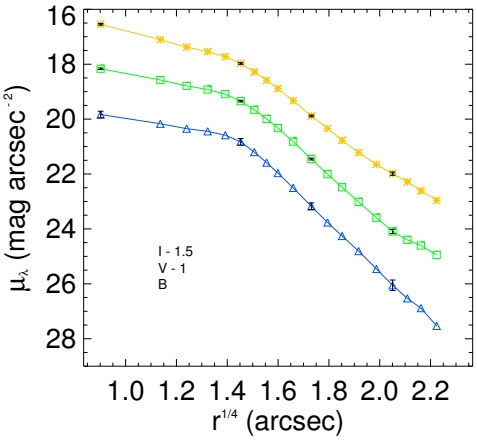
I - 1.5
V - 1
B
μλ (mag arcsec-2)
r1/4 (arcsec)

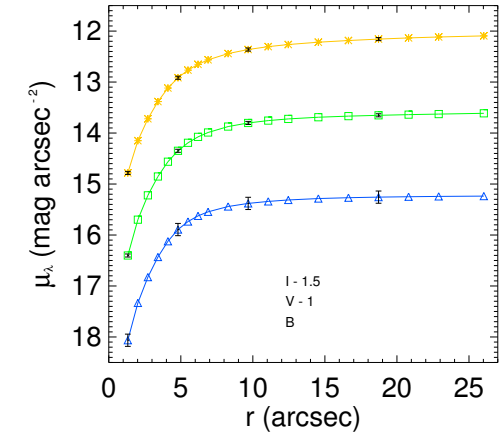
I - 1.5
V - 1
B
μλ (mag arcsec-2)
r (arcsec)

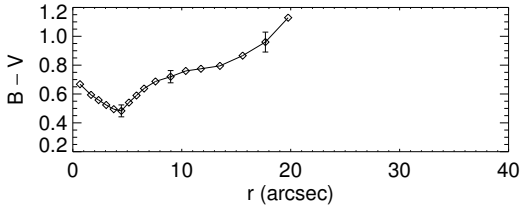
B – V
r (arcsec)

(16) IIZw 44

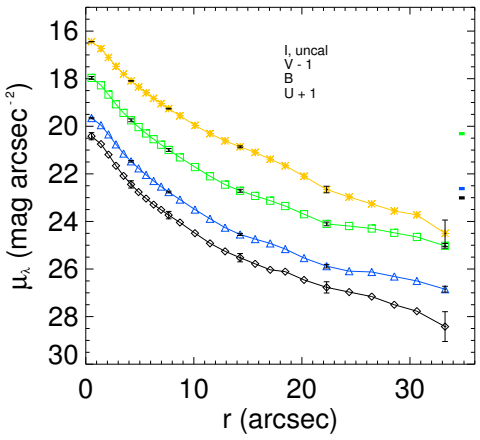
I, uncal
V - 1
B
U + 1
μλ (mag arcsec-2)
r (arcsec)

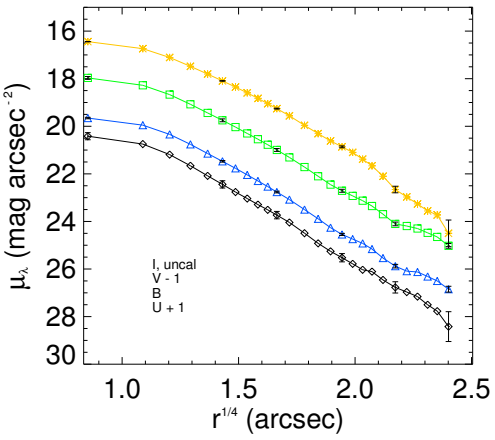
I, uncal
V - 1
B
U + 1
μλ (mag arcsec-2)
r1/4 (arcsec)

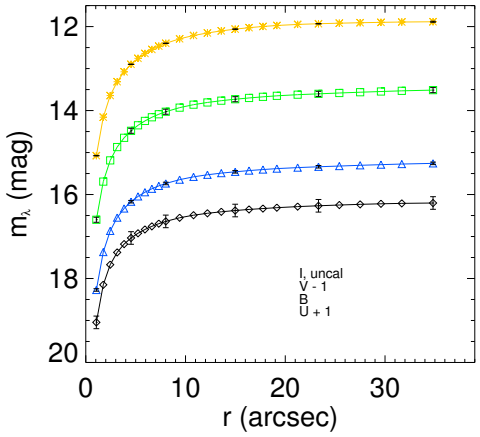
I, uncal
V - 1
B
U + 1
mλ (mag)
r (arcsec)

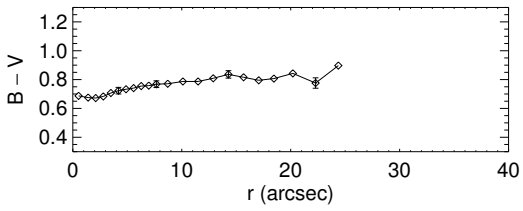
B – V
r (arcsec)

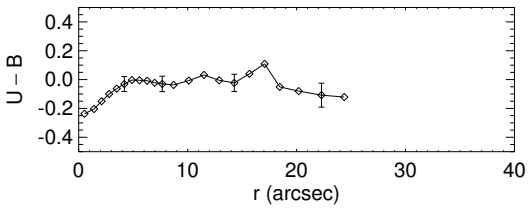
U – B
r (arcsec)

(17) Mrk 139

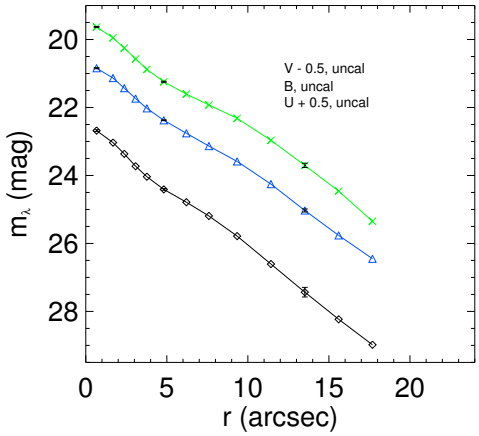
V - 0.5, uncal
B, uncal
U + 0.5, uncal
m$_\lambda$ (mag)
r (arcsec)

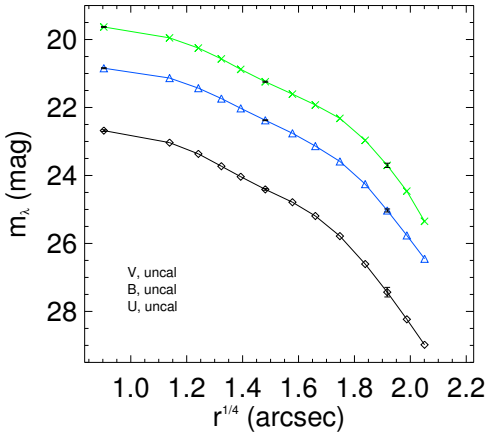
V, uncal
B, uncal
U, uncal
m$_\lambda$ (mag)
r$^{1/4}$ (arcsec)

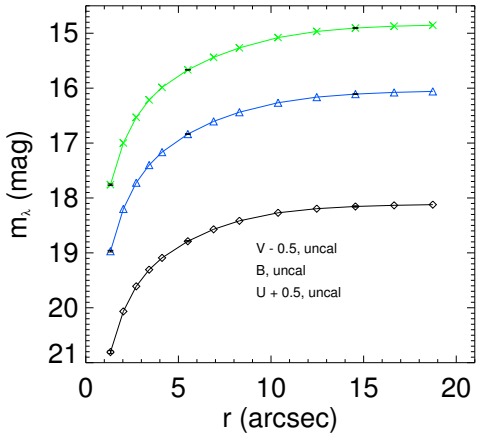
V - 0.5, uncal
B, uncal
U + 0.5, uncal
m$_\lambda$ (mag)
r (arcsec)

(18) Mrk 144

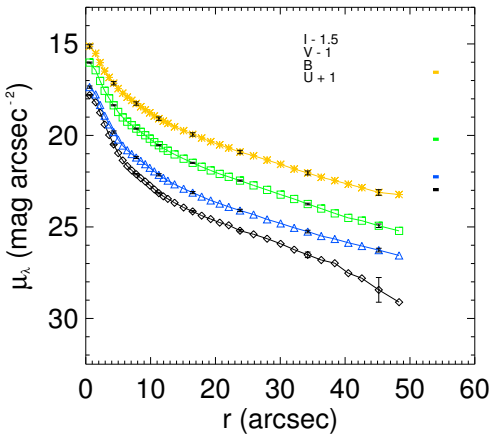
I - 1.5
V - 1
B
U + 1
μλ (mag arcsec-2)
r (arcsec)

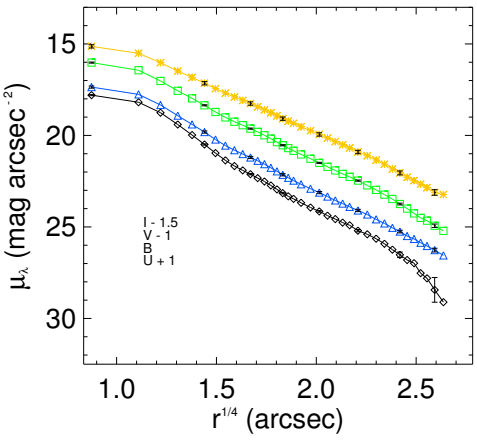
I - 1.5
V - 1
B
U + 1
μλ (mag arcsec-2)
r1/4 (arcsec)

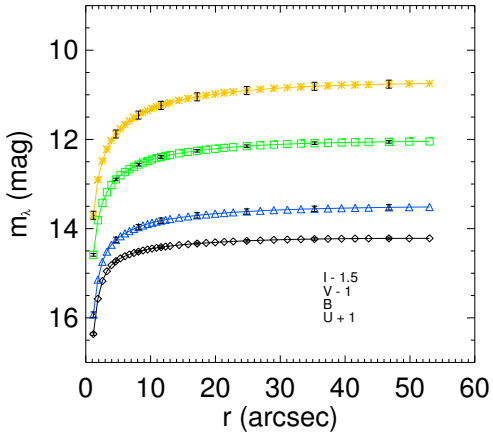
I - 1.5
V - 1
B
U + 1
mλ (mag)
r (arcsec)

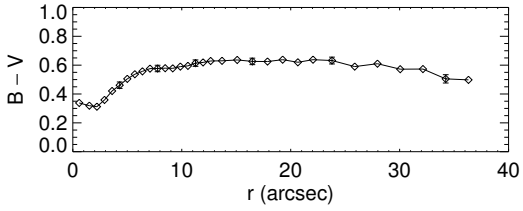
B – V
r (arcsec)

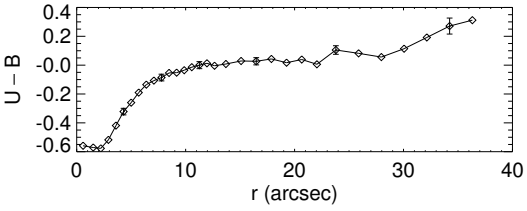
U – B
r (arcsec)

(19) Mrk 33

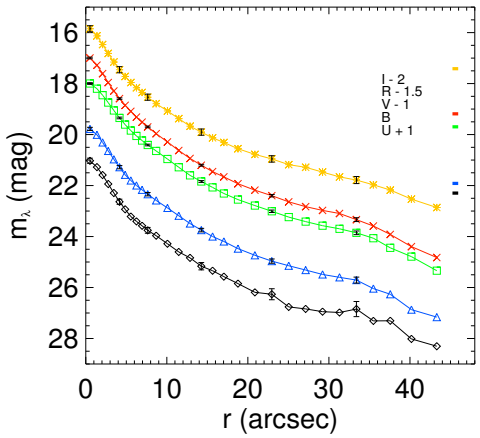
I - 2
R - 1.5
V - 1
B
U + 1
m$_\lambda$ (mag)
r (arcsec)

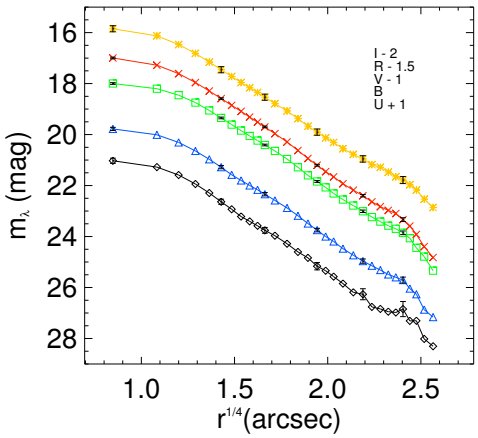
I - 2
R - 1.5
V - 1
B
U + 1
m$_\lambda$ (mag)
r$^{1/4}$(arcsec)

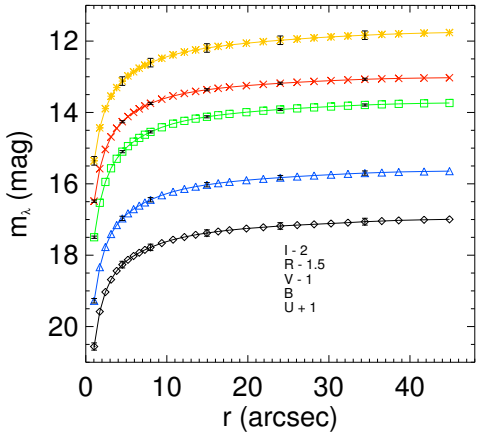
I - 2
R - 1.5
V - 1
B
U + 1
m$_\lambda$ (mag)
r (arcsec)

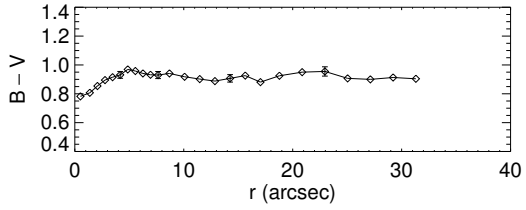
B – V
r (arcsec)

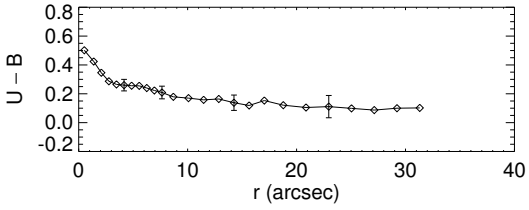
U – B
r (arcsec)

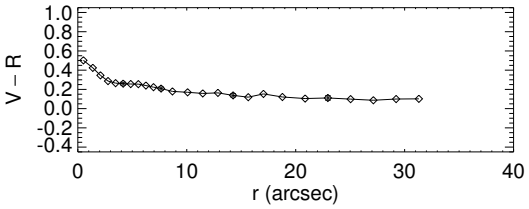
V – R
r (arcsec)

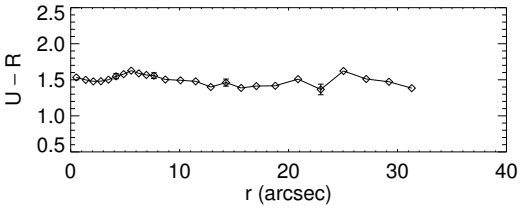
U – R
r (arcsec)

(20) Mrk 148

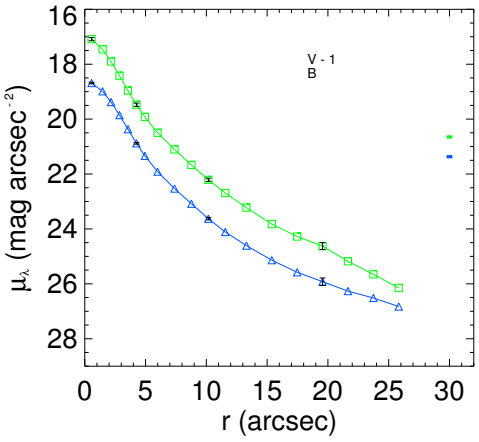
V - 1
B
μλ (mag arcsec-2)
r (arcsec)

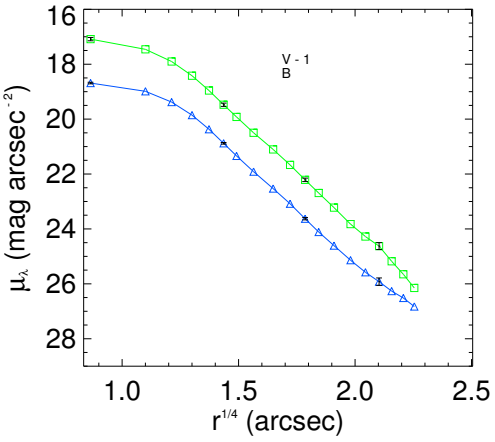
V - 1
B
μλ (mag arcsec-2)
r1/4 (arcsec)

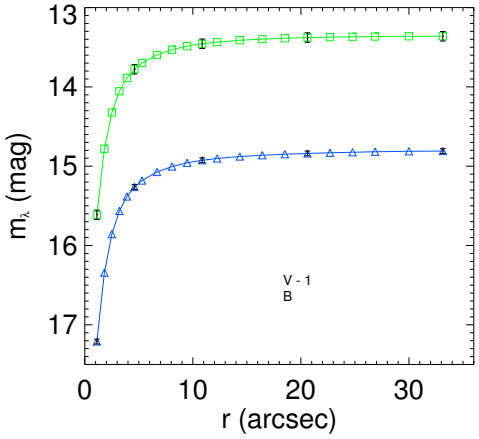
V - 1
B
mλ (mag)
r (arcsec)

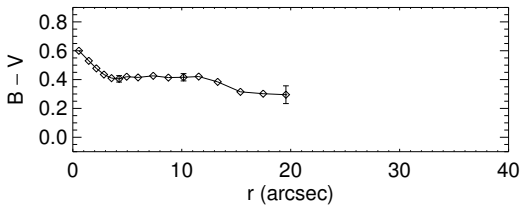
B – V
r (arcsec)

(21) Haro 25

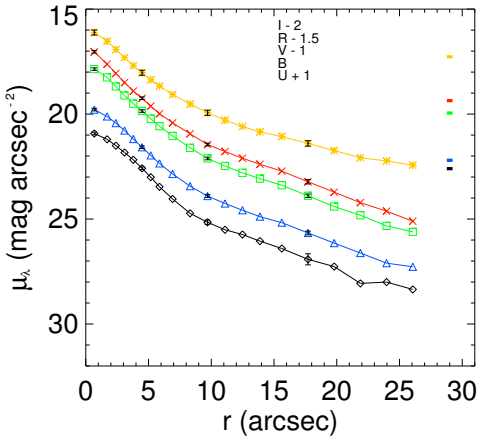
I - 2
R - 1.5
V - 1
B
U + 1
μλ (mag arcsec-2)
r (arcsec)

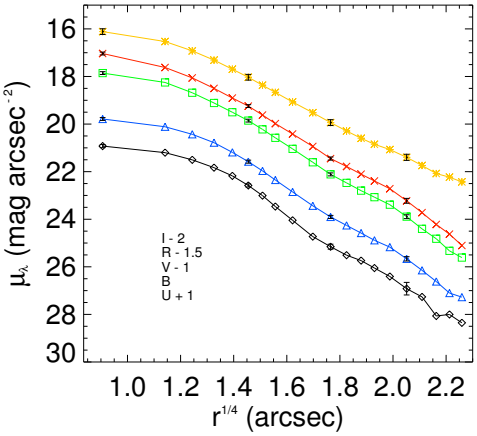
I - 2
R - 1.5
V - 1
B
U + 1
μλ (mag arcsec-2)
r1/4 (arcsec)

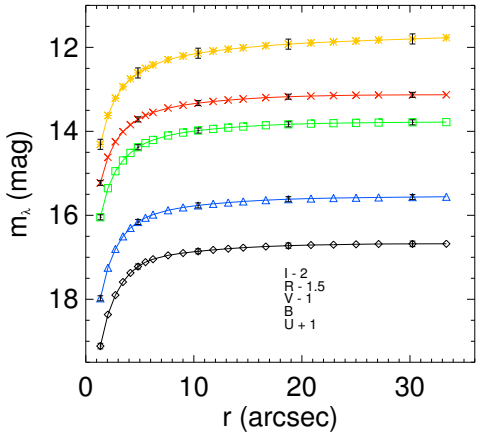
I - 2
R - 1.5
V - 1
B
U + 1
mλ (mag)
r (arcsec)

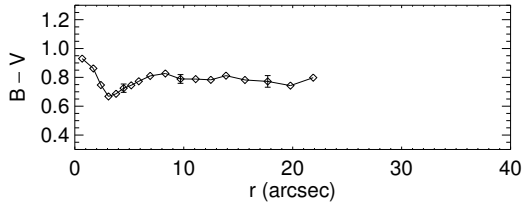
B – V
r (arcsec)

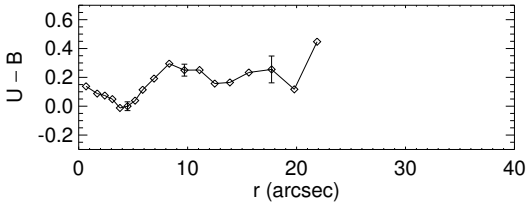
U – B
r (arcsec)

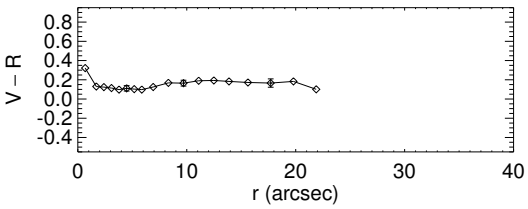
V – R
r (arcsec)

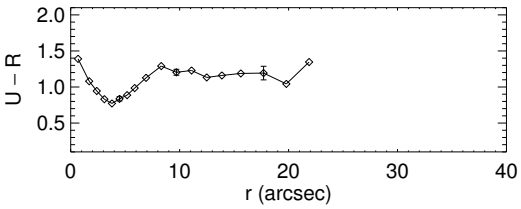
U – R
r (arcsec)

(22) Mrk 154

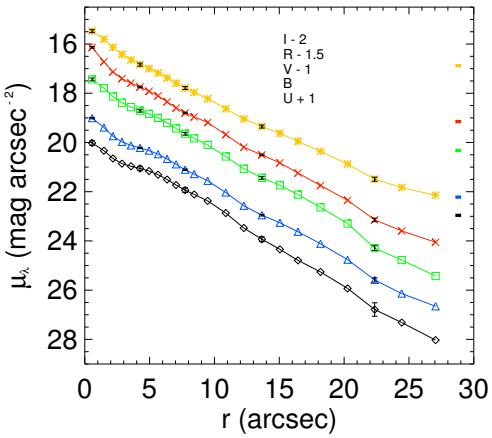
I - 2
R - 1.5
V - 1
B
U + 1
μλ (mag arcsec-2)
r (arcsec)

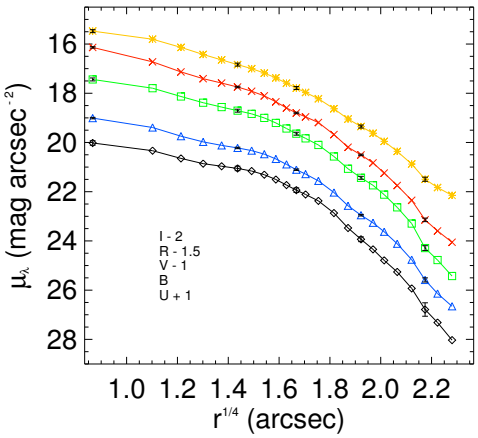
I - 2
R - 1.5
V - 1
B
U + 1
μλ (mag arcsec-2)
r1/4 (arcsec)

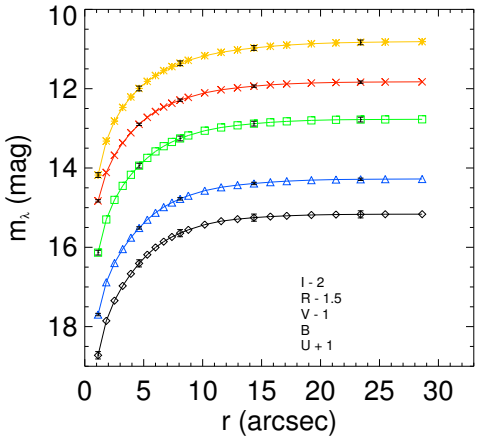
I - 2
R - 1.5
V - 1
B
U + 1
mλ (mag)
r (arcsec)

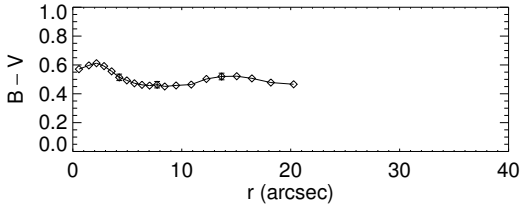
B – V
r (arcsec)

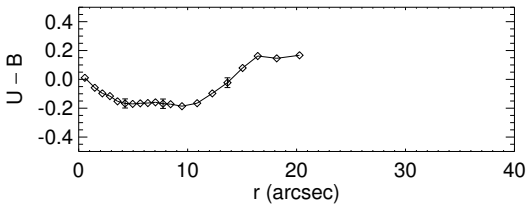
U – B
r (arcsec)

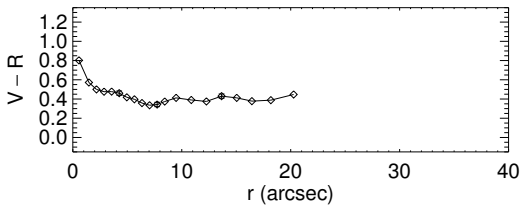
V – R
r (arcsec)

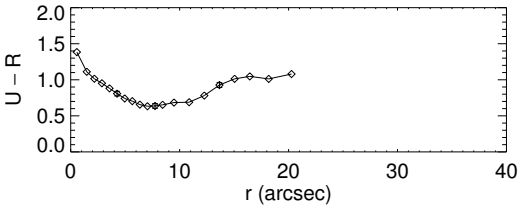
U – R
r (arcsec)

(23) Mrk 181

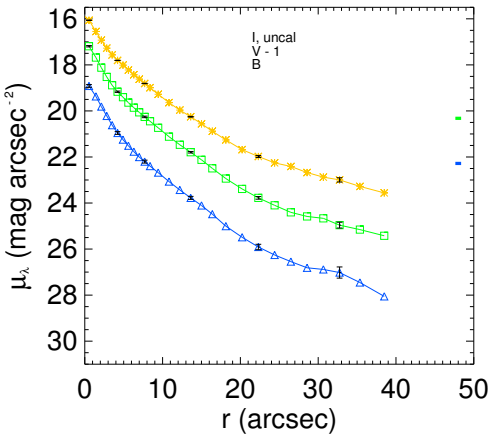
I, uncal
V - 1
B
μλ (mag arcsec-2)
r (arcsec)

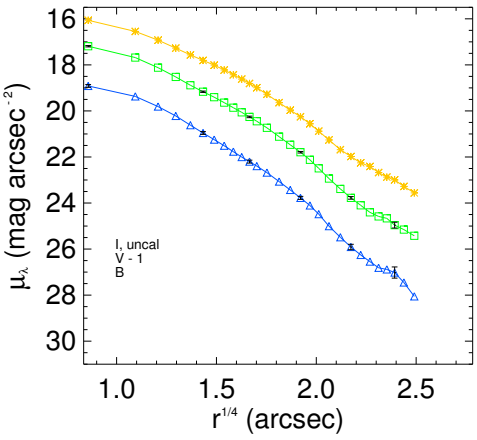
I, uncal
V - 1
B
μλ (mag arcsec-2)
r1/4 (arcsec)

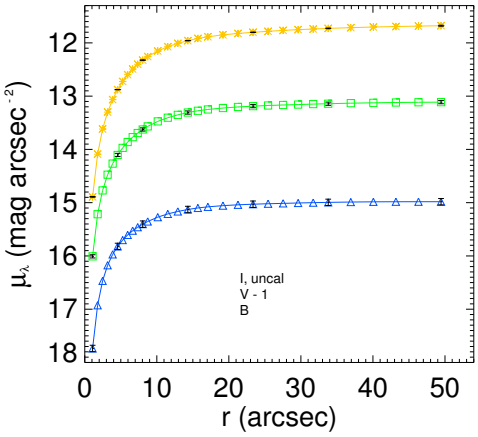
I, uncal
V - 1
B
μλ (mag arcsec-2)
r (arcsec)

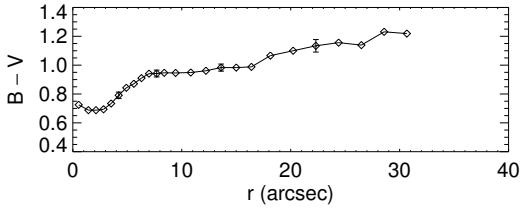
B – V
r (arcsec)

(24) Haro 34

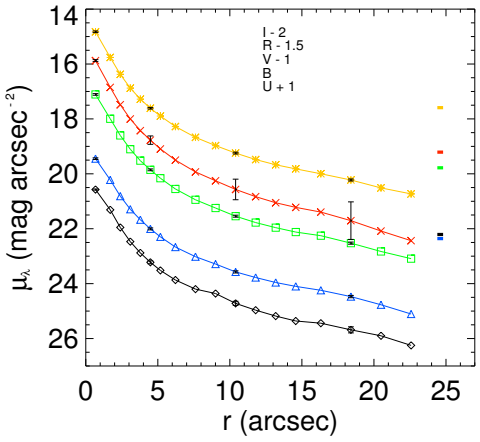
I - 2
R - 1.5
V - 1
B
U + 1
μλ (mag arcsec-2)
r (arcsec)

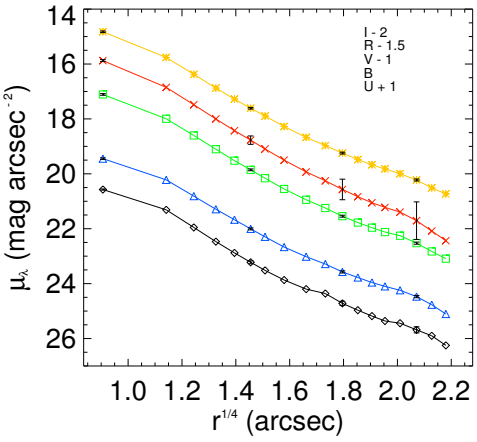
I - 2
R - 1.5
V - 1
B
U + 1
μλ (mag arcsec-2)
r1/4 (arcsec)

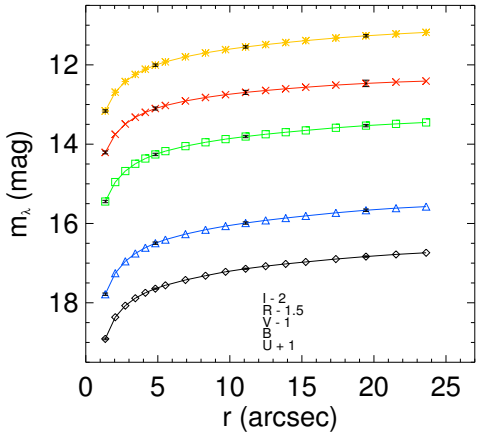
I - 2
R - 1.5
V - 1
B
U + 1
mλ (mag)
r (arcsec)

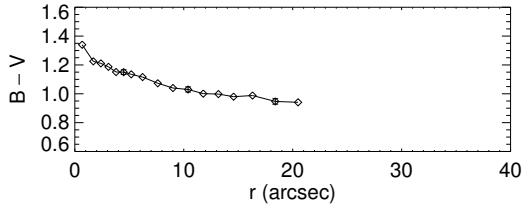
B – V
r (arcsec)

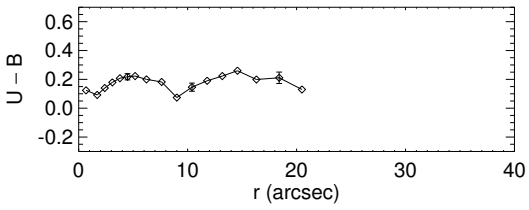
U – B
r (arcsec)

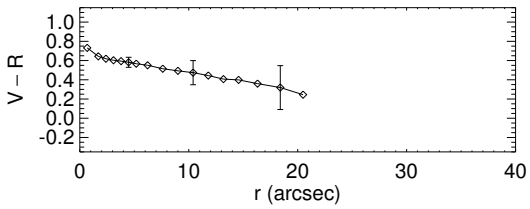
V – R
r (arcsec)

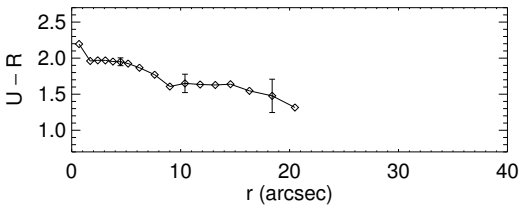
U – R
r (arcsec)

(25) Mrk 248

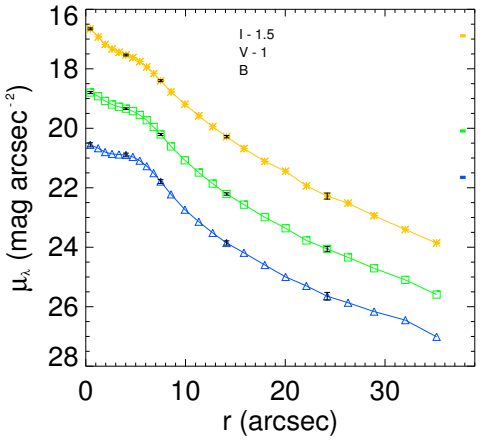
I - 1.5
V - 1
B
μλ (mag arcsec-2)
r (arcsec)

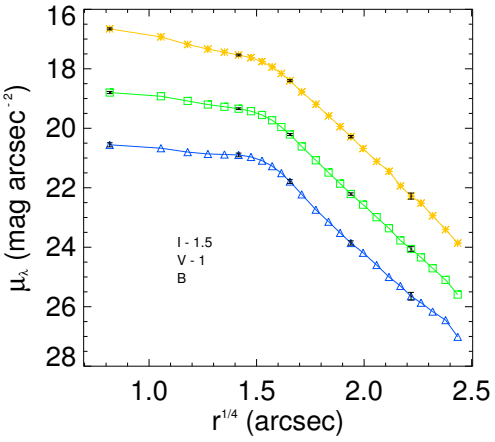
I - 1.5
V - 1
B
μλ (mag arcsec-2)
r1/4 (arcsec)

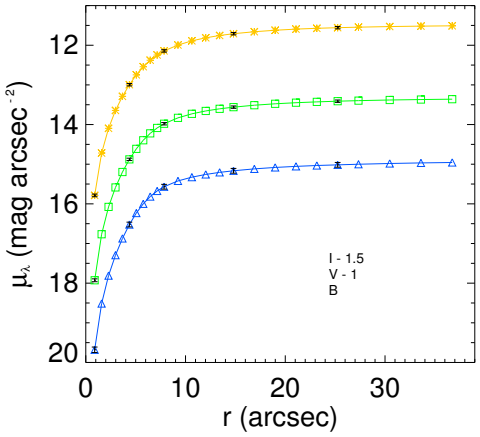
I - 1.5
V - 1
B
μλ (mag arcsec-2)
r (arcsec)

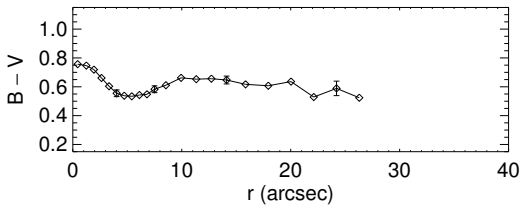
B – V
r (arcsec)

(26) IZw 101

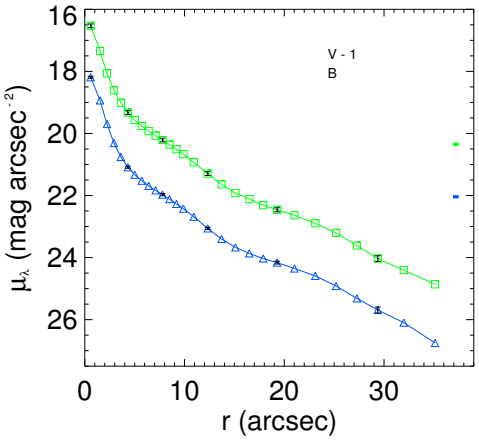
V - 1
B
μλ (mag arcsec-2)
r (arcsec)

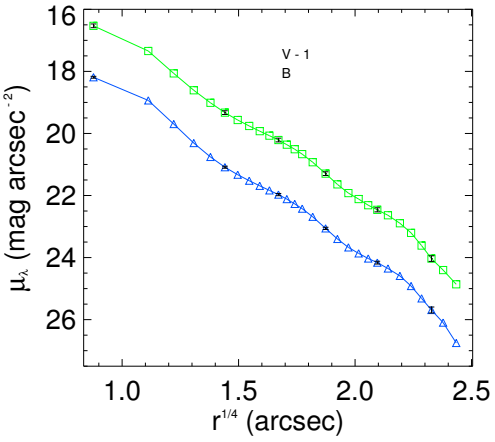
V - 1
B
μλ (mag arcsec-2)
r1/4 (arcsec)

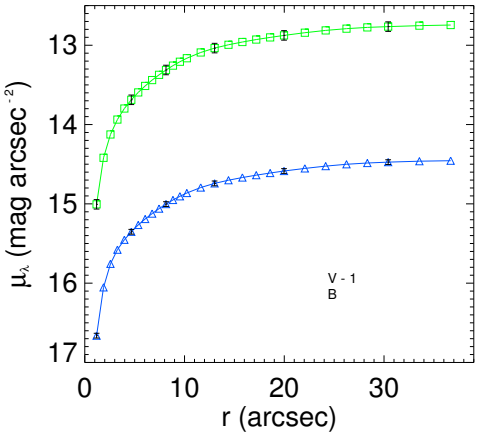
V - 1
B
μλ (mag arcsec-2)
r (arcsec)

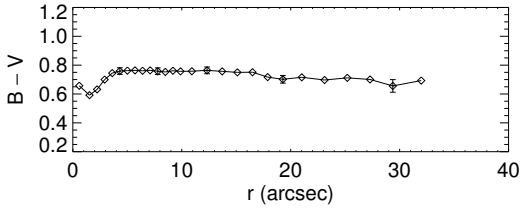
B – V
r (arcsec)

(27) Mrk 492

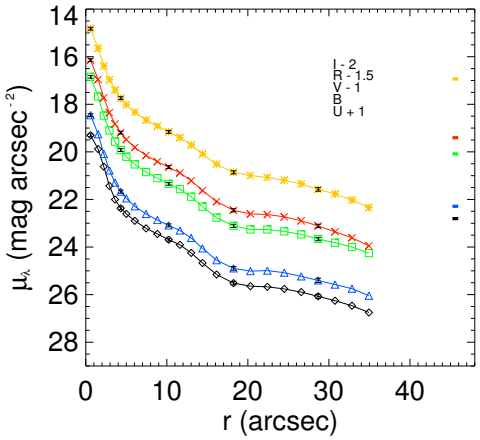
I - 2
R - 1.5
V - 1
B
U + 1
μλ (mag arcsec-2)
r (arcsec)

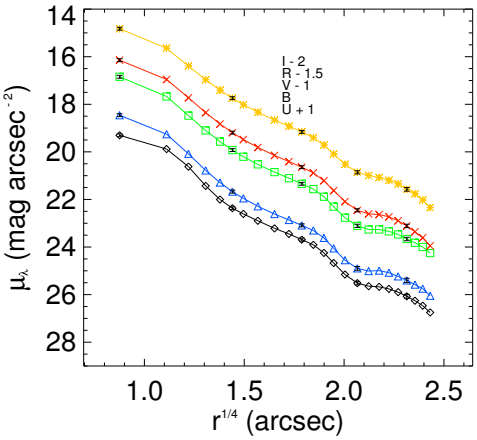
I - 2
R - 1.5
V - 1
B
U + 1
μλ (mag arcsec-2)
r1/4 (arcsec)

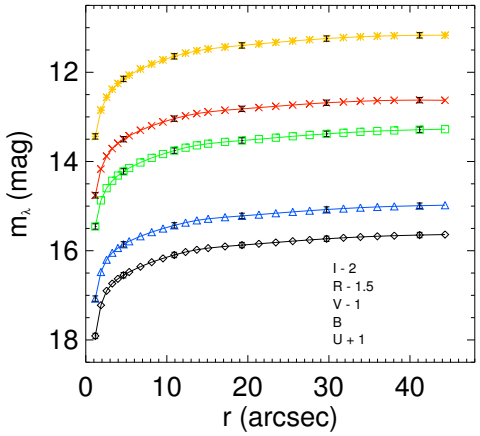
I - 2
R - 1.5
V - 1
B
U + 1
mλ (mag)
r (arcsec)

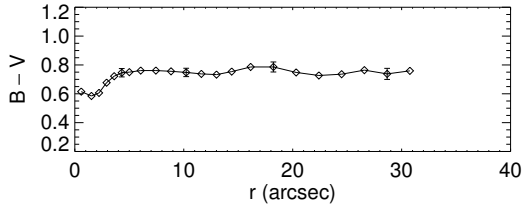
B – V
r (arcsec)

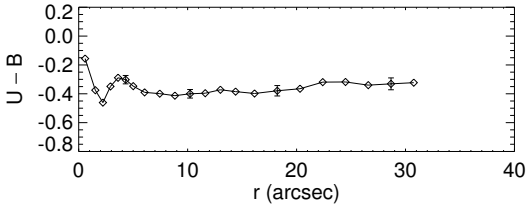
U – B
r (arcsec)

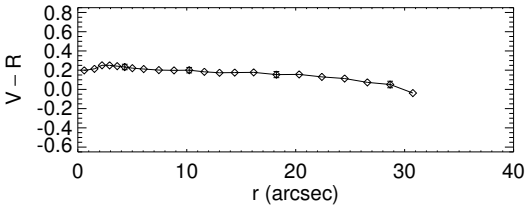
V – R
r (arcsec)

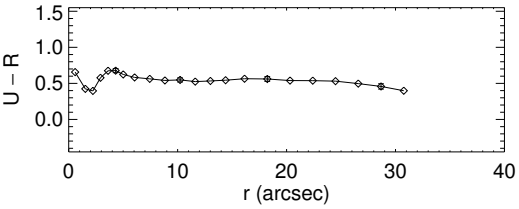
U – R
r (arcsec)

(28) Mrk 300

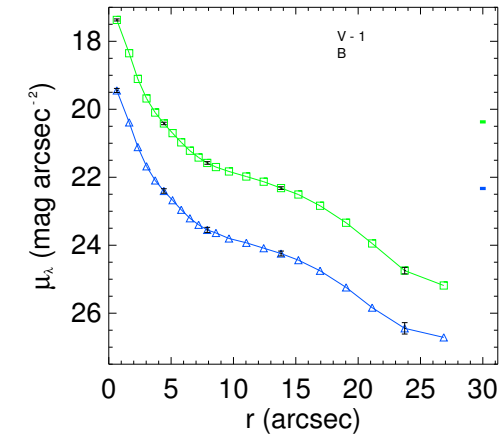
V - 1
B
μλ (mag arcsec-2)
r (arcsec)

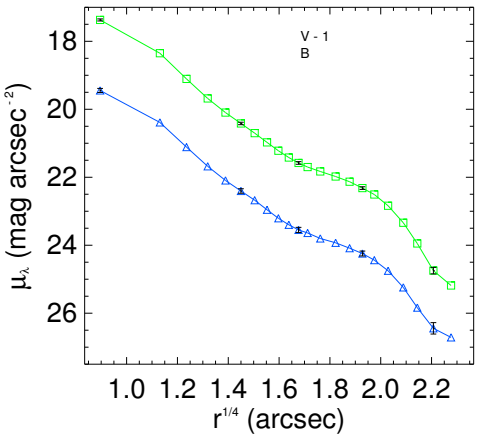
V - 1
B
μλ (mag arcsec-2)
r1/4 (arcsec)

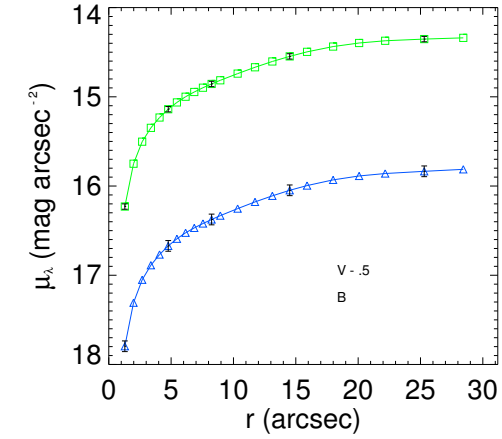
V - .5
B
μλ (mag arcsec-2)
r (arcsec)

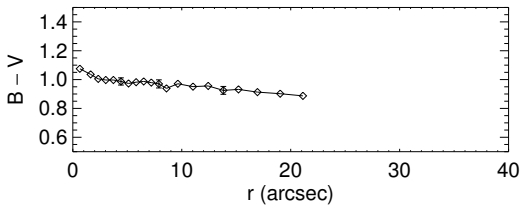
B – V
r (arcsec)

(29) Mrk 697

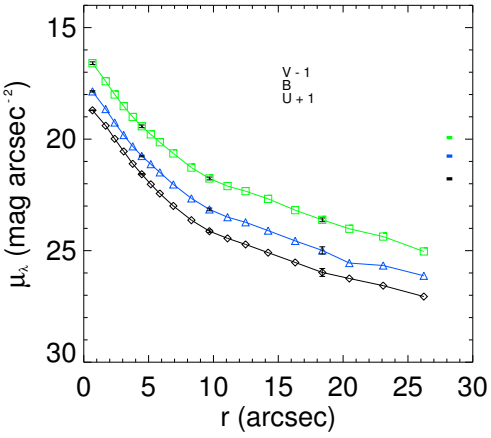
V - 1
B
U + 1
μλ (mag arcsec-2)
r (arcsec)

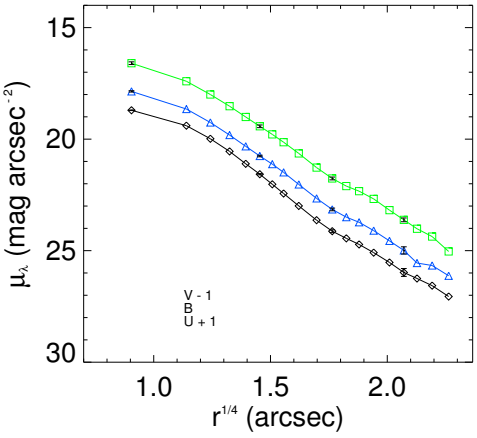
V - 1
B
U + 1
μλ (mag arcsec-2)
r1/4 (arcsec)

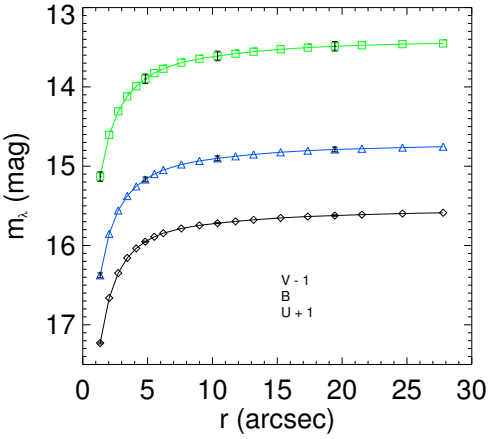
V - 1
B
U + 1
mλ (mag)
r (arcsec)

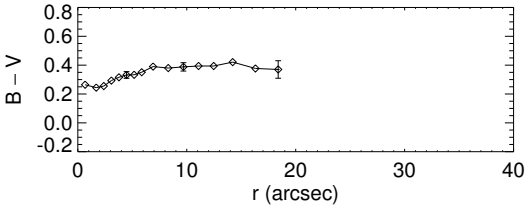
B – V
r (arcsec)

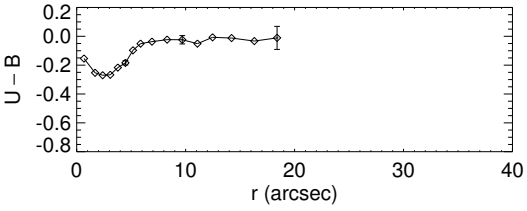
U – B
r (arcsec)

(30) Mrk 499

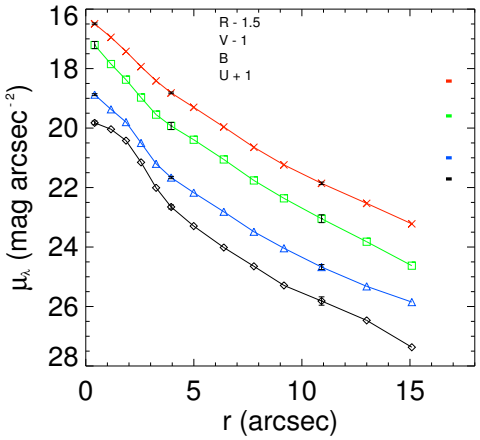
R - 1.5
V - 1
B
U + 1
μλ (mag arcsec-2)
r (arcsec)

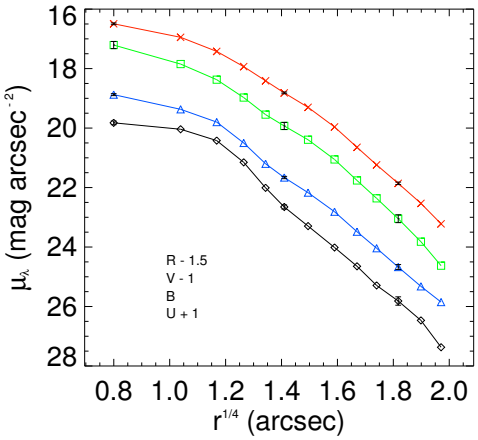
R - 1.5
V - 1
B
U + 1
μλ (mag arcsec-2)
r1/4 (arcsec)

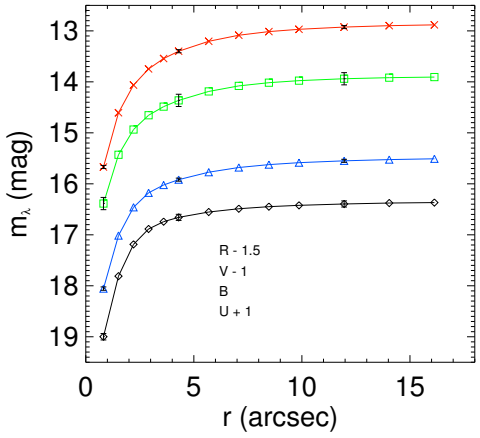
R - 1.5
V - 1
B
U + 1
mλ (mag)
r (arcsec)

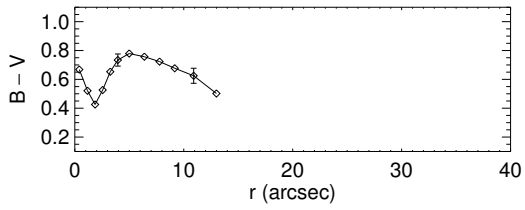
B – V
r (arcsec)

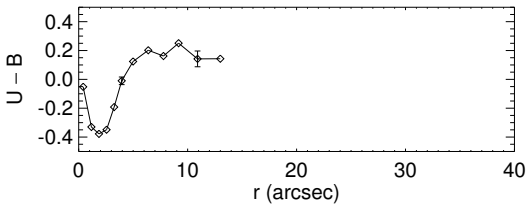
U – B
r (arcsec)

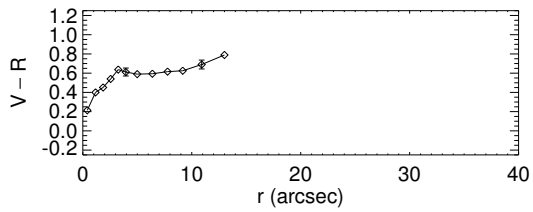
V – R
r (arcsec)

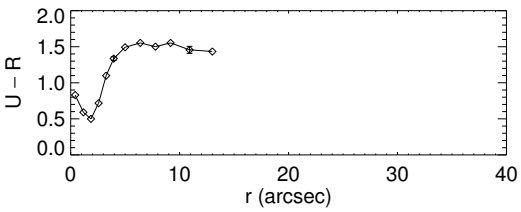
U – R
r (arcsec)

(31) IZw 191

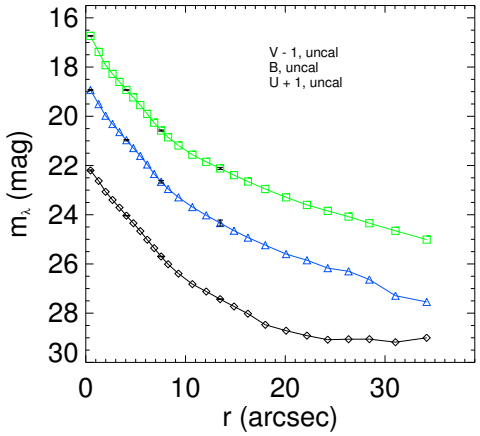
V - 1, uncal
B, uncal
U + 1, uncal
m$_\lambda$ (mag)
r (arcsec)

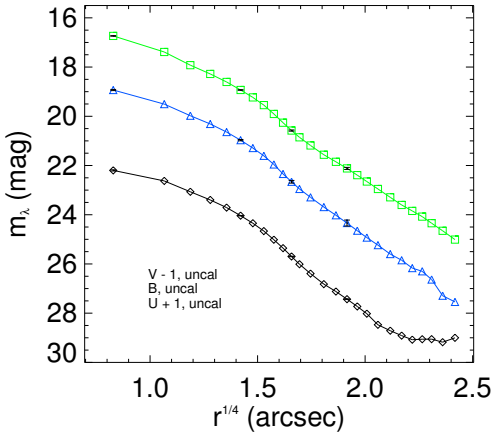
V - 1, uncal
B, uncal
U + 1, uncal
m$_\lambda$ (mag)
r$^{1/4}$ (arcsec)

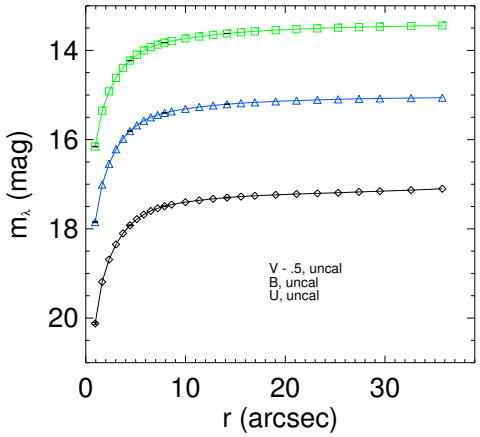
V - .5, uncal
B, uncal
U, uncal
m$_\lambda$ (mag)
r (arcsec)

(32) IIZw 82

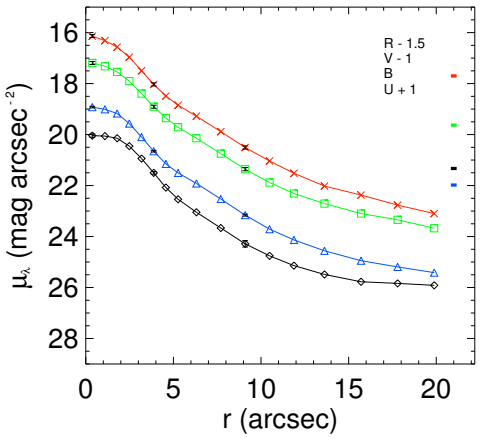
R - 1.5
V - 1
B
U + 1
μλ (mag arcsec-2)
r (arcsec)

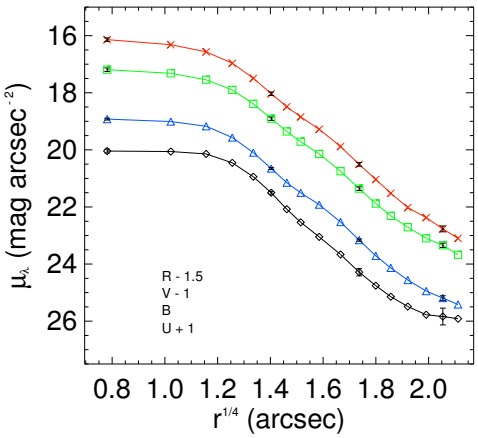
R - 1.5
V - 1
B
U + 1
μλ (mag arcsec-2)
r1/4 (arcsec)

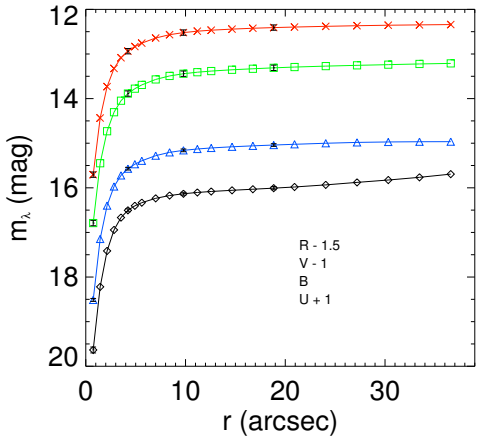
R - 1.5
V - 1
B
U + 1
mλ (mag)
r (arcsec)

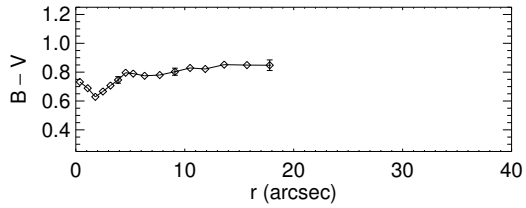
B – V
r (arcsec)

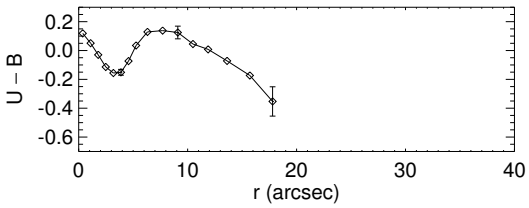
U – B
r (arcsec)

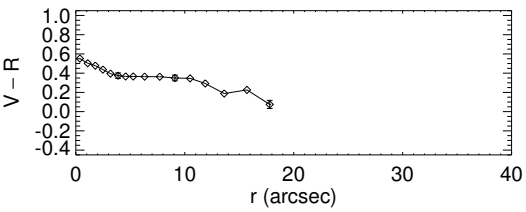
V – R
r (arcsec)

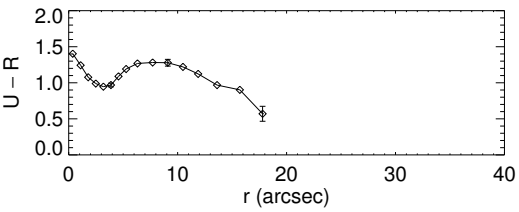
U – R
r (arcsec)

(33) Mrk 512

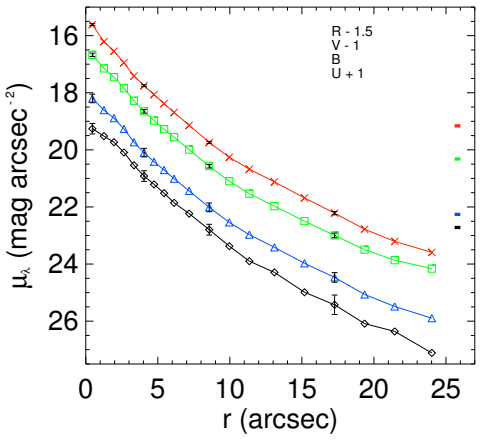
R - 1.5
V - 1
B
U + 1
μλ (mag arcsec-2)
r (arcsec)

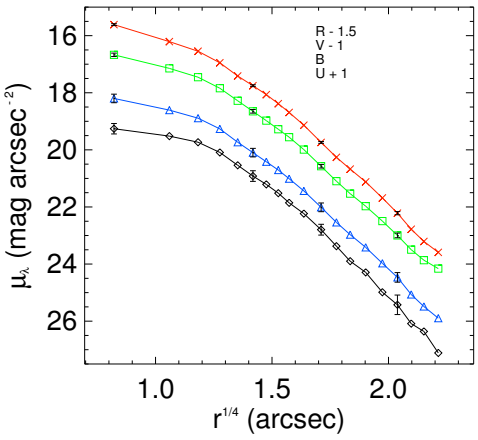
R - 1.5
V - 1
B
U + 1
μλ (mag arcsec-2)
r1/4 (arcsec)

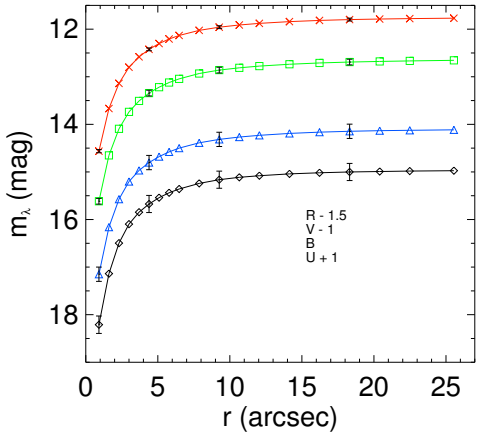
R - 1.5
V - 1
B
U + 1
mλ (mag)
r (arcsec)

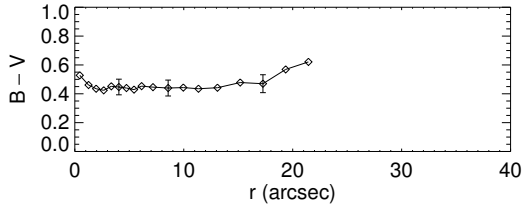
B – V
r (arcsec)

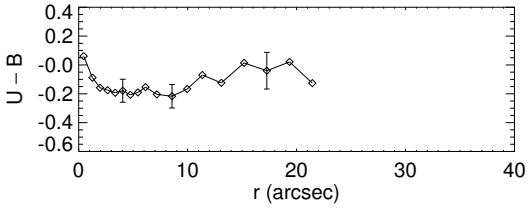
U – B
r (arcsec)

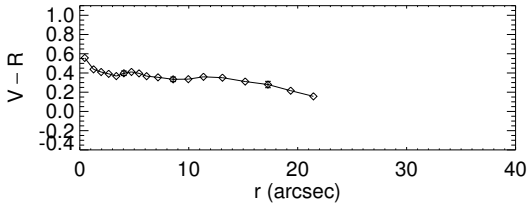
V – R
r (arcsec)

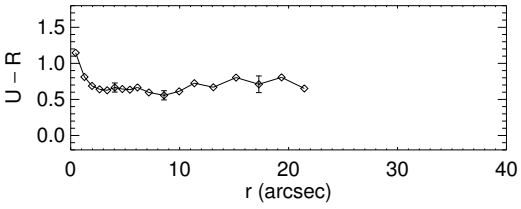
U – R
r (arcsec)

(34) Mrk 518

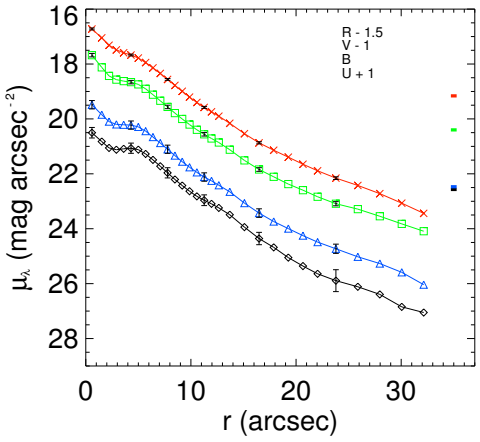
R - 1.5
V - 1
B
U + 1
μλ (mag arcsec-2)
r (arcsec)

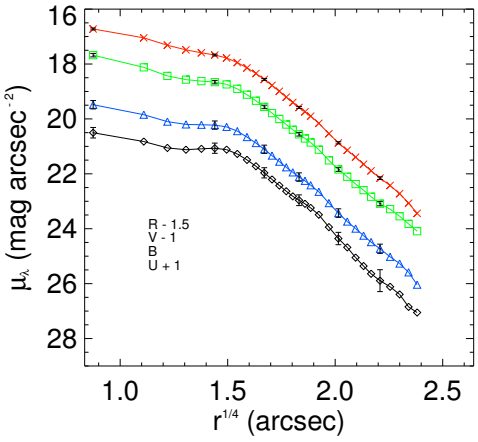
R - 1.5
V - 1
B
U + 1
μλ (mag arcsec-2)
r1/4 (arcsec)

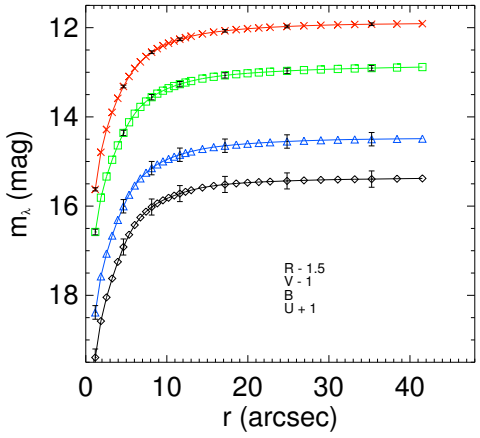
R - 1.5
V - 1
B
U + 1
mλ (mag)
r (arcsec)

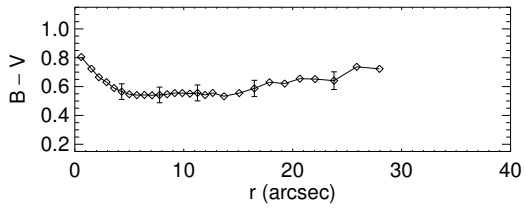
B – V
r (arcsec)

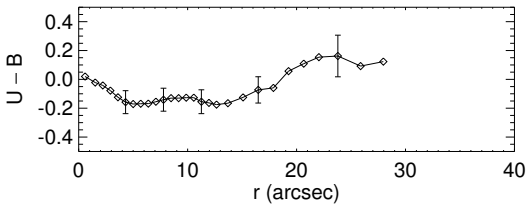
U – B
r (arcsec)

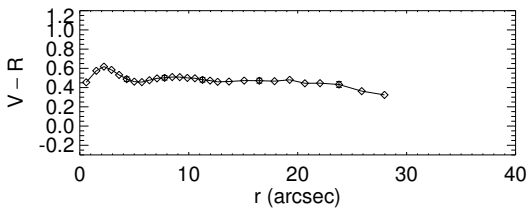
V – R
r (arcsec)

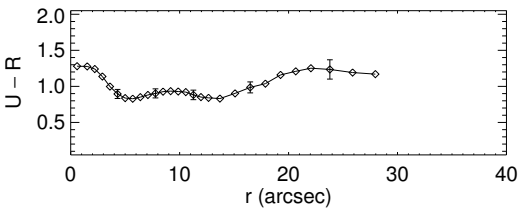
U – R
r (arcsec)

(35) Mrk 303

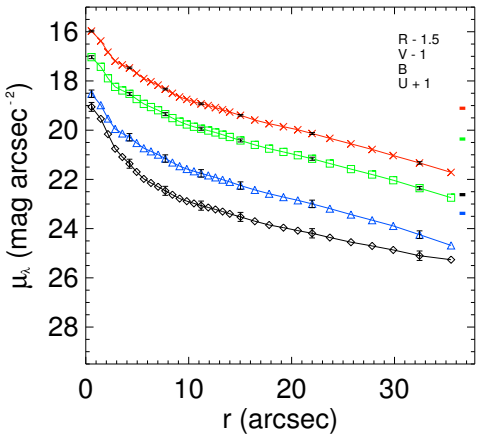
R - 1.5
V - 1
B
U + 1
μλ (mag arcsec-2)
r (arcsec)

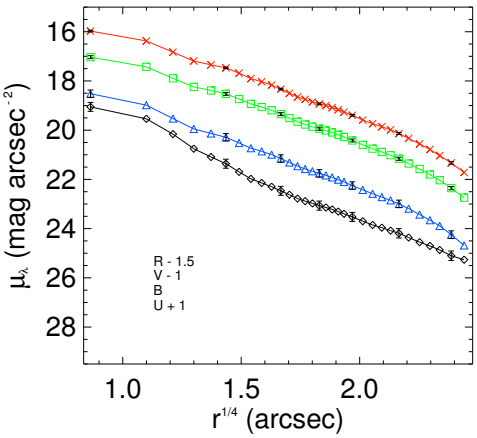
R - 1.5
V - 1
B
U + 1
μλ (mag arcsec-2)
r1/4 (arcsec)

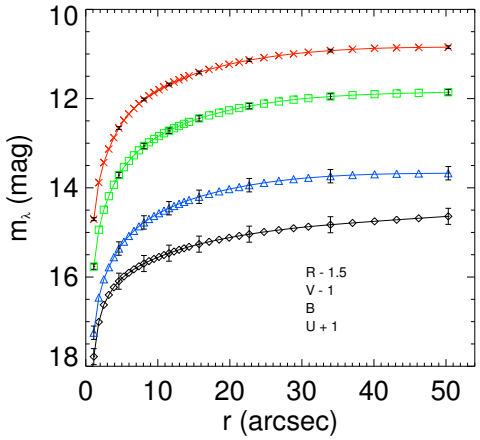
R - 1.5
V - 1
B
U + 1
mλ (mag)
r (arcsec)

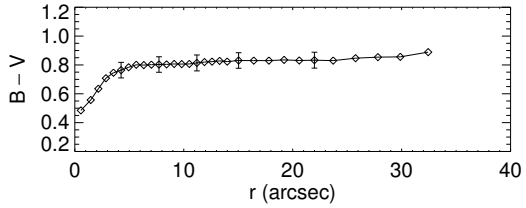
B – V
r (arcsec)

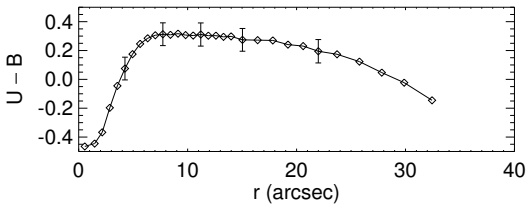
U – B
r (arcsec)

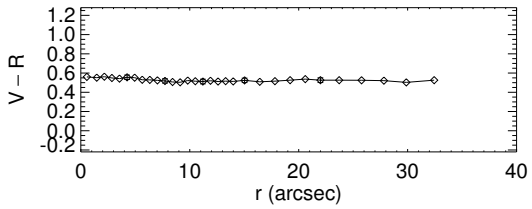
V – R
r (arcsec)

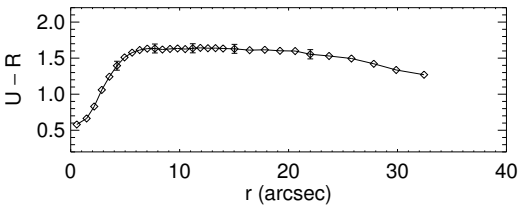
U – R
r (arcsec)

(36) Mrk 531

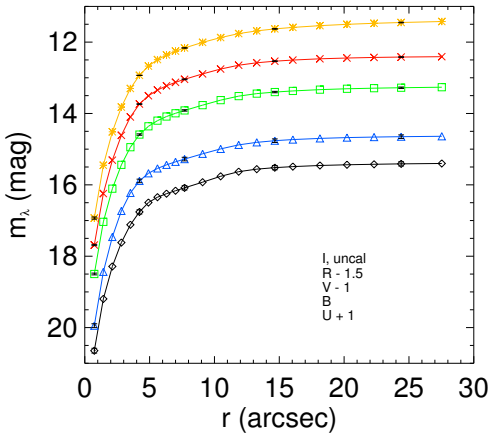

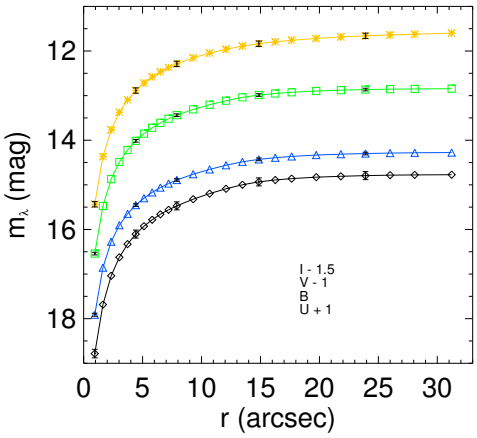

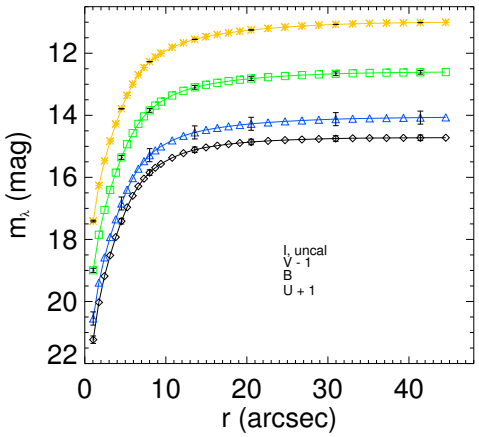

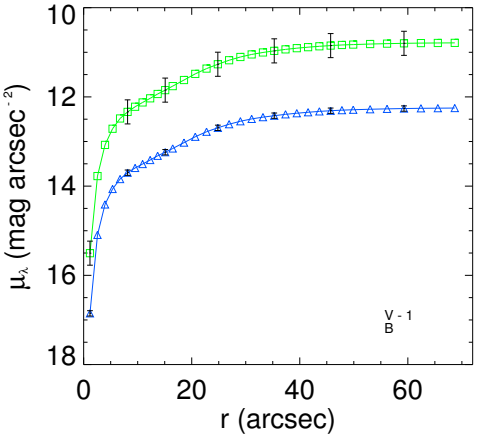

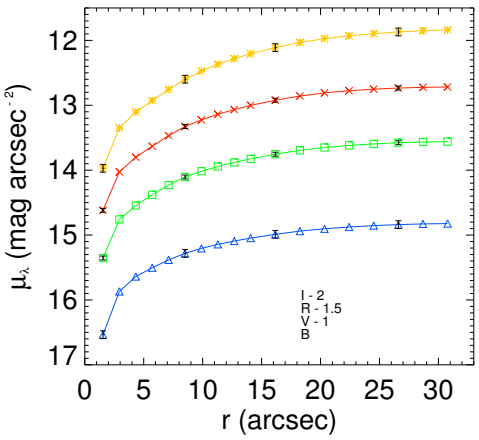

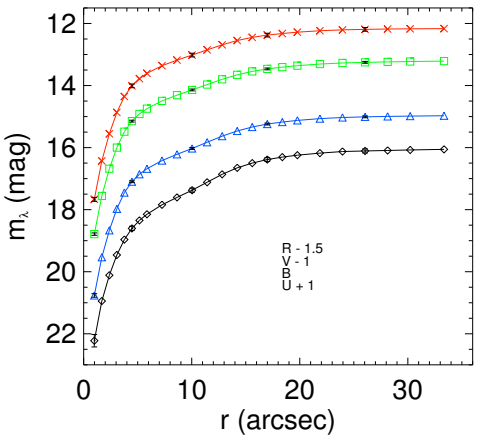

(37) Mrk 360 GC (38) Mrk 1094 GC (39) Mrk 8 GC (40) Mrk 171 GC (41) Mrk 54 GC (42) Mrk 238 GC

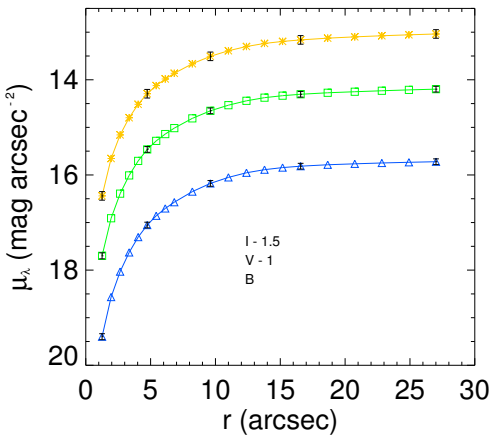

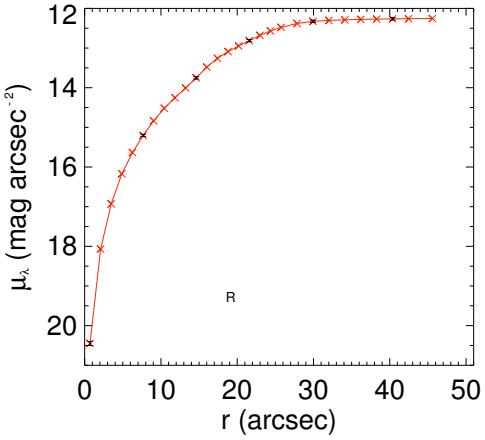

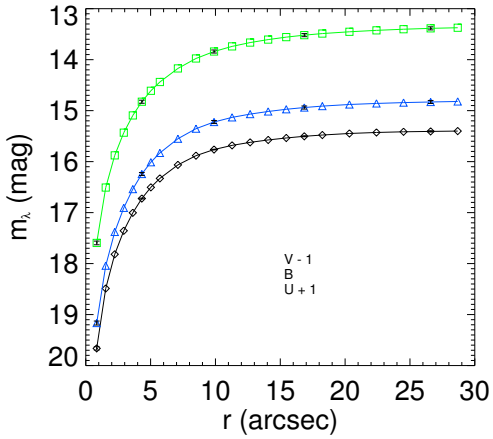

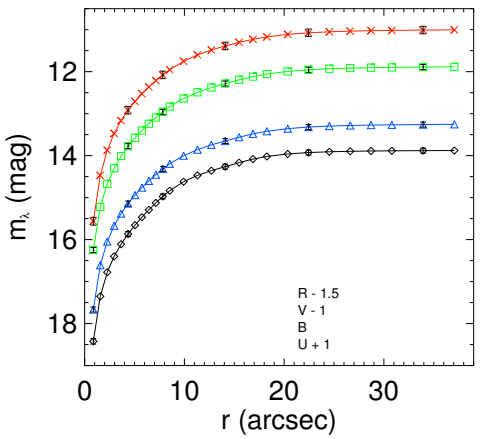

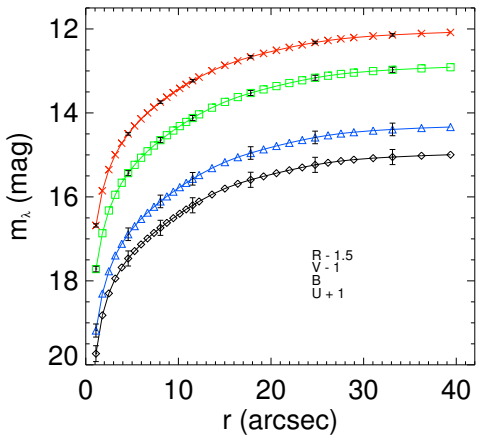

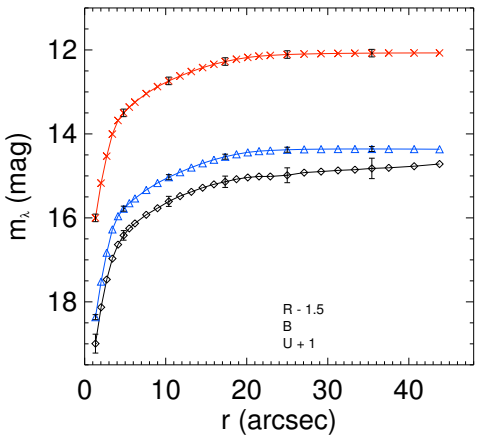

(43) Mrk 255 GC (44) Mrk 271 GC (45) Haro 42 GC (46) Mrk 297 GC (47) Mrk 306 GC (48) IIZw 185 GC

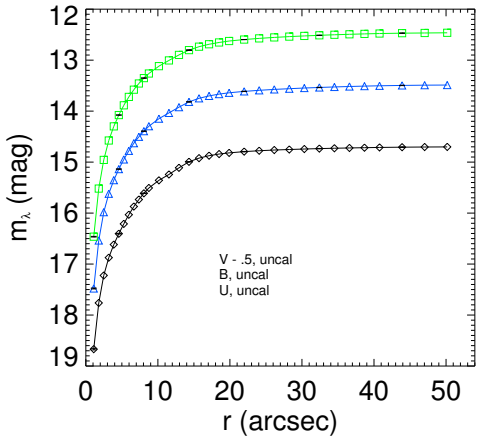
12
13
14
15
16
17
18
19
0
10
20
30
40
50
m$_\lambda$ (mag)
r (arcsec)
V - .5, uncal
B, uncal
U, uncal

(49) Mrk 325 GC

Table 2.5. Photometric Parameters

Name	Ellipticity	Position Angle (°)	Calibration Method
Mrk 342	0.24	34	standard stars
Haro 15 with neighbor	0.04	17	standard stars
Mrk 360 with neighbor	0.13	86	standard stars
Mrk 364	0.00	179	standard stars
Mrk 366	0.03	4	standard stars
Mrk 366 with loop	0.08	112	standard stars
Mrk 367	0.15	16	Sloan survey
Mrk 589	0.13	159	standard stars
Mrk 1184	0.13	139	Sloan survey
Mrk 1404	0.00	178	standard stars
Mrk 1079	0.19	62	none
Mrk 1094	0.06	156	Sloan survey
Mrk 8	0.01	172	standard stars
Haro 1	0.07	177	standard stars
Mrk 385	0.34	178	standard stars
Mrk 385 with loop	0.00	141.39	standard stars
Mrk 1211 with neighbor	0.00	43.24	standard stars
Mrk 390	0.05	161	standard stars

Table 2.5 (continued)

Name	Ellipticity	Position Angle (°)	Calibration Method
Mrk 18	0.30	88	standard stars
Mrk 402	0.00	155	Sloan survey
IIZw 44	0.08	130	Sloan survey
Mrk 139	0.00	159	Sloan survey
Mrk 144	0.00	89	Sloan survey
Mrk 33	0.14	129	Sloan survey
Mrk 148	0.54	132	Sloan survey
Haro 25	0.02	151	Sloan survey
Mrk 154	0.08	75	Sloan survey
Mrk 171	0.18	93	Sloan survey
Mrk 181	0.17	15	Sloan survey
Haro 34	0.20	174	Sloan survey
Mrk 54	0.36	123	Sloan survey
Mrk 238 with neighbor	0.00	99	Sloan survey
Mrk 248	0.20	88	Sloan survey
Mrk 248 with neighbor	0.27	90	Sloan survey
Mrk 255	0.07	158	Sloan survey
Mrk 271 and NGC 5279	0.13	55	Sloan survey

Table 2.5 (continued)

Name	Ellipticity	Position Angle (°)	Calibration Method
Haro 42	0.37	67	Sloan survey
IZw 101	0.12	50	Sloan survey
Mrk 492	0.08	88	Sloan survey
Mrk 297	0.23	179	Sloan survey
Mrk 300	0.18	85	Sloan survey
Mrk 697	0.13	169	Sloan survey
Mrk 499	0.32	152	Sloan survey
IZw 191	0.00	178	Sloan survey
IIZw 82	0.04	84	none
Mrk 512	0.18	6	Sloan survey
Mrk 518	0.00	178	standard stars
Mrk 303	0.36	178	standard stars
Mrk 306	0.55	47	standard stars
Mrk 306 and 305	0.26	47	standard stars
IIZw 185	0.16	178	Sloan survey
Mrk 531	0.18	84	standard stars
Mrk 325	0.17	49	none

Col. (1) Primary galaxy name. Col. (2) The ellipticity of the apertures, decided when hand placing the major and minor axes of the first aperture. The ellipticity is the deviation from perfect circular or spherical form toward elliptic or ellipsoidal form. Col. (3) Position angle of the major axis measured eastward from the north axis Col. (4) The source for calibration, whether it be the use of standard stars, stars in the Sloan survey, or calibration was not possible.

2.4.2 Functional Form of the Surface Brightness Profiles

The SBPs have been analyzed in terms of two standard fitting laws. First, an exponential law describes a typical disk structure. The exponential law is shown in equations 2.9 and 2.10 (in flux units, then magnitudes respectively), where I(0) is the central intensity and R_d is the disk scale length (de Vaucouleurs 1959). On plots that show μ verses R, the exponential law will be linear. Equation 2.11 shows the relation between the intensity at the disk scale length and the central intensity.

$$I(R) = I(0)\exp(-R/R_d) \tag{2.9}$$

$$\mu(R) = \mu(0) + 1.086(R/R_d) \tag{2.10}$$

$$I(R_d) = 1/e \times I(0) \tag{2.11}$$

The de Vaucouleurs law (de Vaucouleurs 1948), also known as the $R^{1/4}$ law, fits elliptical type galaxies, or a bulge. The de Vaucouleurs law is shown below where R_e is the radius of the isophote that encompasses half of the total light of the system, and I(0) is once again the central intensity . The plot of μ versus $R^{1/4}$, will appear linear. The equations below show the exponential law first in flux units, then magnitude.

$$I(R) = I(0)\exp(-7.67(R/R_e)^{1/4}) \tag{2.12}$$

$$\mu(R) = \mu(0) + 8.325(R/R_e)^{1/4} \tag{2.13}$$

Two idl programs were written to fit the profiles for the optical sample of galaxies. The first step was to analyze the SBPs to find which galaxies were bulge dominated,

disk dominated, or a combination. In order to make this classification I inspected the SBPs of each object when plotted against r and $r^{1/4}$ to obtain an initial sense of the functional form of the SBP. As mentioned before, a galaxy that is bulge dominated will appear linear when the surface brightness is plotted against $r^{1/4}$. A disk dominated galaxy will appear linear when its surface brightness is plotted against r. The majority of the galaxies in our sample are bulge dominated. One of the programs would fit either a single bulge, or a bulge and then the disk, and the other would fit either a single disk, or a disk and then a bulge. For example, if a galaxy was bulge dominated, but had traces of a disk at high radius, program 1 would be used. First the SBP points would be read in and the bulge data points would be fit with a line. The slope and y-intercept could be used to solve for I(0) and R_e. Next, all of the data points were converted to flux units so that the fit could be subtracted off. The focus would then switch to the disk data points, and they would be fit. The y-intercept and slope could be used to fine I(0) and R_d of the disk. In many cases the residual light distribution, after subtracting the bulge fit, was negligible indicating no significant disk component.

To convert the magnitude to flux units, the magnitude zero points from Bessel (1990) were used. Not every galaxy from the sample was a viable candidate to be fit. If a galaxy had too many star formation knots, a nearby companion, or interaction feature near the core, a fit would not produce reliable results.

Table 2.6 shows the fit parameters for the galaxies. Six fits are displayed in Figure 2.3 to show the accuracy of our fitting program.

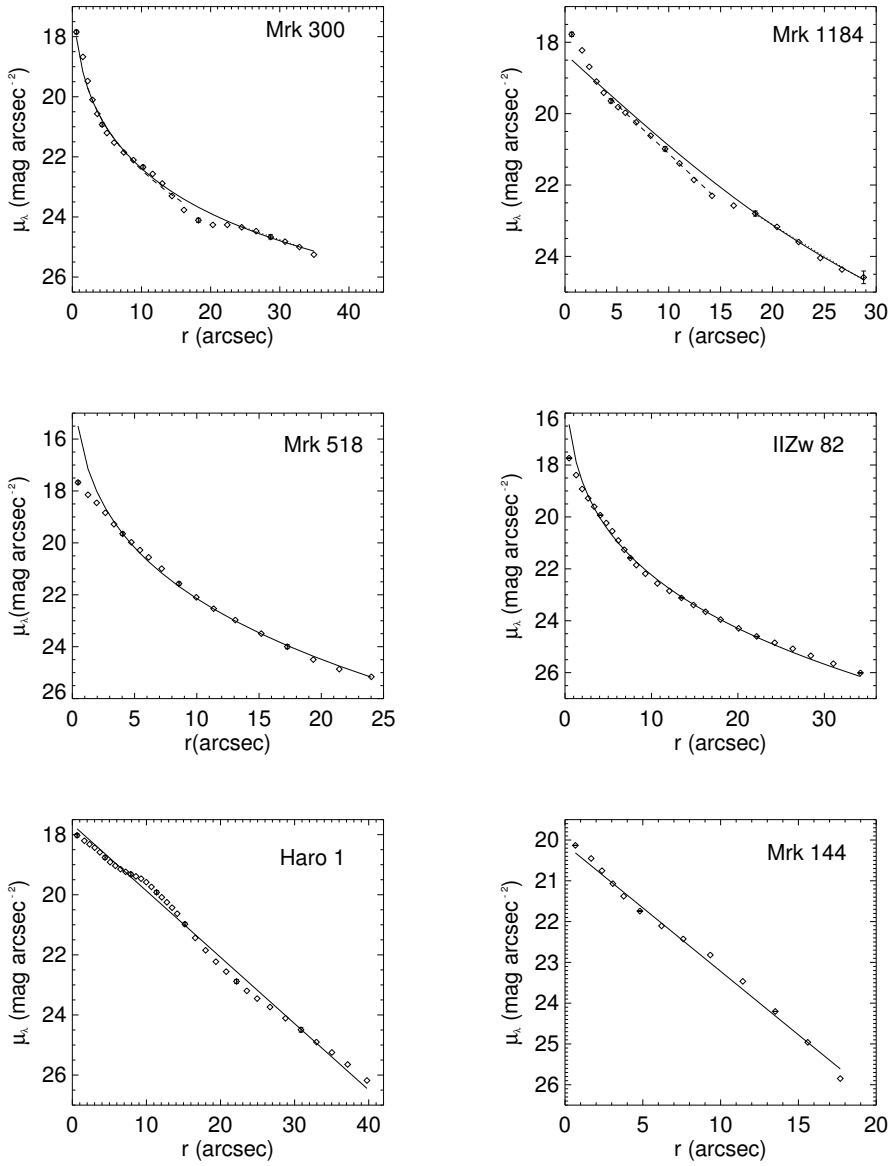

Figure 2.3: Representative examples of fits to the surface brightness profiles, exhibiting the range of observed structures. The diamond symbols are the actual data points. (1) Mrk 300 B-band bulge + disk, dashed line is $R^{1/4}$ law fit, dotted line is exponential fit, and straight line is the combination (2) Mrk 1184 R-band double disk, dashed line is the exponential fit to disk 1, dotted line is the exponential fit to disk 2, and the solid line is the combination (3) Mrk 518 B-band bulge dominated, solid line is $R^{1/4}$ law fit (4) II Zw 82 B-band bulge dominated, solid line is $R^{1/4}$ law fit (5) Haro 1 B-band disk dominated, solid line is exponential fit (6) Mrk 144 B-band disk dominated, solid line is exponential fit

Table 2.6. Structural Parameters

Name	λ	r_e (arcsec)	r_e (kpc)	Bulge μ_0 (mag/arcsec^2)	r_d (arcsec)	r_d (kpc)	Disk μ_0 (mag/arcsec^2)	Class
(1)	(2)	(3)	(4)	(5)	(6)	(7)	(8)	(9)
Mrk 342	U	1.6	1.2	11.9	***	***	***	Bulge
	B	1.8	1.3	12.0	***	***	***	Bulge
	V	2.3	1.7	11.7	***	***	***	Bulge
	I	2.3	1.7	***	***	***	***	Bulge
Haro 15	U	***	***	***	4.0	1.7	18.6	Disk
	B	***	***	***	4.1	4.1	19.1	Disk
	V	***	***	***	4.1	1.7	18.9	Disk
	R	***	***	***	4.2	1.7	***	Disk
	I	***	***	***	4.6	1.9	***	Disk
Mrk 364	U	1.6	0.9	10.6	***	***	***	Bulge
	B	1.5	0.8	10.4	***	***	***	Bulge
	V	1.6	0.9	10.0	***	***	***	Bulge
	R	2.0	1.1	10.2	***	***	***	Bulge
	I	2.8	1.5	***	***	***	***	Bulge
Mrk 366	U	3.6	1.9	12.6	***	***	***	Bulge
	B	6.4	3.4	13.9	***	***	***	Bulge

Table 2.6 (continued)

Name	λ	r_e (arcsec)	r_e (kpc)	Bulge μ_0 (mag/arcsec^2)	r_d (arcsec)	r_d (kpc)	Disk μ_0 (mag/arcsec^2)	Class
(1)	(2)	(3)	(4)	(5)	(6)	(7)	(8)	(9)
	V	7.3	3.9	13.4	***	***	***	Bulge
	R	7.5	4.0	13.0	***	***	***	Bulge
	I	7.7	4.1	***	***	***	***	Bulge
Mrk 367	B	0.7	0.5	7.4	***	***	***	Bulge
Mrk 589	U	1.9	0.4	9.9	154.7	35.0	26.2	Bulge+Disk
	B	2.5	0.6	10.8	24.8	5.6	26.5	Bulge+Disk
	V	2.9	0.7	11.0	8.3	1.9	24.3	Bulge+Disk
	R	3.7	0.8	11.2	***	***	***	Bulge
	I	4.1	0.9	***	***	***	***	Bulge
Mrk 1184	R	***	***	***	4.0	2.3	18.4	DoubleDisk
	R	***	***	***	9.2	5.3	21.5	DoubleDisk
Mrk 1404	U	1.7	1.2	10.4	7.4	5.3	22.6	Bulge+Disk
	B	1.6	1.1	10.2	8.8	6.3	22.7	Bulge+Disk
	V	1.5	1.1	9.7	6.2	4.4	21.4	Bulge+Disk
	R	1.5	1.0	9.2	6.2	4.4	20.9	Bulge+Disk
Mrk 1079	B	2.3	1.3	***	6.9	3.9	***	Bulge+Disk

Table 2.6 (continued)

Name	λ	r_e (arcsec)	r_e (kpc)	Bulge μ_0 (mag/arcsec^2)	r_d (arcsec)	r_d (kpc)	Disk μ_0 (mag/arcsec^2)	Class
(1)	(2)	(3)	(4)	(5)	(6)	(7)	(8)	(9)
	R	3.6	2.0	***	4.5	2.5	***	Bulge+Disk
Haro 1	U	***	***	***	4.9	1.3	17.7	Disk
	B	***	***	***	5.1	1.3	18.1	Disk
	V	***	***	***	4.9	1.3	17.6	Disk
	R	***	***	***	5.1	1.3	17.3	Disk
	I	***	***	***	5.2	1.3	***	Disk
Mrk 385	U	4.4	2.4	12.4	21.7	12.0	25.2	Bulge+Disk
	B	6.2	3.5	13.4	26.4	14.6	25.3	Bulge+Disk
	V	5.9	3.2	12.5	20.8	11.5	24.4	Bulge+Disk
	R	7.3	4.0	12.7	10.5	5.8	23.7	Bulge+Disk
	I	***	***	***	***	***	***	None
Mrk 1211	U	14.6	15.5	15.1	***	***	***	Bulge
	B	9.6	10.2	13.0	***	***	***	Bulge
	V	10.4	11.0	13.7	***	***	***	Bulge
	R	9.6	10.2	13.0	***	***	***	Bulge
Mrk 390	U	3.9	2.0	11.7	***	***	***	Bulge

Table 2.6 (continued)

Name	λ	r_e (arcsec)	r_e (kpc)	Bulge μ_0 (mag/arcsec^2)	r_d (arcsec)	r_d (kpc)	Disk μ_0 (mag/arcsec^2)	Class
(1)	(2)	(3)	(4)	(5)	(6)	(7)	(8)	(9)
	B	4.4	2.3	12.3	***	***	***	Bulge
	V	4.7	2.4	12.0	***	***	***	Bulge
	R	4.7	2.4	11.6	***	***	***	Bulge
Mrk 18	U	3.0	1.6	10.3	***	***	***	Bulge
	B	4.3	2.2	11.3	***	***	***	Bulge
	V	5.0	2.6	11.0	***	***	***	Bulge
	I	8.3	4.3	***	***	***	***	Bulge
Mrk 402	B	1.9	0.9	11.6	8.7	4.3	25.4	Bulge+Disk
	V	2.2	1.1	11.3	13.2	6.6	25.7	Bulge+Disk
	I	3.0	1.5	11.6	6.3	3.1	22.9	Bulge+Disk
IIZw 44	B	0.8	0.3	7.9	***	***	***	Bulge
	V	1.1	0.5	8.4	***	***	***	Bulge
	I	1.9	0.8	9.1	***	***	***	Bulge
Mrk 139	U	4.1	1.5	13.1	***	***	***	Bulge
	B	4.3	1.5	13.2	***	***	***	Bulge
	V	4.8	1.7	12.7	***	***	***	Bulge

Table 2.6 (continued)

Name	λ	r_e (arcsec)	r_e (kpc)	Bulge μ_0 (mag/arcsec^2)	r_d (arcsec)	r_d (kpc)	Disk μ_0 (mag/arcsec^2)	Class
(1)	(2)	(3)	(4)	(5)	(6)	(7)	(8)	(9)
	I	5.0	1.8	***	***	***	***	Bulge
Mrk 144	U	***	***	***	3.0	1.7	***	Disk
	B	***	***	***	3.4	1.9	***	Disk
	V	***	***	***	3.5	2.0	***	Disk
Mrk 33	U	3.6	0.4	10.9	***	***	***	Bulge
	B	5.2	0.6	11.9	***	***	***	Bulge
	V	5.4	0.6	11.5	***	***	***	Bulge
	I	8.0	0.9	11.5	***	***	***	Bulge
Mrk 148	U	8.5	4.2	14.7	***	***	***	Bulge
	B	8.8	4.3	14.3	***	***	***	Bulge
	V	8.7	4.3	13.4	***	***	***	Bulge
	R	7.3	3.6	12.8	***	***	***	Bulge
	I	9.9	4.9	12.7	***	***	***	Bulge
Haro 25	B	1.6	0.8	10.3	***	***	***	Bulge
	V	1.2	0.6	9.1	***	***	***	Bulge
Mrk 154	U	2.0	1.7	11.5	***	***	***	Bulge

Table 2.6 (continued)

Name	λ	r_e (arcsec)	r_e (kpc)	Bulge μ_0 (mag/arcsec^2)	r_d (arcsec)	r_d (kpc)	Disk μ_0 (mag/arcsec^2)	Class
(1)	(2)	(3)	(4)	(5)	(6)	(7)	(8)	(9)
	B	2.4	2.0	11.9	***	***	***	Bulge
	V	2.5	2.1	11.3	***	***	***	Bulge
	R	2.7	2.3	11.4	***	***	***	Bulge
	I	4.4	3.8	11.7	***	***	***	Bulge
Mrk 181	U	***	***	***	3.6	1.5	18.7	Disk
	B	***	***	***	3.8	1.6	19.0	Disk
	V	***	***	***	3.7	1.6	18.4	Disk
	R	***	***	***	3.7	1.6	18.0	Disk
	I	***	***	***	4.2	1.8	17.7	Disk
Haro 34	B	4.5	2.0	12.7	***	***	***	Bulge
	V	6.0	2.7	12.5	***	***	***	Bulge
	I	8.4	3.9	12.3	***	***	***	Bulge
Mrk 248	U	***	***	***	7.9	5.9	22.2	Disk
	B	***	***	***	7.9	5.9	22.0	Disk
	V	***	***	***	7.5	5.6	20.9	Disk
	R	***	***	***	6.5	4.9	20.2	Disk

Table 2.6 (continued)

Name	λ	r_e (arcsec)	r_e (kpc)	Bulge μ_0 (mag/arcsec^2)	r_d (arcsec)	r_d (kpc)	Disk μ_0 (mag/arcsec^2)	Class
(1)	(2)	(3)	(4)	(5)	(6)	(7)	(8)	(9)
	I	***	***	***	7.7	5.7	19.7	Disk
IZw 101	B	2.6	0.9	11.1	***	***	***	Bulge
	V	2.3	0.8	10.1	***	***	***	Bulge
	I	2.2	0.8	8.5	***	***	***	Bulge
Mrk 492	B	***	***	***	4.9	1.5	20.2	DoubeDisk
	B	***	***	***	8.2	2.5	22.4	DoubeDisk
	V	***	***	***	4.9	1.5	19.5	DoubeDisk
	V	***	***	***	9.2	2.8	22.0	DoubeDisk
Mrk 300	U	7.8	6.1	13.9	25.9	20.5	25.2	Bulge+Disk
	B	7.5	5.9	14.2	27.7	21.9	25.4	Bulge+Disk
	V	8.3	6.5	13.7	34.5	27.3	25.1	Bulge+Disk
	R	7.6	6.0	13.3	8.8	7.0	22.7	Bulge+Disk
	I	9.1	7.2	12.7	9.8	7.7	22.2	Bulge+Disk
Mrk 697	B	5.3	3.5	14.4	4.3	2.8	21.5	Bulge+Disk
	V	5.0	3.3	13.3	3.9	2.6	20.2	Bulge+Disk
Mrk499	U	1.7	0.9	10.0	***	***	***	Bulge

Table 2.6 (continued)

Name	λ	r_e (arcsec)	r_e (kpc)	Bulge μ_0 (mag/arcsec^2)	r_d (arcsec)	r_d (kpc)	Disk μ_0 (mag/arcsec^2)	Class
(1)	(2)	(3)	(4)	(5)	(6)	(7)	(8)	(9)
	B	2.0	1.1	10.6	***	***	***	Bulge
	V	2.2	1.2	10.5	***	***	***	Bulge
IZw 191	U	1.1	0.4	10.0	***	***	***	Bulge
	B	1.6	0.6	11.1	***	***	***	Bulge
	V	1.5	0.6	10.3	***	***	***	Bulge
	R	1.7	0.7	10.1	***	***	***	Bulge
IIZw 82	U	3.3	0.9	***	***	***	***	Bulge
	B	2.8	0.7	***	***	***	***	Bulge
	V	3.4	0.9	***	***	***	***	Bulge
Mrk 512	U	1.7	1.1	10.5	***	***	***	Bulge
	B	1.7	1.1	10.4	***	***	***	Bulge
	V	1.9	1.2	9.9	***	***	***	Bulge
	R	1.6	1.0	9.1	***	***	***	Bulge
Mrk 518	U	1.7	1.1	9.5	***	***	***	Bulge
	B	2.0	1.2	10.1	***	***	***	Bulge
	V	2.1	1.3	9.8	***	***	***	Bulge

Table 2.6 (continued)

Name	λ	r_e (arcsec)	r_e (kpc)	Bulge μ_0 (mag/arcsec^2)	r_d (arcsec)	r_d (kpc)	Disk μ_0 (mag/arcsec^2)	Class
(1)	(2)	(3)	(4)	(5)	(6)	(7)	(8)	(9)
	R	1.9	1.2	9.1	***	***	***	Bulge
Mrk 303	U	1.8	0.9	9.0	***	***	***	Bulge
	B	2.4	1.2	9.9	***	***	***	Bulge
	V	2.9	1.5	9.9	***	***	***	Bulge
	R	2.5	1.3	9.0	***	***	***	Bulge
Mrk 531	U	17.3	4.2	14.5	16.1	3.9	23.7	Bulge+Disk
	B	29.2	7.1	15.2	***	***	***	Bulge
	V	34.9	8.5	14.7	***	***	***	Bulge
	R	33.2	8.1	14.1	***	***	***	Bulge

Col. (1) Primary galaxy name, except now I have dropped the extensions saying if a companion or loop was incorporated in the photometry. However, these are in the same order as in Table 2.5, so any time I mentioned a neighbor or loop there, it will be consistent through the rest of the paper. Col (2) Wavelength of image. Col (3) The half light radius from the De Vaucouleurs law in measured in arcseconds. R_e is the radius of the isophote that encompasses half of the total light of the system. Col. (4) Same as column 3 but to a physical scale using distances from Table 2.1. Col. (5) Central intensity of the bulge like galaxies. Col. (6) The disk scale length for disk-like galaxies found using the exponential law, and measured in arcseconds. Col. (7) Same as column 6 but to a physical scale using distances from Table 2.1. Col. (8) Central intensity of the disk like galaxies. Col. (9) Classification of a galaxy after fitting with either a De Vaucouleurs law or exponential law.

2.5 Discussion

2.5.1 Surface Brightness Profiles

Kunth, Maurogordato, & Vigroux (1988) originally called the variety of morphologies and surface brightness profiles for the blue compact dwarf sample a "mixed bag." Kunth's BCG sample included irregular morphologies as well as more common cases with symmetric outer envelopes. Papaderos et al. (1996) agreed with the mixed bad assessment, but believed there was a basic correspondence between morphology and the various intensity distributions. In agreement with our own results, Papderos et al. (1996) found that blue compact dwarfs of the nE type, using the Loose and Thuan classification, were well described with a de Vaucouleurs law. Out of 13 galaxies classified as NE in our optical sample, 8 were bulge dominated. The bulge + disk galaxies do not have as much of a trend. Bulge + disk galaxies seem to average out as IE's, meaning some structure in the core, but an outer envelope is easily distinguished from the rest of the galaxy. The disk galaxies leaned more toward an iI classification, or irregular inner and outer isophotes. Of the disk dominated galaxies only 1 was an nE, and the rest were either iE or iI. From this analysis it appears that as galaxies go from bulge dominated, to a bulge + disk, then finally to disk, the morphology gets more and more irregular.

What remnant is the ultimate result of a major merger? Struck (2006) states that ultraluminous infrared galaxies could be the missing link in Toomres theory for the

formation of elliptical galaxies, first proposed in the 1970s. Toomre suggested that the remnants of disk mergers could account for the population of elliptical galaxies in the universe (Toomre 1972). Much like LBCGs, ULIRGs are thought to be local analogs to the high-z population of high star forming galaxies. ULIRGs are commonly recent mergers with ample star formation ($\sim$176 $M_{\odot}$/yr), and they could eventually consume or heat and disperse the gas. We are positing that a portion of the LBCGs are descendants of ULIRGS, in which the SFR has perhaps declined from a peak in the ULIRG range, and the blue light is produced by the B and A stars formed during several tens of millions of years of previous star formation. When fitting the profiles of high luminosity ULIRGs, Masegosa & Marquez (2003) found that 43% were represented by a spheroid, 23% by an exponential disk, and for the rest a good fit could not be obtained. The results agreed with Veilleux, Kim, & Sander (2002) who found that ULIRGS were better represented by a de Vaucoleurs law. Dasyra et al. (2008) stated that even though mergers are important in ULIRGs at a redshift of 2, the remnant galaxies have disk-like profiles, but local ULIRG remnants are mainly bulge-dominated. Of the galaxies we were able to fit 60% (22/36) were spheroidal, 20% (7/36) were disk, and 20% (7/36) were a combination, which agree with previous results. ULIRGs have high star formation rates and high central gas densities (Sanders et al. 1986), therefore ULIRGs meet the conditions for dissipative mergers (Soto & Martin 2010). Much like the ULIRGs, LBCGs have high central gas density and star formation, just not as extreme. The fact that ULIRGs have similar stellar kinematics

and surface brightness profiles to elliptical galaxies, further makes the point that ULIRGs are in the transition point between mergers and elliptical galaxies (Genzel et al. 2001). In the ULIRG phase the gas mass is much higher than that of an elliptical galaxy, possibly meaning that LBCGs could be an in between stage. The amount of gas blown away by stellar feedback in ULIRGs is not fully known, but half or more is likely consumed by star formation (Soto &Martin 2010). We believe this process of gas being blown away, allowing more and more UV to be shown through the IR, is possibly the LBCG stage. The LBCGs that do not show bulge structure are possible candidates to be the LBCGs that have a starburst on top of an older population, possibly triggered by an interaction. However, there are example of disk galaxies that are in the process of interacting, such as Haro 15.

Figures 2.4 and 2.5 show the effective radius and disk scale length of the bulge and disk component fits respectively. Figure 2.6 shows the relation between the central intensity of the bulges to the B−V colors of the galaxies. We also made plots showing the relation between r_e and r_d to color, but no correlations were visible so they are not shown here. Likewise, no relations were visible when we plotted the individual UBVR&I bands against r_e, r_d, and central intensity. The positive correlation in Figure 2.6 means the bluer galaxies have higher central intensities. Luminous blue compact galaxies have bright blue cores and a lot of star formation concentrated at the center.

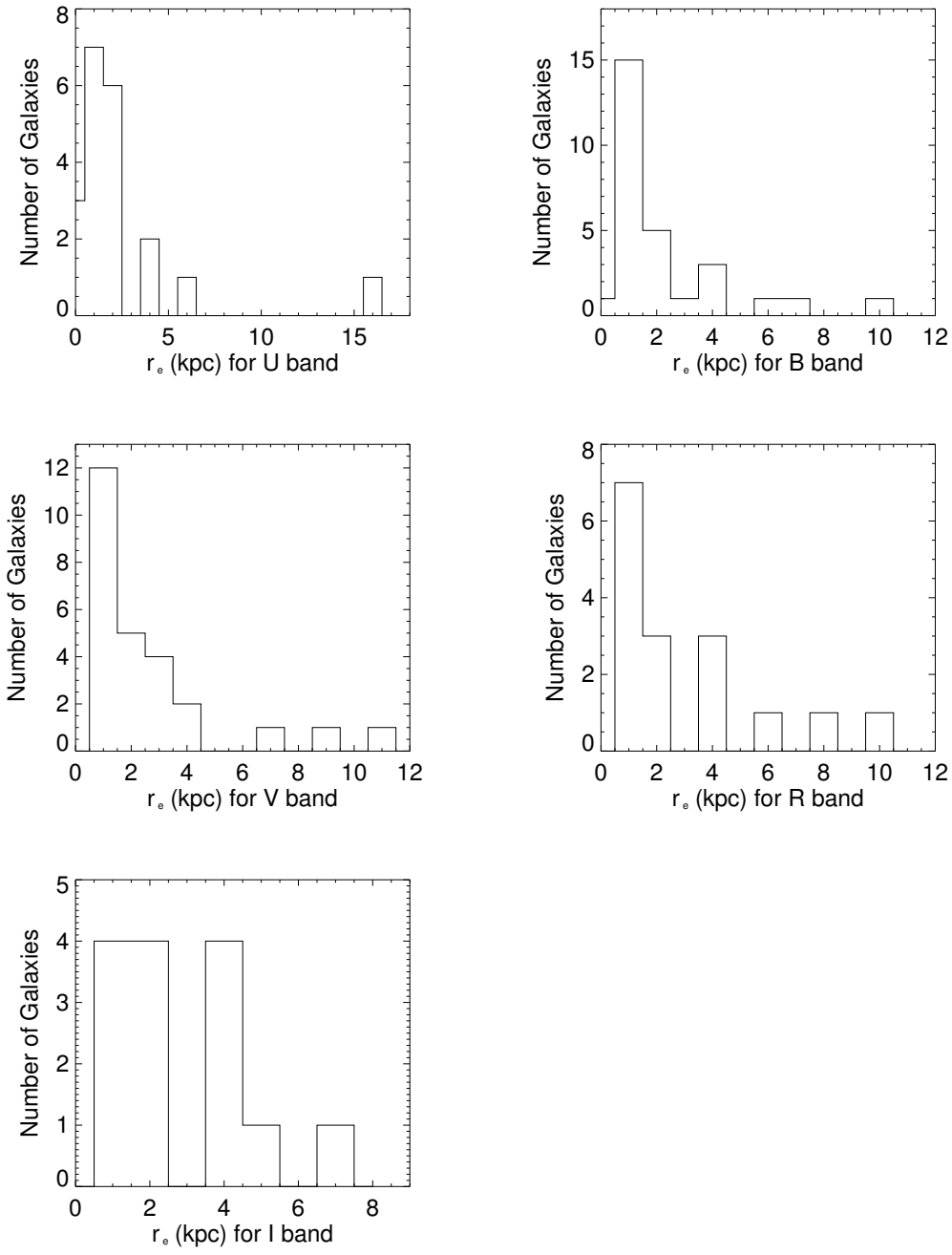

Figure 2.4: Distributions of derived bulge effective radius, r_e, in kiloparsecs as a function of wavelength. Sections of the observed light distributions which matched an $r^{(1/4)}$ radial decline were fit and the resulting effective radii in arcseconds were converted to physical sizes using the distances in Table 2.1.

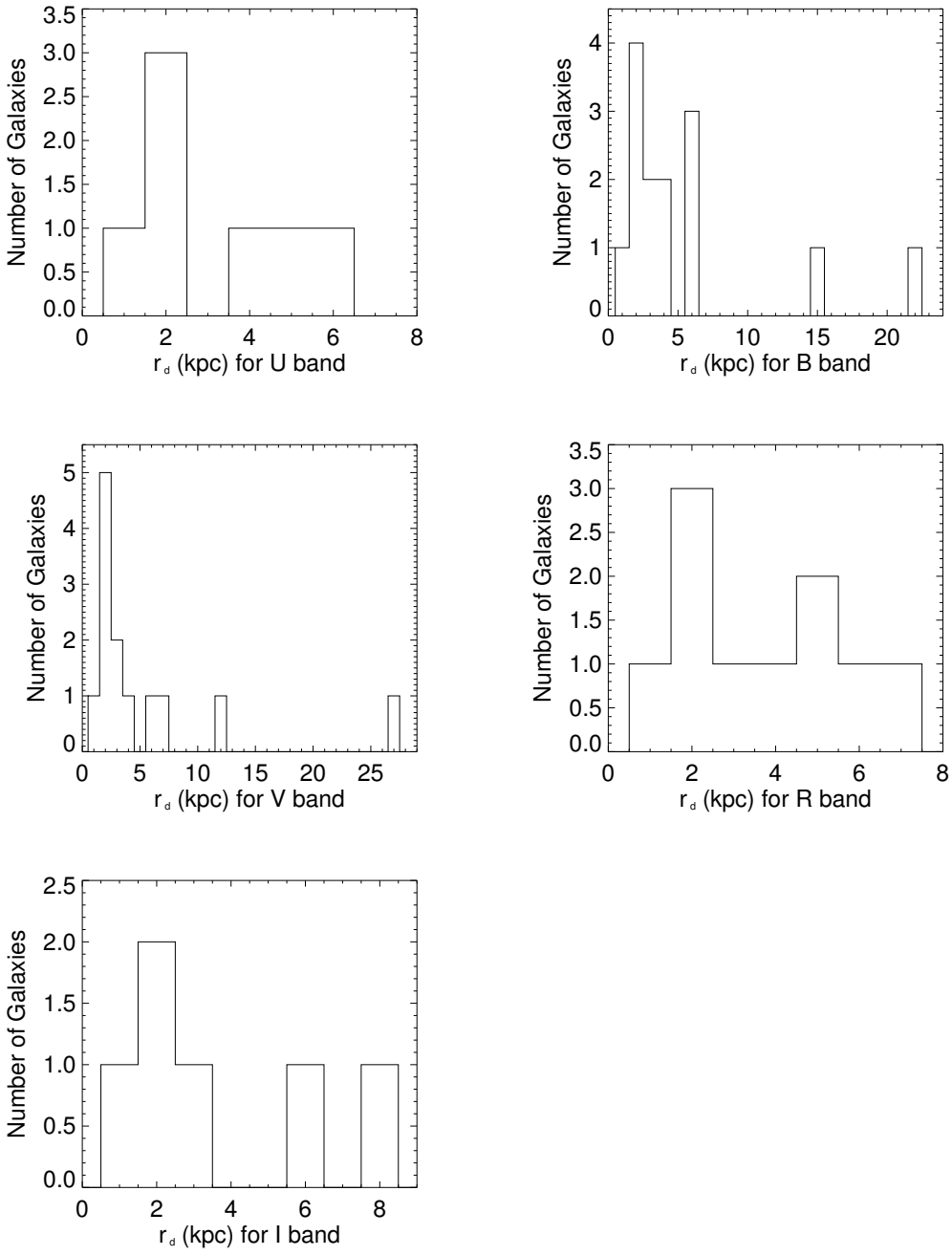

Figure 2.5: Distributions of derived disk scale length, r_d, in kiloparsecs as a function of wavelength. Sections of the observed light distributions which matched an r radial decline were fit and the resulting effective radii in arcseconds were converted to physical sizes using the distances in Table 2.1.

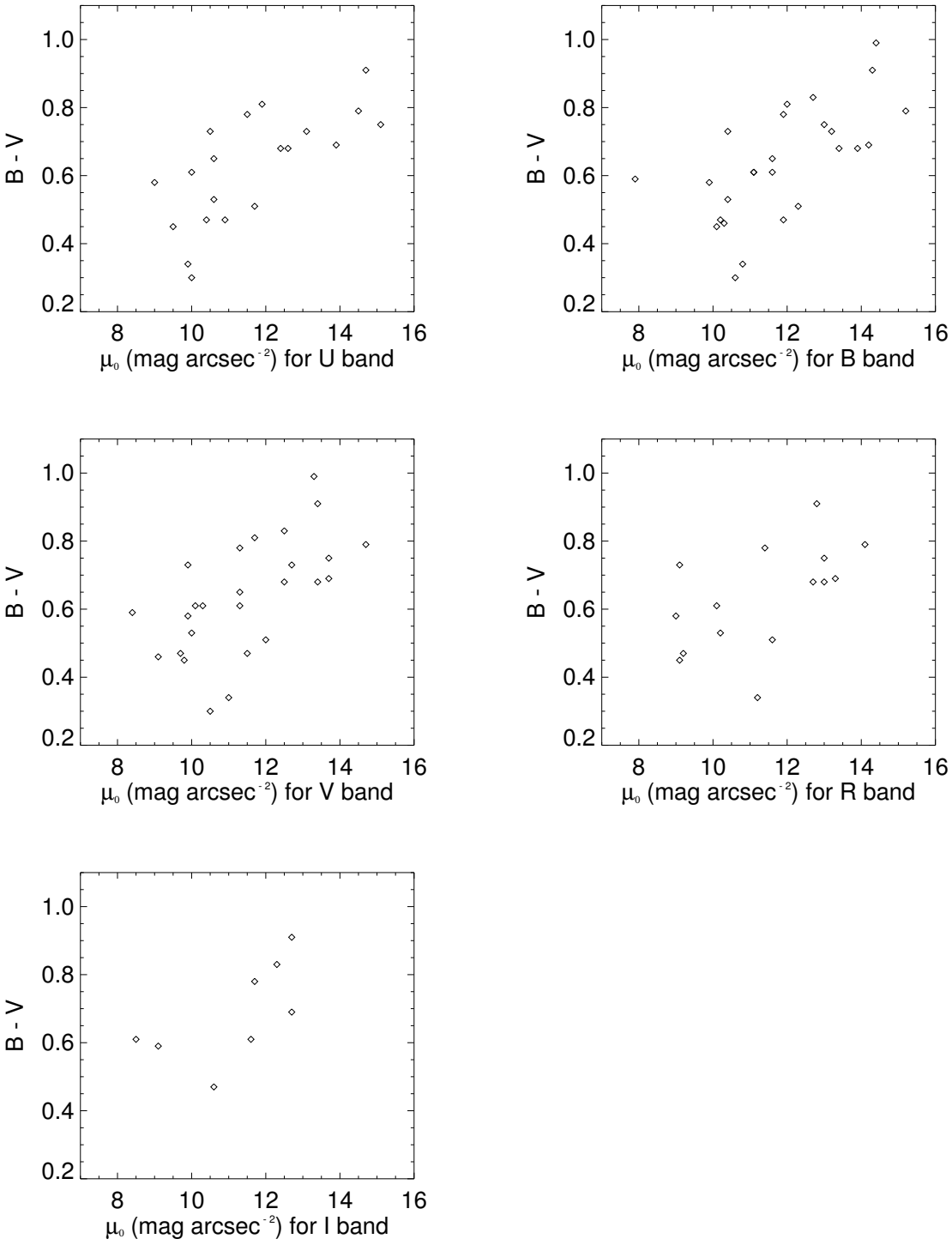

Figure 2.6: Modeled bulge central surface brightness plotted against the integrated B−V color.

2.5.2 Color Profiles

Color profiles were created by a subtraction of curves from different bands in the surface brightness profiles. For example, to get the B−V profiles the V curve was simply subtracted from B curve. The color profiles are in Figure 2.3. The color profile shapes fell into 6 categories. The histograms in Figure 2.7 show the six different categories and their B−V colors. The only category not shown is where the color profile is flat, then turns down; it is not shown because only one galaxy, Mrk 1211, fits this type. The bluest galaxies are the ones that have a mostly flat, or flat and then begin to turn positive, slope. More than likely these 2 shapes are the bluest because a galaxy will appear bluer if it is blue throughout most of the galaxy, not just the central core. Galaxies with a flat profile show a distributed starburst that dominates the galaxy; these galaxies are truly transforming themselves. An elliptical galaxy is typically going to have a flat red profile, the fact that some of our elliptical galaxies have flat blue profiles is really unusual. Some of our elliptical galaxies are not old systems that are no longer forming stars, they are transforming themselves. A profile that rises then flattens out has a blue core, or central starburst, then flattens out into a mean color. A profile that is redder in the middle, then turns blue is a sign of a spiral galaxy. Hα can cause the center of a galaxy to look red. On the flip side, a profile that is blue in the middle and then reddens is a central starburst. A dip to the blue from red, and then back to red, likely indicates a blue ring. Perturbed galaxies have a circumnuclear ring of star formation which shows up best in UV or

blue bands. A central blue color marks a blue-core galaxy, with a strong nuclear starburst in an otherwise normal galaxy. Blue-core galaxies would have an upturn to the blue at small radii. One of the most scientifically interesting questions regarding LBCGs are the presence of blue bulges, i.e., spheroidal components whose integrated colors are $(B-V) < 0.6$. A blue bulge dominated galaxy will have a bulge dominated surface brightness profile and a blue core. The blue cores can be found by looking at the color profiles. Sometimes the overall color of the galaxy may not be below 0.6, but the core could be. Twelve of our galaxies in our optical sample fit both of these criteria: Mrk 364, Mrk 366, Mrk 589, Mrk 1404, Mrk 385, Mrk 390, IIZw 44, Mrk 33, Haro 25, Mrk 499, IZw 191, and Mrk 512. Also interesting was Haro 15 and Mrk 181, which had flat blue profiles, but it was not because of a blue bulge, but because of intense interactions.

2.6 Integrated Magnitudes and Colors

With the use of surface brightness profiles and growth curves, magnitudes were calculated for each galaxy. With the use of the surface brightness profile first, the radius was defined for each object as where the B-band surface brightness reached 25 magnitudes per square arcsecond. A linear interpolation was used to find the radius as exact as possible. Once the galaxy radius was found a linear interpolation could be done for each filter on the growth curve in order to find the integrated magnitude for each galaxy in each filter. Table 2.7 shows the corrected apparent magnitudes,

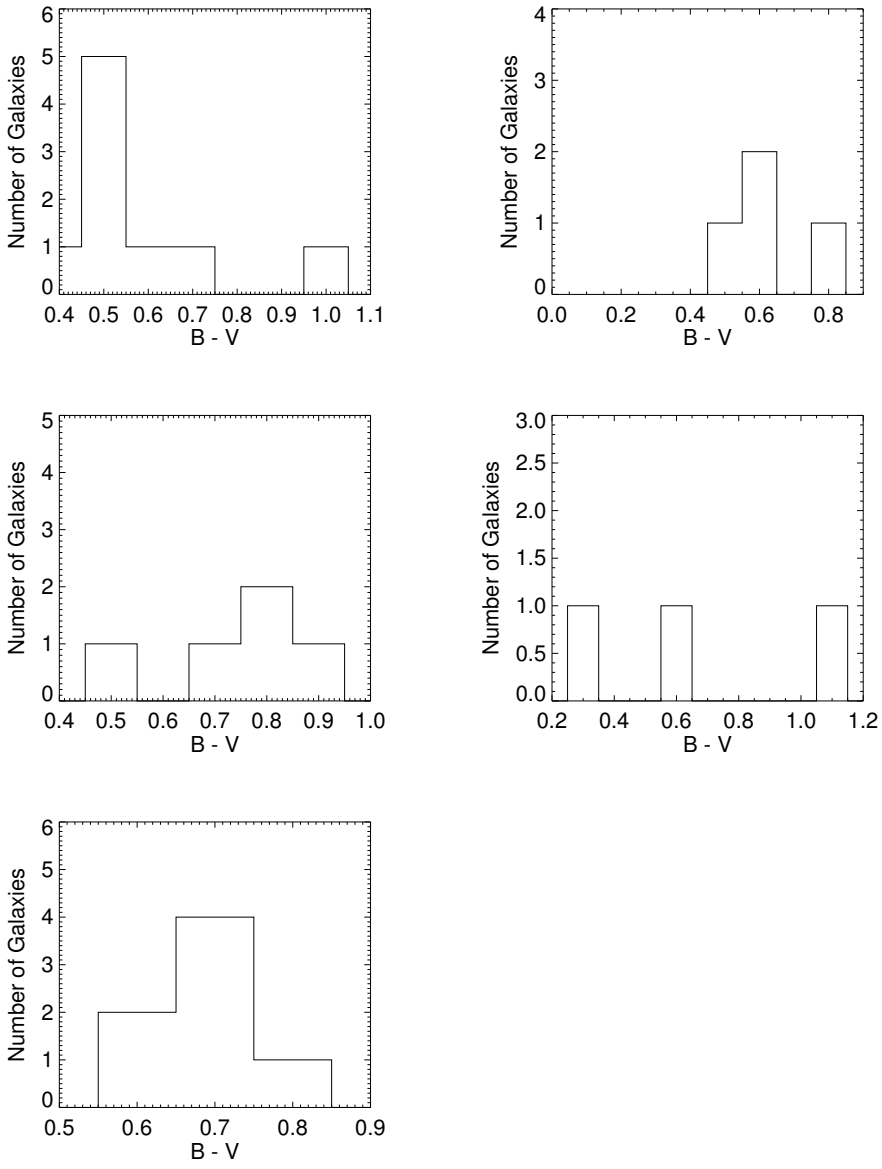

Figure 2.7: Distribution of color profile shapes as a function of integrated source (B−V) color: (1) Straight color profiles in upper left (2) Straight then positive slope color profiles upper right (3) Positive slope then straight color profiles middle left (4) negative slope then straight color profiles middle right (5) Initial dip then straightening out color profiles bottom left

extinction corrections, and the absolute magnitudes for each filter. The apparent magnitudes were found with the method described above, and then turned into absolute magnitudes using the distances from Table 2.1. Note that the magnitudes have already been extinction corrected before insertion into the table. NC represents not calibratable, and *** means that no data was taken. For six galaxies in Table 2.7 we do not provide integrated magnitudes because either we were unable to derive a photometric calibration for them (Mrk 1079, 144, 325, and IIZw 82), or there was no B data available to use to find the radius of the galaxy(Mrk 1184 and 271). Table 2.8 lists the B−V, V−R, and U−B colors.

The errors in the magnitudes calculated at the cutoff radius of the galaxies (where the SBP reached a surface brightness of 25 magnitudes per square arcsec) came from 2 different sources. For the objects calibrated with the use of photometric standard stars, the error came from a combination of the error from the linear least squares fit used during calibration, and the magnitude error derived using 3 sources of error added in quadrature. Error 1 is the random noise inside the sources's aperture, including readout noise and the degree of contamination by nearby sources, as estimated by the scatter in the sky values. Error 2 is the Poisson statistics of the observed brightness. Error 3 is the uncertainty of the mean sky brightness. For the objects calibrated using stars from SDSS, the error came from two sources. First the instrumental magnitude was plotted against the "true" magnitudes for all stars in a specified filter and the error was determined based on the residual between the fitted

line and the measured values. The second error is the magnitude error calculated the same as above using errors 1, 2, and 3. The average errors for the observed magnitudes in the U, B, V, R, and I bands are$\pm$ 0.04, 0.02, 0.02, 0.02, and 0.02 respectively. To find the uncertainties in the colors, rules of error propagation were used, and the results are 0.04, 0.03, and 0.03 for B$-$V, V$-$R, and U$-$B respectively.

A noteworthy find from the galaxy color measurements was a relation between galaxy interactions and B$-$V color. Of the top 30% bluest galaxies (15 in the sample), 9 showed a sign of interaction, companions, or a clear merger. Indeed the bluest galaxies seem to be formed by interactions. The 6 of 15 bluest galaxies that do not show signs of interaction could have accreted a dwarf companion, or there could be a gaseous halo that is accreting at a steady and relatively high rate. In order to be a blue galaxy with a lot of star formation, it is not necessary for an interaction or merger to be taking place. On the flip side, when looking at the top 30% reddest galaxies in our optical sample, 11 of 15 showed signs of interaction or a merger, and 4 of 15 were isolated.

We also noticed that a handful of the galaxies did not have the blue color we expected from a galaxy that made these surveys used to select the sample. We did not, a priori, know the colors of the optical galaxy sample. We knew that they exhibited a blue or UV excess in their low-resolution spectra, and we excluded all systems known to harbor an active nucleus. Only Mrk 1211 turned out to have spectroscopic evidence for an AGN. We did not expect all of the observed systems to

have global blue colors, because some of them would be expected to host a nuclear starburst or post-burst stellar population - producing the blue excess, but not causing the global color to be remarkably blue. The inclusion of the latter galaxies, or what could be termed "blue core" systems is not anamolous. These systems are interesting in their own regard, and some of them could be aged LBCGs.

Table 2.7. Integrated Photometric Properties

Name	U	B	V	R	I	A_u	A_b	A_v	A_r	A_i	M_U	M_B	M_V	M_R	M_I
(1)	(2)	(3)	(4)	(5)	(6)	(7)	(8)	(9)	(10)	(11)	(12)	(13)	(14)	(15)	(16)
Mrk 342	16.52	16.50	15.69	***	NC	0.40	0.31	0.24	0.19	0.14	-19.40	-19.41	-20.23	***	NC
Haro 15	13.61	14.09	13.83	NC	NC	0.13	0.10	0.08	0.06	0.05	-21.08	-20.60	-20.86	NC	NC
Mrk 360	14.44	14.68	14.31	13.95	NC	0.37	0.29	0.22	0.18	0.13	-20.78	-20.54	-20.90	-21.27	NC
Mrk 364	15.18	15.23	14.70	14.26	NC	0.44	0.35	0.27	0.22	0.16	-20.06	-20.02	-20.55	-20.99	NC
Mrk 366	14.84	14.91	14.23	13.80	NC	0.48	0.38	0.29	0.24	0.17	-20.35	-20.28	-20.96	-21.39	NC
Mrk 366	14.82	14.87	14.20	13.76	NC	0.48	0.38	0.29	0.24	0.17	-20.37	-20.32	-20.99	-21.43	NC
Mrk 367	***	15.54	***	***	***	0.52	0.42	0.32	0.26	0.19	***	-20.36	***	***	***
Mrk 589	14.22	14.44	14.10	13.53	NC	0.23	0.18	0.14	0.11	0.08	-19.12	-18.91	-19.25	-19.81	NC
Mrk 1404	14.79	14.65	14.17	13.70	***	0.41	0.33	0.25	0.20	0.15	-21.03	-21.18	-21.65	-22.12	***
Mrk 1094	13.81	14.31	13.88	***	13.18	0.57	0.45	0.35	0.28	0.20	-19.06	-18.56	-18.99	***	-19.68
Mrk 8	13.76	14.13	13.67	***	NC	0.14	0.11	0.09	0.07	0.05	-19.87	-19.49	-19.95	***	NC
Haro 1	12.34	12.71	12.29	11.83	NC	0.23	0.18	0.14	0.11	0.08	-21.29	-20.92	-21.34	-21.80	NC

Table 2.7 (continued)

Name	U	B	V	R	I	A_u	A_b	A_v	A_r	A_i	M_U	M_B	M_V	M_R	M_I
(1)	(2)	(3)	(4)	(5)	(6)	(7)	(8)	(9)	(10)	(11)	(12)	(13)	(14)	(15)	(16)
Mrk 385	15.10	15.26	14.57	14.26	13.52	0.17	0.13	0.10	0.08	0.06	-20.19	-20.03	-20.72	-21.03	-21.77
Mrk 385	15.05	15.19	14.54	14.21	13.49	0.17	0.13	0.10	0.08	0.06	-20.24	-20.10	-20.75	-21.08	-21.79
Mrk 1211	15.13	15.10	14.35	13.85	***	0.18	0.14	0.11	0.09	0.06	-21.56	-21.59	-22.34	-22.84	***
Mrk 390	14.75	15.09	14.58	14.21	13.40	0.22	0.18	0.14	0.11	0.08	-20.37	-20.03	-20.54	-20.91	-21.72
Mrk 18	14.34	14.42	13.77	***	NC	0.23	0.19	0.14	0.11	0.08	-19.11	-19.03	-19.68	***	NC
Mrk 402	***	15.71	15.10	***	14.64	0.11	0.09	0.07	0.05	0.04	***	-19.35	-19.96	***	-20.42
IIZw 44	***	15.29	14.70	***	13.73	0.12	0.10	0.08	0.06	0.04	***	-19.37	-19.96	***	-20.93
Mrk 139	15.34	15.41	14.68	***	NC	0.06	0.05	0.04	0.03	0.02	-19.00	-18.93	-19.66	***	NC
Mrk 33	13.24	13.57	13.10	***	12.33	0.06	0.05	0.04	0.03	0.02	-18.68	-18.35	-18.82	***	-19.59
Mrk 148	16.19	15.84	14.93	14.69	13.99	0.10	0.08	0.06	0.05	0.04	-18.84	-19.20	-20.11	-20.34	-21.04
Haro 25	***	14.87	14.41	***	***	0.18	0.14	0.11	0.09	0.06	***	-20.26	-20.72	***	***
Mrk 154	15.77	15.67	14.89	14.73	14.01	0.08	0.06	0.05	0.04	0.03	-20.44	-20.54	-21.33	-21.48	-22.20

Table 2.7 (continued)

Name	U	B	V	R	I	A_u	A_b	A_v	A_r	A_i	M_U	M_B	M_V	M_R	M_I
(1)	(2)	(3)	(4)	(5)	(6)	(7)	(8)	(9)	(10)	(11)	(12)	(13)	(14)	(15)	(16)
Mrk 171	***	12.27	11.81	***	***	0.09	0.07	0.05	0.04	0.03	***	-21.09	-21.55	***	***
Mrk 181	14.18	14.29	13.79	13.35	12.85	0.14	0.11	0.09	0.07	0.05	-20.51	-20.39	-20.90	-21.34	-21.84
Haro 34	***	15.07	14.24	***	NC	0.22	0.18	0.14	0.11	0.08	***	-19.80	-20.63	***	NC
Mrk 54	***	14.86	14.60	14.26	13.90	0.08	0.06	0.05	0.04	0.03	***	-21.50	-21.76	-22.11	-22.46
Mrk 238	15.15	15.04	14.29	13.72	***	0.09	0.07	0.06	0.05	0.03	-21.44	-21.54	-22.30	-22.87	***
Mrk 248	15.77	15.61	14.48	13.93	13.21	0.10	0.08	0.06	0.05	0.04	-20.16	-20.32	-21.45	-22.00	-22.72
Mrk 248	14.97	14.88	13.86	13.30	12.66	0.10	0.08	0.06	0.05	0.04	-20.96	-21.05	-22.07	-22.63	-23.27
Mrk 255	***	15.83	15.32	***	14.68	0.09	0.07	0.05	0.04	0.03	***	-19.71	-20.22	***	-20.86
Haro 42	14.41	14.84	14.40	***	***	0.08	0.06	0.05	0.04	0.03	-19.64	-19.22	-19.66	***	***
IZw 101	***	15.07	14.46	***	13.11	0.10	0.08	0.06	0.05	0.04	***	-19.21	-19.82	***	-21.17
Mrk 492	***	14.51	13.80	***	***	0.28	0.22	0.17	0.14	0.10	***	-19.47	-20.18	***	***
Mrk 297	12.89	13.27	12.90	12.52	***	0.41	0.33	0.25	0.20	0.15	-21.29	-20.91	-21.28	-21.66	***

Table 2.7 (continued)

Name	U	B	V	R	I	A_u	A_b	A_v	A_r	A_i	M_U	M_B	M_V	M_R	M_I
(1)	(2)	(3)	(4)	(5)	(6)	(7)	(8)	(9)	(10)	(11)	(12)	(13)	(14)	(15)	(16)
Mrk 300	14.83	15.17	14.48	14.27	13.34	0.28	0.23	0.17	0.14	0.10	-21.23	-20.89	-21.58	-21.79	-22.72
Mrk 697	***	15.93	14.94	***	***	0.21	0.17	0.13	0.10	0.08	***	-19.75	-20.74	***	***
Mrk 499	14.63	14.80	14.49	***	***	0.09	0.07	0.05	0.04	0.03	-20.60	-20.43	-20.74	***	***
IZw 191	15.40	15.55	14.94	14.43	***	0.10	0.08	0.06	0.05	0.04	-19.23	-19.08	-19.69	-20.20	***
Mrk 512	15.04	15.06	14.34	13.93	***	0.43	0.34	0.26	0.21	0.15	-20.60	-20.57	-21.30	-21.71	***
Mrk 518	14.00	14.14	13.69	13.29	***	0.50	0.40	0.31	0.25	0.18	-21.57	-21.42	-21.88	-22.27	***
Mrk 303	14.43	14.54	13.96	13.47	***	0.28	0.22	0.17	0.14	0.10	-20.69	-20.57	-21.16	-21.65	***
Mrk 306	14.01	14.35	13.93	13.60	***	0.31	0.25	0.19	0.15	0.11	-20.48	-20.14	-20.56	-20.89	***
Mrk 306 and 305	13.87	14.18	13.73	13.40	***	0.31	0.25	0.19	0.15	0.11	-20.61	-20.30	-20.75	-21.08	***
IZw 185	14.00	14.39	***	13.62	***	0.33	0.26	0.20	0.16	0.12	-21.01	-20.62	***	-21.38	***
Mrk 531	13.78	13.71	12.92	12.39	***	0.22	0.18	0.14	0.11	0.08	-19.71	-19.78	-20.58	-21.10	***

Col. (1) Primary galaxy name, except now I have dropped the extensions saying if a companion or loop was incorporated in the photometry. However, these are in the same order as in Table 2.5, so any time I mentioned a neighbor or loop there, it will be consistent through the rest of the paper. Cols. (2-6) Observed extinction corrected magnitudes. Cols. (7-11) The extinction corrections (Burstein & Heiles 1982). Cols. (12-16) Absolute magnitudes calculated using the distances in Table 2.1 and $H_0 = 73$.

Table 2.8. Galaxy Colors

Name	$B-V$	$V-R$	$U-B$
(1)	(2)	(3)	(4)
Mrk 342	0.81	1.47	0.01
Haro 15	0.26	***	-0.48
Mrk 360	0.37	0.36	-0.24
Mrk 364	0.53	0.44	-0.05
Mrk 366	0.68	0.43	-0.07
Mrk 366	0.67	0.44	-0.05
Mrk 367	***	0.00	***
Mrk 589	0.34	0.57	-0.22
Mrk 1404	0.47	0.47	0.14
Mrk 1094	0.43	***	-0.50
Mrk 8	0.46	***	-0.38
Haro 1	0.42	0.46	-0.37
Mrk 385	0.68	0.31	-0.15
Mrk 385	0.65	0.34	-0.15
Mrk 1211	0.75	0.51	0.03
Mrk 390	0.51	0.37	-0.34
Mrk 18	0.65	***	-0.08
Mrk 402	0.61	***	***

Table 2.8 (continued)

Name	$B-V$	$V-R$	$U-B$
(1)	(2)	(3)	(4)
IIZw 44	0.59	***	***
Mrk 139	0.73	***	-0.07
Mrk 33	0.47	***	-0.33
Mrk 148	0.91	0.24	0.36
Haro 25	0.46	***	***
Mrk 154	0.78	0.16	0.10
Mrk 171	0.46	***	***
Mrk 181	0.51	0.44	-0.12
Haro 34	0.83	***	***
Mrk 54	0.26	0.34	***
Mrk 238	0.76	0.57	0.10
Mrk 248	1.12	0.55	0.17
Mrk 248	1.02	0.56	0.09
Mrk 255	0.51	***	***
Haro 42	0.44	***	-0.43
IZw 101	0.61	***	***
Mrk 492	0.71	***	***
Mrk 297	0.37	0.38	-0.38

Table 2.8 (continued)

Name	$B-V$	$V-R$	$U-B$
(1)	(2)	(3)	(4)
Mrk 300	0.69	0.21	-0.34
Mrk 697	0.99	***	***
Mrk 499	0.30	***	-0.17
IZw 191	0.61	0.51	-0.15
Mrk 512	0.73	0.41	-0.03
Mrk 518	0.45	0.39	-0.14
Mrk 303	0.58	0.50	-0.11
Mrk 306	0.42	0.33	-0.34
Mrk 306 and 305	0.45	0.33	-0.31
IIZw 185	***	***	-0.39
Mrk 531	0.79	0.53	0.07

Col. (1) Primary galaxy name. Col (2) The B−V color found using the magnitudes from Table 2.7. Col (3) The V−R color found using the magnitudes from Table 2.7. Col. (4) The U−B color found using the magnitudes from Table 2.7.

2.7 Hα Imaging

The Hα emission line is a red line created by hydrogen at a wavelength of 6562.8$\mathring{A}$ for galaxies with zero redshift. For our sample, the observed wavelength is shifted according to each objects's redshift, with the largest shift over 400$\mathring{A}$. A set of narrow-band filters is used to observe selected objects in that piece of the spectrum ($\sim$100$\mathring{A}$ wide) in which the redshifted line falls. The Hα images can be used to trace ionized gas in our LBCG sample. High star formation regions have multitudes of massive O and B stars which ionize the surrounding hydrogen. LBCGs total luminosities and colors suggest that the more extreme galaxes could hold from 10^5 to 10^6 massive (OB) stars that formed within the last 10-20 Myr (Fanelli et al 204). O and B stars only appear in areas of new star formation because of their short lives; having masses greater than 16 solar masses and 3-16 solar masses (1 solar mass = $2x10^{30}$kg) respectively causes faster fuel depletion. The lifetimes of main sequence stars range from a million years for a 40$M_\odot$ O-type star, to 560 billion years for a 0.2$M_\odot$ M-type star.

The Hα images are reduced the same as the UBVRI images up until the coadd process. The Hα images are coadded, but the process was a little different. The Hα images are aligned with R band images so that a continuum-subtracted image showing only Hα emission will remain. Once the R band and Hα images are aligned, stars are identified for flux-scaling. Once the flux of the selected stars in the R band images are scaled to match the same stars in the Hα image, the R band image will be

subtracted from the Hα image. The result is a continuum subtracted image, and the flux that remains is Hα emitting gas that is intrinsic to the galaxy, with all foreground stars removed. Figure 2.8 shows the Hα images with a color table (black to orange is high to low flux) wrapped once and Gaussian smoothing with a kernel of 0.5. The top scale bar represents 5 arcseconds, and the bottom scale bar represents 5 kpc.

Continuum subtracted Hα images are useful in photometry. Before isophotes are mapped onto a broad band image, all of the foreground stars must be removed. Continuum subtracted Hα images help discern what objects belong to the galaxy, and which are foreground; only starbursting parts of the galaxy will show up in a continuum subtracted Hα image. If the Hα images were to be calibrated, then the flux values could be used to calculate star formation rates. Conversion between ionizing flux and star formation rates is usually computed with an evolutionary synthesis model. Only stars with masses greater than 10 $M_{\odot}$ and lifetimes less than 20 Myr contribute in any real way to the ionizing flux. Therefore, emission lines provide an instantaneous measure of the SFR. Calibrations have been published by many authors including Kennicutt (1983), Gallagher et al (1984), Kennicutt (1994), and Leitherer & Heckman (1995). Kennicutt (1998) published a relation between the SFR and Hα luminosity based on a Salpeter IMF (0.1 - 100 $M_{\odot}$) and calibrations from Kennicutt et al (1994) and Madau et al (1998).

The Hα images were not taken on the evenings that were both photometric and had sufficient standard images to calibrate with. Therefore we could not do our

standard calibration procedure. The Sloan bootstrap method used on a fraction of the optical band images was also not a possible route to calibration since the Sloan viewing tool does not provide Hα measurements to use for a calibration. Calibrations could be attempted using Sloan spectra, R-band images, or bootstrapping using data straight from the literature. Despite not calibrating, the Hα images are quite detailed and appear to have been taken under good seeing.

The Hα emission in the images from Figure 2.8 show star formation signatures not only in the galaxy cores (or sometimes more than one core for pairs of galaxies), but also in interaction features such as bridges and tails. For example, Hα tracers from the star formation in the tail north of Mrk 181 are easily seen. Many times interacting or merging galaxies will disturb the surrounding gas and dust enough that star formation is triggered. Every galaxy that was viewed with an Hα filter showed Hα, there were no instances of an object that was viewed and showed no Hα emission.

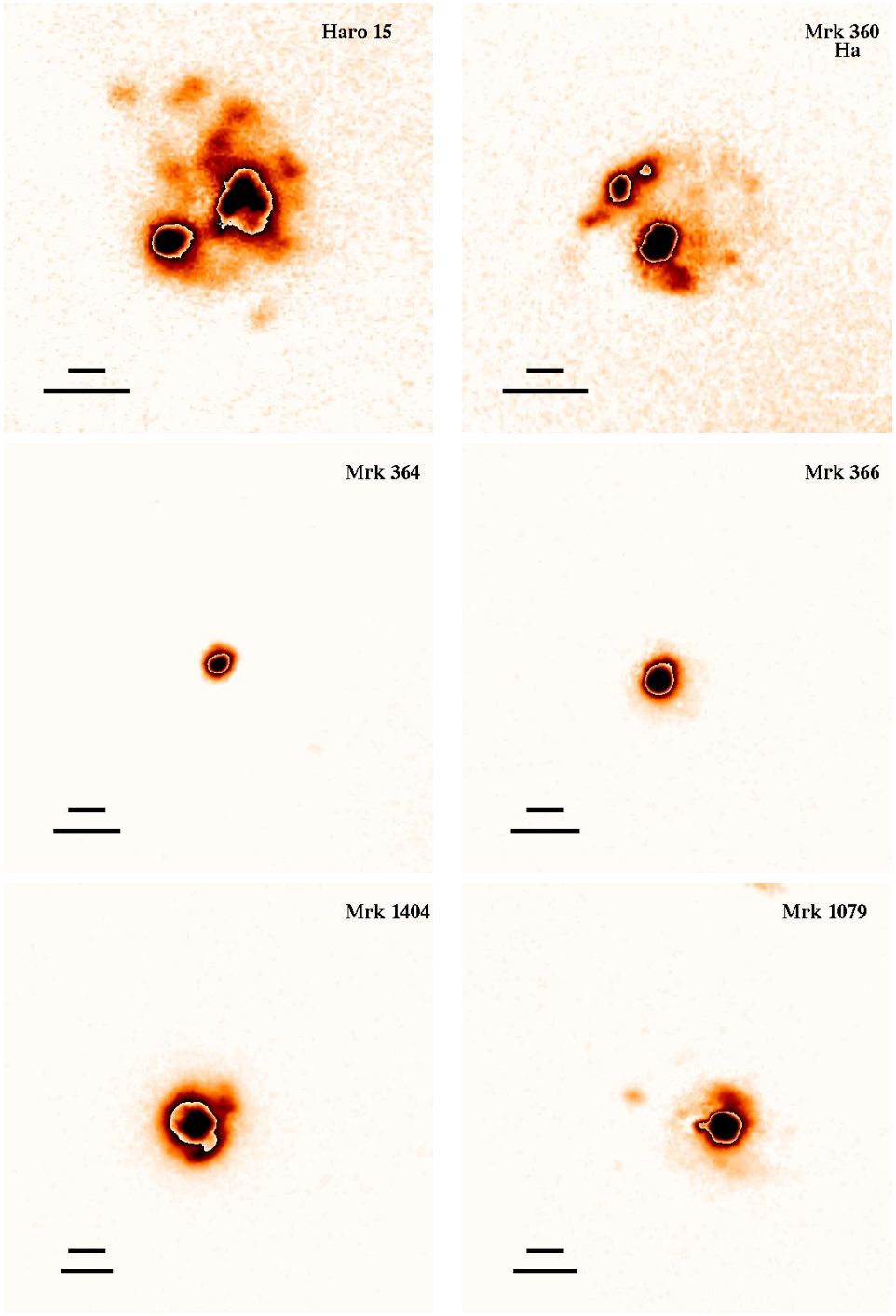

Figure 2.8: Narrow-band Hα images for the McDonald sample: 1 $\times$ 1 arminute images with the top scale bar showing 5 arcseconds, and the bottom showing a physical scale of 5 kpc at the adopted distance (see Table 2.1). Darker to lighter colors (black to orange) show higher to lower intensity. The color table is wrapped once to show more detail in the galaxy. The images are not calibrated. North is up, east is to the left. Images have been Gaussian smoothed.

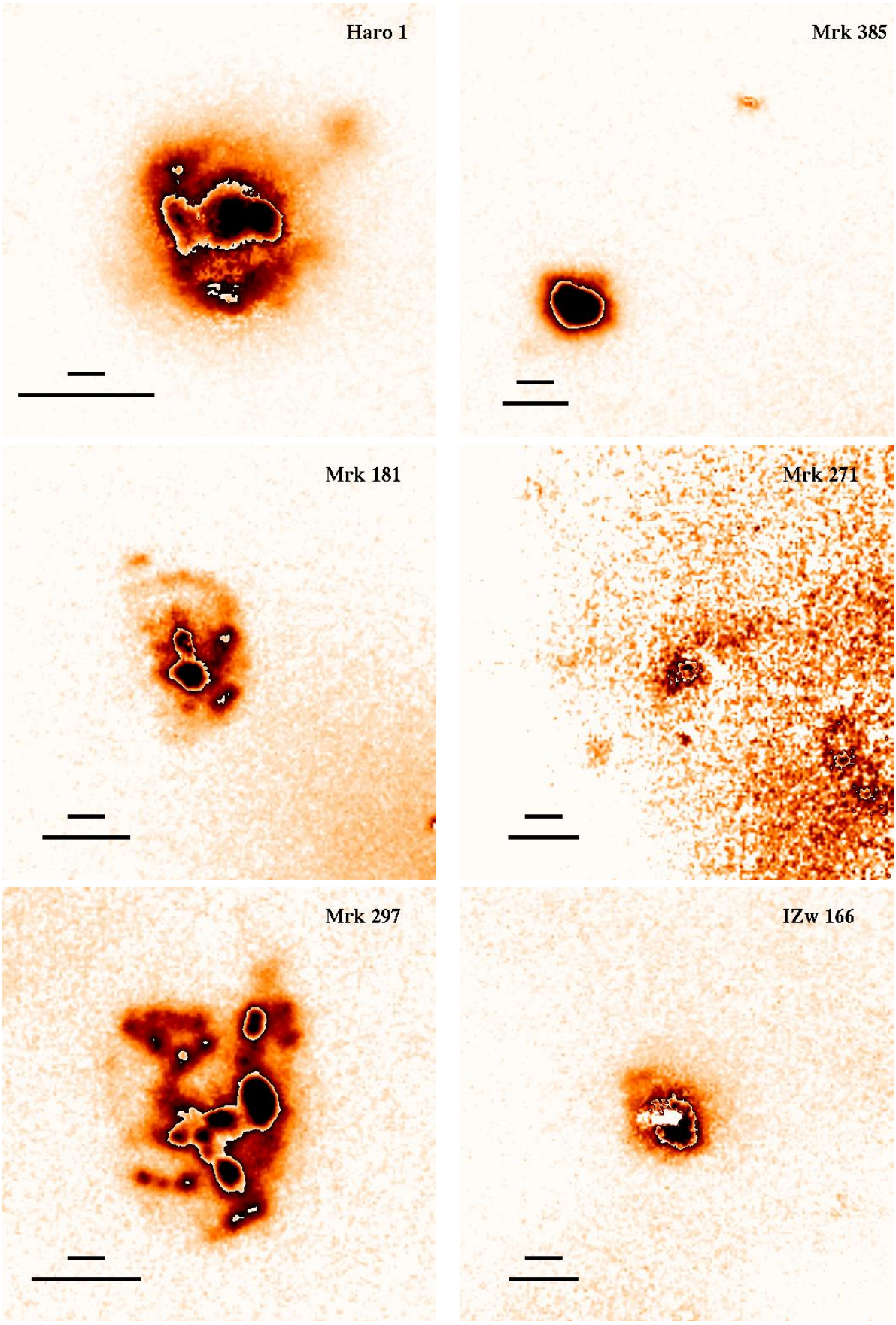
Haro 1
Mrk 385
Mrk 181
Mrk 271
Mrk 297
IZw 166

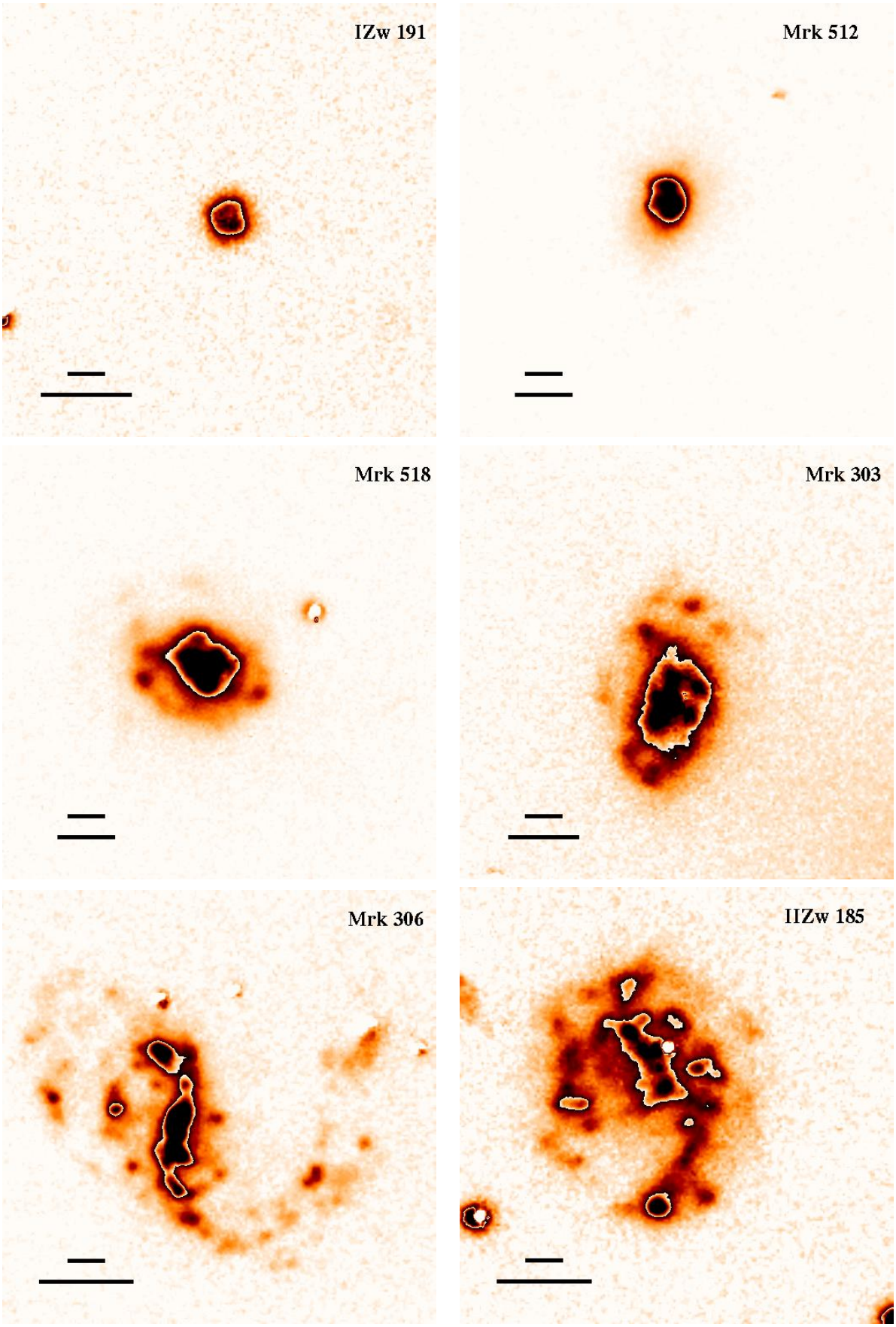
IZw 191
Mrk 512
Mrk 518
Mrk 303
Mrk 306
IIZw 185

2.8 Galaxy Descriptions

No luminous blue compact galaxy is typical. Each one tells a story, and has special traits that can teach us something about its history, and galaxy evolution as a whole. In this section we analyze each galaxy in the optical sample individually and discuss what can be inferred from the optical, Hα, infrared, and UV analysis.

2.8.1 Mrk 342

Mrk 342 is a blue-core objects which turned out to not be globally blue. There was a good bulge fit, with the U and B effective radius smaller than the V and I, as one might expect from a blue-core galaxy. In the McDonald and SDSS images it appears to be elliptical, and so not surprisingly is fit well by a De Vaucouleurs' law. The red color, $B-V \sim 0.81$, is expected due to the red color on the SDSS true color image. Mrk 342 has 2 companions and possible interaction.

2.8.2 Haro 15

Mazzarella, Bothun & Boroson (1991) classified Haro 15 as strongly interacting separated galaxies, or a single highly perturbed system which may be an advanced merger. Cairos et al. 2001 noted two nuclei in the middle of a roughly elliptical envelope and twisted isophotes. The inner gas, visible in the Hα, surrounding the two cores is very disturbed, and there is a tail in the South. One of the most notable features is the high SFR calculated from the UV. With a UV SFR of 4.9 $M_{\odot}$/yr,

Haro 15 is a great example of a further developed LBCG where a significant portion of the stars have migrated outwards allowing more of the UV light out. Young, hot stars and clusters have moved away from regions of high optical extinction (hence the blue color), permitting more of the UV light to escape. This situation can be contrasted with central, dusty starbursts, in which all of the UV/optical starlight is being absorbed by dust. Haro 15 is one of the best examples of a clumpy LBCG and is likely a minor merger.

2.8.3 Mrk 360

Mazzarella & Balazano (1986) classified Mrk 360 as being paired with III Zw 35. III Zw 35 is an odd red + blue galaxy pair located 8.4″ from Mrk 360. The velocity difference between the two objects is only approximatly 200 km/sec, so these 2 objects are probably part of a loose group. Mrk 360 has a tail which extends to east, easiest seen in the U band, although all bands show asymmetry. Both galaxies are bright in Hα, and three different star forming knots become more defined in the Hα. Mrk 360 fits the LBCG class.

2.8.4 Mrk 364

Mrk 364 is an E0 galaxy, with a color bluer that what is typical for an old spheroidal stellar population, B$-$V$\sim$ 0.53. The B$-$V color profile is very flat, so this galaxy stays blue until after about 20″ from the core. The profile shows a slight

bluiing out to about 5″, then a gradual reddening to B−V ∼0.6 at 20″, where the profile is ended. There was a good fit to a bulge and global blue color. SDSS image shows a hint of a dust lane across the nucleus. Mrk 364 is the kind of LBCG that is really interesting because it is a blue spheroid. Note that the bulge has a smaller effective radius at the shorter wavelengths, suggesting that the young stars have a smaller scale length.

2.8.5 Mrk 366

Mrk 366 has a tidal loop, or plume, strongly indicative of a recent or past interaction. A minor merger occurred a few hundred million years ago (a more recent encounter and the galaxy would look more disrupted); gravitational interaction causes a stream of stars to arch out to a large radius, then fall back on the the central part of the galaxy. This process also produces shells and bright-edged arcs; sometimes the disrupted stars slosh back and forth before the kinetic energy is redistributed. Mrk 366 is a great example of what could be called a late stage LBCG. The global color lies midway between blue, star-forming objects, and dead, red systems. There is a blue core and strong Balmer absorption features in the core spectrum (from SDSS), and outer as asymmetric structures which are markers for a past interaction. In Mrk 366 there is a loop in the west. When viewing the SDSS image, the disturbance in the northeast also resembles a loop. The tidal loop does not show up in Hα or UV images, meaning current high star formation in the ring is not likely.

2.8.6 Mrk 367

We only have a B image for this galaxy, but with that image we can tell that there is an asymmetrical core, but regular outer isophotes, hence the iE Loose & Thuan classification. The SBP drops from 19.8 to 21.0 from the first point to the point at $4''$, then there is an inflection point at a$\sim 5''$, probably indicating that the structure producing the asymmetric inner core ends at that radius. Looking at the SDSS images we can see that Mrk 367 has a red core, blue disk, and is possibly an S0 with substantial star formation. Mrk 367 has a UV (1.43 $M_{\odot}/yr$) and IR (13.45 $M_{\odot}/yr$) SFR that is larger than the median for the sample in each bandpass compared to the rest of the sample. Many galaxies only have a SF above the median in either the UV or the IR, so this feature really distinguishes Mrk 367.

2.8.7 Mrk 589

Despite a very blue color, $B - V \sim 0.34$, Mrk 589 has no morphological irregularities or signs of a companion or merger. The U, B, and V bands were fit with a bulge+disk. Mrk 589 has a bright core oriented in the east/west direction, and an outer structure whose major axis is more in the north/south direction. The surface brightness and color profiles are a little odd because the inner $5''$ are possibly affected by very strong emission lines. There is definitely a central starburst, and possibly a disk starburst as well.

2.8.8 Mrk 1184

Mrk 1184 is a spiral galaxy with two arms. The SBP was one of two galaxies best fit with with 2 exponentials, suggesting an inner and outer disk with different slopes. The first disk extends to about 15″, and the second extends to almost 30″. We only have an R-band image for this object, and based on the SDSS image the galaxy does not meet the LBCG criteria. The high star formation seems to be confined to the nucleus. Mrk 1184's IR SFR was one of the highest at $20.48 M_{\odot}$/yr. A lot of gas and dust still surrounds the high star formation.

2.8.9 Mrk 1404

Mrk 1404 is an S0 galaxy with strong Hα, as seen in our Hα image. A bulge+disk combination best fit the SBP, although if there is an older underlying red population, it does not dominate the color because this galaxy is still very blue with a B−V of 0.47, which falls well inside our B−V limit. The optical images show some irregular structure around the core, about 5″ from the center. Mrk 1404 is interesting because of its flat color profiles, blue color, bulge + disk combination, and smooth isophotes. The FUV morphology looks jsut like the B-band, with no bright neighbors.

2.8.10 Mrk 1079

Mrk 1079 is an interacting system in the early stage of interaction, which is characterized by tidal distortions (Chatzichristou 2002). Distortion is seen in the southwest

as a tidal tail, most likely caused by a close passage of the companion to the west. The companion is slightly visible in the stacked FUV/NUV image.

2.8.11 Mrk 1094

There are multiple star formation knots and irregular isophote structure. Mendez et al. (1999) labeled Mrk 1094 as a having a bar-shaped structure and currently undergoing a strong star formation burst that is disbursed in many separated knots. The sizes of the brightest knots are similar to those of giant HII regions in the Local Group. Mendez's final conclusion is that interaction with a companion HI cloud is the reason for the current star formation and bar-shaped distribution. There is a gradient in the ages of the different SF knots from the center outward. The bar is $\sim$ 5 kpc stretching in the north/south direction. Due to the irregular morphology we were not able to fit a SBP to this galaxy. The star formation gives the galaxy a blue color of $B - V \sim 0.43$.

2.8.12 Mrk 8

An unusual optical and Hα morphology in an elongated ring (Bottinelli et al. 1975) have led to this galaxy being classified as a recent merger. The central portion of Mrk 8 has five bright condensations labeled as super-associations that were theoretically formed together and are young (Khachikian 1998). Due to the "clumpiness" a SBP

could not be fit. The high star forming clumps within the ring are quit blue ($M_B \sim$ 0.46), and also UV bright.

2.8.13 Haro 1

The inner isophotes are almost rectangular, and surround a larger than normal asymmetrical nucleus. Due to the large core area and spread out SF, the B−V color profile remains blue for the majority of the galaxy. The odd nucleus is also apparent in the SBP, which only becomes a disk starting 15″ out from the center. The Hα images show much star formation in the core. Haro 1 has high UV (2.65 $M_\odot/yr$) and IR (13.95 $M_\odot/yr$) star formation. The Hα image shows the current star formation pattern. Haro 1 has had an encounter with a dwarfish companion, located to the west, with a tidal tail connecting the two objects. One can see the companion in the SDSS images.

2.8.14 Mrk 385

Mrk 385 has a tidal loop in the northwest, most likely a stream of stars ejected from the galaxy due to a past merger. The loop is visible in every band except U, and becomes more visible in redder bands. In Hα the loop is not visible, but an Hα hot spot is visible at the outer most reaches of the ring, possibly a remnant of a companion being stripped. The southern end of the galaxy appears to be somewhat

disturbed. The Sloan spectrum shows that it is a post burst system. Mrk 385 is a blue core galaxy.

2.8.15 Mrk 1211

Mazzarella & Balazano (1986) believed this to be two or three galaxies in contact. The remnant of a possible companion lies in the northeast. Mrk 1211 has one of the highest IR SFRs at 34.51 $M_{\odot}$/yr. The high star formation rate, derived from the FIR luminosity, is from an unknown combination of reprocessed young star light and light from an accretion disk around a nuclear supermassive black hole, and therefore could be falsely large. Mrk 1211 is an active galaxy.

2.8.16 Mrk 390

Mrk 390 is another tidal loop galaxy, the loop is best seen on the southwest side in the V band, and in the SDSS image. The SDSS image shows more diffuse gas in the northeast, almost like the loop continues around the galaxy. Mazzarella & Balazano (1986) identified a satellite in the southwest, where the loop is. The satellite could be the cause of the tidal loop; it may be stripping the galaxy. The core is slightly asymmetrical in the east, however a De Vaucouleurs law was a good fit. For the most part the color profiles are flat, so this galaxy remains blue even out to its edges. Mrk 390 is UV bright compared with the rest of the sample; it has a substantial UV SFR

of 1.74 $M_{\odot}$/yr. Unlike Mrk 385 this galaxy is blue all over. the profile is clearly bulge-dominated, the B−V profile is flat, and there is good FUV detection.

2.8.17 Mrk 18

Mrk 18 is an elliptical galaxy, when looking at Hubble's classification scheme it would fall somewhere in the E5 to E7 range. There may be an elliptical morphology, de Vaucouleurs law fit, and a Loose & Thuan classification of nE, but this galaxy does not have the typical color and luminosity of a classic elliptical galaxy. The typical elliptical will have a M_B closer to about −18, but Mrk 17 has an M_B of −19.11, putting it safely in LBCG territory.

2.8.18 Mrk 402

Mrk 402 has a tail that extends to the west visible in SDSS and all visible bands except I, and the only reason you can not see it there is because the galaxy is too close to the edge of the image. The surface brightness profile shows a clear inner bulge on top of a disk, where the disk begins to dominate at about 10″ out from the center.

2.8.19 IIZw 44

Chapelon, Contini, & Davoust (1999) labeled this as a barred starburst spiral. The barred spiral morphology is more apparent in the SDSS image, however, the

almost 3 part core viewable in the McDonald images (especially the B band) are due to the bar. Despite being a spiral, the galaxy fit a De Vaucouleurs law, and the B−V color profile turns red very quickly and sharply. The bar and blue blogs(large star-forming regions) make a simple bulge-disk fit problematic. The SBP, due to the bar, changes slightly out to about 5″, then it turns into a profile more fitting for a bulge. The bulge fit could be due to the fact that IIZw 44 is in the process of a starburst, and fits the LBCG definition with a $M_B \sim$ -19.37 and a B−V color of $\sim$ 0.59.

2.8.20 Mrk 139

Mrk 139 has a large (greater than 15kpc) asymmetrical outer envelope, hence the iI Loose & Thuan morphology classification. In SDSS Mrk 139 appears to have multiple shells and arcs, meaning an ongoing merger or accretion event. The optical spectrum is rising strongly to the blue, and it shows strong Balmer absorption lines as well as Hα. The only odd aspect, the B−V color, seems to be too red.

2.8.21 Mrk 144

Mrk 144 is a bit of an anomaly. The its morphology from RC3 is listed as S?. As the McDonald images clearly show, there is a tail feature extending to the northeast. However, when looking at the SDSS image, the same tail is visible, but there seems to be another one on the other side, though not as prominent. So this could be a

starbursting spiral galaxy. The SBP did fit an exponential law, which is typical for a spiral galaxy. Mrk 144 is one of a few blue spirals in our optical sample.

2.8.22 Mrk 33

Mrk 33 is more of a typical dwarf elliptical galaxy with a starburst nucleus. The starburst is likely very young and has yet to produce many supernovae (Beck et al. 2000). Due to the elliptical structure, the De Vaucouleurs law fit well. More than likely due to the recent starbursts activity this galaxy is very blue ($B-V \sim 0.47$). Mrk 33's total blue lluminosity lies below our cutoff for luminous blue compact galaxies yet was included inour survey because, like Haro 1, there was a substantial body of existing data to provide a check on our calibrations and anchor the investigation of LBCGs with a well studied blue compact galaxy. Radio studies have been popular for this galaxy because of a radio bright dust lane offset from the optical center (Mollenhoff 1992).

2.8.23 Mrk 148

Mazzarella & Balazano (1986) labeled Mrk 148 as a having plumes, which are visible on all the McDonald images in the northwest and southeast. The color profiles remain flat, so the galaxy keeps a constant color out to where the galaxy light falls to the level of noise. This system appears highly inclined to our line-of-sight and possesses an odd bulge. The B−V was too red to be a LBCG, and the SF was very

low, almost non-existent in the UV. The ultraviolet star formation was substantially smaller than the far-infrared rate because of this system's edge-on morphology. The UV light passes through a larger column of dust before exiting the galaxy and is highly extincted.

2.8.24 Haro 25

Haro 25, like a handful of others, has a high UV (1.61 $M_\odot$/yr) and IR(13.63 $M_\odot$/yr) SFR. The galaxy is blue, B−V $\sim$ 0.46, and has a high M_B of −20.26. Measuring not even 10 kpc across, the elliptical galaxy is very compact in appearance, and therefore paired with its high star formation, blue color, and high luminosity, is a good poster child for the sample.

2.8.25 Mrk 154

Initially Mrk 154 appears to be an elliptical galaxy, but taking a closer look at both the McDonald images, and SDSS, possible spiral arms are visible north and south of the center of the galaxy. The McDonald U and B filters, and the SDSS image, are best for seeing both arms. The core has some slight asymmetry visible in all images which leads to inflections in the B−V, U−B, and U−R color profiles. Mrk 154 does appear to be a blue spiral.

2.8.26 Mrk 171

Mrk 171 is a pair of galaxies, IC 694 and NGC 3690, which passed each other 700 million years ago. Because of the pass by, the pair experienced a star formation burst. In the last fifteen years six supernovae have been detected, making Mrk 171 well known for supernovae. The optical images show multiple star formation regions, and very disturbed gas and dust. The IR derived SFR is off the chart at $131.13 M_{\odot}$/yr. Not all of the FIR luminosity arises from massive star formation there is some evidence for an AGN in the core of one of the pair. The SFR is close to that of a ULIRG than any other galaxy in the LBCG sample. A typical ULIRG will have a SFR of $10^{2.50.5} M_{\odot}$/yr (Yang et al. 2007). In fact Rujopakarn et al. (2011) labeled Mrk 171 as a LIRG, or luminous infrared galaxy. IC 694 (northeast) contains the majority of the star formation, and contributes more than 46% of the total energy output (Charmandaris, Stacey, & Gull 2002). In fact IC 694 has a supernovae factory, confirming the presence of an extreme starburst that peaked a few million years ago (Neff, Ulvestad, & Teng 2004).

2.8.27 Mrk 181

Mrk 181 is located in a galaxy group, containing 7 bright galaxies within $12'$ and $\pm$ 500 km/sec (per the NASA Extragalactic Database). Mrk 182 is located $2.7''$ to the south of Mrk 181. The distinct galaxies are more apparent in the shorter of the optical wavelengths. At longer wavelengths a tail in the southeast becomes a little

brighter. More than likely the tail is mainly dust, no real star formation activity, so in the UV and shorter optical wavelengths it is not going to be a dominant feature.

2.8.28 Haro 34

The morphology in this galaxy is a great example of an iE galaxy. There is complex inner structure, including 2 distinct star forming knots, setting on top of an outer envelope with normal elliptical structure. In fact this galaxy was fit by a De Vaucouleurs law. Haro 34 seems to be a blue core galaxy, meaning a starburst in the center, then redder regions further out.

2.8.29 Mrk 54

Mrk 54 is a merging system since the B, V, and R bands all show more than one nucleus. Two tail features, shaped like wings, lie northwest and east. Mrk 54 by far had the highest UV SFR, at 12.16 $M_{\odot}$/yr. A significant amount of UV is able to escape the gas and dust in this galaxy, possibly meaning it is further developed, or it is undergoing a strong spell of star formation. Since this galaxy is further developed, it is not surprising that it has the bluest color in the sample, B$-$V $\sim$ 0.26. By developed I mean that the starburst has likely be in progress for tens of millions of years, to allow the ultraviolet bright stars time to escape the dusty regions, and be observed with modest extinction. However, star formation is continuing at an elevated rate as evidenced by the FIR.

2.8.30 Mrk 238

Davoust, Contini (2004) labeled Mrk 238 as a starbursting barred spiral galaxy. Mazzarella, Bothem, & Boroson (1991), classified it as being in a pair. The merger is very obvious in the McDonald optical images. Despite the merger, Mrk 238 is not blue compared with the rest of the sample, it has a B−V of 0.76. The merger could have disturbed the dust to the point where the light from the blue O and B stars is not able to be seen.

2.8.31 Mrk 248

Koss et al. (2010) labeled this as a merging system with obvious signs of disruption. Two possible bridges are directly between the galaxies and arching above them to the north. Mrk 248 (the galaxy on the left) looks to possibly have been a spiral before the disruption, and the companion appears to be a spiralin our McDonald images. Mrk 248 has a red color compared to the rest of the sample. Mrk 248 itself has a B−V of 1.12, and its neighbor as a B−V of 0.91. The neighbor was expected to be a little bluer, as it also appears so in the SDSS true color image. The red colors of both of these galaxies, since the merger seems to be very new due to their spacing, could mean that the current high star formation is due to the interaction, and that there is an older underlying population of stars.

2.8.32 Mrk 255

The asymmetrical core has multiple star forming regions, along with a ~ 6 kpc tail in the north spotted with star formation knots. The outer envelope is also irregular, making this galaxy a great example of an iI morphology classification. Mrk 255 looks to be a disturbed barred spiral, observed face-on, with an unusually blue global color. The star formation knots are more apparent at shorter wavelengths, so the U and B in the optical are best to view, and the UV also shows the inner structure. The B$-$V color of ~ 0.51 does classify Mrk 255 as a LBCG.

2.8.33 Mrk 271

Klimanov & Reshetnikov (2001) called Mrk 271 an M-51 type galaxy. An M 51-type pair includes a bright luminosity spiral galaxy and a satellite with a blue luminosity 1/30 to 1/3 of the primary one. The main galaxies in these pairs are typically barred and have two spiral arms. High star formation can be expected. The UV SFR was not high compared with the rest of the sample. Mrk 271 is a merger in progress, where we can still see the two original galaxies.

2.8.34 Haro 42

Mazzarella, Bothem, & Boroson (1991) believes that Haro 42 has multiple systems. It appears to have three dominant star forming knots, and a tail extending toward the west. The majority of the disturbance in the gas is in the west. The morphology was

too irregular for us to fit a SBP to this galaxy, however the luminosity, $M_B \sim -19.22$, and color (B−V$\sim$ 0.44), and compact appearance easily classify this galaxy as a LBCG.

2.8.35 I Zw 101

I Zw 101 has nearly a completely different morphology in the B band image. With the V and I images the core looks for the most part elliptical, but in the B band we see the emergence of almost a second core and a lot of asymmetry in the inner 5 kpc of the galaxy on top of an elliptical outer envelope. I Zw 101 shows a broken, circumnuclear ring of star formation. The color profile shows this aspect exceedingly well by being red in the center, than dips to the blue, followed by a rise to the red again. The SBP that is plotted against $r^{1/4}$ portrays this iE type morphology well. Out to about the 1.5″ point the profile is nearly flat, then turns down into a perfect bulge type galaxy profile.

2.8.36 Mrk 492

Mrk 492 is an elliptical galaxy with a blue core, just dipping to B−V below 0.6 in the inner core, but overall has a B−V closer to 0.7. The B−V color profile, with the exception of the first few arcseconds, is almost completely flat. Out to 30″ the color changes very little.

2.8.37 Mrk 297

Mazzarella, Bothem & Boroson (1991) labeled Mrk 297 as a tight interacting system, and Ryan & De Robertis (2010) have Mrk 297 in a group of systems undergoing major gravitational interactions. The Ryan & De Robertis (2010) sample was selected from the Arp Atlas of Peculiar Galaxies (Arp 1966). Three nuclei are surrounded by multiple star-forming knots. The high UV SFR of 4.03 $M_{\odot}$/yr means this galaxy has evolved enough for some of the stars to migrate out allowing more of the UV light to be seen. The migration of stars could also be the reason this galaxy is so blue, with a B−V of 0.37. Mrk 297 has properties similiar to Haro 1 and haro 15, UV bright, multiple star forming regions, and lots of ionized gas.

2.8.38 Mrk 300

Mrk 300 is a two armed barred starburst spiral, the bar runs north and south. A satellite galaxy lies in the east and is easily seen in the SDSS image. The true SDSS image is slightly reddish, which matches our B−V of 0.69. Mrk 300 was one of the galaxies best fit with a combination of the 2 major fitting laws, so it had a bulge + disk. However, when looking at the SBP, almost 3 components are visible, possibly due to the bar.

2.8.39 Mrk 697

Mrk 697 is a face-on barred S0 based on its SDSS image. The disk appears featureless except for a weak bar-like structure observed perpendicular to the major axis. This galaxy had no cataloged photometry when our program was started, and was observed based on its luminosity ($M_V = -20.74$) and listing in the Markarian survey. Our integrated color, (B−V) $\sim$ 0.95, is consistent with both its SDSS photometry, and with the colors expected for a normal, passively-evolving S0. The SDSS spectrum shows no blue component or emission lines. Mrk 697 does not meet the criteria for a LBCG and its inclusion in the Markarian survey appears anamolous.

2.8.40 Mrk 499

Mrk 499 is a very compact galaxy, only measuring $\sim$ 8 kpc in the inner region before the light begins to drop off to noise level. The compactness along with the very blue color ($B - V \sim 0.30$), and luminosity ($M_B \sim 20.43$), make this a great example of a LBCG. With no sign of interaction or nearby companions, and no sign of a red underlying disk of older stars, this could be a fairly new galaxy. The UV image also shows strong emission in the core.

2.8.41 I Zw 191

IZw 191 is an E0 galaxy, that sits just on the color and luminosity border that defines a LBCG. Our Hα image shows some star formation in the core. I Zw 191 is a blue core elliptical.

2.8.42 II Zw 82

II Zw 82 is an early type galaxy included because it shows a compact appearance, but like Mrk 697, was inadvertently included. The galaxy appears red in the SDSS true color image. A photometric calibration was not available for the optical data.

2.8.43 Mrk 512

Mrk 512 has a bit of a perturbed core, but for the most part elliptical like contours. There is evidence for an interaction, such as an arc centered at PA $\sim$ 160 degrees, extending about 20 degrees with a sharp outer edge. There is a plume at PA $\sim$ 20 degrees. One of its significant features is having one of the highest IR SFRs at 24.21 $M_{\odot}$/yr. With no obvious merger or interaction effects, Mrk 512 could be an example of a galaxy that had an internal trigger to star formation. The high IR luminosity is due to thick surrounding dust, making this galaxy more similar to the possible ULIRG precursors than others.

2.8.44 Mrk 518

Mrk 518 has an irregular inner structure, especially with the perturbed gas in the east, as seen in the Hα image. The inner structure has more asymmetry at shorter wavelengths. Spiral arms are faintly visible in the McDonald images and the SDSS image. However, the galaxy was best fit by the De Vaucouleurs law for bulge type galaxies. Mrk 518 has one of the highest IR SFRs at 26.86 $M_{\odot}$/yr. The high IR SFR means that this galaxy has significant star formation, with no visible external trigger. the outer isophotes are smooth, even though the inner region shows considerable structure and the global color is blue.

2.8.45 Mrk 303

Mrk 303 appears in the SDSS image to be a loose spiral, such as an Sb or Sc, with much of the activity in the arms. The McDonald image, which shows more detail in the inner few kpcs, reveals multiple star forming knots, or condensations (Khachikyan & Petrosyan 1983), distributed at random about the core. The B−V color profile shows the galaxy begin to get a bit bluer before it flattens out, and starts turning red at the outskirts of the galaxy. The odd color profile shape is caused by these star formation areas in the arms, which (Khachikyan & Petrosyan, 1983) described as a patchy halo.

2.8.46 Mrk 306

Davoust & Contini (2004) labeled Mrk 306 as a starbursting barred spiral galaxy, Mrk 305 is the companion galaxy. Woods et al. (2006) stated that the star formation was tidally triggered due to the close pairing. A bridge connects Mrk 306 and Mrk 305 that shows more structure at shorter optical wavelengths. The core region of Mrk 306 is extended north and south, and has many knots. Due to the irregular shape a SBP was not made. The galaxy appears very blue in SDSS, and we found a B−V of 0.45 and 0.42 for with and without Mrk 305 included respectively. The blue color and high SF could be from the accretion of gas and dust from the companion galaxy.

2.8.47 II Zw 185

Focardi, Zitelli, & Marinoni (2008) classified II Zw 185 as being a spiral pair. The companion spiral, IC 5242, is not seen in the McDonald images presented in this paper, but it is viewable in SDSS. A long spiral arm or tail extends to the south, ending a SF knot. The Hα image is helpful to view for this galaxy because it shows individual star forming knots in much more detail. Looking at Hα, five individual star forming knots are in the core area, and then seven surround the core. The UV based star formation rate was on the high end for this sample, 5.67 $M_{\odot}$/yr, which is not surprising for an active blue spiral galaxy with a companion.

2.8.48 Mrk 531

Mrk 531 is an S0 galaxy that for the most part has elliptical contours, but there is some asymmetry in the core that is also visible in the SDSS image. The V-band image shows the profile the best, a small bulge then a smooth exponential decline for the disk. The B−V color profile shows that the core starts out blue, around B−V $\sim$ 0.5, put quickly rises and flattens out at B−V of 0.8 by $\sim$ 4 or 5″. Mrk 531 is a blue core object.

2.8.49 Mrk 325

Mrk 325 is a starburst galaxy with inner asymmetric spiral structure, and ripples in the outer structure (Conselice, C.J., et al. 2000). The ripples are more than likely due to a merger or interaction (Homeier & Gallagher 1999). Due to its irregular shape there is no SBP. The SDSS image does show Mrk 325 as being blue.

Chapter 3

Star Formation and Supernovae in LBCGs

3.1 Motivation and Background

Observations of star formation rates (SFRs) in galaxies provide vital clues to the physical nature of the Hubble sequence, and are key probes of the evolutionary histories of galaxies (Kennicutt 1998). Because star forming galaxies are discovered in different ways, it is vital to compare various methods for measuring the star formation in a galaxy (Sargysan & Weedman 2009). Studies have attempted to measure cosmic evolution of star formation rates using the UV, optical, and near-infrared bands (Martin et al. 2007, etc). The most direct measurement of the star formation rate in a starburst is to observe the ultraviolet continuum luminosity from the young, hot stars in the starburst (Salim et al. 2007). Early type O and B stars produce significant amounts of UV compared to less massive stars, and since these hot massive stars have short lifetimes (less than 100 million years), they are a great tracer of star formation. The flux emitted in the UV in spiral and irregular galaxies is an excellent measure of the current star formation rate (Kennicutt 1998; Donas, Deharveng, & Lager 1987). However, the light emitted in the UV can be very efficiently absorbed

by dust and then re-emitted at far-infrared wavelengths. Therefore, an analysis of the energy budget using a comparison of the infrared and UV emission is a powerful tool to determine the dust attenuation of light at all wavelengths (Buat, Iglesias-Paramo, & Seibert 2005).

A number of studies have been completed to compare UV and recombination line based star formation rates to dust-free star formation indicators such as those based on infrared luminosity and radio luminosity. Dust attenuation increases with the star formation rate in nearby galaxies (Hopkins et al. 2001). The dust attenuation dependence on SFR stems from the relationship between the dust attenuation and far-IR luminosity found in Wang & Heckman (1996). Sargysan & Weedman (2009) likewise found an IR luminosity dependence of attenuation. Bell & Kennicutt (2001) support the notion that attenuation increases with SFR.

We will use ultraviolet data obtained with the galaxy evolution explorer satellite (Martin et al. 2005), and infrared data obtained with the infrared astronomical satellite (Helou 1995), to derive SFRs using synthesis models derived in Kennicutt (1998). Star formation rates will be used to examine the relationship between UV and IR star formation rates along with the luminosity, color, k-band dependencies, and attenuation.

3.2 Data Sample

3.2.1 High Star Formation Sample Selection

The optical sample of galaxies introduced in Chapter 2 was also used in this section along with a high star formation rate sample. The high star formation sample was taken from the Markarian survey. Our definition for high star formation is defined as having a FIR-derived star formation rate greater than 10 $M_{\odot}$/yr. *IRAS* fluxes for all 1,500 Markarian survey objects were extracted from the Nasa Extragalactic Database (NED) by Heather Appleby during her Master's Thesis, and converted to FIR luminosities and SFRs. All objects with SFRs greater than 10 $M_{\odot}$/yr were selected. Using the galaxies' photographic magnitudes as listed in NED, Heather and Dr. Fanelli derived an absolute magnitude which was assumed to be roughly approximate to the B-band absolute magnitude. Objects with M_B less than -18.5 were removed. All sources with spectroscopic evidence for an active nuclei were removed to ensure that the FIR luminosity originated in dust heated by the UV-optical radiation from young high-mass stars and not from accretion onto a supermassive black hole. Table 3.1 lists the high star formation galaxy sample. The column headings are the same as in Table 2.1.

Table 3.1. Properties of the High Star Formation Sample

Name	Alternate Name	R.A. (J2000.0)	Dec (J2000.0)	V (km s^{-1})	D (Mpc)	a x b (′)	a x b (Kpc)
(1)	(2)	(3)	(4)	(5)	(6)	(7)	(8)
Mrk 2	UGC 01385	01 54 53.8	+36 55 05	5747	78.7	0.7 x 0.6	16.0 x 13.7
Mrk 83	SBS 0744+53	07 48 10.9	+54 12 42	14605	200.1	...	...
Mrk 91	SBS 0828+527	08 32 28.1	+52 36 22	5289	72.4	0.8 x 0.7	16.8 x 14.7
Mrk 97	CGCG 311-019	08 50 58.6	+65 38 15	7219	98.9	...	...
Mrk 103	KUG 0911+679	09 16 04.7	+67 45 32	9479	129.8	0.4 x 0.3	15.1 x 11.3
Mrk 114	UGC 05055	09 30 11.7	+55 51 09	7754	106.2	1.5 x 1.3	46.3 x 40.2
Mrk 126	SBS 0949+524	09 52 36.9	+52 13 18	11952	163.7	0.5 x 0.5	23.8 x 23.8
Mrk 143	KUG 1023+625	10 26 53.2	+62 20 11	9832	134.7	0.6 x 0.5	23.5 x 19.6
Mrk 161	UGC 06103	11 01 59.0	+45 13 41	6208	85.0	0.8 x 0.7	19.8 x 17.3
Mrk 183	CGCG 334-046	11 38 50.0	+68 32 45	12493	171.1	...	...
Mrk 204	PGC 039868	12 20 54.6	+61 59 34	17734	242.9	0.5 x 0.4	35.3 x 28.3
Mrk 217	VIIZw 472	12 35 02.6	+66 22 33	14325	196.2	0.5 x 0.4	28.5 x 22.8
Mrk 237	CGCG 245-012	13 01 17.5	+48 03 34	9203	126.1	0.8	29.3
Mrk 254	SBS 1320+519	13 22 50.6	+51 44 18	9185	125.8	0.5 x 0.4	18.3 x 14.6
Mrk 261	VIIZw 518	13 30 01.1	+75 34 08	9436	129.3	...	...
Mrk 264	SBS 1332+521	13 34 11.9	+51 53 21	19078	261.3	0.5 x 0.3	38.0 x 22.8
Mrk 265	KUG 1335+280C	13 38 16.8	+27 46 17	10235	140.2	0.7 x 0.3	28.5 x 12.2

Table 3.1 (continued)

Name	Alternate Name	R.A. (J2000.0)	Dec (J2000.0)	V (km s^{-1})	D (Mpc)	a x b (′)	a x b (Kpc)
(1)	(2)	(3)	(4)	(5)	(6)	(7)	(8)
Mrk 269	PGC 048404	13 40 49.1	+65 49 26	14466	198.2	0.6 x 0.5	34.6 x 28.8
Mrk 286	NGC 5607	14 19 26.7	+71 35 18	7914	108.4	0.9 x 0.8	28.4 x 25.2
Mrk 311	IC 1461	22 58 34.3	+15 10 22	9302	127.4	0.5 x 0.5	18.5 x 18.5
Mrk 312	KUG 2258+160	23 00 37.8	+16 21 36	9768	133.8	0.4 x 0.2	15.6 x 7.8
Mrk 319	UGC 12490	23 18 38.3	+25 13 58	8232	112.8	0.8 x 0.6	26.2 x 19.7
Mrk 321	NGC 7620	23 20 05.7	+24 13 16	9720	133.2	0.9 x 0.8	34.9 x 31.0
Mrk 327	CGCG 476-078	23 37 05.9	+23 19 14	11749	161.0	0.4 x 0.3	18.7 x 14.0
Mrk 349	PGC 003149	00 53 34.4	+21 30 48	6987	95.7	0.5 x 0.4	13.9 x 11.1
Mrk 353	NGC 0354	01 03 16.4	+22 20 34	4750	65.1	0.8 x 0.4	15.1 x 7.6
Mrk 354	PGC 003811	01 04 07.0	+20 26 01	14155	193.9	0.6 x 0.2	33.8 x 11.3
Mrk 368	IC 0235	02 32 50.8	+20 38 28	8796	120.5	0.4 x 0.3	14.0 x 10.5
Mrk 387	CGCG 089-016	08 24 14.3	+17 19 55	11184	153.2	0.5 x 0.5	22.3 x 22.3
Mrk 413	CGCG 153-009	09 59 15.9	+31 42 00	11691	160.1	0.5 x 0.4	23.3 x 18.6
Mrk 414	KUG 1010+355	10 13 05.8	+35 16 55	11486	157.3	0.6 x 0.4	27.5 x 18.3
Mrk 440	PGC 040866	12 27 29.8	+36 41 53	15192	208.1	0.7 x 0.3	42.4 x 18.2
Mrk 477	IZw 092	14 40 38.1	+53 30 16	11614	159.1	0.6 x 0.4	27.8 x 18.5
Mrk 489	NGC 5992	15 44 21.5	+41 05 11	9820	134.5	0.9 x 0.7	35.2 x 27.4

Table 3.1 (continued)

Name	Alternate Name	R.A. (J2000.0)	Dec (J2000.0)	V (km s^{-1})	D (Mpc)	a x b (′)	a x b (Kpc)
(1)	(2)	(3)	(4)	(5)	(6)	(7)	(8)
Mrk 496	NGC 6090	16 11 40.7	+52 27 24	9111	124.8	1.7	61.7
Mrk 540	CGCG 381-045	23 47 00.4	-00 26 51	21332	292.3	0.5 x 0.4	42.5 x 34.0
Mrk 545	NGC 0023	00 09 53.4	+25 55 26	4699	64.4	2.1 x 1.3	39.3 x 24.4
Mrk 551	IVZw 023	00 29 25.2	+30 33 30	15230	208.6	...	...
Mrk 556	UM 071	00 48 51.5	+04 19 56	12443	170.5	...	...
Mrk 559	CGCG 410-022	00 59 17.9	+06 55 14	13177	180.5	0.5 x 0.3	26.3 x 15.8
Mrk 560	...	01 06 23.9	-00 08 42	14372	196.9	0.7 x 0.5	40.1 x 22.3
Mrk 567	UM 093	01 19 18.1	+04 34 41	9901	135.6	...	...
Mrk 569	CGCG 385-087	01 22 35.8	+01 53 27	9622	131.8	0.7 x 0.4	26.8 x 15.3
Mrk 575	UGC 01260	01 48 33.1	+12 36 50	5199	75.3	0.8 x 0.6	17.5 x 13.1
Mrk 579	PGC 006907	01 51 58.4	+07 16 42	19500	267.1	...	...
Mrk 582	UGC 01449	01 58 06.7	+03 05 15	5544	76.0	0.8 x 0.5	17.7 x 11.1
Mrk 592	UGC 01794	02 19 41.1	-00 15 20	7638	104.6	0.8 x 0.4	24.3 x 12.2
Mrk 593	NGC 0927	02 26 37.3	+12 09 19	8240	112.9	1.2 x 1.2	39.4 x 39.4
Mrk 606	PGC 012502	03 20 23.1	+04 08 55	8900	121.9	...	...
Mrk 619	PGC 019190	06 31 32.1	+57 13 50	13330	182.6	...	...
Mrk 629	PGC 030049	10 17 20.0	+15 29 21	9760	133.7	0.8 x 0.3	31.1 x 11.7

Table 3.1 (continued)

Name	Alternate Name	R.A. (J2000.0)	Dec (J2000.0)	V (km s^{-1})	D (Mpc)	a x b (′)	a x b (Kpc)
(1)	(2)	(3)	(4)	(5)	(6)	(7)	(8)
Mrk 632	IC 0638	10 43 48.0	+15 53 43	11931	163.4	0.8 x 0.4	38.0 x 19.0
Mrk 637	KUG 1136+212	11 38 51.5	+20 58 57	19673	269.5	0.9 x 0.4	70.6 x 31.4
Mrk 639	KUG 1140+241	11 43 20.5	+23 54 06	10131	138.8	1.0 x 0.4	40.4 x 16.2
Mrk 681	PGC 051544	14 26 17.3	+22 56 01	21081	288.8	0.3 x 0.3	25.2 x 25.2
Mrk 688	CGCG 106-026	15 16 39.9	+19 05 37	11763	161.1	0.8 x 0.6	37.5 x 28.1
Mrk 693	KUG 1551+232B	15 54 02.9	+23 07 52	4656	63.8	1.0 x 0.5	18.6 x 9.3
Mrk 702	CGCG 090-003	08 45 33.5	+16 05 46	16093	220.5	0.7 x 0.5	44.9 x 32.1
Mrk 717	IC 2551	10 10 40.3	+24 24 51	6453	88.4	0.9 x 0.7	23.1 x 18.0
Mrk 718	UGC 05501	10 12 11.7	+04 55 24	8515	116.6	0.5 x 0.5	17.0 x 17.0
Mrk 719	ARK 236	10 15 59.9	+04 57 17	9586	131.3	0.6 x 0.4	22.9 x 15.3
Mrk 726	CGCG 155-006	10 45 49.8	+27 37 11	13413	183.7	0.7 x 0.6	37.4 x 32.1
Mrk 753	PGC 037441	11 55 35.3	+13 06 19	16786	229.9	0.4 x 0.4	26.8 x 26.8
Mrk 785	ARK 410	13 16 15.9	+30 15 52	14973	205.1	0.5 x 0.5	29.8 x 29.8
Mrk 789	VIIZw 323	13 32 24.2	+11 06 23	9579	131.2	0.5 x 0.3	19.1 x 11.4
Mrk 799	NGC 5430	14 00 45.7	+59 19 42	3315	45.4	2.6 x 1.0	34.3 x 13.2
Mrk 809	NGC 5591	14 22 34.0	+13 43 00	7863	107.7	1.5	47.0
Mrk 823	PGC 052868	14 48 12.4	+15 33 53	13927	190.8	...	...

Table 3.1 (continued)

Name	Alternate Name	R.A. (J2000.0)	Dec (J2000.0)	V (km s^{-1})	D (Mpc)	a x b (′)	a x b (Kpc)
(1)	(2)	(3)	(4)	(5)	(6)	(7)	(8)
Mrk 834	UGC 09639	14 58 36.0	+44 53 01	11098	152.0	1.0	44.2
Mrk 837	CGCG 105-093	15 01 36.3	+16 43 47	9803	134.3	0.4 x 0.3	15.6 x 11.7
Mrk 839	UGC 09668	14 56 07.0	+83 31 23	4216	57.8	1.5 x 0.8	25.2 x 13.5
Mrk 848	VV 705	15 18 06.3	+42 44 37	12344	169.1	0.9	44.3
Mrk 851	CGCG 049-148	15 22 05.2	+05 51 18	10837	148.5	0.7 x 0.7	30.2 x 30.2
Mrk 858	PGC 05547	15 34 29.2	+14 28 38	9674	132.5	0.7 x 0.3	27.0 x 11.6
Mrk 860	CGCG 136-042	15 39 26.8	+24 56 44	7133	97.8	...	...
Mrk 863	CGCG 079-011	15 56 25.9	+09 03 19	12886	176.5	0.7 x 0.5	35.9 x 25.7
Mrk 867	IC 1166	16 02 08.9	+26 19 38	21864	299.5	0.4	34.8
Mrk 881	KUG 0881	16 25 49.2	+40 20 43	8947	122.6	0.7 x 0.5	25.0 x 17.8
Mrk 891	SBS 1657+575	16 58 28.8	+57 31 21	15464	211.8	...	...
Mrk 904	CGCG 377-019	22 04 12.7	-00 01 56	9890	135.5	0.7 x 0.4	27.6 x 15.8
Mrk 923	IC 1460	22 57 04.1	+04 40 37	7370	101.0	0.4 x 0.3	11.8 x 8.8
Mrk 932	PGC 071964	23 38 04.9	+01 33 47	17162	235.1	0.4 x 0.3	27.4 x 20.5
Mrk 938	NGC 0017	00 11 06.5	-12 06 26	5826	79.8	2.2 x 0.8	51.1 x 18.6
Mrk 940	KUG 0011+339	00 14 22.3	+34 12 10	19149	262.3	0.3 x 0.2	22.9 x 15.3
Mrk 941	PGC 001000	00 15 02.0	+34 48 30	14468	198.2	...	...

Table 3.1 (continued)

Name	Alternate Name	R.A. (J2000.0)	Dec (J2000.0)	V (km s^{-1})	D (Mpc)	a x b (′)	a x b (Kpc)
(1)	(2)	(3)	(4)	(5)	(6)	(7)	(8)
Mrk 948	CGCG 409-017	00 28 14.3	+07 07 45	12035	164.9	0.6 x 0.3	28.8 x 14.4
Mrk 955	CGCG 383-044	00 37 35.8	+00 16 50	10469	143.4	0.9 x 0.6	37.5 x 25.0
Mrk 984	UGC 00849	01 19 24.1	+12 26 49	14272	195.5	1.3 x 0.6	73.9 x 34.1
Mrk 995	PGC 005434	01 27 29.2	-08 33 15	14553	199.4	0.5 x 0.4	29.0 x 23.2
Mrk 1001	PGC 005811	01 33 42.1	+11 41 44	16332	223.7	0.5 x 0.3	32.5 x 19.5
Mrk 1005	PGC 006207	01 40 43.4	-04 39 07	12533	171.7	0.6 x 0.5	30.0 x 25.0
Mrk1027	IC 0214	02 14 05.6	+05 10 24	9009	123.4	0.8 x 0.6	28.7 x 21.5
Mrk 1029	CGCG 413-068	02 17 03.5	+05 17 31	9023	123.6	0.8 x 0.4	28.8 x 14.4
Mrk 1050	UGC 02105	02 37 39.9	+32 25 54	5016	68.7	1.2 x 0.8	24.0 x 16.0
Mrk 1056	UGC 02288	02 49 13.1	+35 20 05	12471	170.8	1.0 x 0.5	49.7 x 24.8
Mrk 1057	KUG 0246+338	02 49 38.9	+34 02 20	11642	159.5	0.3	13.9
Mrk 1088	NGC 1691	04 54 38.3	+03 16 05	4488	61.5	1.7 x 1.5	30.4 x 26.8
Mrk 1097	MCG +12-15-006	15 24 08.2	+70 55 27	17848	244.5	...	...
Mrk 1101	UGC 10099	15 56 36.4	+41 52 51	10706	146.7	0.5 x 0.4	21.3 x 17.1
Mrk 1111	IC 4630	16 55 09.6	+26 39 46	10650	145.9	0.8 x 0.5	34.0 x 21.2
Mrk 1112	CGCG 169-016	16 57 18.3	+28 11 16	10700	146.6	0.4 x 0.3	17.1 x 12.8
Mrk 1115	IZw 172	17 02 59.1	+33 03 43	19291	264.3	0.5 x 0.4	38.4 x 30.8

Table 3.1 (continued)

Name	Alternate Name	R.A. (J2000.0)	Dec (J2000.0)	V (km s^{-1})	D (Mpc)	a x b ($'$)	a x b (Kpc)
(1)	(2)	(3)	(4)	(5)	(6)	(7)	(8)
Mrk 1116	UGC 10923	17 19 31.4	+86 44 18	8211	112.5	1.2 x 0.7	39.3 x 22.9
Mrk 1117	PGC 060673	17 40 21.6	+39 15 18	13771	188.6	...	...
Mrk 1122	CGCG 228-007	18 26 41.1	+42 40 14	12345	169.1	...	...
Mrk 1143	UM 060	00 42 33.9	+03 15 25	11034	151.1	0.7 x 0.4	30.8 x 17.6
Mrk 1151	PGC 004053	01 08 28.9	-12 58 48	16219	222.2	0.7 x 0.6	45.2 x 38.8
Mrk 1156	KUG 0129+329	01 32 04.3	+33 10 46	10584	145.0	0.6 x 0.3	25.3 x 12.7
Mrk 1159	KUG 0132+327	01 35 17.5	+33 03 02	20741	284.1	0.6 x 0.5	49.6 x 41.3
Mrk 1194	NGC 1819	05 11 46.1	+05 12 02	4387	60.1	1.7 x 1.2	29.7 x 21.0
Mrk 1198	UGC 03726	07 11 07.0	+25 54 56	7682	105.2	1.0 x 0.4	30.6 x 12.2
Mrk 1205	PGC 022206	07 55 48.9	+16 33 23	13953	191.1	0.5 x 0.4	27.8 x 22.2
Mrk 1206	PGC 022288	07 57 10.4	+14 39 32	14256	195.3	0.4 x 0.4	22.7 x 22.7
Mrk 1224	IC 2431	-9 04 35.3	+14 35 39	14948	204.8	0.5	29.8
Mrk 1229	IC 2453	09 15 54.5	+26 55 44	9082	124.4	0.8 x 0.4	28.9 x 14.5
Mrk 1231	MCG -02-24-010	09 19 32.7	-10 29 56	11204	153.5	0.7 x 0.6	31.3 x 26.8
Mrk 1277	CGCG 010-065	11 03 35.5	-01 23 30	10864	148.8	0.8 x 0.5	34.6 x 21.6
Mrk 1286	PGC 034604	11 18 49.0	+78 05 02s	25339	347.1	...	...
Mrk 1298	PG 1126-041	11 29 16.6	-04 24 08	18563	254.3	...	...

Table 3.1 (continued)

Name	Alternate Name	R.A. (J2000.0)	Dec (J2000.0)	V (km s^{-1})	D (Mpc)	a x b (′)	a x b (Kpc)
(1)	(2)	(3)	(4)	(5)	(6)	(7)	(8)
Mrk 1300	PGC 035761	11 34 30.6	+24 24 47	10239	140.3	0.3 x 0.2	12.2 x 8.2
Mrk 1314	PGC 039048	12 14 01.6	-09 34 11	19185	262.8	0.7 x 0.4	53.5 x 30.6
Mrk 1332	CGCG 014-105	12 41 59.2	-03 35 00	14478	198.3	0.7 x 0.3	40.4 x 17.3
Mrk 1339	CGCG 043-058	12 54 14.0	+05 21 53	14603	200.0	0.7 x 0.7	40.7 x 40.7
Mrk 1340	PGC 044186	12 56 46.6	+05 54 59	9457	129.5	0.4 x 0.3	15.1 x 11.3
Mrk 1362	PGC 049070	13 49 54.5	+23 19 10	17017	233.1	0.5 x 0.3	33.9 x 20.3
Mrk 1365	UGC 08827	13 54 31.2	+15 02 39	5730	78.5	0.8 x 0.7	18.3 x 16.0
Mrk 1380	PGC 051278	14 21 08.1	+30 37 49	15670	214.7	0.5 x 0.4	31.2 x 25.0
Mrk 1382	VIIIZw 421	14 28 09.8	-01 40 32	9292	127.3	0.5	18.5
Mrk 1387	CGCG 105-009	14 43 52.3	+16 28 27	16466	225.6	0.6 x 0.5	39.4 x 32.8
Mrk 1391	CGCG 105-091	15 00 55.3	+16 56 49	9300	127.4	0.4 x 0.3	14.8 x 11.1
Mrk 1405	UGC 02836	03 43 56.9	+39 17 43	5113	70.0	1.0 x 0.9	20.4 x 18.3
Mrk 1406	PGC 021127	07 29 32.1	+55 01 56	12011	164.5	0.4 x 0.4	19.1 x 19.1
Mrk 1420	KUG 0938+482	09 42 09.9	+48 00 46	16780	229.9	0.3	20.1
Mrk 1428	KUG 1002+445	10 05 11.2	+44 19 05	21538	295.0	...	...
Mrk 1432	CGCG 240-043	10 26 47.5	+47 04 56	17873	244.8	0.4 x 0.3	28.5 x 21.4
Mrk 1433	UGC 05733	10 33 47.8	+52 22 17	11147	152.7	0.9 x 0.5	40.0 x 22.2

Table 3.1 (continued)

Name	Alternate Name	R.A. (J2000.0)	Dec (J2000.0)	V (km s^{-1})	D (Mpc)	a x b (′)	a x b (Kpc)
(1)	(2)	(3)	(4)	(5)	(6)	(7)	(8)
Mrk 1464	CG 1480	11 55 57.1	+43 35 35	11103	152.1	0.5 x 0.5	22.1 x 22.1
Mrk 1490	SBS 1417+494	14 19 43.2	+49 14 12	8016	109.8	0.5 x 0.4	16.0 x 12.8
Mrk 1497	SBS 1625+496	16 27 01.7	+49 32 07	14572	199.6	0.6 x 0.4	34.8 x 23.2

Col. (1) Primary galaxy name. Col. (2) Alternate name. Most galaxies in this sample have multiple alternate designations, reflecting their inclusion in a number of catalogs. Cols. (3)-(4) Right Ascension and Declination, obtained from NASA's Extragalactic Database (NED). The coordinates are from the J2000 epoch. Col. (5) Recessional velocity, corrected for Galactic motion and Virgo infall, obtained from NED. Col. (6) Distance in megaparsecs, derived using Col. (5) and $H_0 = 73$ km $s^{-}1$ $Mpc^{-}1$. Col. (7) Angular diameter of the major and minor axes, expressed in arcminutes. Col. (8) Corresponding physical diameter expressed in kiloparsecs derived using the distances in Col. (6).

3.2.2 Ultraviolet Data and *GALEX*

GALEX (Martin et al. 2005) is a NASA small explorer class mission, launched on 2003 April 28, that is performing a series of imaging and spectroscopic sky surveys in two ultraviolet bands, FUV and NUV. The instrument consists of a 50cm aperture Ritchy-Chrétien telescope with a circular field of view of 1.2° in diameter and a resolution of ≈4.2″-5.3″ for FUV−NUV (Morrissey et al. 2007). The effective wavelengths of the two *GALEX* bands are 1516 and 2267 $\mathring{A}$, and their full widths at half-maximum are 269 and 616 $\mathring{A}$ respectively, for the FUV and NUV channels. The compilation of *GALEX* UV data will allow researchers to provide fundamental clues for solving some of the many open questions regarding the UV properties of galaxies in the local universe.

The photometric system used by *GALEX* is based on the AB magnitude scale (Oke & Gunn 1983). Magnitudes are defined as a relative unit, such as

$$m_1 - m_2 = -2.5 \log(f_1/f_2) = -2.5 \log f_1 + 2.5 \log f_2. \tag{3.1}$$

In order to tie this to a physical scale the star Vega can be used, which by definition has m=0 in all passbands if you are in the Johnson magnitude system. Then

$$m = -2.5 \log f(\lambda) + 2.5 \log f(\lambda) Vega. \tag{3.2}$$

The last term is called the zeropoint, the different magnitude systems each define this zeropoint differently. The Vega spectrum is different from a constant flux density. Therefore, m= 0 corresponds to very different physical fluxes in different passbands.

To avoid the changing flux densities in the Johnson system and exceedingly small fluxes outside the ultraviolet and near-infrared, the AB magnitude system was devised by Oke and Gunn in 1983. In the AB magnitude system the reference spectrum is flat in f = const [ergs s^{-1} cm^{-2} Hz^{-1}]; this constant is chosen so that m_v(vega) = m_v(AB). If you are not in the AB magnitude system, for example if you are in the Johnson System, the zero point will change with wavelength. Both the *GALEX* and SDSS data are in the AB magnitude system.

We corrected the UV photometry for foreground Galactic extinction using E(B−V) values calculated using V band extinctions tabulated in NED and R_v = 3.1. We adopted the Wyder et al. 2007 coefficients of the interstellar dust extinction law in the *GALEX* bandpasses:

$$A_{FUV} = 8.24 \times E(B-V) \tag{3.3}$$

and

$$A_{NUV} = 8.2 \times E(B-V). \tag{3.4}$$

The extinction A_x of a star in some waveband X is defined to be the difference between the observed X-band magnitude m(X) and the magnitude m_0(X) that would be observed in the absence of dust. The reddening, or color excess, E(X−Y) in some color X-Y is defined to be the difference between the observed color m(X)−m(Y) and the intrinsic color m_0(X)−m_0(Y). The most often cited color excess is E(B−V). R, is the ratio of selective to total extinction. An extinction curve shows the ratio A_λ/A_J of the extension at wavelength λ to that in the Johnson J-band. A_λ peaks in

the far-UV, near 73nm. Shorter wavelengths, like X-rays, pass right through grains, while much longer wavelength radiation refracts around them. The extinction curve is unchanging in the R-band and redward from it, hence us not correcting for reddening with our infrared data, but variable (shows variations based on location in the sky) at V and blueward of V. The ratio of A_λ/A_J changes with varying lines of sight. If the type of dust was the same in all directions, the ratio of the extinctions at any two frequencies would be the same for all lines of sight.

The observed and corrected *GALEX* photometry is presented in Table 3.2 along with the derived UV luminosity for both samples. Seventeen galaxies did not have data available in the *GALEX* archive, and therefore are not listed.

Table 3.2. Ultraviolet Photometry and Star Formation Rates for the Combined Sample

Name	FUV	NUV	FUV_c	NUV_c	FUV−NUV	$E(B-V)$	log L_{FUV} (erg s^{-1} Hz^{-1})	SFR_{FUV} ($M_\odot$/yr)
(1)	(2)	(3)	(4)	(5)	(6)	(7)	(8)	(9)
McDonald Sample								
Mrk 342	19.79	19.33	19.19	18.73	0.46	0.07	27.33	0.30
Haro 15	15.10	14.86	14.91	14.67	...	0.02	28.55	4.97
Mrk 360	16.98	16.46	16.42	15.90	0.53	0.07	28.16	2.00
Mrk 364	18.90	17.99	18.22	17.32	0.90	0.08	27.45	0.39
Mrk 366	18.23	17.64	17.50	16.91	0.59	0.09	27.71	0.72
Mrk 367	18.27	17.70	17.47	16.90	0.57	0.10	28.01	1.43
Mrk 589	17.50	16.85	17.15	16.51	0.65	0.04	27.11	0.18
Mrk 1184	18.23	17.16	17.92	16.85	1.07	0.04	27.62	0.58
Mrk 1404	18.32	17.39	17.70	16.77	0.93	0.07	27.89	1.08
Mrk 1079	17.19	16.31	16.71	15.83	0.88	0.06	28.08	1.68
Mrk 8	...	15.50	...	15.28	...	0.03	...	...
Haro 1	14.89	14.28	14.54	13.93	0.61	0.04	28.28	2.65
Mrk 1211	18.27	17.50	17.99	17.22	0.77	0.03	28.12	1.85

Table 3.2 (continued)

Name	FUV	NUV	FUV_c	NUV_c	FUV−NUV	$E(B-V)$	log L_{FUV} (erg s^{-1} Hz^{-1})	SFR_{FUV} ($M_\odot$/yr)
(1)	(2)	(3)	(4)	(5)	(6)	(7)	(8)	(9)
Mrk 390	16.82	16.42	16.48	16.08	0.40	0.04	28.09	1.74
Mrk 18	17.31	16.79	16.90	16.38	0.52	0.05	27.26	0.25
Mrk 402	17.35	16.80	17.19	16.64	0.55	0.02	27.79	0.86
IIZw 44	17.92	17.43	17.73	17.24	0.49	0.02	27.41	0.36
Mrk 144	17.53	17.04	17.42	16.93	0.49	0.01	27.79	0.87
Mrk 33	14.97	14.72	14.88	14.62	0.26	0.01	27.46	0.40
Mrk 148	19.09	18.31	18.93	18.16	0.78	0.02	27.08	0.17
Haro 25	16.85	16.32	16.58	16.05	0.53	0.03	28.06	1.61
Mrk 154	17.78	17.35	17.66	17.24	0.42	0.01	28.06	1.61
Mrk 171	15.54	15.07	15.40	14.93	0.47	0.02	27.82	0.93
Mrk 181	16.69	16.07	16.48	15.85	0.63	0.03	27.92	1.17
Haro 34	17.42	16.89	17.08	16.55	0.53	0.04	27.75	0.80
Mrk 54	15.73	15.47	15.61	15.35	0.26	0.01	28.94	12.16
Mrk 238	19.14	...	19.00	...	...	0.02	27.67	0.66
Mrk 248	19.18	...	19.02	...	...	0.02	27.40	0.35
Mrk 255	16.81	16.49	16.68	16.36	0.32	0.02	28.18	2.14

Table 3.2 (continued)

Name	FUV	NUV	FUV_c	NUV_c	FUV−NUV	$E(B-V)$	log L_{FUV} (erg s^{-1} Hz^{-1})	SFR_{FUV} ($M_\odot$/yr)
(1)	(2)	(3)	(4)	(5)	(6)	(7)	(8)	(9)
Mrk 271	18.66	17.93	18.59	17.86	0.73	0.01	27.26	0.25
IZw 101	17.40	16.92	17.24	16.77	0.48	0.02	27.45	0.40
Mrk 492	19.33	18.19	18.91	17.77	1.13	0.05	26.67	0.07
Mrk 297	15.26	14.80	14.63	14.17	0.46	0.08	28.46	4.03
Mrk 300	19.11	18.20	18.68	17.77	0.91	0.05	27.59	0.54
Mrk 697	...	20.90	...	20.59	...	0.04	...	...
Mrk 499	16.72	16.17	16.58	16.03	0.55	0.02	28.10	1.75
Mrk 518	22.45	...	21.68	...	...	0.09	26.19	0.02
Mrk 303	17.35	16.84	16.93	16.42	0.51	0.05	27.91	1.15
Mrk 306	16.53	16.06	16.06	15.59	0.47	0.06	28.01	1.43
IIZw 185	...	22.07	...	21.56	0.06	...	...	
Mrk 531	18.63	17.22	18.29	16.89	1.40	0.04	26.72	0.07
Mrk 325	14.80	14.50	14.44	14.15	0.30	0.04	28.24	2.42

High Star Formation Rate Sample

Table 3.2 (continued)

Name	FUV	NUV	FUV_c	NUV_c	FUV−NUV	$E(B-V)$	$\log L_{FUV}$ (erg s^{-1} Hz^{-1})	SFR_{FUV} ($M_\odot$/yr)
(1)	(2)	(3)	(4)	(5)	(6)	(7)	(8)	(9)
Mrk 2	16.91	16.29	16.24	15.63	0.62	0.08	27.93	1.20
Mrk 83	18.22	17.76	17.80	17.34	0.46	0.05	28.12	1.85
Mrk 91	19.12	17.67	18.76	17.30	1.46	0.04	26.86	0.10
Mrk 97	18.99	18.02	18.46	17.49	0.97	0.06	27.24	0.25
Mrk 103	18.12	17.47	17.41	16.76	0.65	0.09	27.90	1.12
Mrk 114	17.89	17.19	17.61	16.91	0.70	0.03	27.65	0.62
Mrk 126	18.03	17.32	17.93	17.22	0.71	0.01	27.90	1.10
Mrk 143	...	17.79	...	17.72	...	0.01	...	...
Mrk 161	16.89	15.53	16.81	15.46	1.35	0.01	27.77	0.83
Mrk 183	17.22	16.94	17.10	16.82	0.28	0.01	28.27	2.59
Mrk 204	18.33	17.97	18.18	17.82	0.36	0.02	28.14	1.92
Mrk 217	19.09	18.31	18.94	18.16	0.78	0.02	27.65	0.62
Mrk 237	17.21	16.62	17.07	16.48	0.58	0.02	28.01	1.45
Mrk 254	17.13	16.86	17.02	16.75	0.27	0.01	28.03	1.50
Mrk 261	17.63	16.92	17.33	16.63	0.71	0.04	27.93	1.19
Mrk 264	18.53	17.81	18.47	17.75	0.72	0.01	28.09	1.71

Table 3.2 (continued)

Name	FUV	NUV	FUV_c	NUV_c	FUV−NUV	$E(B-V)$	log L_{FUV} (erg s^{-1} Hz^{-1})	SFR_{FUV} ($M_\odot$/yr)
(1)	(2)	(3)	(4)	(5)	(6)	(7)	(8)	(9)
Mrk 265	18.82	18.05	18.70	17.93	0.77	0.01	27.45	0.40
Mrk 269	18.42	17.78	18.24	17.60	0.64	0.02	27.94	1.21
Mrk 286	16.23	15.49	16.06	15.31	0.74	0.02	28.29	2.70
Mrk 319	17.67	16.71	16.82	15.86	0.95	0.10	28.02	1.45
Mrk 327	...	20.36	...	19.93	...	0.05	...	...
Mrk 349	18.05	17.47	17.71	17.13	0.58	0.04	27.52	0.46
Mrk 353	17.88	17.03	17.50	16.66	0.85	0.04	27.26	0.26
Mrk 354	18.50	17.84	18.21	17.55	0.66	0.04	27.93	1.19
Mrk 368	17.12	16.64	16.23	15.75	0.49	0.11	28.31	2.84
Mrk 387	17.26	16.94	16.94	16.61	0.32	0.04	28.23	2.40
Mrk 413	18.70	17.60	18.58	17.47	1.11	0.01	27.62	0.58
Mrk 414	17.97	17.48	17.80	17.31	0.49	0.02	27.91	1.14
Mrk 440	18.47	17.82	18.36	17.72	0.64	0.01	27.93	1.20
Mrk 489	16.48	15.93	16.31	15.76	0.55	0.02	28.37	3.30
Mrk 496	16.29	15.66	16.12	15.49	0.63	0.02	28.38	3.37
Mrk 540	19.13	18.22	18.76	17.85	0.91	0.04	28.07	1.63

Table 3.2 (continued)

Name	FUV	NUV	FUV_c	NUV_c	FUV−NUV	$E(B-V)$	log L_{FUV} (erg s^{-1} Hz^{-1})	SFR_{FUV} ($M_\odot$/yr)
(1)	(2)	(3)	(4)	(5)	(6)	(7)	(8)	(9)
Mrk 545	16.48	15.55	16.16	15.24	0.92	0.04	27.79	0.87
Mrk 556	18.61	18.27	18.43	18.09	0.34	0.02	27.73	0.75
Mrk 559	18.84	18.12	18.32	17.60	0.72	0.06	27.83	0.94
Mrk 560	19.95	19.01	19.68	18.73	0.95	0.03	27.36	0.32
Mrk 567	18.08	17.21	17.88	17.00	0.87	0.03	27.75	0.79
Mrk 569	17.22	16.82	16.98	16.58	0.40	0.03	28.09	1.70
Mrk 575	18.91	16.90	18.14	16.13	2.02	0.09	27.14	0.19
Mrk 579	19.27	18.39	18.84	17.96	0.88	0.05	27.96	1.27
Mrk 582	16.98	16.51	16.77	16.29	0.47	0.03	27.69	0.69
Mrk 592	17.35	16.53	17.06	16.24	0.82	0.04	27.85	1.00
Mrk 593	...	16.13	...	15.43	...	0.09	...	...
Mrk 629	17.93	17.25	17.61	16.93	0.67	0.04	27.85	0.99
Mrk 632	19.37	18.74	19.10	18.48	0.63	0.03	27.42	0.37
Mrk 637	18.49	17.67	18.27	17.46	0.82	0.03	28.19	2.17
Mrk 639	18.32	17.75	18.01	17.43	0.58	0.04	27.72	0.73
Mrk 681	19.64	18.80	19.18	18.34	0.84	0.06	27.89	1.08

Table 3.2 (continued)

Name	FUV	NUV	FUV_c	NUV_c	FUV−NUV	$E(B-V)$	log L_{FUV} (erg s^{-1} Hz^{-1})	SFR_{FUV} ($M_\odot$/yr)
(1)	(2)	(3)	(4)	(5)	(6)	(7)	(8)	(9)
Mrk 688	17.77	17.07	17.42	16.71	0.71	0.04	28.09	1.71
Mrk 693	19.09	18.18	18.59	17.68	0.91	0.06	26.81	0.09
Mrk 702	17.31	16.91	17.10	16.71	0.40	0.03	28.48	4.27
Mrk 717	18.12	17.08	17.82	16.78	1.04	0.04	27.40	0.36
Mrk 718	17.57	16.83	17.33	16.59	0.73	0.03	27.84	0.97
Mrk 719	17.20	16.70	16.97	16.47	0.50	0.03	28.09	1.72
Mrk 726	17.30	16.71	17.08	16.49	0.59	0.03	28.33	3.02
Mrk 753	19.18	18.68	18.90	18.40	0.50	0.03	27.80	0.89
Mrk 785	16.74	16.52	16.65	16.43	0.22	0.01	28.60	5.62
Mrk 789	17.31	16.76	17.05	16.49	0.55	0.03	28.06	1.60
Mrk 799	...	15.34	...	15.21	...	0.01	...	...
Mrk 809	17.66	16.71	17.48	16.54	0.94	0.02	27.71	0.72
Mrk 823	17.32	16.88	17.02	16.57	0.45	0.04	28.39	3.46
Mrk 834	18.14	17.08	17.99	16.93	1.06	0.02	27.81	0.90
Mrk 837	16.93	16.38	16.56	16.02	0.54	0.04	28.27	2.61
Mrk 839	16.52	16.08	15.48	15.04	0.44	0.13	27.97	1.31

Table 3.2 (continued)

Name	FUV	NUV	FUV_c	NUV_c	FUV−NUV	$E(B-V)$	log L_{FUV} (erg s^{-1} Hz^{-1})	SFR_{FUV} ($M_\odot$/yr)
(1)	(2)	(3)	(4)	(5)	(6)	(7)	(8)	(9)
Mrk 848	17.87	17.10	17.66	16.88	0.77	0.03	28.03	1.51
Mrk 851	18.92	17.90	18.50	17.48	1.02	0.05	27.58	0.53
Mrk 858	...	19.39	...	18.88	...	0.06	...	...
Mrk 860	17.92	17.51	17.53	17.12	0.42	0.05	27.61	0.56
Mrk 863	17.63	17.07	17.28	16.72	0.04	28.22	2.33	
Mrk 867	...	19.33	...	18.88	...	0.05	...	...
Mrk 881	16.89	16.42	16.83	16.36	0.47	0.01	28.08	1.70
Mrk 891	16.93	16.61	16.77	16.45	0.32	0.02	28.58	5.35
Mrk 904	18.29	17.55	17.78	17.04	0.73	0.06	27.79	0.87
Mrk 923	17.81	17.20	17.25	16.64	0.60	0.07	27.75	0.79
Mrk 932	18.68	17.85	18.33	17.50	0.83	0.04	28.05	1.57
Mrk 938	17.21	16.19	16.99	15.97	1.02	0.03	27.65	0.62
Mrk 940	19.41	18.71	18.99	18.29	0.70	0.05	27.88	1.06
Mrk 941	19.47	18.93	19.00	18.45	0.54	0.06	27.63	0.60
Mrk 948	18.95	18.27	18.71	18.02	0.68	0.03	27.59	0.55
Mrk 955	...	17.44	...	17.26	...	0.02	...	...

Table 3.2 (continued)

Name	FUV	NUV	FUV_c	NUV_c	FUV−NUV	$E(B-V)$	log L_{FUV} (erg s^{-1} Hz^{-1})	SFR_{FUV} ($M_\odot$/yr)
(1)	(2)	(3)	(4)	(5)	(6)	(7)	(8)	(9)
Mrk 984	16.78	16.30	16.52	16.05	0.47	0.03	28.61	5.75
Mrk 995	19.56	18.41	19.32	18.17	1.15	0.03	27.51	0.45
Mrk 1001	18.72	18.22	18.33	17.84	0.50	0.05	28.01	1.42
Mrk 1005	17.66	17.22	17.45	17.02	0.44	0.03	28.13	1.88
Mrk 1027	17.04	...	16.67	...	...	0.04	28.16	2.00
Mrk 1029	19.81	18.65	19.46	18.30	1.16	0.04	27.04	0.15
Mrk 1050	...	17.35	...	16.76	...	0.07	...	...
Mrk 1056	...	18.13	...	17.46	...	0.08	...	...
Mrk1057	17.68	17.15	16.91	16.38	0.53	0.09	28.28	2.68
Mrk 1101	16.22	15.79	16.07	15.64	0.43	0.02	28.54	4.90
Mrk 1111	19.86	18.42	19.25	17.81	1.44	0.07	27.27	0.26
Mrk 1112	...	18.90	...	18.34	...	0.07	...	...
Mrk 1115	19.89	18.62	19.67	18.41	1.27	0.03	27.61	0.58
Mrk 1117	18.36	17.45	18.01	17.10	0.91	0.04	27.98	1.35
Mrk 1122	19.62	18.21	19.25	17.84	1.40	0.04	27.40	0.35
Mrk 1143	18.63	17.87	18.42	17.66	0.76	0.03	27.63	0.60

Table 3.2 (continued)

Name	FUV	NUV	FUV_c	NUV_c	FUV−NUV	$E(B-V)$	log L_{FUV} (erg s^{-1} Hz^{-1})	SFR_{FUV} ($M_\odot$/yr)
(1)	(2)	(3)	(4)	(5)	(6)	(7)	(8)	(9)
Mrk 1151	20.75	19.47	20.53	19.25	1.28	0.03	27.12	0.18
Mrk 1156	17.41	17.04	16.96	16.60	0.37	0.05	28.18	2.10
Mrk 1159	18.37	17.71	18.00	17.34	0.67	0.04	28.35	3.10
Mrk 1198	17.85	17.09	17.34	16.58	0.76	0.06	27.75	0.78
Mrk 1205	18.57	18.13	18.29	17.84	0.45	0.03	27.89	1.07
Mrk 1206	18.07	17.44	17.76	17.14	0.64	0.04	28.11	1.82
Mrk 1224	16.64	16.18	16.23	15.77	0.46	0.05	28.77	8.26
Mrk 1229	19.07	18.37	18.79	18.09	0.70	0.04	27.31	0.29
Mrk 1231	18.37	17.53	17.92	17.07	0.84	0.06	27.85	0.98
Mrk 1277	18.68	17.52	18.28	17.12	1.16	0.05	27.67	0.66
Mrk 1286	18.74	18.16	18.52	17.93	0.59	0.03	28.31	2.87
Mrk 1298	16.28	15.69	15.83	15.23	0.59	0.06	29.12	18.38
Mrk 1300	18.34	17.96	18.17	17.78	0.39	0.02	27.66	0.65
Mrk 1314	19.82	18.48	19.13	17.78	1.34	0.08	27.83	0.94
Mrk 1332	18.64	18.17	18.41	17.94	0.47	0.03	27.87	1.04
Mrk 1339	18.21	17.74	17.92	17.45	0.47	0.04	28.07	1.66

Table 3.2 (continued)

Name	FUV	NUV	FUV_c	NUV_c	FUV−NUV	$E(B-V)$	log L_{FUV} (erg s^{-1} Hz^{-1})	SFR_{FUV} ($M_\odot$/yr)
(1)	(2)	(3)	(4)	(5)	(6)	(7)	(8)	(9)
Mrk 1340	18.10	17.43	17.82	17.15	0.68	0.03	27.73	0.76
Mrk 1362	18.92	18.54	18.81	18.43	0.38	0.01	27.85	0.99
Mrk 1365	17.52	16.64	17.33	16.45	0.88	0.02	27.50	0.44
Mrk 1380	17.65	17.21	17.49	17.06	0.44	0.02	28.30	2.82
Mrk 1382	17.86	17.11	17.43	16.69	0.74	0.05	27.88	1.05
Mrk 1387	18.15	17.56	17.92	17.33	0.59	0.03	28.18	2.11
Mrk 1391	17.62	17.18	17.35	16.91	0.44	0.03	27.91	1.14
Mrk 1405	18.78	17.93	16.49	15.64	0.85	0.28	27.73	0.76
Mrk 1406	18.71	18.33	18.18	17.79	0.39	0.07	27.80	0.88
Mrk 1420	17.48	17.00	17.38	16.89	0.49	0.01	28.41	3.61
Mrk 1428	18.57	18.26	18.48	18.17	0.31	0.01	28.19	2.15
Mrk 1432	18.48	17.92	18.40	17.84	0.56	0.01	28.06	1.60
Mrk 1433	17.58	16.85	17.44	16.71	0.73	0.02	28.03	1.50
Mrk 1464	17.08	16.82	16.95	16.69	0.25	0.02	28.22	2.35
Mrk 1490	...	19.33	...	19.18	...	0.02	...	...
Mrk 1497	18.31	17.52	18.12	17.34	0.79	0.02	27.99	1.37

Table 3.2 (continued)

Name	FUV	NUV	FUV_c	NUV_c	FUV−NUV	$E(B-V)$	log L_{FUV} (erg s^{-1} Hz^{-1})	SFR_{FUV} ($M_\odot$/yr)
(1)	(2)	(3)	(4)	(5)	(6)	(7)	(8)	(9)

Col. (1) Primary galaxy name. Cols. (2 & 3) The FUV and NUV magnitudes are from GALEX's 5th data release on the Mikulski Archive for Space Telescopes (MAST). Cols. (4 & 5) Corresponding integrated magnitudes corrected for foreground Galactic extinction. Col. (6) The FUV−NUV color. Col. (7) Line-of-sight color excess, obtained from the V band extinctions tabulated in NED and $R_V = 3.1; A_{FUV} = 8.24 * E(B-V); A_{NUV} = 8.2 * E(B-V)$. Extinction law coefficients for the GALEX bands are from Wyder et al. (2007). Col (8). Log of the far-UV luminosity derived from the extinction-corrected FUV magnitude listed in Col.4 and the distances listed in Tables 2.1 and 3.1. Col. (9) Star formation rates derived from the far-UV luminosity in Col. 7 and the scaling relation from Kennicutt (1998), presented in Eq. 3.5.

3.2.3 Thermal Infrared Data and *IRAS*

IRAS was a joint NASA, Netherlands, and United Kingdom mission to perform an unbiased, sensitive all sky survey at 12, 25, 60 and 100 μm. Table 3.3 lists the *IRAS* data. The infrared data is not extinction corrected because the corrections would be within the uncertainty. The galaxies which had no *IRAS* data were left out of the table.

Table 3.3. Thermal Infrared Photometry and Star Formation Rates for the Combined Samples

Name	12μm	25μm	60μm	100μm	Log F_{IR}	Log L_{IR}	Log $L/L_\odot$	SFR_{IR}
	Jy	Jy	Jy	Jy	(J s^{-1} m^{-2})	(erg s^{-1})		($M_\odot$/yr)
(1)	(2)	(3)	(4)	(5)	(6)	(7)	(8)	(9)
McDonald Sample								
Haro 15	0.12	0.30	1.36	1.97	-12.81	44.14	10.56	6.26
Mrk 360	0.14	0.19	0.64	1.64	-12.95	44.21	10.63	7.36
Mrk 364	0.08	0.15	0.88	1.51	-12.99	44.18	10.60	6.90
Mrk 366	0.11	0.19	1.01	1.68	-12.91	44.24	10.66	7.81
Mrk 367	0.10	0.21	0.81	1.51	-12.96	44.48	10.89	13.45
Mrk 589	0.17	0.39	2.72	3.34	-12.58	43.84	10.26	3.11
Mrk 1184	0.13	0.32	2.52	4.97	-12.57	44.66	11.07	20.48
Mrk 1404	0.10	0.14	1.32	3.29	-12.80	44.61	11.02	18.25
Mrk 1079	0.15	0.31	2.70	5.16	-12.55	44.66	11.07	20.46
Mrk 1094	0.06	0.12	0.69	2.20	-13.01	43.22	9.64	0.75
Mrk 8	0.09	0.37	2.46	3.97	-12.62	43.91	10.33	3.68
Haro 1	0.61	1.19	8.75	13.58	-12.04	44.49	10.91	13.95
Mrk 385	0.06	0.14	0.92	1.65	-12.99	44.20	10.62	7.17
Mrk 1211	0.25	0.25	0.59	1.29	-12.87	44.88	11.30	34.51

Table 3.3 (continued)

Name	12μm	25μm	60μm	100μm	Log F_{IR}	Log L_{IR}	Log $L/L_{\odot}$	SFR_{IR}
	Jy	Jy	Jy	Jy	(J s^{-1} m^{-2})	(erg s^{-1})		($M_{\odot}$/yr)
(1)	(2)	(3)	(4)	(5)	(6)	(7)	(8)	(9)
Mrk 390	0.07	0.16	0.58	0.93	-13.12	44.01	10.42	4.58
Mrk 18	0.14	0.25	2.16	2.97	-12.67	43.79	10.21	3.75
Mrk 402	0.11	0.14	0.34	0.53	-13.19	43.92	10.33	3.72
IIZw 44	0.10	0.25	1.24	2.08	-12.85	44.09	10.51	5.60
Mrk 139	0.08	0.12	0.44	0.62	-13.20	43.61	10.03	1.83
Mrk 144	0.10	0.11	0.54	1.32	-13.08	44.12	10.54	5.96
Mrk 33	0.21	1.05	4.77	5.99	-12.32	43.53	9.94	1.51
Mrk 148	0.10	0.11	0.34	0.83	-13.18	43.91	10.33	3.68
Haro 25	0.10	0.53	2.30	2.42	-12.65	44.48	10.90	13.63
Mrk 154	0.09	0.09	0.60	1.15	-13.10	44.46	10.88	13.11
Mrk 171	3.90	24.14	121.64	122.45	-10.96	45.46	11.88	131.13
Mrk 181	0.12	0.24	2.11	4.49	-12.64	44.32	10.73	9.37
Haro 34	0.17	0.28	1.30	3.11	-12.74	44.29	10.70	8.75
Mrk 54	0.10	0.14	0.94	1.83	-12.94	44.68	11.09	21.47
Mrk 255	0.11	0.07	0.23	0.62	-13.26	44.03	10.45	4.85
Haro 42	0.09	0.14	0.80	1.08	-13.04	43.66	10.08	2.08
IZw 101	0.06	0.06	0.29	0.95	-13.30	43.49	9.90	1.39

Table 3.3 (continued)

Name	12μm	25μm	60μm	100μm	Log F_{IR}	Log L_{IR}	Log $L/L_{\odot}$	SFR_{IR}
	Jy	Jy	Jy	Jy	(J s^{-1} m^{-2})	(erg s^{-1})		($M_{\odot}$/yr)
(1)	(2)	(3)	(4)	(5)	(6)	(7)	(8)	(9)
Mrk 492	0.20	0.79	3.26	2.92	-12.49	44.18	10.60	6.88
Mrk 297	0.28	0.83	6.79	10.57	-12.19	44.56	10.98	16.53
Mrk 300	0.08	0.10	0.66	2.13	-13.01	44.50	10.91	17.17
IZw 191	0.08	0.08	0.71	1.22	-13.09	43.84	10.25	3.09
Mrk 512	0.15	0.28	2.54	3.83	-12.60	44.73	11.15	24.21
Mrk 518	0.38	0.33	2.84	3.61	-12.50	44.81	11.22	28.86
Mrk 306	0.10	0.16	1.10	2.37	-12.88	43.99	10.41	4.44
IIZw 185	0.10	0.10	0.54	2.54	-12.98	44.10	10.52	5.67
Mrk 531	0.17	0.67	4.79	8.32	-12.32	44.16	10.57	6.42
Mrk 325	0.13	0.52	4.98	6.89	-12.36	44.10	10.51	5.60
High Star Formation Rate Sample								
Mrk 2	0.21	0.99	5.89	7.81	-12.25	44.62	11.03	18.63
Mrk 83	0.08	0.14	0.44	0.88	-13.16	44.53	10.94	15.05
Mrk 91	0.20	0.70	4.89	7.33	-12.33	44.47	10.89	13.34
Mrk 97	0.10	0.24	1.90	2.83	-12.73	44.34	10.75	9.77

Table 3.3 (continued)

Name	12μm	25μm	60μm	100μm	Log F_{IR}	Log L_{IR}	Log $L/L_{\odot}$	SFR_{IR}
	Jy	Jy	Jy	Jy	(J s^{-1} m^{-2})	(erg s^{-1})		($M_{\odot}$/yr)
(1)	(2)	(3)	(4)	(5)	(6)	(7)	(8)	(9)
Mrk 103	0.08	0.24	0.94	1.74	-12.93	44.38	10.79	10.72
Mrk 114	0.08	0.18	1.48	2.94	-12.80	44.33	10.75	9.65
Mrk 126	0.10	0.12	0.55	1.56	-13.04	44.46	10.88	13.04
Mrk 143	0.09	0.09	0.60	1.15	-13.10	45.13	11.55	60.95
Mrk 161	0.12	0.40	2.27	4.50	-12.60	44.34	10.76	9.90
Mrk 183	0.06	0.13	0.36	1.31	-13.18	44.37	10.78	10.49
Mrk 204	0.07	0.07	0.23	0.78	-13.32	44.53	10.95	15.30
Mrk 217	0.08	0.10	0.46	0.72	-13.21	44.44	10.86	12.92
Mrk 237	0.12	0.15	1.49	2.74	-12.79	44.49	10.90	13.78
Mrk 254	0.09	0.11	1.13	2.24	-12.90	44.37	10.79	10.67
Mrk 261	0.09	0.08	0.98	1.92	-12.96	44.34	10.76	9.95
Mrk 264	0.09	0.11	0.76	2.46	-12.95	44.96	11.37	40.86
Mrk 265	0.11	0.13	0.90	1.23	-12.99	44.38	10.80	10.91
Mrk 269	0.09	0.06	0.32	0.72	-13.26	44.41	10.83	11.60
Mrk 286	0.22	0.70	4.35	6.85	-12.35	44.80	11.21	28.12
Mrk 311	0.10	0.24	1.82	3.31	-12.72	44.57	10.99	16.73
Mrk 312	0.15	0.23	0.65	1.30	-12.95	44.38	10.79	10.74

Table 3.3 (continued)

Name	12μm	25μm	60μm	100μm	Log F_{IR}	Log L_{IR}	Log $L/L_{\odot}$	SFR_{IR}
	Jy	Jy	Jy	Jy	(J s^{-1} m^{-2})	(erg s^{-1})		($M_{\odot}$/yr)
(1)	(2)	(3)	(4)	(5)	(6)	(7)	(8)	(9)
Mrk 319	0.22	0.54	4.27	7.06	-12.37	44.82	11.23	29.48
Mrk 321	0.18	0.26	2.41	5.74	-12.55	44.78	11.20	27.15
Mrk 327	0.13	0.12	0.33	1.18	-13.10	44.39	10.80	11.05
Mrk 349	0.14	0.34	1.95	2.49	-12.70	44.34	10.76	9.88
Mrk 353	0.23	0.57	3.88	5.71	-12.41	44.30	10.72	8.98
Mrk 354	0.12	0.15	0.70	0.90	-13.04	44.62	11.03	18.56
Mrk 368	0.08	0.19	0.69	2.83	-12.92	44.32	10.74	9.48
Mrk 387	0.17	0.35	0.67	1.00	-12.91	44.54	10.95	15.57
Mrk 413	0.09	0.19	1.25	2.13	-12.86	44.63	11.04	19.00
Mrk 414	0.06	0.14	0.55	1.57	-13.09	44.38	10.80	10.88
Mrk 440	0.07	0.15	0.81	1.37	-13.03	44.69	11.10	21.86
Mrk 489	0.11	0.22	1.81	4.69	-12.67	44.67	11.09	21.04
Mrk 496	0.26	1.24	6.48	9.41	-12.19	45.08	11.50	54.54
Mrk 540	0.10	0.16	0.81	1.66	-12.97	45.03	11.45	48.75
Mrk 545	0.66	1.29	9.03	15.66	-12.01	44.69	11.10	21.97
Mrk 551	0.24	0.80	4.66	5.69	-12.35	45.37	11.79	106.07
Mrk 556	0.09	0.24	0.18	0.82	-13.17	44.37	10.78	10.50

Table 3.3 (continued)

Name	12μm	25μm	60μm	100μm	Log F_{IR}	Log L_{IR}	Log $L/L_{\odot}$	SFR_{IR}
	Jy	Jy	Jy	Jy	(J s^{-1} m^{-2})	(erg s^{-1})		($M_{\odot}$/yr)
(1)	(2)	(3)	(4)	(5)	(6)	(7)	(8)	(9)
Mrk 559	0.15	0.22	0.52	1.30	-12.98	44.61	11.02	18.24
Mrk 560	0.17	0.15	0.21	1.15	-13.07	44.60	11.02	18.00
Mrk 567	0.23	0.43	3.03	4.93	-12.49	44.86	11.27	32.24
Mrk 569	0.11	0.20	0.74	1.34	-12.98	44.33	10.75	9.73
Mrk 575	0.22	0.49	2.79	5.37	-12.49	44.35	10.76	9.99
Mrk 579	0.10	0.18	0.49	1.23	-13.06	44.87	11.28	33.27
Mrk 592	0.21	0.28	1.62	2.41	-12.71	44.41	10.83	11.55
Mrk 593	0.17	0.37	0.82	2.29	-12.81	44.38	10.79	10.70
Mrk 606	0.12	0.15	0.80	1.97	-12.94	44.31	10.73	9.28
Mrk 619	0.10	0.09	0.20	1.14	-13.21	44.39	10.81	11.09
Mrk 629	0.09	0.22	0.94	1.58	-12.94	44.39	10.81	11.06
Mrk 632	0.09	0.17	0.89	1.47	-12.98	44.53	10.94	15.10
Mrk 637	0.13	0.31	1.93	2.49	-12.71	45.23	11.64	76.00
Mrk 639	0.09	0.12	1.40	2.70	-12.83	44.53	10.95	15.40
Mrk 681	0.09	0.14	0.32	1.64	-13.09	44.91	11.32	36.30
Mrk 688	0.11	0.09	0.51	1.27	-13.09	44.40	10.82	11.28
Mrk 693	0.10	0.12	0.56	1.04	-13.10	43.59	10.01	1.75

Table 3.3 (continued)

Name	12μm	25μm	60μm	100μm	Log F_{IR}	Log L_{IR}	Log $L/L_{\odot}$	SFR_{IR}
	Jy	Jy	Jy	Jy	(J s^{-1} m^{-2})	(erg s^{-1})		($M_{\odot}$/yr)
(1)	(2)	(3)	(4)	(5)	(6)	(7)	(8)	(9)
Mrk 702	0.08	0.19	0.67	1.17	-13.06	44.71	11.13	23.09
Mrk 717	0.22	0.76	3.84	4.01	-12.42	44.55	10.96	15.85
Mrk 718	0.14	0.20	1.23	3.31	-12.77	44.44	10.86	12.45
Mrk 719	0.15	0.44	1.16	1.78	-12.79	44.53	10.94	15.08
Mrk 726	0.14	0.18	1.81	2.86	-12.73	44.88	11.29	33.87
Mrk 753	0.11	0.26	0.32	0.79	-13.10	44.70	11.12	22.74
Mrk 785	0.12	0.12	0.68	2.06	-12.96	44.74	11.16	24.94
Mrk 789	0.15	0.62	3.35	5.07	-12.47	44.85	11.26	31.56
Mrk 799	0.50	1.94	10.10	20.34	-11.94	44.45	10.86	12.65
Mrk 809	0.21	0.21	1.99	3.39	-12.65	44.49	10.91	14.02
Mrk 823	0.07	0.15	0.21	1.13	-13.22	44.42	10.84	11.84
Mrk 834	0.21	0.42	2.40	4.85	-12.54	44.90	11.32	36.14
Mrk 837	0.09	0.17	0.76	2.31	-12.95	44.39	10.80	11.02
Mrk 839	0.29	0.89	5.24	8.49	-12.26	44.34	10.76	9.91
Mrk 848	0.31	1.47	9.57	10.75	-12.07	45.47	11.88	131.18
Mrk 851	0.11	0.17	0.75	1.65	-12.97	44.45	10.87	12.74
Mrk 858	0.09	0.17	1.16	2.73	-12.85	44.47	10.89	13.38

Table 3.3 (continued)

Name	12μm	25μm	60μm	100μm	Log F_{IR}	Log L_{IR}	Log $L/L_{\odot}$	SFR_{IR}
	Jy	Jy	Jy	Jy	(J s^{-1} m^{-2})	(erg s^{-1})		($M_{\odot}$/yr)
(1)	(2)	(3)	(4)	(5)	(6)	(7)	(8)	(9)
Mrk 860	0.10	0.54	2.37	2.67	-12.63	44.42	10.84	11.97
Mrk 863	3.00	2.44	2.98	2.12	-11.95	45.63	12.04	190.11
Mrk 867	0.09	0.14	0.52	1.20	-13.09	44.95	11.36	39.69
Mrk 881	0.09	0.16	1.39	2.63	-12.83	44.43	10.85	12.12
Mrk 891	0.07	0.12	0.63	0.69	-13.16	44.57	10.99	16.82
Mrk 904	0.06	0.13	0.85	1.49	-13.03	44.31	10.73	9.21
Mrk 923	0.14	0.19	1.41	2.55	-12.79	44.30	10.71	8.96
Mrk 932	0.09	0.17	0.54	0.94	-13.09	44.73	11.14	24.05
Mrk 938	0.35	2.39	17.05	16.86	-11.85	45.03	11.45	48.21
Mrk 940	0.13	0.11	0.32	0.94	-13.14	44.78	11.20	27.13
Mrk 941	0.08	0.10	0.23	0.85	-13.26	44.42	10.83	11.74
Mrk 948	0.20	0.16	0.45	0.98	-12.99	44.52	10.94	15.02
Mrk 955	0.15	0.41	0.94	1.78	-12.82	44.57	10.98	16.64
Mrk 984	0.11	0.20	0.52	1.69	-13.00	44.66	11.08	20.56
Mrk 995	0.19	0.47	3.60	6.82	-12.42	45.26	11.67	81.39
Mrk 1001	0.17	0.16	0.33	0.79	-13.07	44.71	11.12	22.97
Mrk 1005	0.09	0.23	0.35	0.68	-13.15	44.40	10.81	11.27

Table 3.3 (continued)

Name	12μm	25μm	60μm	100μm	Log F_{IR}	Log L_{IR}	Log $L/L_{\odot}$	SFR_{IR}
	Jy	Jy	Jy	Jy	(J s^{-1} m^{-2})	(erg s^{-1})		($M_{\odot}$/yr)
(1)	(2)	(3)	(4)	(5)	(6)	(7)	(8)	(9)
Mrk 1027	0.33	0.68	5.58	9.23	-12.24	45.02	11.43	46.74
Mrk 1029	0.12	0.32	1.90	2.10	-12.73	44.53	10.95	15.25
Mrk 1050	0.28	0.68	5.10	7.28	-12.30	44.45	10.87	12.70
Mrk 1056	0.10	0.10	0.17	0.98	-13.22	44.32	10.74	9.47
Mrk 1057	0.09	0.22	1.09	1.29	-12.94	44.55	10.97	15.96
Mrk 1088	0.36	1.05	6.78	10.53	-12.16	44.50	10.91	14.08
Mrk 1097	0.09	0.12	0.70	1.35	-13.05	44.80	11.22	28.52
Mrk 1101	0.12	0.21	1.90	3.28	-12.71	44.71	11.12	22.91
Mrk 1111	0.09	0.07	0.46	2.12	-13.05	44.36	10.77	10.24
Mrk 1112	0.08	0.11	0.39	2.41	-13.04	44.37	10.79	10.57
Mrk 1115	0.06	0.10	0.56	1.26	-13.14	44.78	11.20	27.40
Mrk 1116	0.31	0.49	4.70	9.73	-12.29	44.89	11.31	35.04
Mrk 1117	0.07	0.11	0.62	1.09	-13.12	44.51	10.92	14.41
Mrk 1122	0.08	0.07	0.29	1.52	-13.18	44.36	10.77	10.26
Mrk 1143	0.12	0.23	0.49	1.43	-13.01	44.43	10.85	12.10
Mrk 1151	0.12	0.14	0.30	0.55	-13.18	44.59	11.01	17.57
Mrk 1156	0.08	0.08	0.57	1.98	-13.05	44.35	10.77	10.07

Table 3.3 (continued)

Name	12μm	25μm	60μm	100μm	Log F_{IR}	Log L_{IR}	Log $L/L_{\odot}$	SFR_{IR}
	Jy	Jy	Jy	Jy	(J s^{-1} m^{-2})	(erg s^{-1})		($M_{\odot}$/yr)
(1)	(2)	(3)	(4)	(5)	(6)	(7)	(8)	(9)
Mrk 1159	0.10	0.12	0.21	0.84	-13.22	44.77	11.18	26.27
Mrk 1194	0.36	0.74	6.85	12.05	-12.16	44.48	10.89	13.45
Mrk 1198	0.23	0.25	0.98	2.75	-12.76	44.36	10.78	10.33
Mrk 1205	0.08	0.16	0.14	0.64	-13.27	44.37	10.78	10.47
Mrk 1206	0.09	0.11	0.47	1.23	-13.12	44.54	10.96	15.72
Mrk 1224	0.18	0.50	4.12	6.98	-12.39	45.31	11.73	92.26
Mrk 1229	0.18	0.20	1.34	2.73	-12.76	44.51	10.93	14.62
Mrk 1231	0.08	0.20	1.12	1.99	-12.90	44.55	10.97	16.06
Mrk 1277	0.09	0.14	0.52	1.67	-13.05	44.37	10.79	10.66
Mrk 1286	0.06	0.05	0.21	0.78	-13.37	44.79	11.21	28.01
Mrk 1298	0.14	0.34	0.60	3.09	-12.83	45.06	11.48	51.90
Mrk 1300	0.28	0.19	0.63	0.64	-12.90	44.47	10.89	13.31
Mrk 1314	0.09	0.26	0.88	2.35	-12.89	45.03	11.45	48.15
Mrk 1332	0.11	0.15	0.37	1.09	-13.11	44.56	10.98	16.50
Mrk 1339	0.07	0.15	0.43	1.07	-13.15	44.53	10.94	15.19
Mrk 1340	0.16	0.23	1.09	1.63	-12.86	44.45	10.86	12.62
Mrk 1362	0.09	0.09	0.15	0.69	-13.30	44.51	10.93	14.59

Table 3.3 (continued)

Name	12μm	25μm	60μm	100μm	Log F_{IR}	Log L_{IR}	Log $L/L_{\odot}$	SFR_{IR}
	Jy	Jy	Jy	Jy	(J s^{-1} m^{-2})	(erg s^{-1})		($M_{\odot}$/yr)
(1)	(2)	(3)	(4)	(5)	(6)	(7)	(8)	(9)
Mrk 1365	0.16	0.64	4.20	6.11	-12.39	44.47	10.89	13.41
Mrk 1380	0.11	0.14	0.52	0.85	-13.11	44.63	11.05	19.39
Mrk 1382	0.13	0.19	0.82	1.45	-12.95	44.34	10.76	9.86
Mrk 1387	0.09	0.10	1.09	2.30	-12.91	44.88	11.29	34.06
Mrk 1391	0.15	0.13	1.33	2.34	-12.82	44.47	10.89	13.28
Mrk 1405	0.35	0.54	4.58	11.22	-12.26	44.51	10.92	14.54
Mrk 1406	0.07	0.14	0.52	1.15	-13.13	44.38	10.79	10.77
Mrk 1420	0.09	0.17	0.85	1.44	-12.99	44.81	11.23	29.38
Mrk 1428	0.05	0.14	0.18	0.52	-13.37	44.65	11.07	20.24
Mrk 1432	0.10	0.11	1.67	2.10	-12.82	45.04	11.45	48.95
Mrk 1433	0.10	0.09	0.88	1.79	-12.97	44.47	10.89	13.40
Mrk 1464	0.13	0.06	0.38	1.43	-13.10	44.35	10.76	10.03
Mrk 1490	0.15	0.84	6.01	8.47	-12.26	44.90	11.31	35.54
Mrk 1497	0.07	0.09	0.36	0.85	-13.23	44.45	10.87	12.73

Col. (1) Primary galaxy name. Cols. (2 - 5) The 12, 25, 60, and 100 micron band fluxes from IRAS. The values were extracted from NED. Col. (6) An estimate for the total far-IR flux, found by combining the flux densities in the four IRAS bands using the relation from Sanders & Mirabel (1996), given in Eq. 3.7. Col. (7) Log of the far-IR luminosity calculated using eq. 3.6 with fluxes from Col 6 and distances from Tables 2.1 and 3.1. Col. (8) Log of the ratio of the thermal IR luminosity to the Sun's bolometric luminosity. Col. (9) Star formation rates derived from the far-IR luminosity in Col. 7 and the scaling relation from Kennicutt (1998), presented in Eq. 3.9.

3.3 Star Formation Rates

The UV is more sensitive to hot stellar components, such as young massive stars, and to dust, than are the optical and near-IR bands (Marcum et al. 2001). FUV magnitudes were turned into fluxes using using eq. 3.5. A flux can then be turned into a luminosity using eq. 3.6. Kennicutt (1998) provides a calibration of the star formation rate as a function of the FUV luminosity. Kennicutt's calibration is rooted in synthesis modeling. The construction of a synthesis model begins with a grid of stellar evolution tracks being used to derive the effective temperatures and bolometric luminosities for various stellar masses as a function of time, and these are converted in broadband luminosities using stellar atmosphere models or spectral libraries. A stellar library relates quantities in the isochrone such as bolometric luminosity, abundances, mass loss rates, and instantaneous mass, with observed quantities such as monochromatic luminosities, ionizing spectrum, and kinetic power. Once evolutionary tracks are decided on, the stellar birth rate must be decided. The stellar birth rate is the probability of what form a given amount of stars, in a given mass interval, at a given age, will take. The stellar birth rate can be divided into 2 functions. First is the initial mass function, or IMF. An IMF provides the probability of obtaining a certain amount of stars in a given mass range. It is normalized to the total amount of gas that will be turned into stars. The stellar templates are summed together and weighted by the IMF to synthesize the luminosities or colors of single-age populations as functions of age. The isochrones can be added in linear combination to synthesize

the spectrum or colors of a galaxy with an arbitrary star formation history. A star formation history provides the amount of gas transformed into stars at a certain age. The conversion between the UV flux over a given wavelength interval and the SFR can be found with a synthesis model. Calibrations, such as the one by Madau et al (1998), have been published for wavelengths between 1500 and 2800 $\mathring{A}$. Assuming that the SFR has remained constant over time scales that are long compared to the lifetimes of the dominant UV emitting population ($<10^8$ years), in the continuum star formation approximation, and converting the Madau et al (1998) calibrations to Salpeter's (1955) IMF (mass limits 0.1 and 100 $M_\odot$) yields equation 3.7. Extinction corrections were applied before calculating the SFR. Table 3.2 lists the UV SFRs.

$$F_{FUV}(\text{ergs m}^{-2}\ \text{s}^{-1}\ \text{Hz}^{-1}) = 10^{((m_{FUV})\ +\ 48.6)/(-2.5))} \tag{3.5}$$

$$L_{FUV}(\text{ergs}\ \ \text{s}^{-1}\ \text{Hz}^{-1}) = 4\pi D^2 F_{FUV} \tag{3.6}$$

$$\text{SFR}(M_\odot\ \text{year}^{-1}) = 1.4 \times 10^{-28} L_\nu(\text{ergs s}^{-1}\ \ \text{Hz}^{-1}) \tag{3.7}$$

The UV star formation rates do not account for the UV light absorbed in the galaxy. UV-based diagnostics are biased in that absorption by dust plays a major role, we only observe some unknown fraction of the emergent UV light. Starting with *IRAS* astronomers have used the FIR flux as another measure of the recent star formation. A large portion of the bolometric luminosity of a galaxy is absorbed by interstellar dust and re-emitted in the thermal IR. The relation to convert FIR flux

densities from IRAS into FIR fluxes is provided by Sanders & Mirabel (1996).

$$F_{IR}(\text{J s}^{-1}\ \text{m}^{-2}) = 1.8 \times 10^{-14}[13.48f_{12} + 5.16f_{25} + 2.58f_{60} + f_{100}]. \quad (3.8)$$

FIR fluxes were turned into luminosities using the same method as in the UV. IR SFRs are determined using the relation

$$\text{SFR}(M_{\odot}\ \text{year}^{-1}) = 4.5 \times 10^{-44} L_{FIR}(\text{ergs s}^{-1}) \quad (3.9)$$

from (Kennicutt 1998). Equation 3.9 was derived using synthesis modeling and Leitherer & Heckman (1995) continuous bursts models of age 10 - 100 Myr, and adopting the Salpeter IMF. Table 3.3 lists the IR SFRs.

When calculating the SFRs, there are 2 types of error to deal with, the systematic error, and the measurement error. Systematic error is due to biases in the methods of calculation. The dependence on the assumed IMF is a major systematic error with Kennicutt's calculations. In the spectrum range of 1500 to 2500 $\mathring{A}$, stars with masses greater than 5 $M_{\odot}$ are the dominate factor. Therefore, the SFR calculation consists of a large estimate to lower stellar masses. Also, the IR SFR could have uncertainty if the dust is heated partly by other sources, or by use of a fixed continuous burst model (Kennicutt 1998). On top of the IMF dependence the UV has the added uncertainty of obscuration. Typical extinction correction in the integrated UV magnitudes are 0-3 magnitudes (Buat 1992, Buat & Xu 1996.)

The measurement error for infrared SFRs will come from uncertainty in the *IRAS* fluxes and the distance. We are not considering the uncertainty in the Hubble con-

stant, so the distance uncertainty comes from the velocity. The measurement error for the UV SFRs comes from the uncertainty in the *GALEX* UV magnitudes, and distance. Error bars for the average error are shown in each plot in this chapter.

3.4 Discussion

3.4.1 Comparison of UV to FIR Star Formation Rates

The infrared based star formation rates were higher than the ultraviolet based SFRs. The results are below in Figures 3.1 and 3.2. The LBCGs are enshrouded with gas and dust fueling the star formation, so attenuation of the UV is not surprising.

Sargsyan & Weedman (2009) derived a correction for the ultraviolet based star formation rate due to absorption. Using a plot of the ratio of PAH to UV SFRs vs. IR luminosity, they calculated how much much of the ultraviolet light was not able to penetrate through the dust. PAH (Polycyclic Aromatic Hydrocarbon molecules) are pumped by the FUV photon flux from the stars (Tielens, et al. 2004). Sargysan & Weedman (2009) found that SFRs determined with UV luminosities requires dust corrections by a factor of 10 for typical starbursts, and can increase to over 700 for extremely luminous starbursts at z$\sim$2.5. Our data agrees that the UV luminosity cannot be used to find the total SFR. However, our plot in Figure 3.3 of the ratio of FIR to UV SFRs vs. IR luminosity shows a weak correlation for us to fit and calculate a correction. Sargysan & Weedman (2009) have a weak fit themselves. Although we

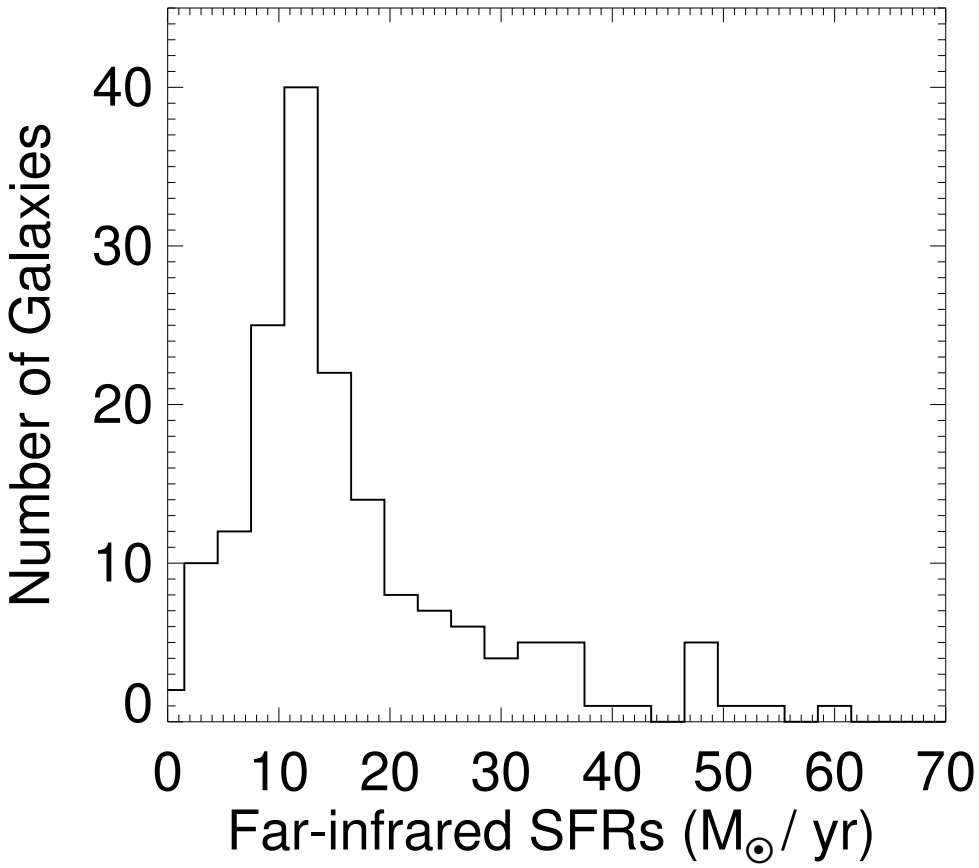

Figure 3.1: Distribution of far-infrared derived star formation rates, in solar masses per year, for the combined sample.

can say that there needs to be a correction to star formation rates found using the ultraviolet, we cannot say that there is a direct relationship between that correction and IR luminosity. Many factors could contribute to this; for example galaxy angle, age, and morphology type can all affect the relationship of the ratio of SFRs to IR luminosity.

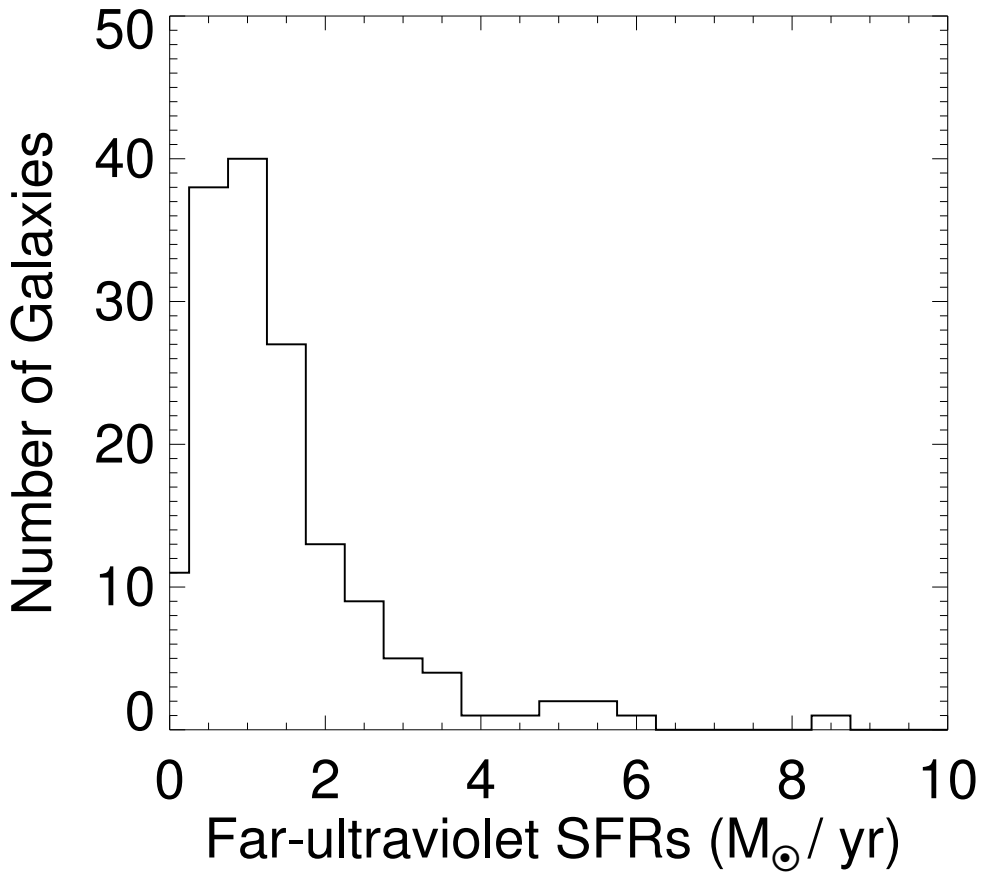

Figure 3.2: Distribution of far-ultraviolet derived star formation rates, in solar masses per year, for the combined sample

An interesting correlation that did come from the data was the relationship between the ratio of FIR to UV SFRs vs. UV luminosity, shown in Figure 3.4. The UV luminous systems may have longer high mass star formation. The longer a SFR stays high, the more the stars migrate away from the dust and more of the UV light becomes visible. The relationship between the ratio of SFRs and UV luminosity is shown in equation 3.10. The process of more UV light being measurable over time

falls into our posited scenario of LBCGs being the next stage after ULIRGs. To think about this idea one step further, if more of the UV light is visible, wouldn't more of the blue light from the O and B stars be visible? To test the previously stated idea we plotted the UV SFR against the B−V optical color, and found a correlation. For the galaxies with higher UV star formation, the color was bluer. The plot showing this relation is Figure 3.5.

$$\log \frac{\mathrm{SFR(IR)}}{\mathrm{SFR(UV)}} = -0.78 \times \log(\mathrm{L}_{UV}) + 22.78. \tag{3.10}$$

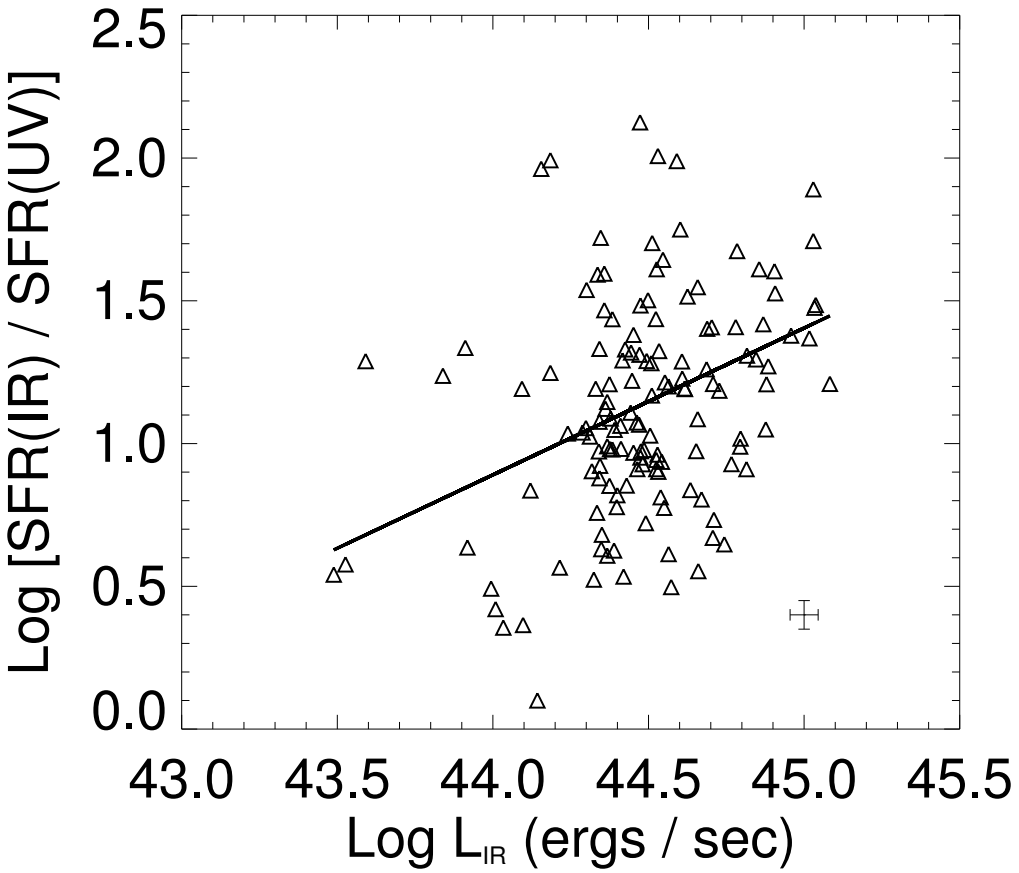

Figure 3.3: The ratio of star formation rates derived from the thermal infrared emission to those derived from the observed far-UV emission for the combined sample, as a function of the infrared luminosity. The plotted line shows our weak correlation. $\log \frac{\mathrm{SFR(IR)}}{\mathrm{SFR(UV)}} = 0.51 \times \log(\mathrm{L}_{UV}) - 21.73$

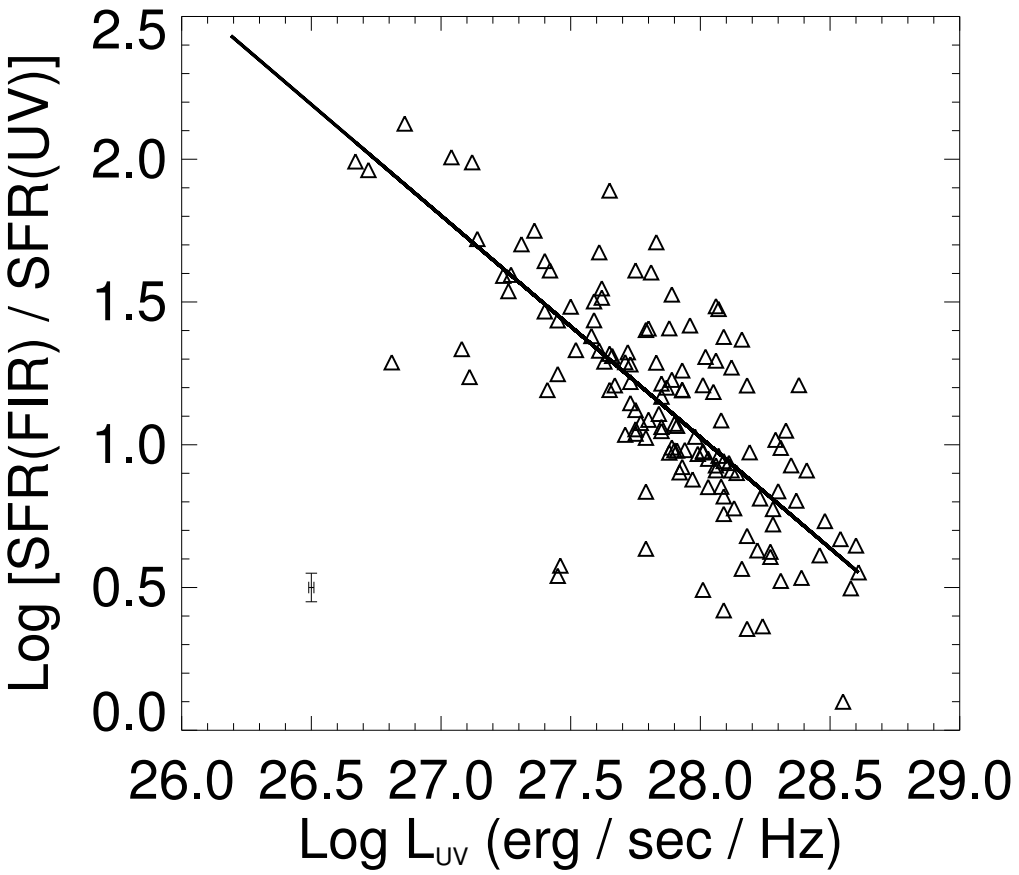

Figure 3.4: The ratio of star formation rates derived from the thermal infrared emission to those derived from the observed far-UV emission for the combined sample, as a function of the far-UV luminosity. The plotted line shows the correlation of the ratio of SFRs to the UV luminosity.

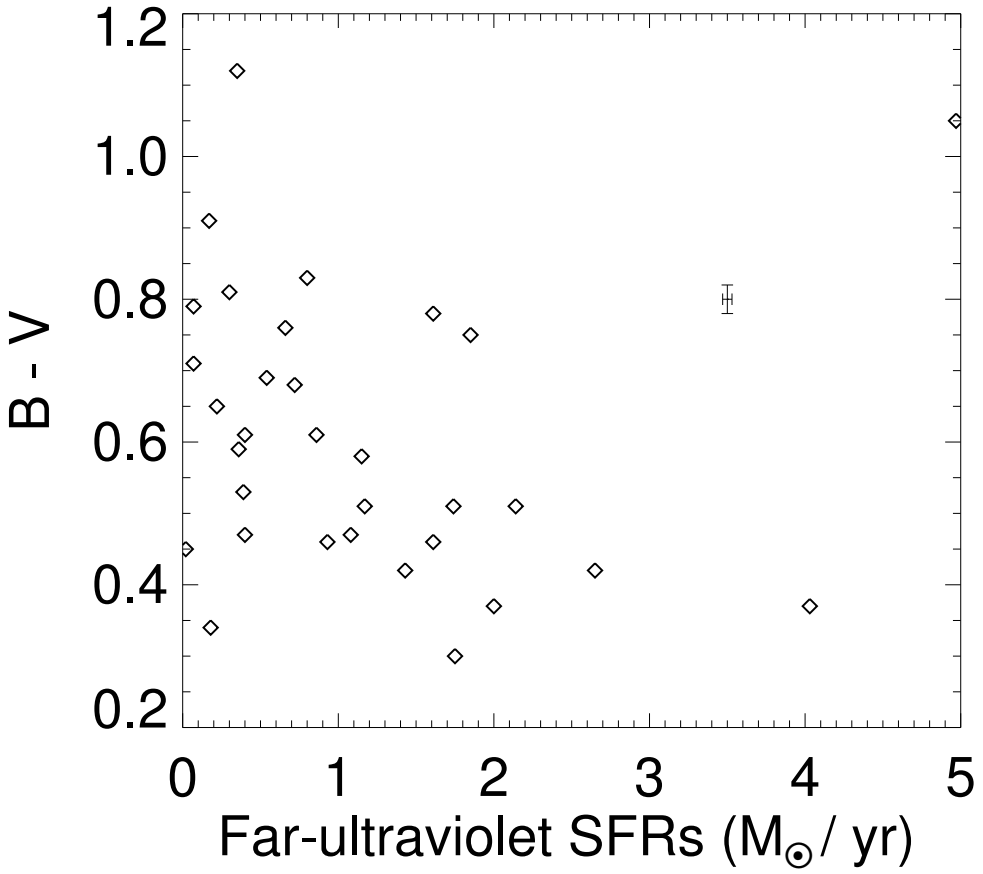

Figure 3.5: Ultraviolet star formation rates relation to B−V colors from Table 2.8. Mrk 54 is left off of the plot because its UV SFR of 12.2 $M_{\odot}$/yr was too high to logically put on this plot with the others.

3.4.2 Star Formation Rates as a Function of Environment

Evidence exists for a connection between galaxy interactions and high star formation. A large amount of the most luminous infrared galaxies are assumed to have underlying starbursts (Genzel et al. 1998), and occur in galaxies with clearly disturbed morphologies that are presumably interacting or merging (Knapen 2009). However, Knapen & James (2009) found that the presence of a close companion raises the star formation rate by a factor of just below two, meaning that although statistically galaxies with close companions form stars at a higher rate, they do this over extended periods of time and not as bursts. Woods, Geller, & Barton(2006) found that pairs consisting of similarly luminous galaxies have the most intense bursts of star formation, compared to other pairs.

Our LBCG sample can be divided into 2 groups, interacting and non-interacting. To be selected for the interacting group a galaxy must be in the process of a merger with one or more companion galaxies, or interactions have left marks such as bridges, tails, and tidal loops. For the optical sample we were able to make these classifications using a combination of images from the Sloan Digital Sky Survey (SDSS), and images obtained in the optical survey described in Chapter 2. For the high star formation sample we were only able to use SDSS images. Fifty galaxies were found to be interacting, and 95 were found not to be. The missing 43 galaxies in this classification scheme are from sample 2 because they were not in the Sloan field and we had no images from McDonald Observatory. However, classifying 145 galaxies was a

sufficient sample to see the patterns we were looking for. When comparing the FIR star formation rates for these two groups, it is found that environment is not as dominant of a factor as expected in creating high SFRs. The median SFR for the non-interacting sample is 13.3 $M_{\odot}$/yr, and the median for the interacting sample is 15.0. Figures 3.6 and 3.7 show the respective distributions. Our results agree with the Knapen & James (2009) conclusion that interactions are not the main trigger to a star formation burst. A starbursting galaxy can occur in any environment.

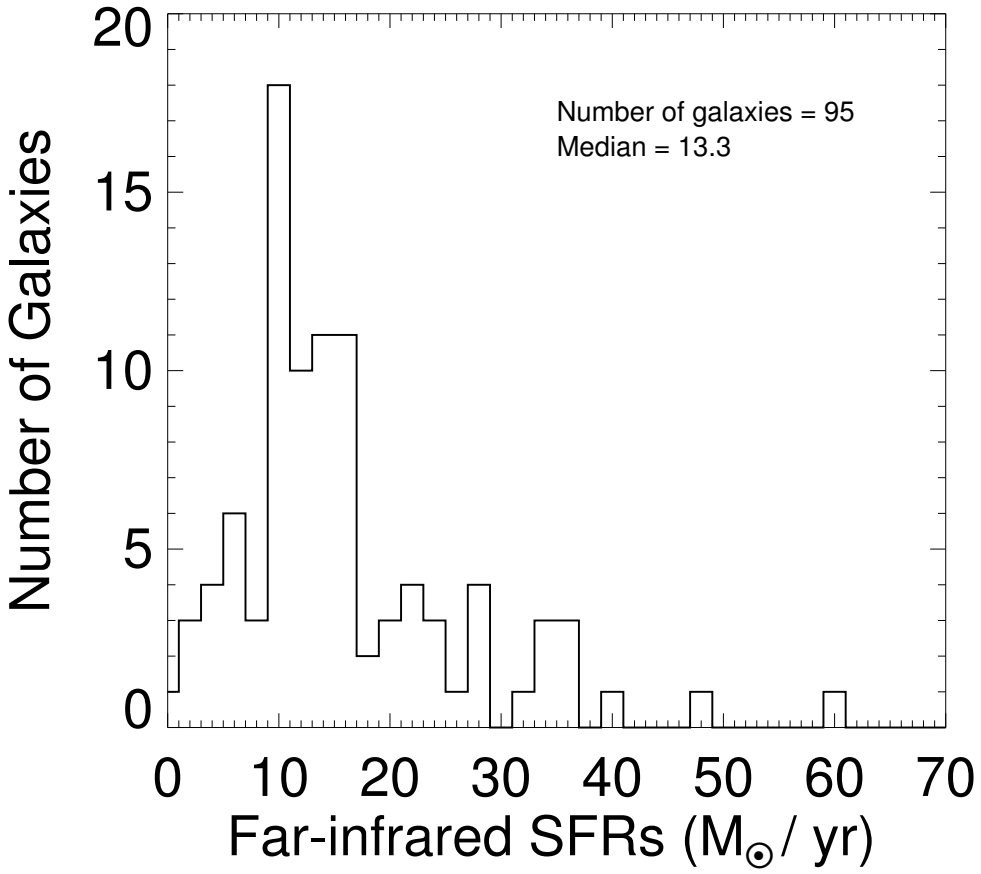

Figure 3.6: Distribution of far-infrared derived star formation rates, in solar masses per year, for the galaxies in the combined sample which are classified as non-interacting

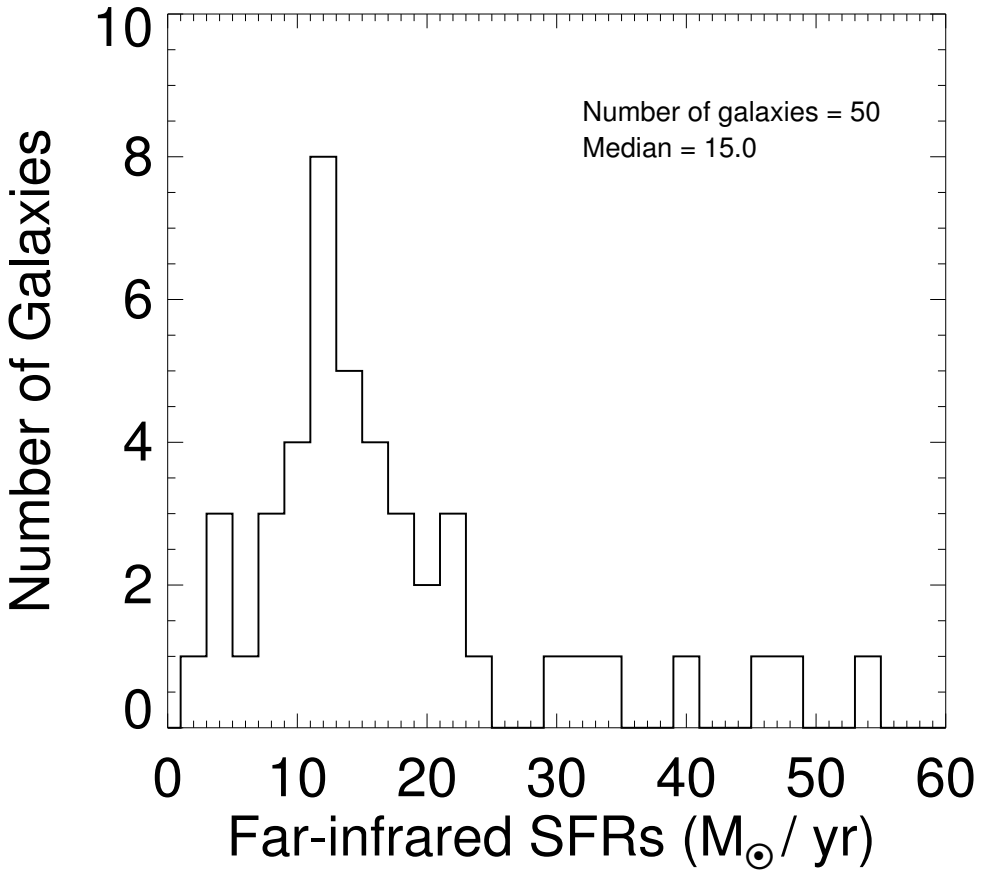

Figure 3.7: Distribution of far-infrared derived star formation rates, in solar masses per year, for galaxies in the combined sample classified as interacting

3.4.3 Star Formation Rates as a Function of Surface Brightness Distribution

A second method to divide our sample of galaxies is by the surface brightness distribution. Some galaxies have formed stars in large discrete knots over their disks, and some have high star formation only in a compact core. The sample was divided into these categories using a combination of images from McDonald Observatory and SDSS as before. A total of 77 galaxies have asymmetrical distribution of surface brightness, or a "clumpy" morphology, and 68 have a smooth surface brightness distribution showing no knots. The median star formation in $M_{\odot}$/year for the galaxies with an asymmetrical light is 13.5, and for smooth galaxies the median is 13.4. The $\sim 1\%$ difference in the median star formation rates means that a starbursting galaxy does not always have large knots over a disk, but can have equally high rates with just a starbursting core. FIgures 3.8 and 3.9 show the distributions of far-infrared SFRs for the two types of morphologies.

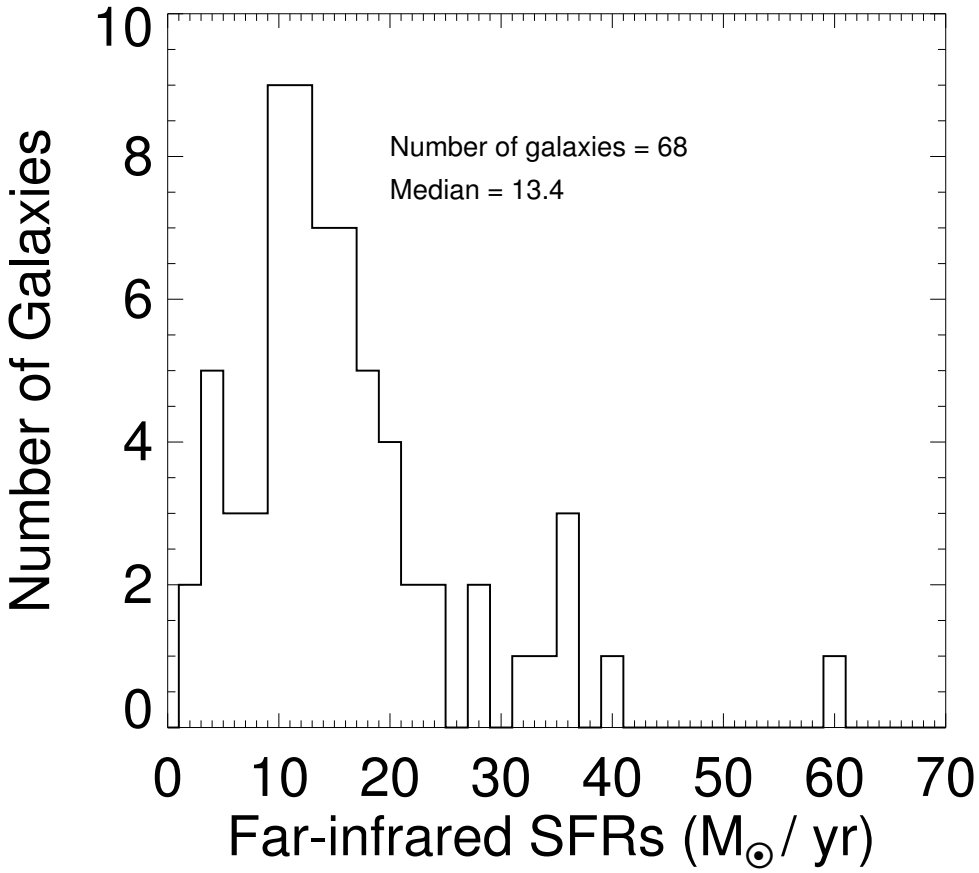

Figure 3.8: Distribution of far-infrared derived star formation rates, in solar masses per year, for galaxies in the combined sample which display smooth surface brightness distributions.

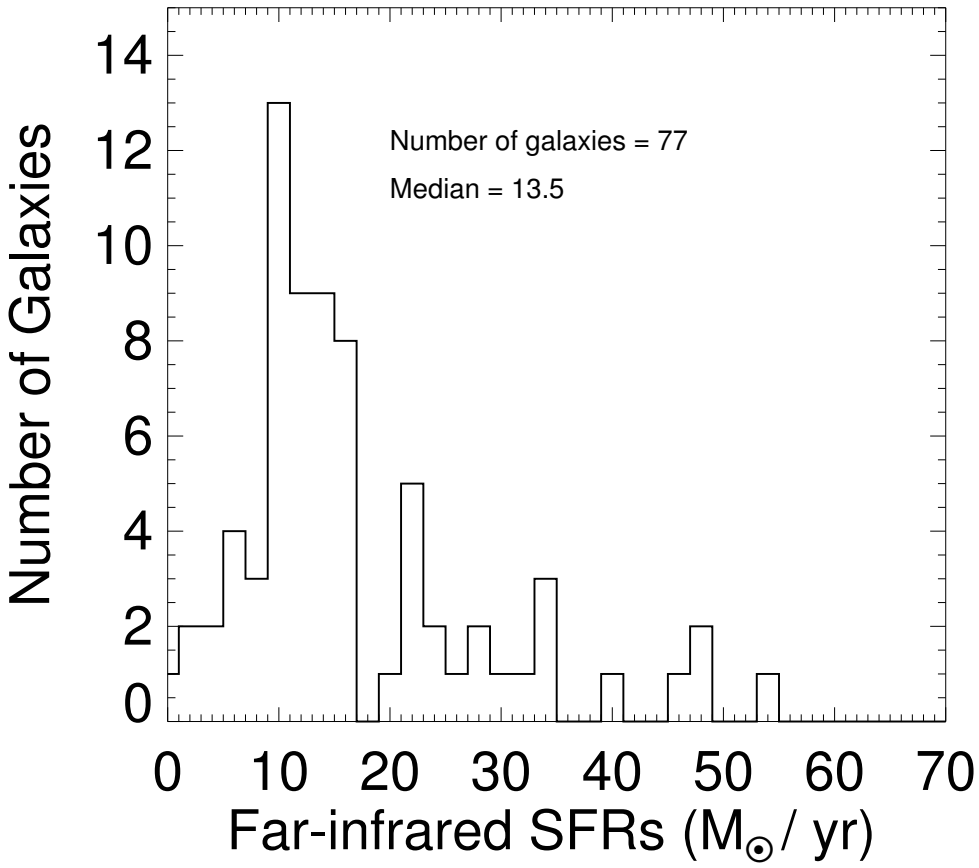

Figure 3.9: Distribution of far-infrared derived star formation rates, in solar masses per year, for galaxies in the combined sample which display multiple brightness peaks, i.e., a clumpy morphology

3.4.4 Star Formation as a Function of K-band Luminosity

Star formation rates are built on many parameters. Before it can be shown that the high star formation rates are results of mergers, interactions, or new galaxy formation, it must first be shown that the star formation is not solely mass dependent. To analyze this dependence a comparison was made of K-band magnitudes to both ultraviolet and far-infrared SFRs. The K-band data used, from the *Two Micron All Sky Survey (2MASS)*, is the total extrapolated K magnitude of each galaxy. The K-band is dominated by cool stars, and cool stars dominate the mass, therefore if the derived star formation rates are not strongly correlated with the K-band luminosity then the observed star formation is unlikely to just track the the galaxy's total mass. K-band observed and absolute magnitudes in tabular form is presented in Table 3.4. The distances used to get the absolute magnitudes are the same ones from Tables 2.1 and 3.1. The K-band values are not corrected for extinction. We were just looking for a K-band relation to the SFRs, so extinction corrections were not necessary. Looking at Figures 3.10 and 3.11, we see no correlation, meaning the star formation is not solely mass dependent. The error bars on Figures 3.10 and 3.11 come from using the rules of error propagation with the measurement error from *2MASS* and the distance error.

Table 3.4. K-band Photometry for the Combined Sample

Name	K	±K	M_K
(1)	(2)	(3)	(4)
McDonald Sample			
Mrk 342	12.53	0.08	-23.39
Haro 15	11.53	0.10	-23.16
Mrk 360	12.41	0.12	-22.80
Mrk 366	11.44	0.07	-23.75
Mrk 367	12.09	0.08	-23.81
Mrk 589	11.27	0.06	-22.07
Mrk 1184	10.76	0.04	-24.62
Mrk 1404	11.13	0.04	-24.69
Mrk 1079	10.31	0.03	-25.00
Mrk 1094	11.96	0.08	-20.90
Haro 1	9.78	0.02	-23.86
Mrk 385	11.83	0.06	-23.46
Mrk 390	12.27	0.06	-22.85
Mrk 18	10.38	0.03	-23.07

Table 3.4 (continued)

Name	K	±K	M_K
(1)	(2)	(3)	(4)
Mrk 402	12.80	0.12	-22.26
IIZw 44	11.81	0.05	-22.85
Mrk 139	11.82	0.10	-22.51
Mrk 144	11.93	0.07	-23.39
Mrk 33	10.43	0.04	-21.49
Mrk 148	12.16	0.07	-22.87
Haro 25	12.27	0.06	-22.86
Mrk 154	12.38	0.09	-23.83
Mrk 171	8.42	0.02	-24.93
Mrk 181	11.24	0.05	-23.45
Haro 34	11.55	0.07	-23.32
Mrk 54	12.83	0.11	-23.53
Mrk 248	10.82	0.07	-25.11
Mrk 255	13.46	0.20	-22.08
Haro 42	12.73	0.11	-21.32
IZw 101	11.74	0.06	-22.54
Mrk 492	10.70	0.05	-23.28

Table 3.4 (continued)

Name	K	±K	M_K
(1)	(2)	(3)	(4)
Mrk 300	11.36	0.04	-24.70
Mrk 697	11.82	0.08	-23.86
Mrk 499	12.23	0.07	-23.00
IIZw 82	10.31	0.03	-23.36
Mrk 512	11.30	0.05	-24.34
Mrk 518	11.06	0.04	-24.50
Mrk 303	11.13	0.04	-23.98
Mrk 306	11.69	0.12	-22.79
IIZw 185	12.08	0.11	-22.92
Mrk 531	9.70	0.03	-23.80
Mrk 325	10.73	0.03	-22.71
High Star Formation Rate Sample			
Mrk 2	10.64	0.03	-23.99
Mrk 83	13.26	0.14	-21.22
Mrk 91	10.75	0.05	-25.76

Table 3.4 (continued)

Name	K	±K	M_K
(1)	(2)	(3)	(4)
Mrk 97	11.24	0.05	-23.06
Mrk 103	12.11	0.08	-22.86
Mrk 114	10.80	0.04	-24.77
Mrk 126	11.53	0.05	-23.60
Mrk 143	11.83	0.09	-24.24
Mrk 161	10.75	0.03	-24.90
Mrk 183	12.05	0.07	-22.60
Mrk 204	12.26	0.07	-23.91
Mrk 217	11.98	0.07	-24.95
Mrk 254	12.08	0.07	-23.42
Mrk 261	12.36	0.08	-23.14
Mrk 264	12.00	0.06	-23.56
Mrk 265	11.96	0.07	-25.13
Mrk 269	12.37	0.10	-23.37
Mrk 286	10.58	0.05	-25.91
Mrk 311	11.25	0.05	-23.96
Mrk 312	11.79	0.07	-24.72

Table 3.4 (continued)

Name	K	±K	M_K
(1)	(2)	(3)	(4)
Mrk 319	10.63	0.03	-24.54
Mrk 321	10.32	0.04	-25.20
Mrk 349	11.73	0.06	-24.31
Mrk 353	10.31	0.03	-24.60
Mrk 368	11.74	0.07	-24.69
Mrk 387	11.75	0.07	-23.66
Mrk 413	12.00	0.05	-23.93
Mrk 414	11.50	0.05	-24.52
Mrk 440	12.41	0.09	-23.57
Mrk 489	11.30	0.06	-25.29
Mrk 540	11.90	0.07	-23.58
Mrk 545	8.88	0.02	-28.45
Mrk 556	12.95	0.13	-21.10
Mrk 559	11.88	0.06	-24.28
Mrk 560	11.45	0.08	-24.83
Mrk 567	10.66	0.03	-25.81
Mrk 569	11.81	0.08	-23.81

Table 3.4 (continued)

Name	K	±K	M_K
(1)	(2)	(3)	(4)
Mrk 575	10.25	0.03	-25.41
Mrk 579	13.37	0.12	-21.02
Mrk 582	12.17	0.09	-24.97
Mrk 592	11.52	0.06	-22.88
Mrk 593	10.15	0.06	-24.95
Mrk 606	12.39	0.07	-23.62
Mrk 619	11.96	0.08	-24.64
Mrk 629	12.12,	0.06	-23.14
Mrk 632	11.56	0.06	-24.07
Mrk 637	12.35	0.06	-23.72
Mrk 639	12.50	0.08	-24.65
Mrk 681	13.28	0.15	-22.44
Mrk 688	12.04	0.09	-25.26
Mrk 693	10.32	0.03	-25.72
Mrk 717	10.74	0.04	-25.97
Mrk 718	10.58	0.05	-24.16
Mrk 719	11.93	0.07	-23.40

Table 3.4 (continued)

Name	K	±K	M_K
(1)	(2)	(3)	(4)
Mrk 726	11.31	0.06	-24.28
Mrk 753	12.42	0.09	-23.90
Mrk 785	11.64	0.05	-25.16
Mrk 789	11.43	0.07	-25.13
Mrk 799	8.98	0.02	-26.61
Mrk 834	10.49	0.03	-25.91
Mrk 837	12.52	0.09	-23.39
Mrk 839	10.50	0.05	-25.14
Mrk 851	11.82	0.07	-24.32
Mrk 858	11.37	0.03	-24.48
Mrk 863	11.35	0.07	-23.60
Mrk 881	11.80	0.08	-25.58
Mrk 891	13.25	0.13	-22.19
Mrk 904	11.78	0.06	-24.85
Mrk 923	11.09	0.06	-24.57
Mrk 932	12.41	0.08	-22.61
Mrk 938	10.07	0.03	-26.78

Table 3.4 (continued)

Name	K	±K	M_K
(1)	(2)	(3)	(4)
Mrk 940	11.97	0.06	-22.54
Mrk 941	12.36	0.09	-24.73
Mrk 948	11.70	0.06	-24.78
Mrk 955	10.76	0.05	-25.33
Mrk 984	11.18	0.07	-24.60
Mrk 995	11.30	0.05	-25.16
Mrk 1001	12.62	0.11	-23.88
Mrk 1005	11.54	0.06	-25.21
Mrk 1029	11.97	0.06	-24.20
Mrk 1050	10.12	0.03	-25.34
Mrk 1056	11.11	0.04	-23.08
Mrk 1088	9.20	0.03	-26.23
Mrk 109,	12.55	0.10	-23.76
Mrk 1101	11.62	0.06	-24.39
Mrk 1111	10.81	0.03	-25.02
Mrk 1112	10.86	0.04	-24.96
Mrk 1115	12.19	0.06	-23.64

Table 3.4 (continued)

Name	K	±K	M_K
(1)	(2)	(3)	(4)
Mrk 1116	10.56	0.04	-24.89
Mrk 1117	12.30	0.07	-24.81
Mrk 1143	11.79	0.07	-24.59
Mrk 1151	11.95	0.07	-24.19
Mrk 1156	12.50	0.09	-23.39
Mrk 1159	11.67	0.05	-25.07
Mrk 1194	9.23	0.03	-24.72
Mrk 1198	10.26	0.04	-25.55
Mrk 1205	12.22	0.11	-25.04
Mrk 1206	11.78	0.06	-23.33
Mrk 1229	11.00	0.04	-25.45
Mrk 1231	11.05	0.05	-25.51
Mrk 1277	11.57	0.07	-23.91
Mrk 1286	12.98	0.12	-22.95
Mrk 1298	11.04	0.03	-24.82
Mrk 1300	12.60	0.09	-25.10
Mrk 1314	11.95	0.08	-25.08

Table 3.4 (continued)

Name	K	±K	M_K
(1)	(2)	(3)	(4)
Mrk 1332	11.89,	0.07	-23.85
Mrk 1339	12.22	0.12	-24.88
Mrk 1340	12.22	0.09	-24.26
Mrk 1362	12.36	0.09	-24.15
Mrk 1365	10.32	0.03	-25.24
Mrk 1380	12.09	0.09	-24.75
Mrk 1387	12.20	0.07	-24.46
Mrk 1405	9.71	0.02	-27.05
Mrk 1406	11.96	0.06	-23.56
Mrk 1432	12.25	0.10	-24.55
Mrk 1464	12.79	0.11	-24.16
Mrk 1490	11.30	0.04	-24.62

Col. (1) Primary galaxy name. Col. (2) K-band photometry from 2MASS. The K-band values are not corrected for extinction. Col. (3) Measurement error in the K-band photometry. Col. (4) K-band absolute magnitudes calculated using the distances from Tables 2.1 and 3.1.

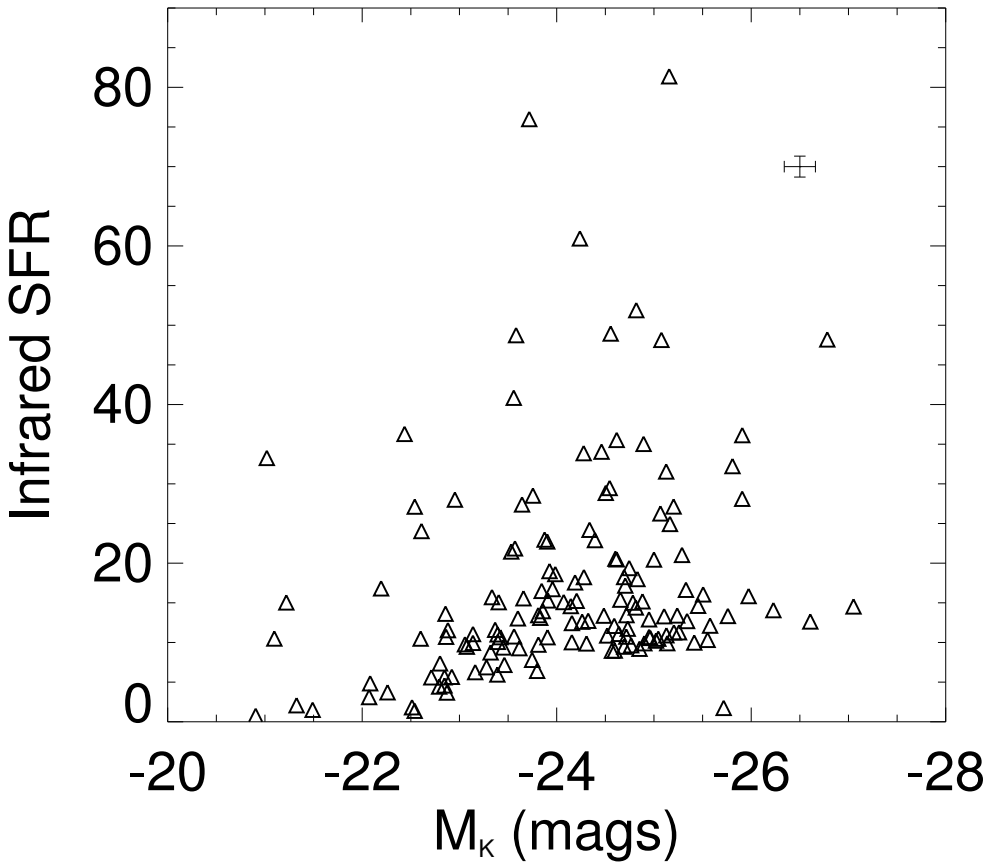

Figure 3.10: Infrared star formation rates versus absolute K-band luminosity for the combined sample

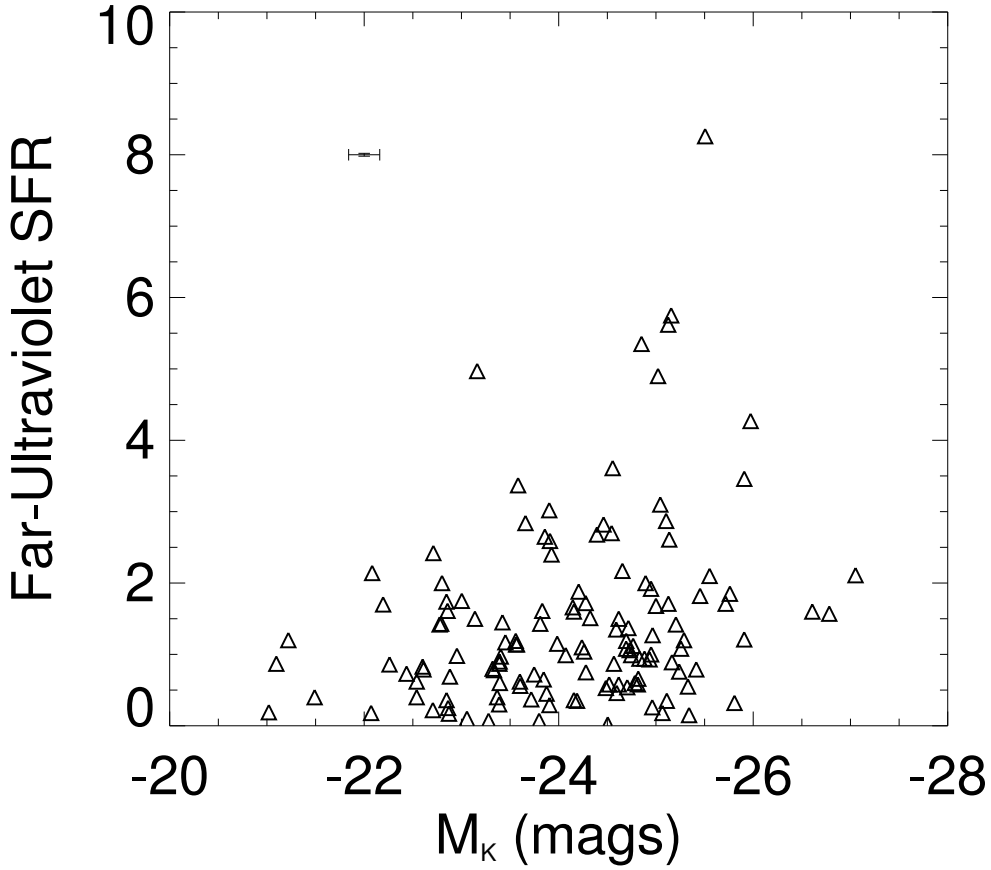

Figure 3.11: Far-ultraviolet star formation rates versus absolute K-band luminosity for the combined sample

3.5 Supernovae

A supernovae (SN) is an exploding star in the process of ending its life; SN can outshine their parent galaxy and have a visibility lasting from a few weeks to a few months. There are 2 main types of SN. Type 1 are hydrogen poor and occur when white dwarf stars accumulate material from a companion star until they reach the Chandrasekhar limit and undergo runaway fusion in their interior. The resulting explosion can expel nearly all stellar materials. Type 2 supernovae are hydrogen rich and come from stars with masses of 8 $M_{\odot}$ or higher. Stars above this mass limit are the only ones with cores capable of fusing H, He, C, O and heavier elements up to iron in their inner core. Once the core begins to change to iron, the temperature gets so high that the photons break nuclei into constituent parts. The star begins to collapse until neutron degeneracy pressure kicks in and the star explodes leaving behind a neutron star or black hole.

We expect the type 2 supernova rate in LBCGs to be significantly elevated compared to normal galaxies, since for continuous star formation, the SNR scales with the SFR. Therefore, SN events should be detected in significant numbers within the population of LBCGs. Given the level of SF, and the expected number of SN, these SN may drive powerful starburst winds out of the galaxy, heating and removing gas, and possibly stopping the star formation. These SN will be more difficult to detect against the bright star-forming regions within LBCGs, but given the high SFRs, we expect many to be detected. We examined three years of the Lick Observatory Super-

nova Search data to assess the separation between detected SN and the host galaxy core, and an estimate of the supernova rate, SNR, for LBCGs using a starburst evolutionary synthesis model. The LOSS team uses the Katzman Automatic Imaging Telescope (KAIT) to discover nearby supernovae to be used for a wide variety of studies. The telescope has a fully robotic 0.76m reflector with a CCD imaging camera that can observe 1200 galaxies a night. The camera cycles back every 3 to 4 nights, then the software automatically subtracts template images to identify possible SN (Filippenko, 2001).

3.5.1 Supernovae Locations Within Galaxies

The LOSS team releases the right ascension and declination values for the cores of the galaxies used in their searches and the SN that are found. Using the Pythagorean theorem we could take the RA and Dec. for the galaxies and SN and calculate the angular separation between the two in degrees. To find the physical separation in kpc we used the small angle formula and the distances from Tables 2.1 and 3.1.

Most SN are observed between 5″-20″ or 5 to 10 kpc. The odd part of this result is the gap in SN between 0 and 10 kpc. The cores of many galaxies are the densest part and should have high star density and therefore more SN. A discussion with the LOSS team revealed that they ignored the core incase there was an active galactic nuclei. We also believe that the core is so bright that distinguishing a SN would be difficult.

3.5.2 Supernovae Rates

Leitherer et al. (1999) provided models that describe the evolution of stellar populations, calculating their integrated properties and observables as a function of user-selected input parameters such as star formation rates. Supernova rates can be calculated based on the properties of the evolving stellar population. From Figure 3.12 (a model from Leitherer et al. 1999) the SNR can be derived from a star formation rate. For an assumed SFR of 1 $M_{\odot}$/yr in the chart, the SNR levels off at 0.02/yr. Making the assumption that there is continuous star formation, solar abundances, and normal stellar initial mass distribution, it can be seen that the supernovae rate becomes constant after 4×10^7 years. Once star formation began, the O and B0-4 stars had to have time to burn through their fuel and become supernovae before any supernovae were visible.

Making the assumptions described above, we took the star formation rates for our combined sample and calculated the supernovae rates. The median years between supernovae of the LBCG sample was 3.1 years. Type 2 SN are not expected in elliptical type galaxies, so to see a rate this high for a sample with elliptical galaxies is a new concept. Type 2 supernovae are expected in spiral arms mostly. Of the galaxies we had data for within the 3 years of LOSS data we mined, mid to late type spiral galaxies had the most SN. The lack of SN in elliptical galaxies could be due to the make-up of the list though, and not natural causes. The Milky Way is judged to have $\sim$ 1.4 SN per century (Cappellaro et al. 1999).

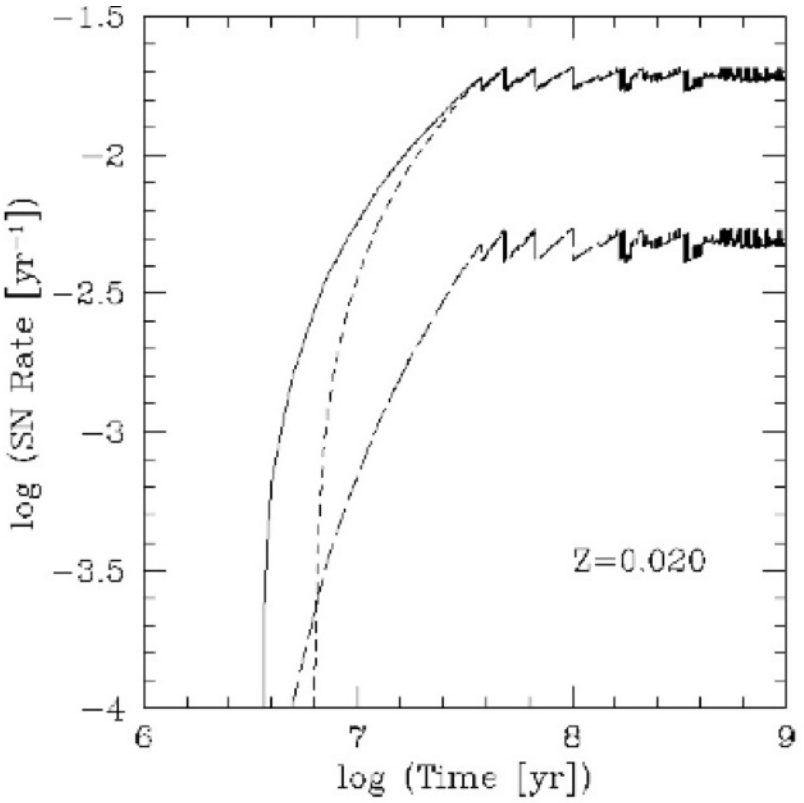

Figure 3.12: Evolution of the massive star supernova rate for a starburst with a continous star formation rate of 1 $M_\odot$ yr^-1. The supernova rate saturates after ∼40 Myr at a value of ∼0.02 SN per year or 1 SN every 50 years. The adopted model is for a standard initial mass function with slope -2.35, upper mass limit of 100 $M_\odot$ and solar abundances from (Leitherer 1999)

Chapter 4

Evolutionary State of Luminous Blue Compact Galaxies

Massive young stars emit most of their energy in the ultraviolet part of the spectrum, and at least in star forming galaxies, they outshine the emission from any other evolutionary stage of a composite stellar population (Bruzual &Charlot 2003). The observation of nearby galaxies in the UV is important in order to understand the evolution of galaxies from the high-redshift universe (where their properties are commonly derived from rest-frame UV observations) to the present. UV data can address fundamental questions such as the relation between the qualitative (optical) morphology of these galaxies and more quantitative properties such as colors, luminosities, total-infrared-to-UV ratios, etc. (Gil De Paz et al. 2007). Comparing UV and optical colors to evolutionary tracks of instantaneous burst models can help us find the age range, and extinction values for the LBCG sample.

4.1 Ultraviolet Morphology

Figure 4.1 shows stacked FUV and NUV images for all of the galaxies in the optical sample that were viewed with *GALEX*. A red color template was used for

the FUV, and a blue color template was used for the NUV. The *GALEX* archive images are large tiles, so the images displayed here have been cut to a size of $5'$ x $5'$. In Figure 4.2 we show zoomed in detailed views of the galaxies with the most interesting UV structure. Figure 4.2 shows FUV and NUV images from the *GALEX* archive of a handful of galaxies from the optical sample that have been Gaussian smoothed, and displayed on a logarithmic scale. A color table was applied using DS9, an astronomical imaging and data visualization application. The face that our optical sample of galaxies show structure in the UV is consistent with the scenario that LBCGs could be ULIRGs (or LIRGS), further along in their development phase. The latter systems have higher SFRs, more dust, and are not intensity UV-bright or unusually blue. The select sample shown in Figure 4.2, with the exception of Haro 25, show more UV structure than the others. The galaxies with more UV structure could be in later stages, meaning that star formation has been continuous giving the O and B stars time to migrate from their initial star formation locations, and more UV light is able to be seen.

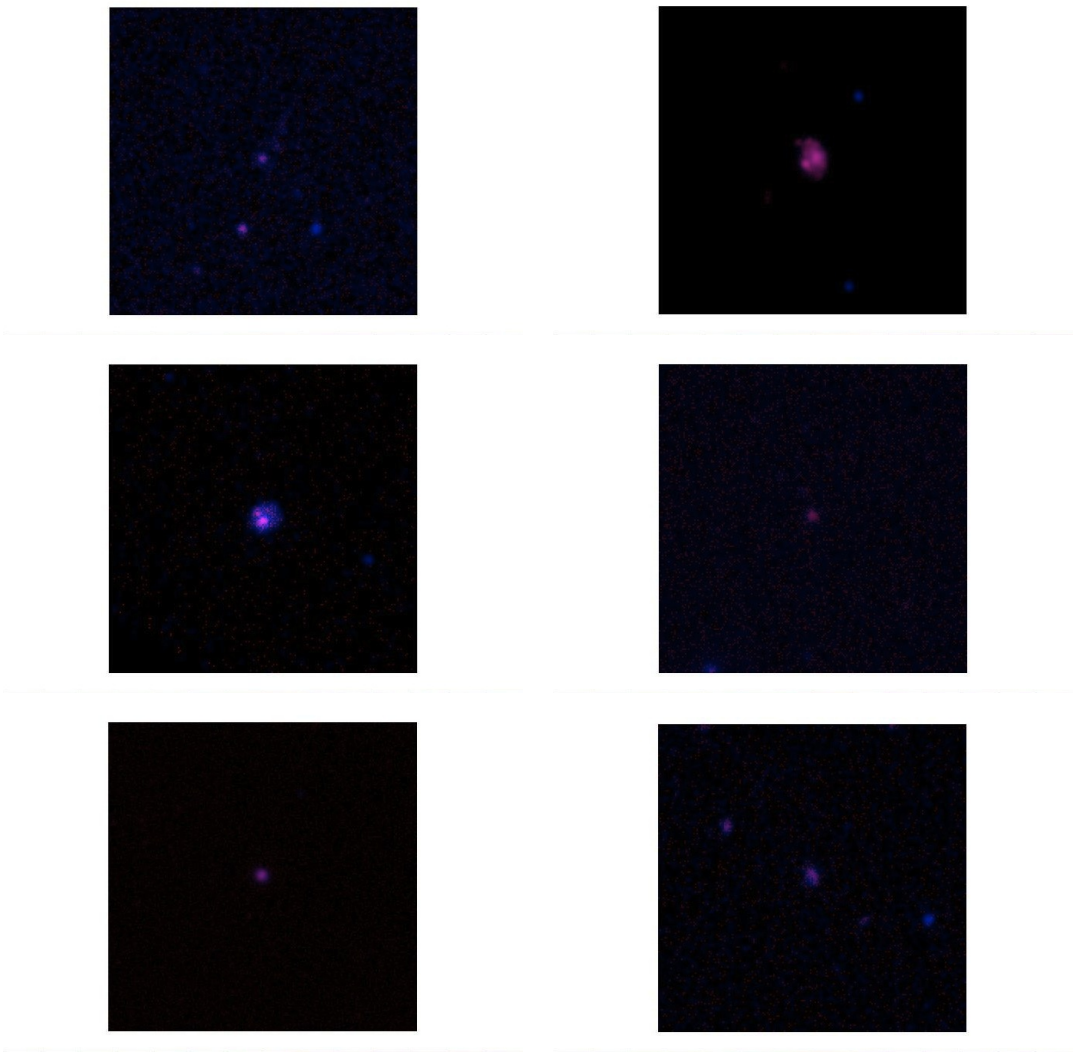

Mrk 342: top left; Haro 15: top right; Mrk 360: middle left; Mrk 364: middle right; Mrk 366: bottom left; Mrk 367: bottom right

Figure 4.1: Ultraviolet images of selected objects created by stacking *GALEX* far (red)- and near (blue)-UV data to create a pseudo true-color image. UV emission directly traces the recently-formed massive stars which produce most of their luminosity in the UV band. North is up and east is to the left. A log scale has been applied, but no calibration. The images are $5' \times 5'$, and have a resolution of $4.2''$-$5.3''$. Gaussian smoothing has been applied. These are intensity maps with units of (photons / pixel / sec).

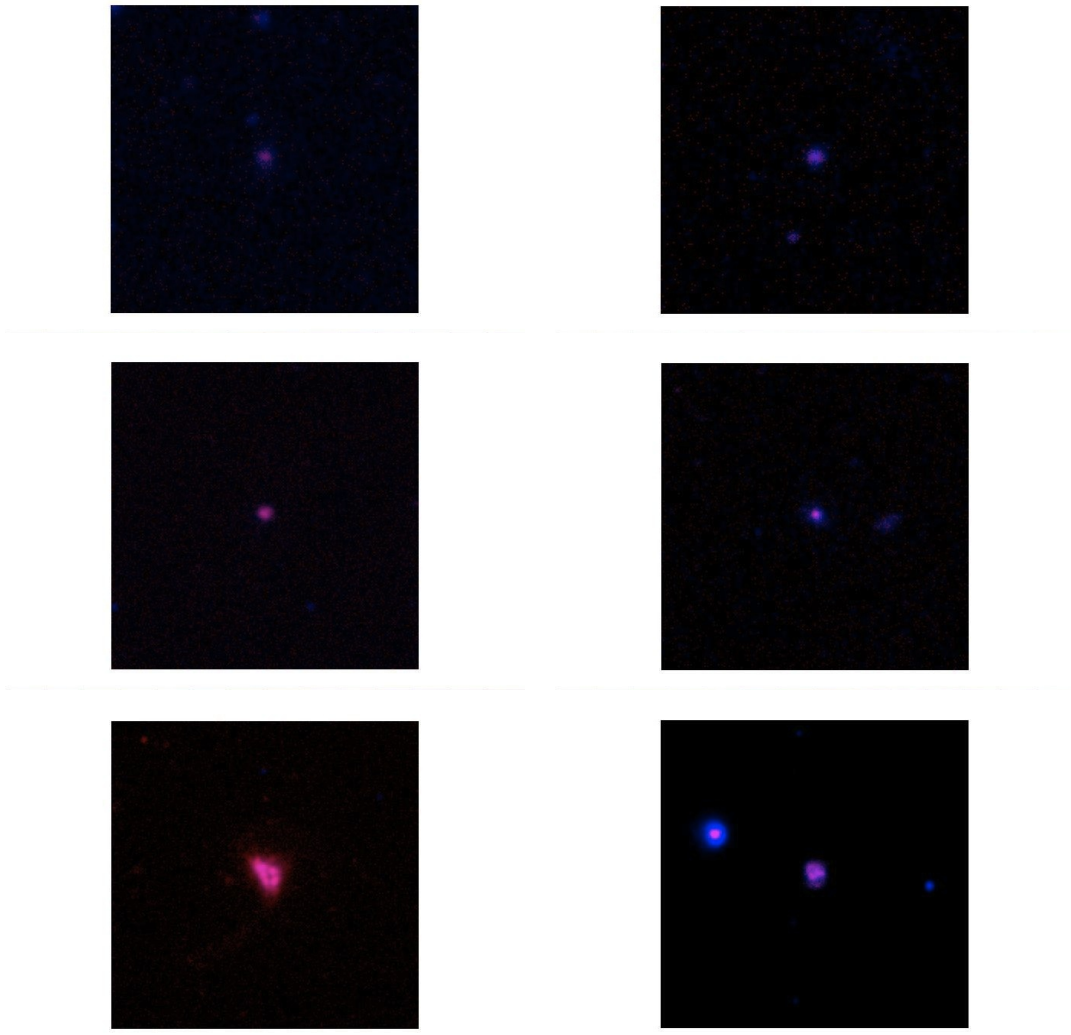

Mrk 589: top left; Mrk 1184: top right; Mrk 1404: middle left; Mrk 1079: middle right; Mrk 8: bottom left; Haro 1: bottom right

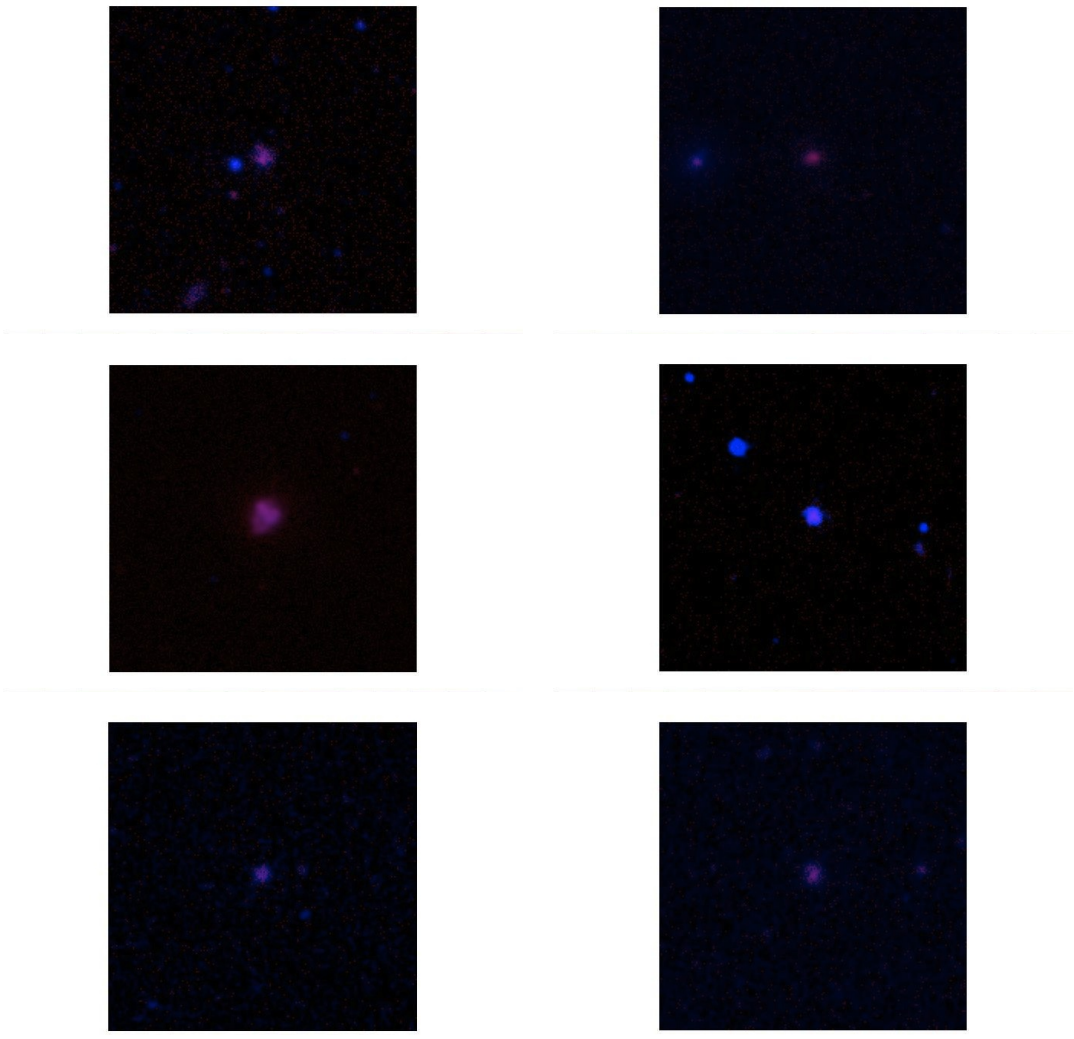

Mrk 1211: top left; Mrk 1184: top right; Mrk 325: middle left; Mrk 402: middle right; IIZw 44: bottom left; Mrk 144: bottom right

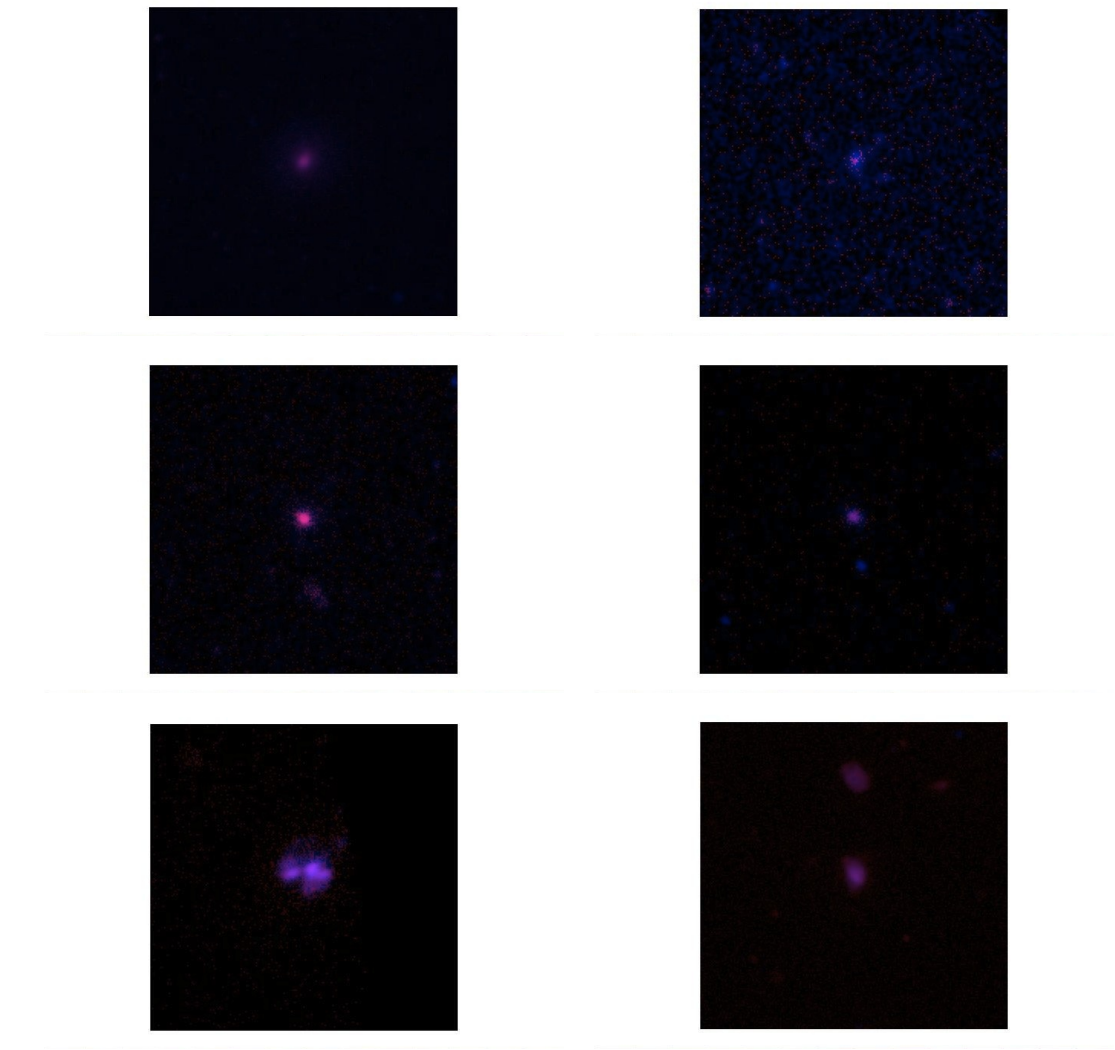

Mrk 33: top left; Mrk 148: top right; Haro 25: middle left; Mrk 154: middle right; Mrk 171: bottom left; Mrk 181: bottom right

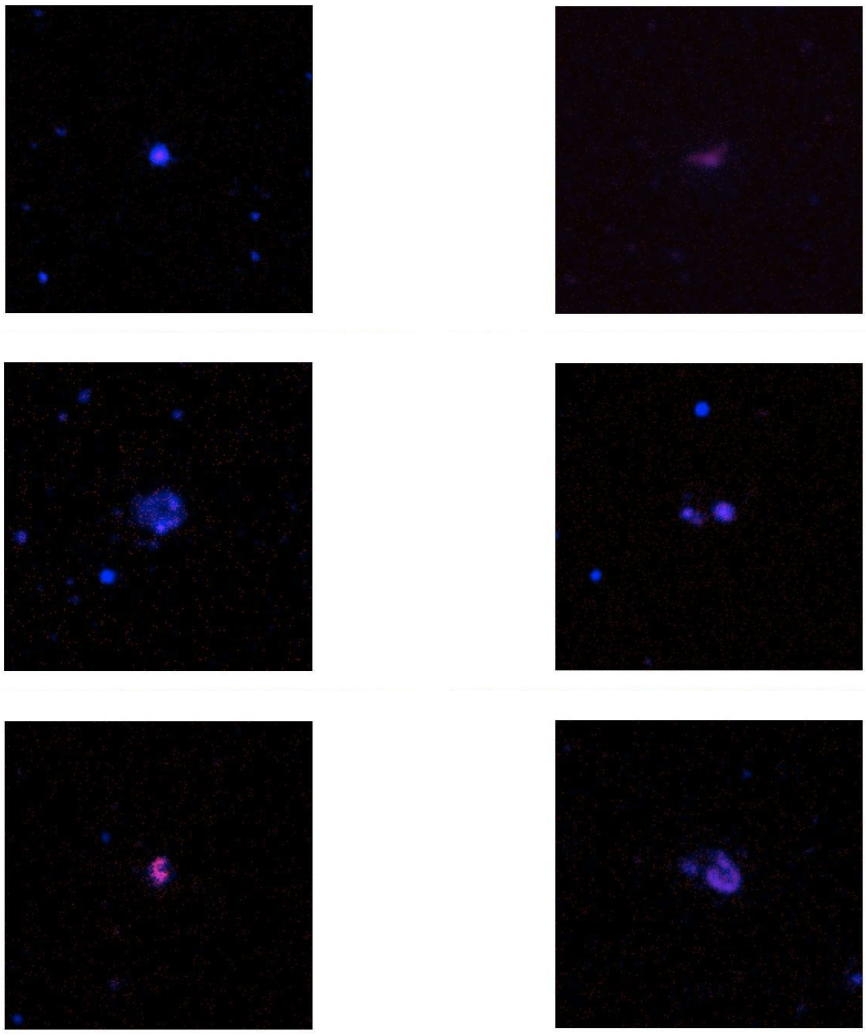

Haro 34: top left; Mrk 54: top right; Mrk 238: middle left; Mrk 248: middle right; Mrk 255: bottom left; Mrk 271: bottom right

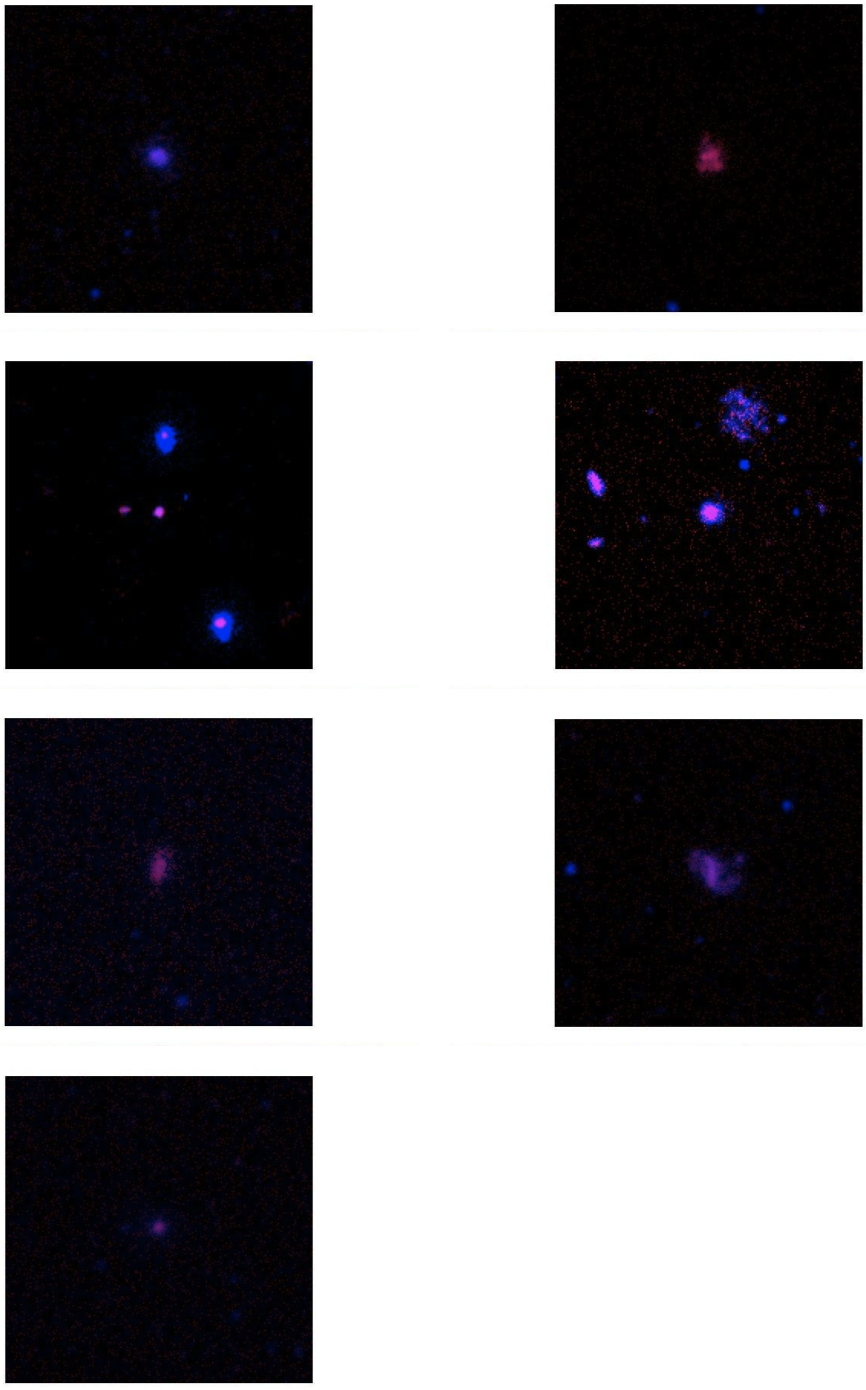

IZw 101: top left; Mrk 297: top right; Mrk 300: second row left; Mrk 499: second row right; Mrk 303: third row left; Mrk 306: third row right; Mrk 531: bottom left

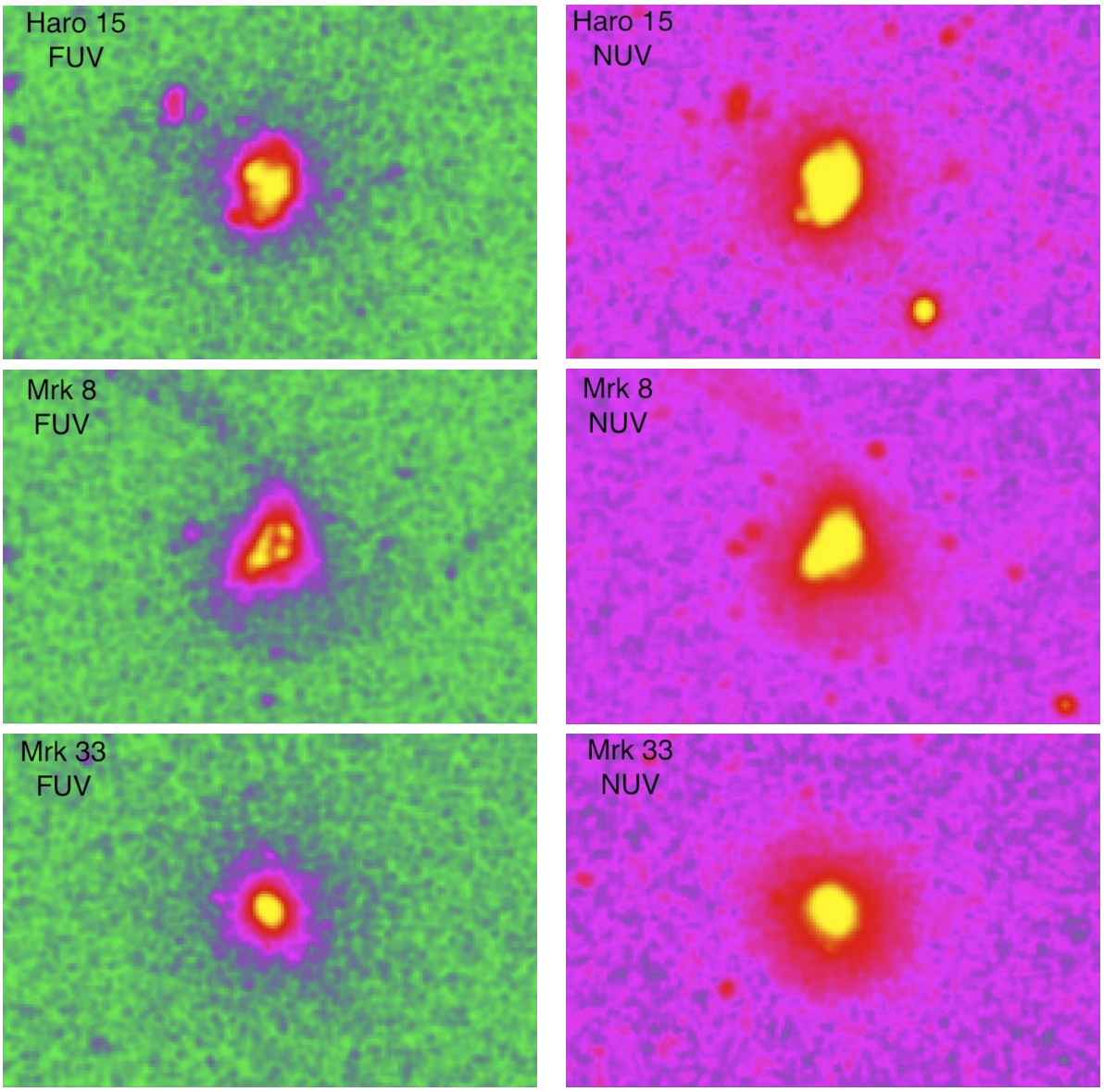

Figure 4.2: FUV and NUV images from the *GALEX* archive of a handful of galaxies from the optical sample that have been Gaussian smoothed and displayed on a logarithmic scale. A color table was applied using DS9.

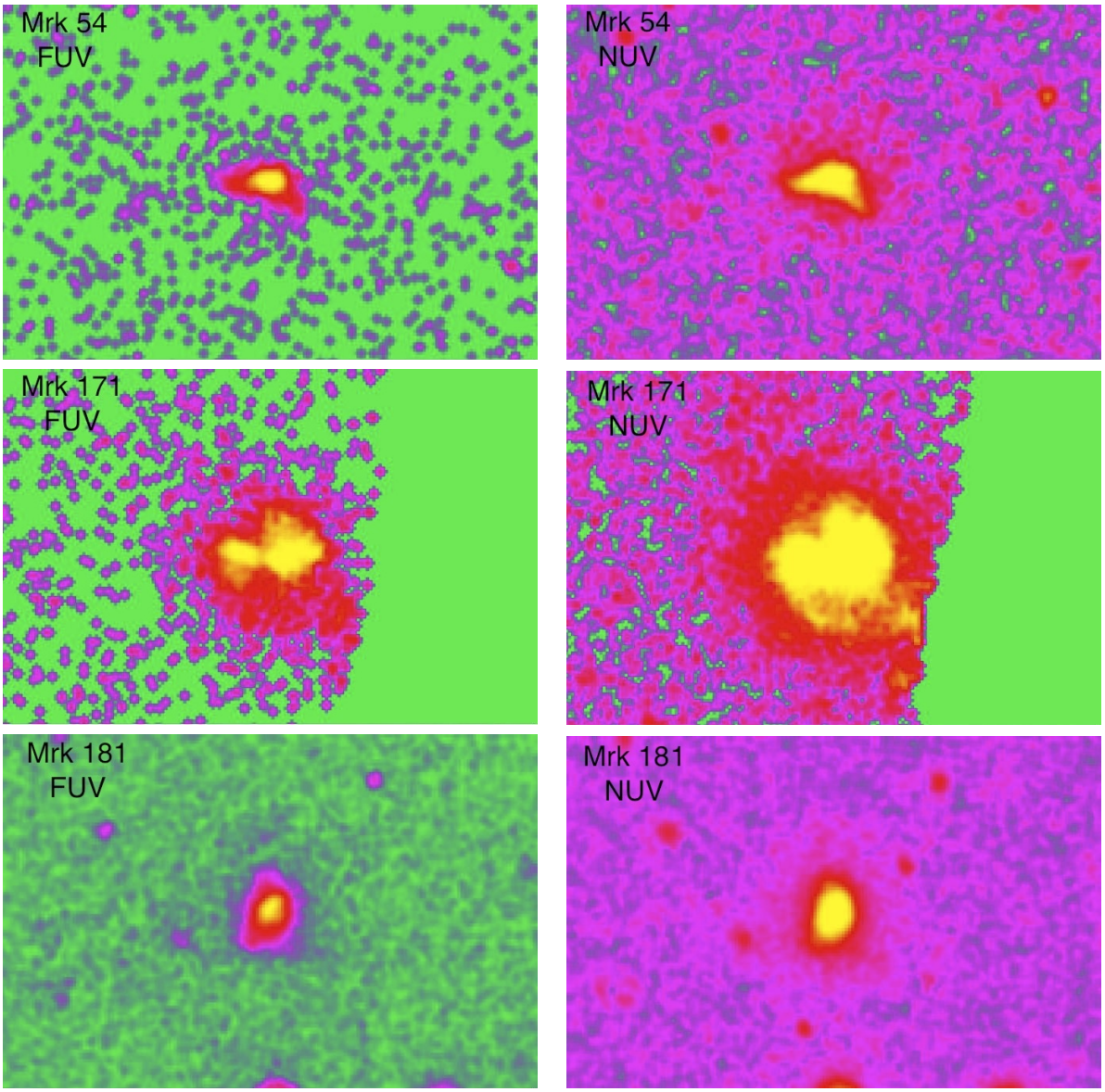
Mrk 54
FUV
Mrk 54
NUV
Mrk 171
FUV
Mrk 171
NUV
Mrk 181
FUV
Mrk 181
NUV

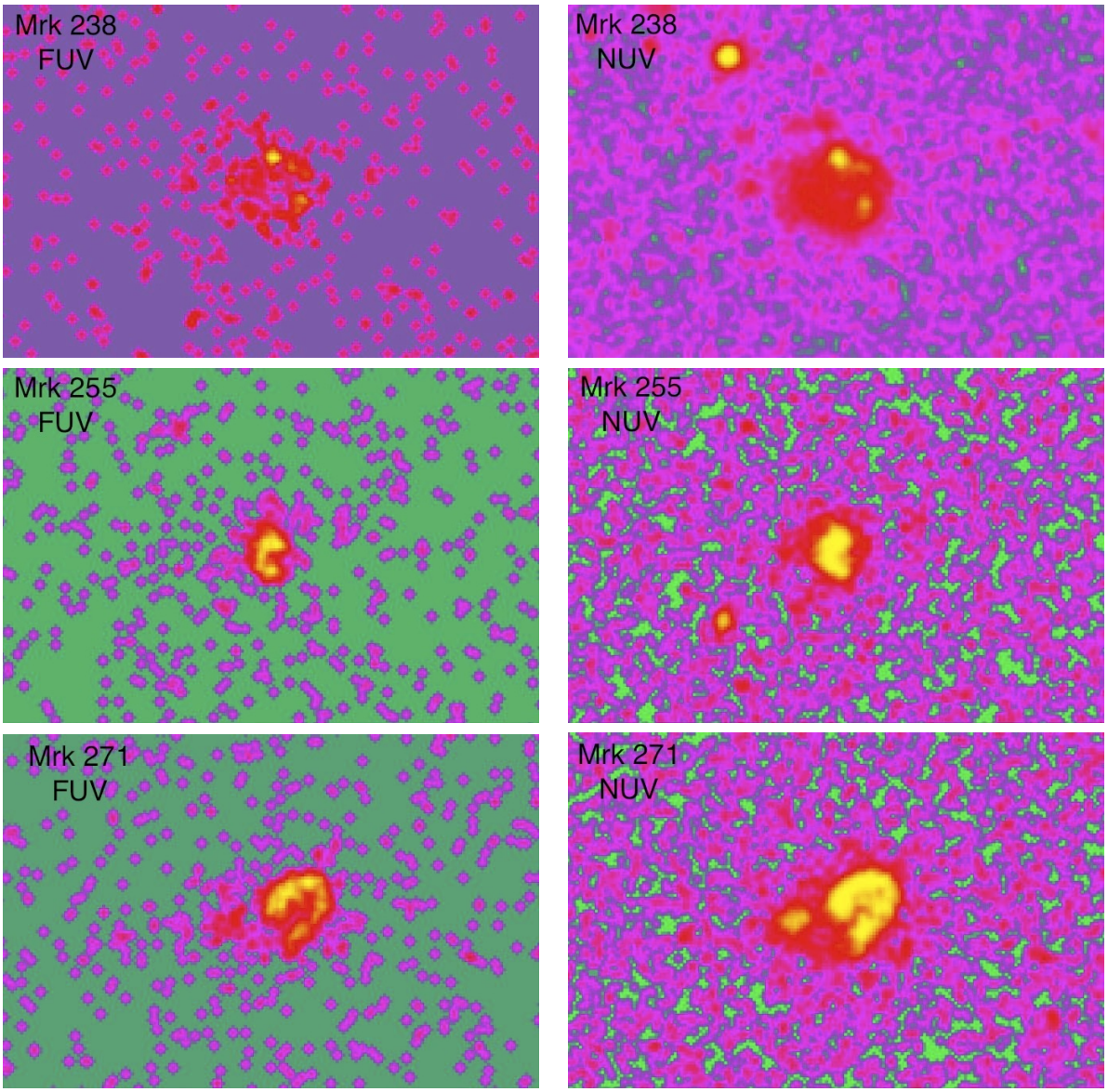
Mrk 238
FUV
Mrk 238
NUV
Mrk 255
FUV
Mrk 255
NUV
Mrk 271
FUV
Mrk 271
NUV

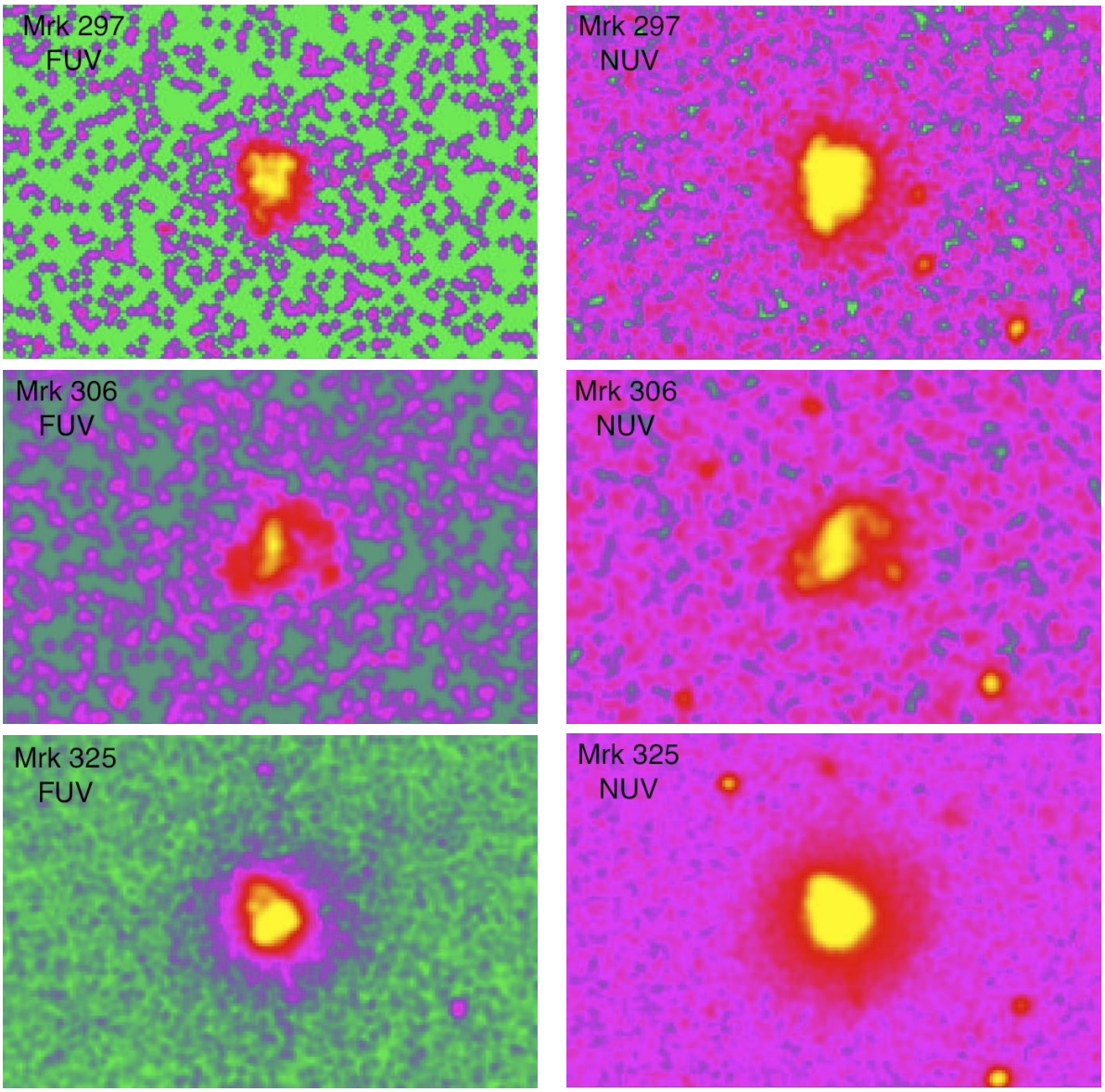
Mrk 297
FUV
Mrk 297
NUV
Mrk 306
FUV
Mrk 306
NUV
Mrk 325
FUV
Mrk 325
NUV

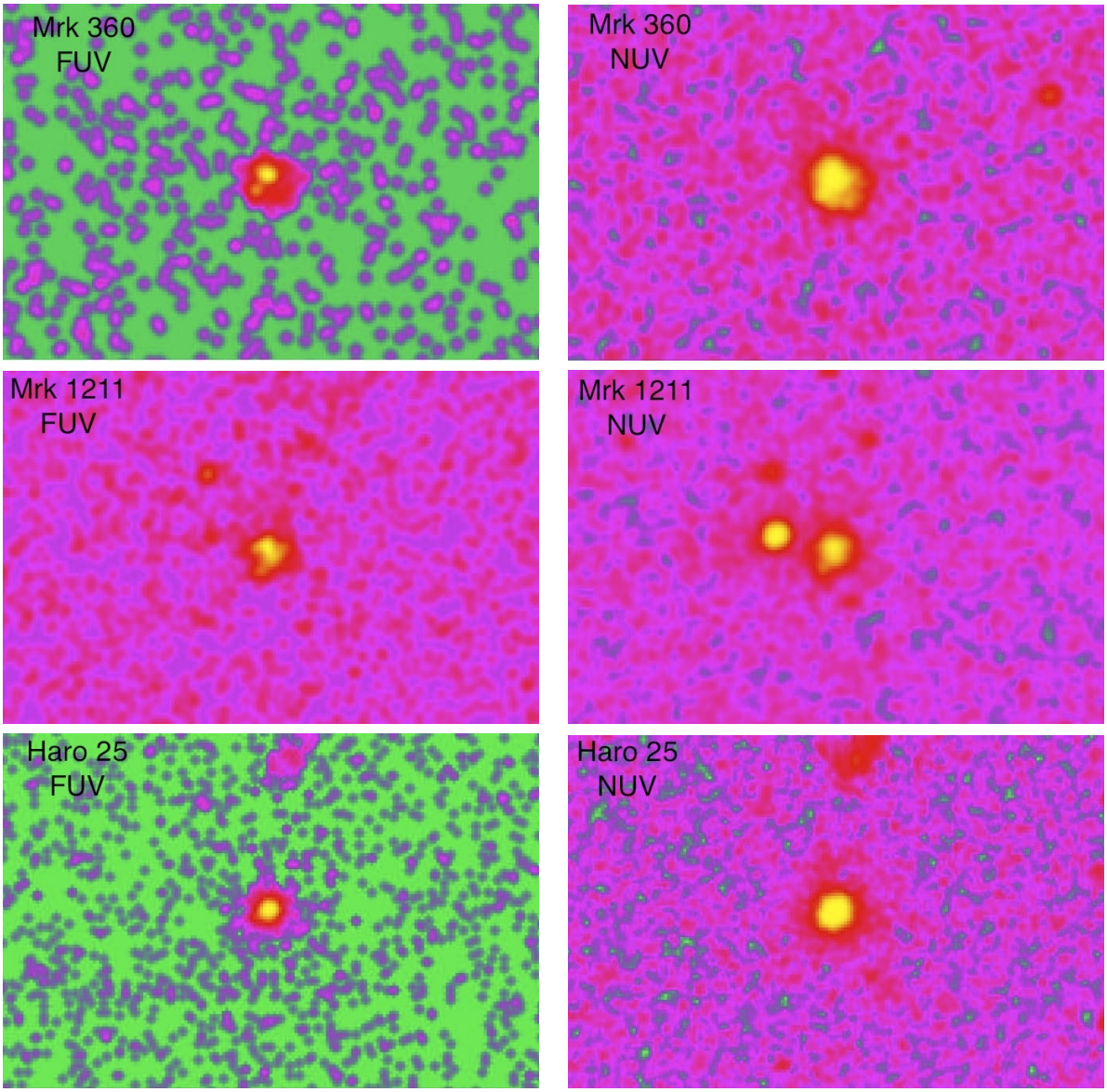
Mrk 360
FUV
Mrk 360
NUV
Mrk 1211
FUV
Mrk 1211
NUV
Haro 25
FUV
Haro 25
NUV

4.2 UV-Optical Photometry Compared to Models

4.2.1 Synthesis Models

Synthesis models, introduced in section 3.3, for comparison with observed galaxy properties are increasingly used to interpret multiwavelength observations of galaxies. Starburst99 is a comprehensive set of model predictions for spectrophotometric and related properties of galaxies with active star formation (Leitherer et al. 1999). The code was first used by Leitherer & Heckman (1995) for compiling a set of observable parameters of evolving young stellar populations. New models have been added since 1995 to include new knowledge of stellar atmospheres and evolution models.

In Figures 4.3-4.7 we plot various UV-optical color-color plots for the optical and high star formation sample of galaxies. The optical colors used here are the Sloan ugriz bands. On the color-color plots are superimposed evolutionary tracks from version 5.1 of the Starburst99 population synthesis code (Leitherer et al. 1999), assuming instantaneous bursts, Kroupa (2002) initial mass functions, and an initial mass range of 0.1-100$M_{\odot}$. Padova asymptotic giant-branch stellar models (Vazquez & Leitherer 2005) were used in this version of the code.

An initial mass function (IMF), $\xi(M)$ specifies the distribution in mass of a freshly formed stellar population. Specifically, after a burst of star formation, let there be

$$dN = N_0 \xi(M) dM \tag{4.1}$$

stars with masses in $(M, M + dM)$ range. The IMF is frequently assumed to be a simple power law of the form:

$$\xi \propto M^{-\alpha}. \tag{4.2}$$

The Kroupa (2001) initial mass function is a multi-power-law IMF; it summarizes the standard model for the IMF as a 2-component power law with the break at a mass of $0.5M_{\odot}$. Two IMF exponents, 1.3 and 2.3 are specified, and refer to low and high mass exponents separately. The mass boundaries corresponding to these low and high mass intervals are from 0.1 to 0.5 and 0.5 to 100 $M_{\odot}$ respectively.

Padova stellar models are best shown in Figure 4.8 (Walcher et al. 2009). The evolutionary tracks of stars are shown comparing 4 different models. The one we are using is in black (Padova, Marigo & Girardi 2007). The stellar tracks first need a chemical abundance assigned to them. The Padova tracks have the solar abundance tables from Anders & Grevesse (1989) as a baseline. Values for carbon, nitrogen, and iron, have been updated using Grevesse & Anders (1991), Grevesse et al. (1991), Hannaford et al. (1992), and Grevesse & Noels (1993). Other than for Helium, the zero-age main-sequence abundances were used from Anders & Grevesse (1989). For nonsolar abundance models in the Padova tracks, heave-element compositions were found by applying scaling of the heavy-element abundances to solar abundance models, and by keeping the metal abundance ratios unchanged. In order to incorporate convective energy transport into the synthesis models, work from Yi (2003) was used. The efficiency of convective energy transport has a major effect on the evolution of

massive stars. To account for convective overshooting (increase the rate of energy transport by increasing the size of convective core) low-mass stars have an allowed core over-shoot of $d/H_p = 0.25$, where the overshoot distance is d and the pressure scale height is H_p. Massive stars have a value of 0.5. The Padova model does not consider the effects of rotation. The next consideration in building the Padova models was stellar mass loss, which is an important parameter when dealing with evolution of massive stars in particular. To account for mass loss, the Padova models use parameterization of de Jager et al. (1988). He created mall-loss ranges across the HRD.

The solar metallicity models, shared with us by Smith et al. (2010), have an extinction of E(B−V)=0 (blue), E(B−V)=0.5 (red), and E(B−V)=1 (yellow). The model colors have the Hα line added to them, which can contribute significantly to the r-band flux for very young ages. The ages are increasing from the bottom starting at 1 Myr, by step sizes of 1 Myr to 20 Myr, then by 5 Myr steps to 50 Myr, then 10 Myr steps to 100 Myr, 100 Myr steps to 1 Gyr, and 500 Myr steps to 10 Gyr. Smith et al. (2010) studied stellar populations and star formation morphology in a sample of 42 nearby optically selected pre-merger interacting galaxy pairs.

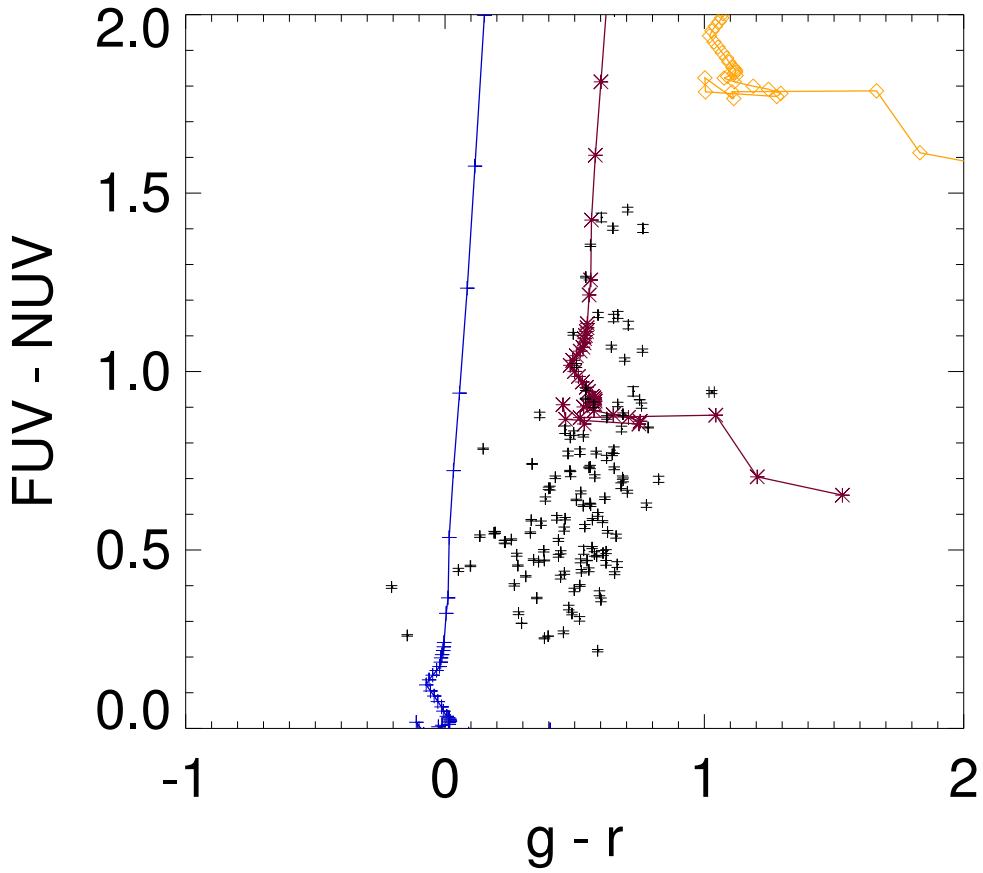

Figure 4.3: FUV−NUV vs. g−r colors for the combined sample, plotted against the corresponding colors for the evolution of a stellar population obtained from Starburst99 (Leitherer etal 1999). The solar metallicity models have an extinction of E(B−V)=0 (blue), E(B−V)=0.5 (red), and E(B−V)=1 (yellow). The model colors have the Hα line added to them, which can contribute significantly to the r-band flux for very young ages. The ages are increasing from the bottom starting at 1 Myr, by step sizes of 1 Myr to 20 Myr, then by 5 Myr steps to 50 Myr, then 10 Myr steps to 100 Myr, 100 Myr steps to 1 Gyr, and 500 Myr steps to 10 Gyr. The evolutionary tracks assume an instantaneous burst, Kroupa (2002) initial mass functions, and an initial mass range of 0.1-100$M\odot$. Padova asymptotic giant-branch stellar models (Vazquez & Leitherer 2005) were used.

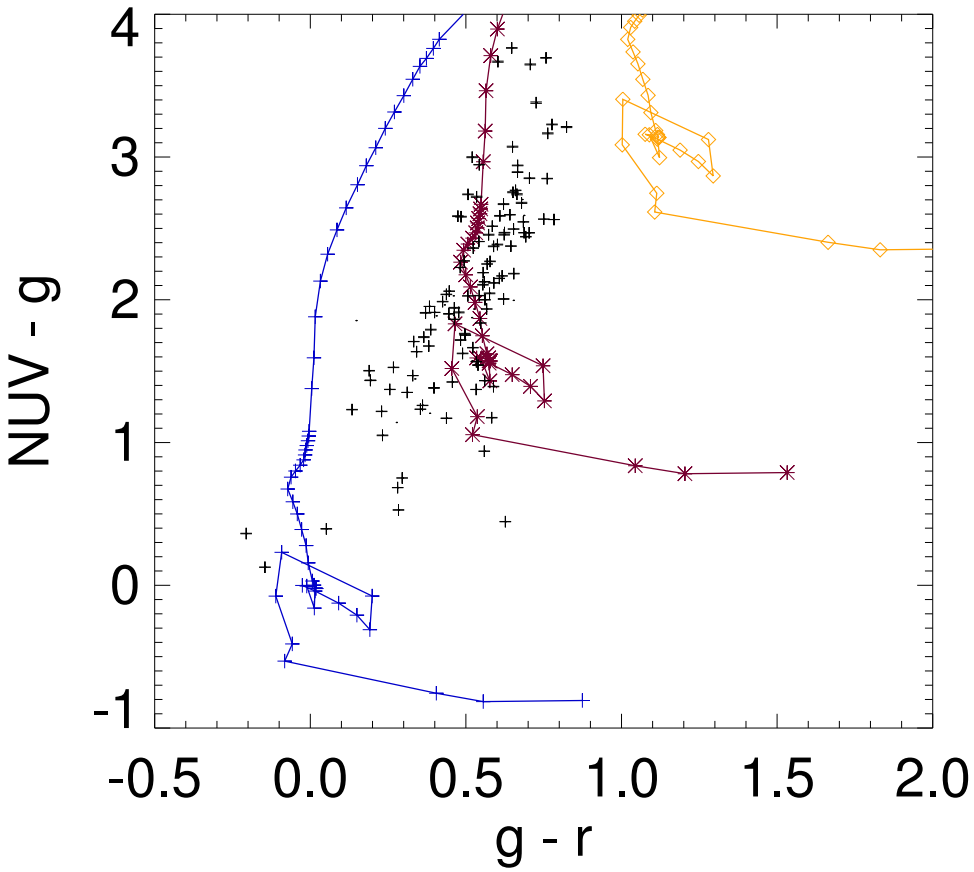

Figure 4.4: NUV−g vs. g−r Color-Color Plot

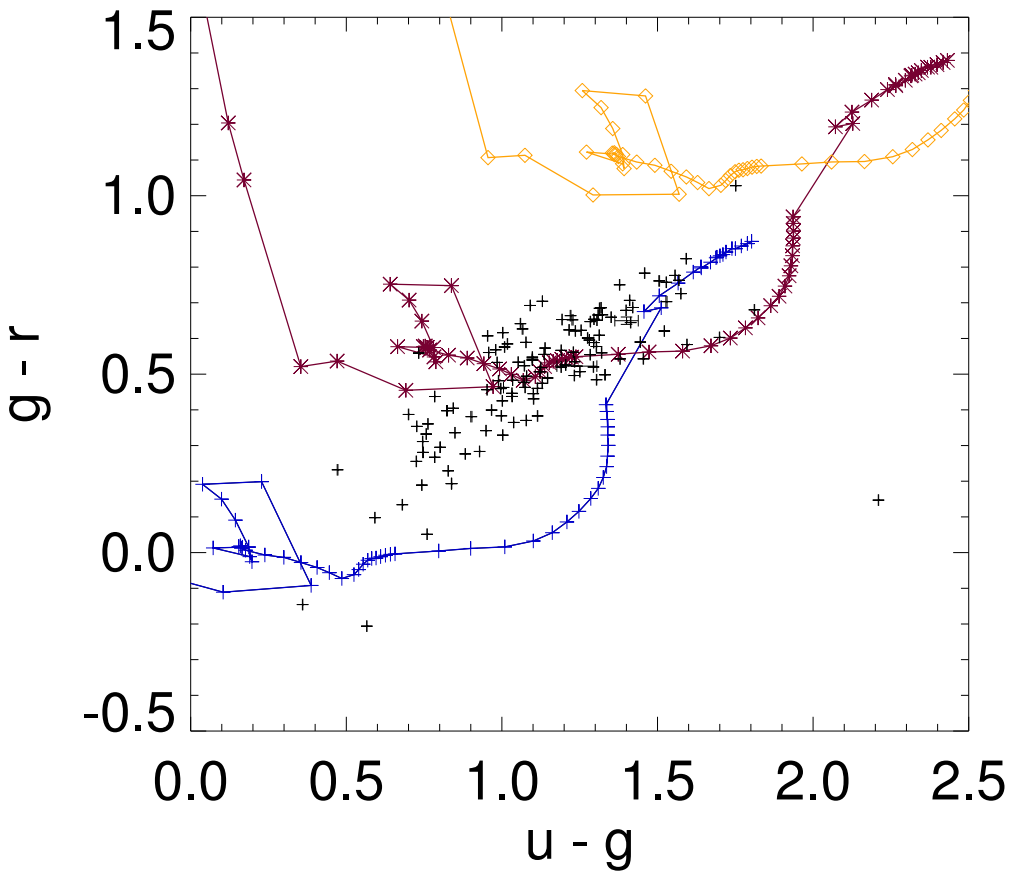

Figure 4.5: g−r vs. u−g Color-Color Plot

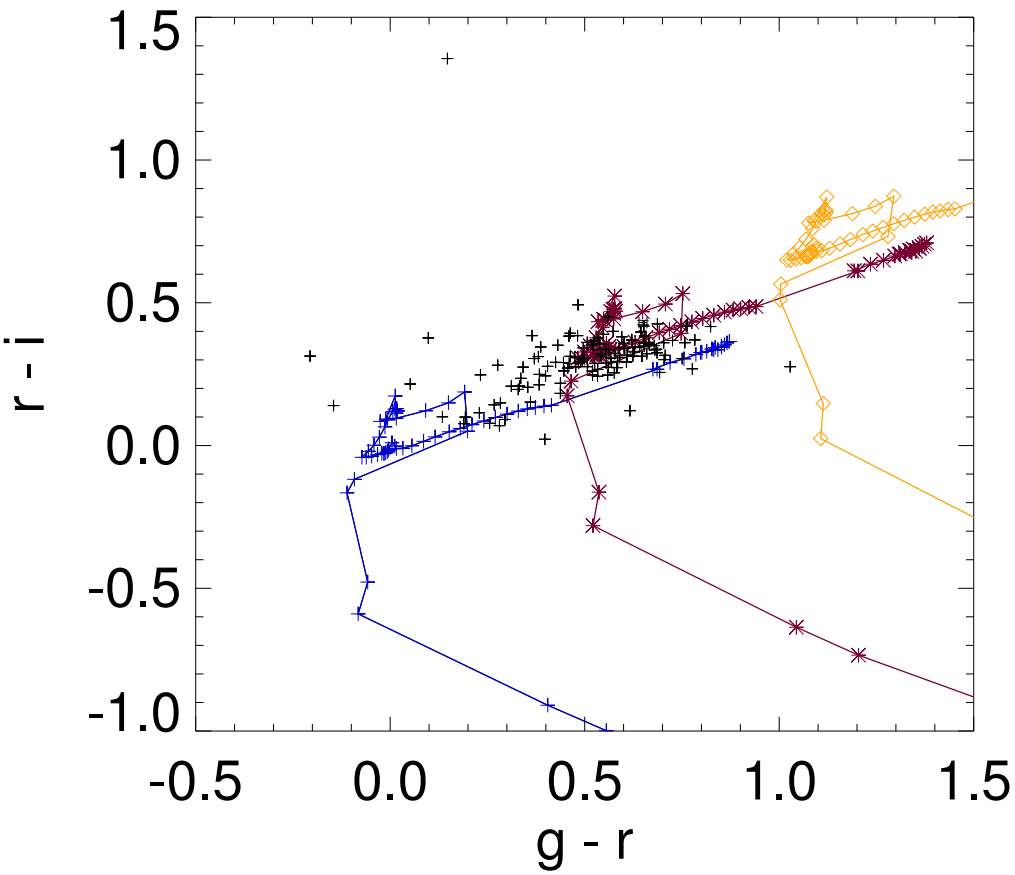

Figure 4.6: r−i vs. g−r Color-Color Plot

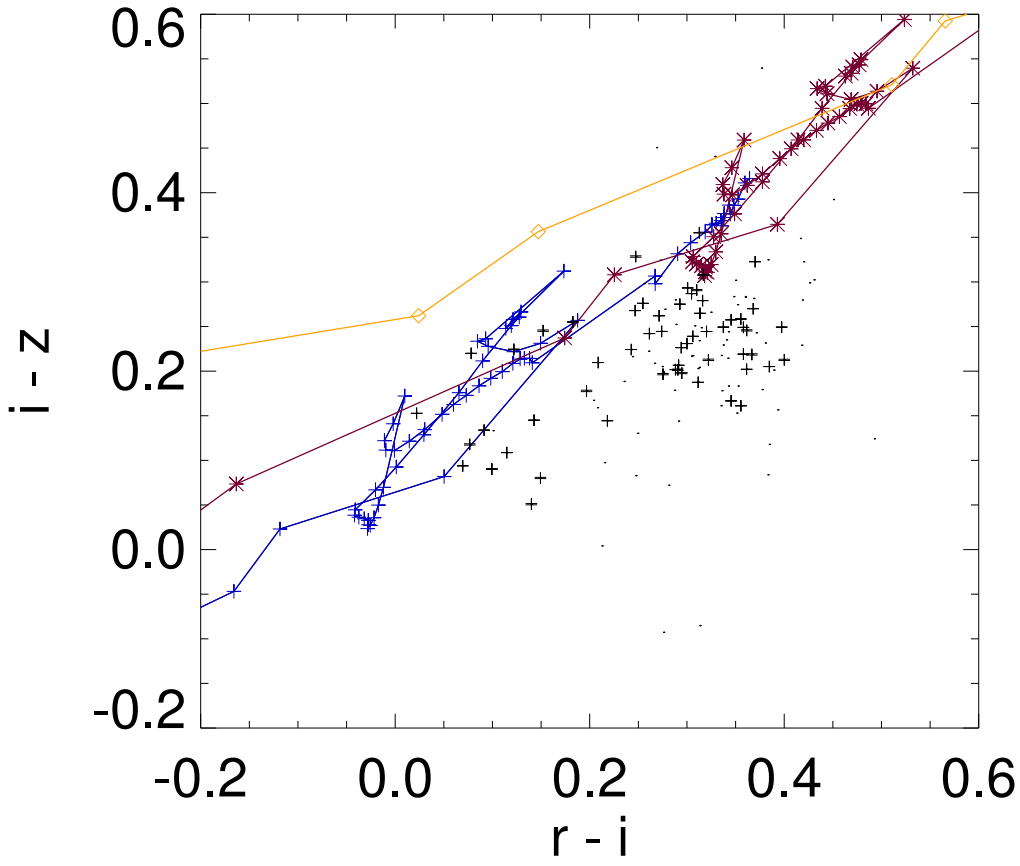

Figure 4.7: i−z vs. r−i Color-Color Plot

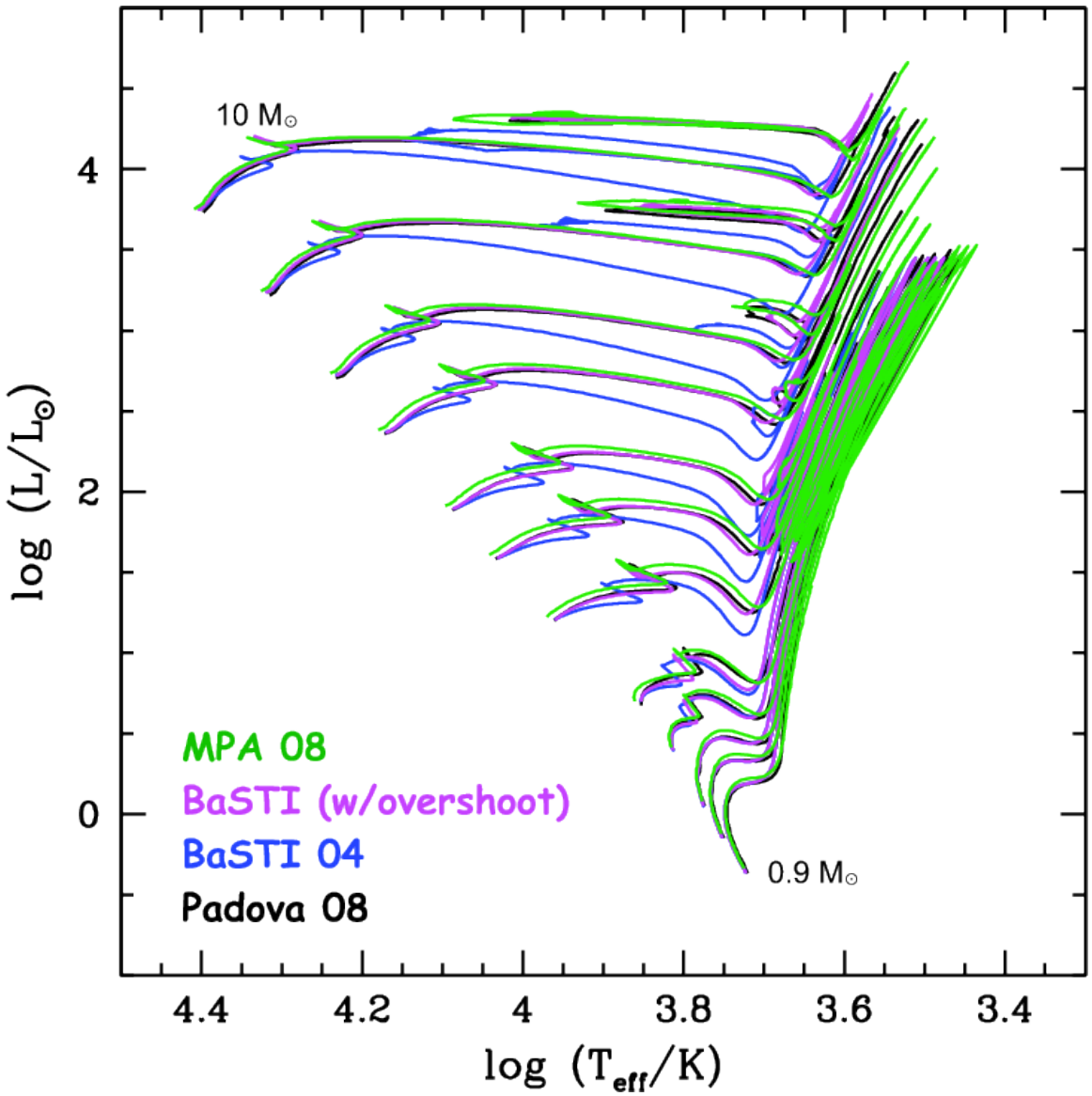

Figure 4.8: Padova Stellar Models

4.2.2 Sloan Survey Photometry

The models in this section use photometry from the Sloan Digital Sky Survey, so background on the survey is provided here. The Sloan Digital Sky Survey (SDSS) is an imaging survey that covers approximately one-quarter of the celestial sphere and collect spectra of $\approx 10^6$ galaxies, 100,000 quasars, 30,000 stars, and 30,000 serendipity targets (Stoughton et al. 2002). SDSS used a 2.5m telescope to view five optical bands, u, g, r, i, and z in the AB magnitude system. The data in this paper came from Sloan's data release 8. The SDSS data is shown in Table 4.1. Since SDSS data was used in multiple locations throughout the dissertation, some images have also been included for reference in Figure 4.9. To correct for extinction, values of 5.16, 3.79, 2.75, 2.09, and 1.48 for the u,g,r,i, and z bands respectively were used for $A_\lambda/E(B-V)$ as found in Schlegel, Finkbeiner, & Davis (1998).

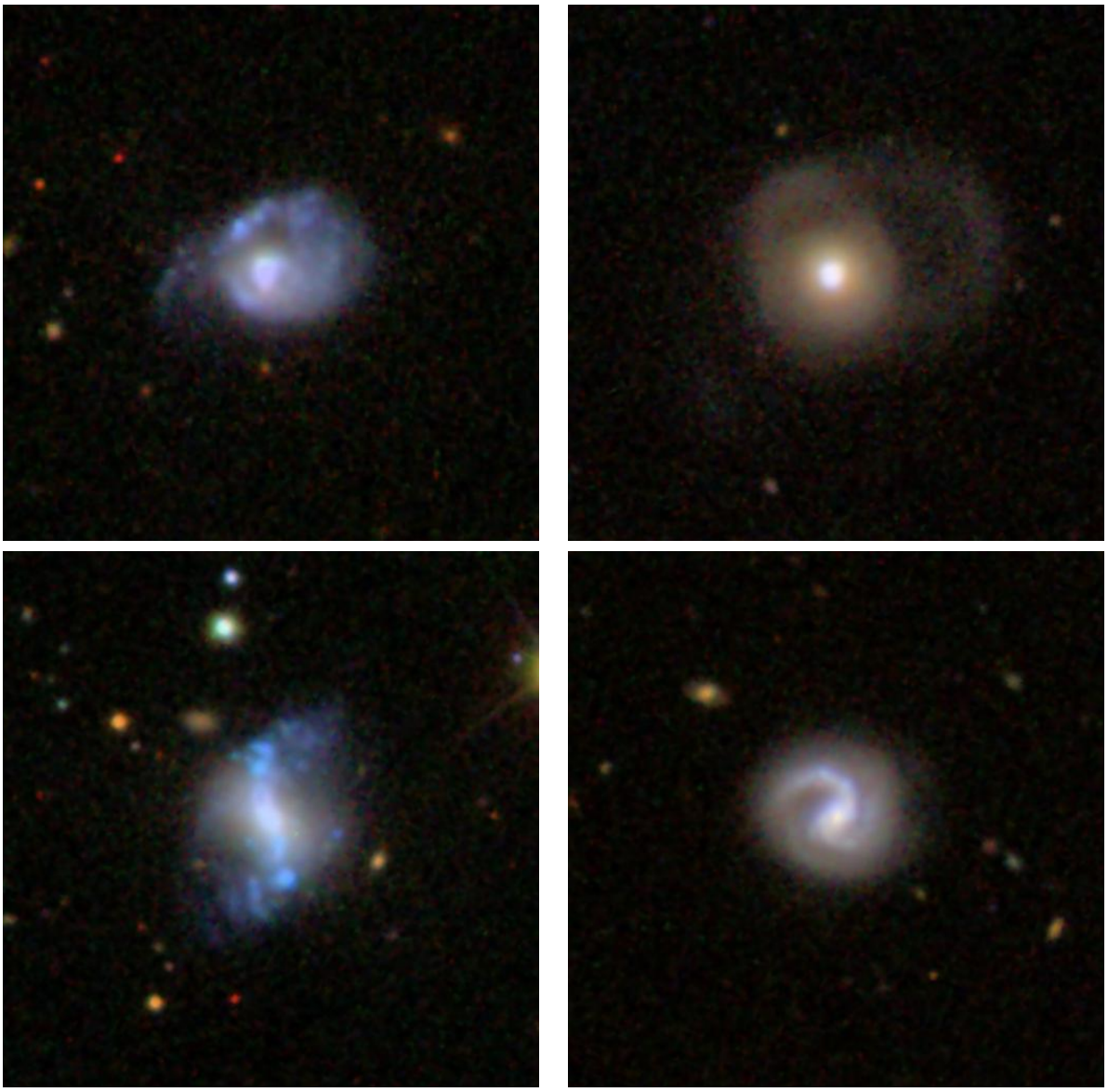

(1) Mrk 360 SDSS image (2) Mrk 366 SDSS image3) Mrk 1094 SDSS image (4) Mrk 144 SDSS image

Figure 4.9: Selected examples of luminous blue compact galaxies taken from the Sloan Digital Sky Survey. The rgb true color images use the g (blue), r (green), and i (red) filters. The images presented here are $\sim 1.7'' \times 1.7''$. Each galaxy was also observed at McDonald, and was selected to also include an SDSS image because of the complex morphologies such as the tidal loop with Mrk 366 and the barred spiral of Mrk 144.

Table 4.1. Sloan Digital Sky Survey Photometry for the Combined Samples

Name	u	g	r	i	z	u_c	g_c	r_c	i_c	z_c
(1)	(2)	(3)	(4)	(5)	(6)	(7)	(8)	(9)	(10)	(11)
McDonald Sample										
Mrk 342	17.59	16.27	15.53	15.12	14.83	17.21	15.99	15.33	14.97	14.72
Mrk 360	15.86	14.94	14.64	14.48	14.33	15.51	14.68	14.45	14.34	14.23
Mrk 366	16.10	15.00	14.34	13.99	13.73	15.65	14.67	14.10	13.81	13.60
Mrk 367	16.96	15.73	15.09	14.67	14.45	16.46	15.36	14.82	14.47	14.31
Mrk 589	15.56	14.50	13.84	13.69	13.44	15.34	14.34	13.72	13.60	13.38
Mrk 1184	15.51	14.40	13.72	13.35	13.07	15.32	14.26	13.62	13.27	13.02
Mrk 1404	15.85	14.65	14.03	13.66	13.37	15.46	14.37	13.82	13.50	13.26
Mrk 1094	15.35	14.54	14.18	14.02	13.85	14.81	14.14	13.89	13.80	13.69

Table 4.1 (continued)

Name	u	g	r	i	z	u_c	g_c	r_c	i_c	z_c
(1)	(2)	(3)	(4)	(5)	(6)	(7)	(8)	(9)	(10)	(11)
Haro 1	19.99	19.76	22.65	19.17	20.11	19.77	19.60	22.53	19.08	20.05
Mrk 385	15.99	14.94	14.46	14.23	14.02	15.84	14.83	14.38	14.17	13.98
Mrk 1211	16.43	14.97	14.29	13.87	13.60	16.25	14.84	14.20	13.80	13.55
Mrk 390	15.55	14.71	14.40	14.23	14.06	15.34	14.55	14.29	14.14	14.00
Mrk 18	15.27	14.13	13.41	13.10	12.81	15.01	13.94	13.27	13.00	12.74
Mrk 402	15.98	15.21	15.00	14.91	14.78	15.88	15.13	14.94	14.87	14.75
IIZw 44	16.32	15.28	14.68	14.41	14.12	16.20	15.19	14.62	14.36	14.09
Mrk 139	15.76	14.55	14.14	13.91	13.75	15.70	14.50	14.11	13.88	13.73
Mrk 144	15.97	14.92	14.46	14.19	13.94	15.90	14.87	14.42	14.16	13.92
Mrk 33	14.12	13.28	12.87	12.84	12.68	14.06	13.23	12.84	12.81	12.66
Mrk 148	16.55	15.23	14.69	14.43	14.09	16.45	15.16	14.64	14.39	14.06

Table 4.1 (continued)

Name	u	g	r	i	z	u_c	g_c	r_c	i_c	z_c
(1)	(2)	(3)	(4)	(5)	(6)	(7)	(8)	(9)	(10)	(11)
Haro 25	15.57	14.80	14.51	14.41	14.17	15.40	14.67	14.42	14.34	14.12
Mrk 154	16.51	15.39	14.93	14.63	14.42	16.44	15.34	14.89	14.60	14.40
Mrk 181	15.60	14.58	14.02	13.76	13.52	15.47	14.48	13.95	13.71	13.48
Haro 34	15.51	14.67	14.19	13.98	13.70	15.30	14.51	14.08	13.89	13.64
Mrk 54	15.66	15.28	15.41	15.26	15.20	15.58	15.22	15.37	15.23	15.18
Mrk 248	16.73	15.07	14.29	13.87	13.56	16.63	15.00	14.23	13.83	13.53
Mrk 255	16.84	15.89	15.59	15.43	15.34	16.76	15.83	15.55	15.40	15.32
Haro 42	15.52	14.83	14.65	14.59	14.47	15.44	14.77	14.61	14.56	14.45
Mrk 492	15.80	14.32	13.56	13.21	12.90	15.54	14.13	13.42	13.10	12.82
Mrk 297	14.63	13.78	13.42	13.30	13.16	14.24	13.49	13.21	13.14	13.05
Mrk 300	16.46	15.08	14.36	13.97	13.68	16.19	14.88	14.22	13.86	13.60

Table 4.1 (continued)

Name	u	g	r	i	z	u_c	g_c	r_c	i_c	z_c
(1)	(2)	(3)	(4)	(5)	(6)	(7)	(8)	(9)	(10)	(11)
Mrk 697	17.53	15.63	14.79	14.37	14.03	17.33	15.49	14.69	14.29	13.97
Mrk 499	15.52	14.66	14.45	14.34	14.24	15.44	14.60	14.41	14.31	14.22
IZw 191	16.08	15.13	14.52	14.24	14.00	15.98	15.06	14.47	14.20	13.97
IIZw 82	15.87	14.12	13.27	12.87	12.56	14.89	13.40	12.74	12.47	12.28
Mrk 512	16.35	15.15	14.52	14.17	13.86	15.94	14.85	14.30	14.01	13.74
Mrk 518	15.74	14.50	13.98	13.68	13.46	15.26	14.15	13.72	13.49	13.32
Mrk 303	15.94	14.68	14.06	13.72	13.45	15.68	14.49	13.92	13.61	13.37
Mrk 306	15.39	14.55	14.13	13.94	13.66	15.10	14.33	13.97	13.82	13.58
IIZw 185	15.76	14.75	14.37	14.19	14.05	15.45	14.52	14.20	14.06	13.96
Mrk 531	14.62	13.28	12.59	12.25	11.87	14.41	13.12	12.48	12.16	11.81
Mrk 325	14.42	13.56	13.22	13.10	12.94	14.20	13.40	13.10	13.01	12.88

Table 4.1 (continued)

Name	u	g	r	i	z	u_c	g_c	r_c	i_c	z_c
(1)	(2)	(3)	(4)	(5)	(6)	(7)	(8)	(9)	(10)	(11)
High Star Formation Rate Sample										
Mrk 91	15.81	14.62	13.87	13.54	13.22	15.58	14.45	13.75	13.45	13.15
Mrk 114	15.85	14.49	13.77	13.41	13.14	15.67	14.36	13.68	13.34	13.09
Mrk 126	16.32	15.00	14.41	14.08	13.86	16.26	14.95	14.38	14.05	13.84
Mrk 143	16.38	14.99	14.32	13.96	13.70	16.33	14.96	14.30	13.94	13.69
Mrk 161	15.03	14.06	13.49	13.21	12.96	14.98	14.03	13.47	13.19	12.95
Mrk 204	16.80	15.50	14.88	14.51	14.28	16.71	15.43	14.83	14.47	14.25
Mrk 217	16.81	15.48	14.81	14.44	14.18	16.72	15.41	14.76	14.40	14.15
Mrk 237	15.62	14.84	14.49	14.27	14.05	15.53	14.78	14.44	14.23	14.02

Table 4.1 (continued)

Name	u	g	r	i	z	u_c	g_c	r_c	i_c	z_c
(1)	(2)	(3)	(4)	(5)	(6)	(7)	(8)	(9)	(10)	(11)
Mrk 254	16.35	15.38	14.91	14.63	14.36	16.28	15.33	14.87	14.60	14.34
Mrk 264	16.55	15.55	15.06	14.67	14.46	16.51	15.52	15.04	14.65	14.45
Mrk 265	16.55	15.40	14.91	14.59	14.29	16.47	15.34	14.87	14.56	14.27
Mrk 269	16.62	15.89	15.48	15.12	14.94	16.51	15.81	15.42	15.07	14.91
Mrk 311	15.80	14.76	14.16	13.82	13.49	15.57	14.59	14.04	13.73	13.42
Mrk 312	17.04	15.50	14.75	14.36	14.04	16.68	15.24	14.56	14.22	13.94
Mrk 319	15.75	14.23	13.58	13.20	12.95	15.22	13.84	13.30	12.99	12.80
Mrk 321	15.41	13.92	13.20	12.82	12.53	15.01	13.62	12.99	12.66	12.41
Mrk 327	18.21	16.36	15.39	14.99	14.63	17.94	16.16	15.25	14.88	14.55
Mrk 349	16.15	15.14	14.49	14.17	13.87	15.94	14.98	14.38	14.08	13.81
Mrk 353	15.79	14.27	13.44	13.04	12.69	15.56	14.10	13.32	12.95	12.62

Table 4.1 (continued)

Name	u	g	r	i	z	u_c	g_c	r_c	i_c	z_c
(1)	(2)	(3)	(4)	(5)	(6)	(7)	(8)	(9)	(10)	(11)
Mrk 354	16.44	15.32	14.76	14.37	14.13	16.26	15.19	14.66	14.30	14.08
Mrk 368	16.17	14.99	14.44	14.15	13.94	15.61	14.58	14.14	13.92	13.78
Mrk 387	16.34	15.14	14.61	14.29	14.04	16.14	14.99	14.50	14.21	13.98
Mrk 413	16.36	15.26	14.75	14.44	14.20	16.28	15.20	14.71	14.41	14.18
Mrk 414	16.14	14.80	14.17	13.84	13.52	16.04	14.72	14.11	13.80	13.49
Mrk 440	16.88	15.74	15.22	14.85	14.64	16.81	15.69	15.18	14.82	14.62
Mrk 477	15.86	14.00	84.00	14.70	14.48	15.80	13.96	83.97	14.68	14.46
Mrk 489	15.40	14.37	14.02	13.81	13.62	15.30	14.29	13.96	13.77	13.59
Mrk 496	15.39	14.63	14.05	13.79	13.51	15.29	14.55	13.99	13.75	13.48
Mrk 540	16.77	15.57	14.95	14.52	14.28	16.54	15.40	14.83	14.43	14.21
Mrk 545	14.25	12.82	12.03	11.70	11.39	14.05	12.68	11.93	11.62	11.33

Table 4.1 (continued)

Name	u	g	r	i	z	u_c	g_c	r_c	i_c	z_c
(1)	(2)	(3)	(4)	(5)	(6)	(7)	(8)	(9)	(10)	(11)
Mrk 551	19.77	18.76	18.33	18.22	17.94	19.45	18.52	18.16	18.09	17.85
Mrk 556	17.36	16.26	15.76	15.47	15.26	17.25	16.18	15.70	15.42	15.23
Mrk 559	16.65	15.26	14.71	14.38	14.14	16.33	15.02	14.54	14.25	14.05
Mrk 560	17.10	15.48	14.72	14.33	14.04	16.93	15.35	14.63	14.26	13.99
Mrk 567	15.88	14.63	13.98	13.65	13.37	15.75	14.54	13.91	13.60	13.33
Mrk 569	16.35	15.12	14.57	14.29	14.05	16.20	15.01	14.49	14.23	14.01
Mrk 575	15.31	13.99	13.24	12.83	12.49	14.83	13.64	12.98	12.64	12.35
Mrk 579	17.53	16.42	16.00	15.58	15.43	17.26	16.22	15.85	15.47	15.35
Mrk 582	15.59	14.44	14.03	13.80	13.78	15.46	14.34	13.96	13.75	13.74
Mrk 592	15.91	14.81	14.24	13.95	13.72	15.73	14.68	14.14	13.88	13.67
Mrk 606	17.21	16.03	15.43	15.08	14.72	16.46	15.48	15.03	14.78	14.50

Table 4.1 (continued)

Name	u	g	r	i	z	u_c	g_c	r_c	i_c	z_c
(1)	(2)	(3)	(4)	(5)	(6)	(7)	(8)	(9)	(10)	(11)
Mrk 629	16.19	15.17	14.73	14.46	14.22	15.99	15.02	14.62	14.38	14.16
Mrk 632	16.97	15.37	14.56	14.27	13.80	16.81	15.25	14.47	14.20	13.75
Mrk 637	16.91	15.84	15.33	14.82	14.68	16.78	15.74	15.26	14.77	14.64
Mrk 639	16.80	15.67	15.26	14.93	14.69	16.60	15.53	15.16	14.85	14.63
Mrk 681	17.69	16.61	16.09	15.66	15.47	17.41	16.40	15.94	15.55	15.39
Mrk 688	15.95	14.89	14.42	14.10	13.93	15.73	14.73	14.30	14.01	13.87
Mrk 693	15.83	14.22	13.40	13.00	12.68	15.52	13.99	13.23	12.87	12.59
Mrk 702	17.04	16.44	16.62	16.29	16.36	16.91	16.35	16.55	16.24	16.32
Mrk 717	15.62	14.48	13.75	13.47	13.15	15.43	14.34	13.65	13.39	13.10
Mrk 718	15.94	14.58	13.99	13.52	13.11	15.79	14.47	13.91	13.46	13.07
Mrk 719	15.84	14.90	14.49	14.16	13.94	15.70	14.79	14.41	14.10	13.90

Table 4.1 (continued)

Name	u	g	r	i	z	u_c	g_c	r_c	i_c	z_c
(1)	(2)	(3)	(4)	(5)	(6)	(7)	(8)	(9)	(10)	(11)
Mrk 726	15.84	14.73	14.24	13.91	13.69	15.71	14.63	14.17	13.86	13.65
Mrk 753	17.09	15.81	15.24	14.84	14.64	16.91	15.68	15.15	14.77	14.59
Mrk 785	16.39	15.08	14.48	14.13	13.94	16.33	15.04	14.45	14.11	13.92
Mrk 789	17.28	16.17	15.51	15.16	14.70	17.12	16.05	15.42	15.09	14.65
Mrk 799	14.90	13.05	12.11	11.64	11.25	14.82	12.99	12.07	11.61	11.23
Mrk 809	24.63	22.85	21.80	21.51	21.59	24.52	22.77	21.74	21.47	21.56
Mrk 823	17.13	16.32	16.23	15.99	15.87	16.94	16.18	16.13	15.91	15.82
Mrk 834	15.68	14.15	13.37	12.94	12.70	15.59	14.08	13.32	12.90	12.67
Mrk 837	15.70	14.96	14.78	14.65	14.49	15.47	14.79	14.66	14.56	14.42
Mrk 848	17.44	15.81	15.20	14.91	14.57	17.31	15.71	15.13	14.86	14.53
Mrk 851	16.26	14.94	14.38	14.07	13.84	16.00	14.75	14.24	13.96	13.76

Table 4.1 (continued)

Name	u	g	r	i	z	u_c	g_c	r_c	i_c	z_c
(1)	(2)	(3)	(4)	(5)	(6)	(7)	(8)	(9)	(10)	(11)
Mrk 858	17.23	15.49	14.62	14.16	13.76	16.92	15.26	14.45	14.03	13.67
Mrk 881	15.71	14.75	14.40	14.12	13.91	15.67	14.72	14.38	14.10	13.90
Mrk 904	16.31	15.09	14.47	14.14	13.85	15.99	14.85	14.30	14.01	13.76
Mrk 923	15.70	14.53	13.87	13.51	13.22	15.35	14.27	13.68	13.37	13.12
Mrk 932	17.19	15.90	15.36	14.99	14.75	16.97	15.74	15.24	14.90	14.69
Mrk 940	17.51	16.02	15.28	14.82	14.49	17.25	15.83	15.14	14.71	14.41
Mrk 941	17.34	15.91	15.19	14.83	14.47	17.04	15.69	15.03	14.71	14.38
Mrk 948	16.90	15.46	14.75	14.38	14.06	16.75	15.35	14.67	14.32	14.02
Mrk 955	15.84	14.47	13.77	13.38	13.09	15.73	14.39	13.71	13.33	13.06
Mrk 984	15.47	14.33	13.75	13.34	13.12	15.31	14.21	13.66	13.28	13.07
Mrk 995	16.65	15.21	14.53	14.08	13.76	16.50	15.10	14.45	14.02	13.72

Table 4.1 (continued)

Name	u	g	r	i	z	u_c	g_c	r_c	i_c	z_c
(1)	(2)	(3)	(4)	(5)	(6)	(7)	(8)	(9)	(10)	(11)
Mrk 1001	17.31	16.01	15.34	14.94	14.63	17.07	15.83	15.21	14.84	14.56
Mrk 1005	16.26	14.93	14.25	13.85	13.51	16.13	14.84	14.18	13.80	13.47
Mrk 1027	16.14	15.18	14.66	14.30	14.01	15.91	15.01	14.54	14.21	13.94
Mrk 1029	16.90	15.52	14.81	14.43	14.13	16.68	15.36	14.69	14.34	14.07
Mrk 1057	16.29	15.69	15.36	15.05	14.91	15.81	15.33	15.10	14.85	14.77
Mrk 1101	15.13	14.36	14.03	13.81	13.64	15.04	14.29	13.98	13.77	13.61
Mrk 1111	16.23	14.43	13.75	13.36	13.08	15.85	14.15	13.55	13.21	12.97
Mrk 1112	16.53	14.76	13.88	13.44	13.06	16.17	14.50	13.69	13.30	12.96
Mrk 1115	17.05	15.56	14.99	14.66	14.41	16.92	15.46	14.92	14.61	14.37
Mrk 1122	16.48	14.85	14.04	13.59	13.24	16.25	14.68	13.92	13.50	13.17
Mrk 1143	16.59	15.30	14.65	14.29	14.03	16.46	15.20	14.58	14.24	13.99

Table 4.1 (continued)

Name	u	g	r	i	z	u_c	g_c	r_c	i_c	z_c
(1)	(2)	(3)	(4)	(5)	(6)	(7)	(8)	(9)	(10)	(11)
Mrk 1156	16.37	15.57	15.16	14.92	14.72	16.09	15.37	15.01	14.81	14.64
Mrk 1159	16.63	15.04	14.29	13.90	13.59	16.40	14.87	14.17	13.81	13.52
Mrk 1205	17.20	15.87	15.28	14.92	14.67	17.02	15.74	15.19	14.85	14.62
Mrk 1206	16.56	15.28	14.68	14.32	14.08	16.37	15.14	14.58	14.24	14.03
Mrk 1224	18.74	18.08	17.93	17.52	16.95	18.48	17.89	17.79	17.42	16.88
Mrk 1229	16.65	15.01	14.15	13.71	13.34	16.47	14.88	14.05	13.64	13.29
Mrk 1277	16.70	15.19	14.55	14.21	13.93	16.45	15.01	14.42	14.11	13.86
Mrk 1300	17.47	16.11	15.59	15.27	15.04	17.36	16.03	15.53	15.23	15.01
Mrk 1332	16.94	15.38	14.73	14.34	14.08	16.80	15.27	14.65	14.28	14.04
Mrk 1339	17.21	15.92	15.36	15.00	14.80	17.02	15.78	15.26	14.92	14.75
Mrk 1340	16.28	15.39	14.95	14.65	14.36	16.10	15.26	14.86	14.58	14.31

Table 4.1 (continued)

Name	u	g	r	i	z	u_c	g_c	r_c	i_c	z_c
(1)	(2)	(3)	(4)	(5)	(6)	(7)	(8)	(9)	(10)	(11)
Mrk 1362	17.39	16.09	15.48	15.09	14.85	17.32	16.04	15.44	15.06	14.83
Mrk 1365	15.30	13.95	13.24	12.90	12.62	15.18	13.86	13.18	12.85	12.59
Mrk 1380	16.38	15.24	14.76	14.46	14.27	16.28	15.17	14.71	14.42	14.24
Mrk 1382	16.36	15.44	15.05	14.78	14.56	16.09	15.24	14.91	14.67	14.48
Mrk 1387	16.61	15.47	15.01	14.64	14.47	16.47	15.36	14.93	14.58	14.43
Mrk 1391	16.35	15.10	14.54	14.23	13.93	16.18	14.97	14.45	14.16	13.88
Mrk 1405	16.19	14.00	13.03	12.51	12.18	14.76	12.95	12.27	11.93	11.77
Mrk 1420	16.70	15.80	15.51	15.22	15.14	16.63	15.75	15.47	15.19	15.12
Mrk 1428	17.48	16.34	15.81	15.45	15.26	17.42	16.30	15.78	15.43	15.24
Mrk 1432	16.86	15.85	15.38	14.99	14.90	16.81	15.81	15.35	14.97	14.89
Mrk 1433	16.03	14.78	14.11	13.68	13.39	15.94	14.72	14.06	13.64	13.36

Table 4.1 (continued)

Name	u	g	r	i	z	u_c	g_c	r_c	i_c	z_c
(1)	(2)	(3)	(4)	(5)	(6)	(7)	(8)	(9)	(10)	(11)
Mrk 1464	16.57	15.55	15.15	14.89	14.75	16.49	15.49	15.11	14.86	14.73
Mrk 1490	16.96	15.36	14.54	14.12	13.77	16.87	15.29	14.49	14.08	13.74
Mrk 1497	17.81	15.57	15.40	14.03	13.88	17.70	15.49	15.34	13.98	13.85

Col. (1) Primary galaxy name. Cols. (2 - 6) Sloan Digital Sky Survey observed magnitudes. Col. (7-11) Extinction corrected Sloan magnitudes. The extinction corrections were found using R = $A/E(B-V)$, where the R values are 5.16, 3.79, 2.75, 2.09, and 1.48 for u, g, r, i, and z respectively as found in Schlegel (1998).

4.2.3 Internal Extinction

Using the model - to - data comparison we can make a statement regarding the extinction due to the galaxies themselves. Recall the calculation to correct for extinction due to the milky way, where R_λ is the ratio of total to selective extinction at a particular wavelength, A_λ is the total extinction in magnitudes at that wavelength, and the color excess defines the selective extinction between the V and B bands, otherwise known as reddening.

$$R_\lambda = \frac{A_\lambda}{E(B-V)} \tag{4.3}$$

The models take the absolute magnitudes of an evolving stellar population (from Starbrst 99) and add extinction in each band. These absolute magnitudes are then differenced to obtain the reddened colors for each model timestep, which are displayed in the plots. A color excess of 0.5 is the best estimate of a mean extinction for the entire sample. Once E(B−V) was figured, and R's found for each filter, it was simple to solve for the extinction in each waveband of the LBCGs sample. Table 4.2 shows the extinction values. Note that throughout the paper when we have corrected for extinction, we have been referring to extinction due to the Milky Way. The values calculated here are the estimated extinctions from the LBCGs themselves.

Table 4.2. Extinction Values for LBCGs

λ	A
u	2.58
g	1.90
r	1.38
i	1.05
z	0.74

Col. (1) Wavelength. Col. (2) Extinction values by each band for the LBCGs themselves found using R values from Schlegel, Finkbeiner, & Davis (1998) and a color excess calculated from plots 4.4 - 4.8 in equation 4.3.

4.2.4 Star Formation History

Along with extinction values, the synthesis models can help find the ages of the luminous blue compact galaxy sample. Studies by Zhao, Gu, & Gao (2011) of blue compact dwarfs showed older systems with episodic star formation histories, confirming previous studies such as that by Lee et al. (2009). Lee et al. (2009) found in dwarf galaxy starbursts that the percentage of dwarfs undergoing large-scale starbursts is only 6%. Approximately 70% of star formation in the overall dwarf population is going through a continuous mode. This view is somewhat new; previously it had been thought that BCDs were chemically primitive and would experience strong bursts intermittent long quiet periods (Searle, Sargent, & Bagnuolo 1973). Kong et al. (2003)

who studied blue compact dwarfs found that some galaxies might be undergoing a first round star forming burst, but for others older stars could account for half of the optical emission. Looking at our LBCG sample overlaid on synthesis models, we also see a variety of ages. Our data agrees that LBCGs can be older systems. Figres 4.3 through 4.7 shows galaxies ranging from abut 5 Myr to 1 Gyr. Astronomers using the Hubble space Telescope discovered the oldest known spiral galaxy in 2012, which was 10.7 billion years old. Analyzing the models in Figure 4.4 we see a shift to the blue for NUV−g without a large shift in g−r. This is more than likely an age effect (Smith et al. 2010). Star formation rather than dust extinction is the main factor causing the bluer NUV−g colors. the models also show that as (FUV−NUV) reddens very quickly with age, the (g−r) does not.

Chapter 5

Summary and Conclusions

Luminous blue compact galaxies are some of the most dynamic, changing, intriguing galaxies in the universe. However, this fact which makes them so exciting, also means that there are no black and white answers to their history or evolution. We know that LBCGs are a stage in galaxy evolution, and that they are building blocks to many of the galaxies that surround us today. Our study of LBCGs was to better understand where they came from, what kind of galaxy are they now, what are their traits such as color or star formation, and where they are headed.

The journey begins with the optical wavelengths; this is by far where the majority of the time was spent with this dissertation. A major question going into this project was, what are the morphologies for these galaxies? The morphology question is answered two ways, first with the Loose & Thuan classification scheme, and secondly with the profile fitting. Using Loose & Thuan's scheme we found that the majority of the sample has an irregular core and irregular outer envelope, and second place is an irregular core on top of a fairly normal outer envelope with regular isophotes. Cairos et al. (2001) found a similar division of their blue compact dwarfs. Looking at the surface brightness profile fittings with the De Vaucouleurs and exponential law, it was possible to see if the galaxy flux falls off at higher radi in the same format as spiral or elliptical galaxies. The majority of our sample is bulge dominated, meaning the

SBP is fit well by a De Vaucouleurs law. A correspondence between morphology and the intensity distributions is seen. Eight of the thirteen nE galaxies are bulges, which would be expected. However, half of the iE are also bulges. The star formation in the galaxies is not just in the core in most cases, it could be throughout the galaxies, making any underlying, older, red population very difficult to see or fit. As the color profiles show, the bluest galaxies have flat profiles all the way out to where the galaxy light begins to fall off to noise level. The iI galaxies tend to lean toward the disk classification, meaning they have an exponential fit.

The environment of the LBCG is very important to observe, because it needs to be known if the galaxy traits, such as high star formation, are only environmentally triggered, or if there are internal triggers. The majority, 60%, of our optical sample shows either signs of interactions or 1 or more companions. Much of the high star formation, resulting in blue colors and high luminosities, is due to interactions and mergers. However, there is the 40% that could be new galaxies, or had some other kind of internal trigger to the high star formation. The sample as a whole does not have one type of triggering mechanism, but interactions may cause bluer colors and higher star formations compared to the rest of the sample. Of the top 30% bluest galaxies (fifeteen in the sample), nine have interactions or companions. When comparing the median SFRs for interacting vs. non-interacting galaxies in the combined optical and high star formation sample, the interacting have a slightly higher rate than the non-interacting. However, this gap could be bigger because there is possible error in

the interacting/non-interacting classifications, and we are not sure how many of the interacting sample of galaxies would actually fall under a LBCG classification.

The most promising scenario from our results is that LBCGs are the stage in galaxy evolution after ultraluminous infrared galaxies. ULIRGs are recent mergers with high star formation that could eventually consume or heat and disperse the gas. As more and more of the gas is dispersed, and stars migrate out of the dust, more UV and blue light would become visible. Figure 3.4 is one of our strongest results backing this scenario. A correlation exist between the ratio of FIR to UV star formation and UV luminosity. As the UV SFR becomes a more dominant factor, the galaxy becomes more UV bright, showing a possible evolutionary path from ULIRGs to UV bright LBCGs. On the same note, as the LBCGs get bluer in B−V, the UV SFR gets higher, as can be seen in Figure 3.5. As more of the gas is dispersed from ULIRGs, more of the UV and blue light can be seen. However, the star formation is still extremely high, although usually tapering off from the ULIRG stage, and that is why we have blue galaxies with high UV and IR SFRs.

The M_B magnitudes calculated using the SBPs and GCs match what we had expected based on literature. However, a handful of the sample did not have a blue enough ($B - V < 0.6$) color overall to be classified as a LBCG. However, even if the overall color did not make the cutt-off point, the core was still blue so their inclusion in the sample was still viable. Figure 5.1 shows a color magnitude diagram for the

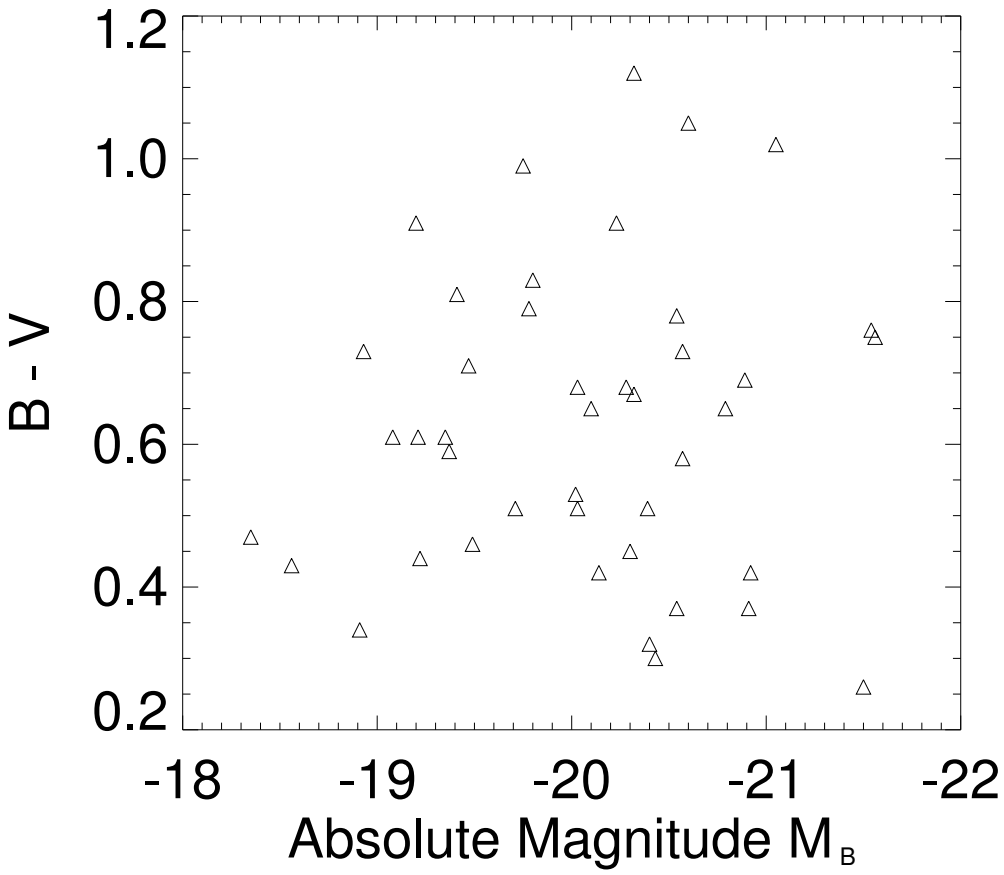

Figure 5.1: Color-magnitude diagram for the optical sample made using colors from Table 2.8 and M_B values from Table 2.7.

combined samples which graphically presents a significant piece of this project, and shows which galaxies actually met the LBCG criteria.

Each individual LBCG told a story, but I would like to highlight a few. For example, the tidal loop galaxies are an amazing and unexpected find. Mrk 366, for example, has a tidal loop on its West side, caused by either material being tidally stripped from a nearby galaxy, or a smaller galaxy colliding along the plane of rotation

of the host galaxy. The loop is not viewable in the Hα or UV, meaning that current high star formation in the loop is not likely. With Mrk 390 a satellite in the southwest is a visible cause of the loop; Mrk 390 appears to be stripping the companion.

Barred spiral galaxies are typical for this sample. The bar structure in a galaxy can be a hub of star formation, so to have high star formation, blue, barred spirals makes sense. A bar is typically created by a density wave from the center of the galaxy; this wave reshapes the orbit of the inner stars and channels gas inwards from the spiral arms. A flow is made which creates new stars. IIZw 44 and Mrk 300 are 2 examples of barred spirals from our sample. Mrk 306 is a starbursting barred spiral with a spiral companion, Mrk 305. Mrk 305 and 306 are a great example of Toomres theory, in which disk mergers account for the population of elliptical galaxies in the Universe. In Toomre's theory it is believed that the collision would go through a ULIRG stage, which according to our theory means it would next go through a LBCG phase. Mrk 248 and its companion also appear to be merging spirals.

A possible remnant of these mergers are blue ellipticals, not a stranger in our sample. Elliptical galaxies are known to be red, low star formation, quite galaxies. But our sample proved that this was not always the case. Mrk 17 for example is an E5 to E7 elliptical galaxy with a color bluer than typical by 2.79 magnitudes. Other examples from out sample include Mrk 364, Haro 25, and Mrk 499.

Of course many of the most interesting LBCGs in the sample are mergers. Many have a merger of multiple galaxies, such as Mrk 181, which is a small group of 4

galaxies. Mrk 181 is not believed to be a new merger due to the galaxies close proximity to each other, $\sim$ 7 kpc. Mrk 1211 possibly consists of 3 galaxies, and has such a high SFR it is sometimes classified as a luminous infrared galaxy.

From the varying environments, morphologies, colors, and star formation rates, it becomes apparent that not all LBCGs are the same age. Some could be new galaxies, and some could be older galaxies with newly triggered star formation from a nearby companion or merger. The resulting ages from the synthesis models shows that LBCGs can have a variety of ages. Results from literature agree with our finding.

Luminous blue compact galaxies are a piece of the galaxy assembly story. Through studying LBCGs we have learned more about the morphology, environment, color, magnitude, star formation, supernovae rates, Hα distribution, extinction, and history of galaxy building blocks. Galaxy evolution is a complex topic, but LBCGs have proven to be a great tool to develop assembly scenarios, and will continue to do so.

Chapter 6

Glossary

Active Galactic Nuclei: The central energy source of an active galaxy, powered by a supermassive black hole.

Bias Frame: 0 exposure time, shows granularity of the CCD chip.

Bolometric Magnitude: Magnitude we would observe if we could detect all wavelengths.

Chandrasekhar limit: The maximum mass of a white dwarf, about $1.4M_{\odot}$; a white dwarf of greater mass cannot support itself and will collapse.

Color Index: A numerical measure of the color of a star, e.g. (B?V)

Dark Frame: Non-zero exposure time; counts from thermal motion in the system.

Dithering: Slightly moving telescope between images of the same target to help remove cosmic rays later.

Eccentricity: A measure of the flattening of an ellipse. An ellipse of e = 0 is circular. The closer to 1 e becomes, the more flattened the ellipse.

Flat Field: Non-zero exposure time taken with dome open at sunrise or sunset; accounts for gradients across detector where sensitivity drops off.

Flux: A measure of the flow of energy onto or through a surface, measured in energy per time per area.

Hertzsprung-Russell diagram: A plot of the intrinsic brightness versus the sur-

face temperature of stars. An H-R diagram separates the effects of temperature and surface area on stellar luminosity; commonly absolute magnitude versus spectral type, but also luminosity versus surface temperature or color.

Hubble Constant: A measure of the rate of expansion of the universe; the average value of velocity of recession divided by distance.

Inclination: The angle between the normal to the disk and the line of sight.

Interstellar Dust: Microscopic solid grains in the interstellar medium.

Light curve: Intensity of radiation as a function of time.

Luminosity: The total amount of energy radiated in 1 second.

Luminosity Function: Distribution of galaxy luminosities.

Magnitude: The astronomers brightness scale; the larger the number the fainter the star.

Metallicity: A measure of an objects chemical composition.

Morphology: System used by astronomers to divide galaxies into groups based on their visual appearance. The most famous system is the Hubble sequence which divides galaxies into elliptical, spiral, lenticular, and irregular galaxies.

Nucleosynthesis: The production of elements heavier than helium by the fusion of atomic nuclei in stars during supernovae explosions.

Parsec: 3.26 light years, kpc = 1000pc, Mpc = 106 pc

Population I Star: Star rich in atoms heavier than helium; nearly always a relatively young star found in the disk of the galaxy.

Population II Star: Star poor in atoms heavier than helium; nearly always a relatively old star found in the halo, globular clusters, or the nuclear bulge.

Red shift: The lengthening of the wavelengths of light seen when the source and observer are receding from each other.

Solar luminosity: Luminosity of the sun, $L_{\odot}$ (3.8x1026W)

Solar mass: Mass of the sun, $M_{\odot}$ (1.99x1030 kg)

Star formation rate: Solar masses of stars made per year.

Supernovae rate: Number of supernovae per year.

Supernovae Type 1: The explosion of a star, believed caused by the transfer of matter to a white dwarf.

Supernovae Type 2: The explosion of a star, believed caused by the collapse of a massive star.

Surface brightness: Radiative flux per unit solid angle of the source.

Surface Brightness Profile (SBP): Radial Distribution of flux vs. radius of a galaxy.

Ultraluminous Infrared Galaxy: A highly luminous galaxy so filled with dust that most of its energy escapes as infrared photons emitted by warmed dust.

Chapter 7

Appendix

Table 7.1. Sloan Coordinates Of Stars Used For Bootstrap Calibration

Name	R.A.	Dec.
(1)	(2)	(3)
Mrk 366	32.90760	13.92316
...	32.89241	13.92448
Mrk 367	33.41011	17.07764
...	33.39928	17.07896
...	33.41436	17.06972
Mrk 1184	41.49591	-5.64661
...	41.48297	-5.64804
...	41.47733	-5.62857
Mrk 1094	77.70284	-2.67243
...	77.70240	-2.66957
...	77.70813	-2.67749
...	77.70615	-2.69201
Mrk 385	120.00000	0.85877
...	120.87505	25.11213
...	120.86910	25.11984
...	120.85792	25.10124
Mrk 390	128.87549	30.52735

Table 7.1 (continued)

Name	R.A.	Dec.
(1)	(2)	(3)
...	128.87549	30.54583
...	128.90743	30.52999
Mrk 402	143.82898	30.40053
...	143.82796	30.42055
...	143.83919	30.41307
...	143.83510	30.40471
...	143.85297	30.41395
IIZw 44	153.80021	21.10988
...	153.82215	21.11538
...	153.81932	21.11604
...	153.81437	21.12066
Mrk 139	153.96495	43.80016
...	153.93568	43.80148
...	153.94086	43.78916
...	153.97561	43.78916
...	153.94574	43.78366
Mrk 33	158.11518	54.39792

Table 7.1 (continued)

Name	R.A.	Dec.
(1)	(2)	(3)
...	158.11481	54.39946
...	158.15639	54.40056
...	158.15564	54.41090
...	158.11027	54.40364
...	158.13711	54.38868
...	158.11556	54.39462
...	158.10951	54.40804
Mrk 148	158.91192	44.31473
...	158.91284	44.32155
...	158.88393	44.31099
...	158.90700	44.32089
...	158.89131	44.30527
...	158.90976	44.31891
...	158.89623	44.32287
Haro 25	162.18944	26.02973
...	162.18490	26.03138
...	162.19323	26.03887

Table 7.1 (continued)

Name	R.A.	Dec.
(1)	(2)	(3)
...	162.17829	26.06153
Mrk 154	162.68575	50.15509
...	162.71047	50.15046
...	162.70841	50.15553
...	162.67990	50.18039
...	162.72113	50.17247
...	162.66925	50.17797
Mrk 171	172.15229	58.55006
...	172.10294	58.55160
...	172.16368	58.55226
...	172.16369	58.55952
Mrk 181	174.22995	19.98645
...	174.23346	19.98425
...	174.23885	19.97369
...	174.21262	19.97941
...	174.21964	19.98822
...	174.23276	19.97633

Table 7.1 (continued)

Name	R.A.	Dec.
(1)	(2)	(3)
...	174.21567	19.96423
...	174.23533	19.97303
Haro 34 191.28345	21.18088	
...	191.28487	21.18462
...	191.29525	21.16900
...	191.29832	21.16306
Mrk 54	194.25018	32.44090
...	194.23610	32.46224
...	194.23193	32.45828
...	194.24966	32.44904
...	194.23558	32.44002
Mrk 238	195.32490	64.98945
...	195.34729	65.00507
...	195.34937	64.99781
...	195.29625	65.01277
...	195.30564	64.98593
Mrk 248	198.79548	44.41338

Table 7.1 (continued)

Name	R.A.	Dec.
(1)	(2)	(3)
...	198.80226	44.42020
...	198.80934	44.42417
...	198.81674	44.41932
...	198.80473	44.40084
...	198.79764	44.41822
...	198.79980	44.40986
Mrk 255	200.76812	52.97802
...	200.77323	52.96020
...	200.73852	52.97648
...	200.74473	52.98749
Mrk 271	205.40463	55.67838
...	205.43585	55.68344
...	205.43545	55.65836
Haro 42	217.78337	27.25031
...	217.80515	27.24635
IZw 101	225.93379	42.70060
...	225.94218	42.68410

Table 7.1 (continued)

Name	R.A.	Dec.
(1)	(2)	(3)
...	225.92197	42.69279
...	225.92825	42.70489
Mrk 492	239.68356	26.82642
...	239.68307	26.83346
...	239.68553	26.80288
Mrk 297	241.29124	20.54266
...	241.29054	20.55190
...	241.31545	20.53958
...	241.31780	20.55300
Mrk 300	241.57568	18.17255
...	241.57244	18.17266
...	241.57429	18.17805
...	241.56734	18.16495
...	241.56839	18.16572
...	241.57151	18.17585
...	241.56769	18.19202
...	241.55403	18.18608

Table 7.1 (continued)

Name	R.A.	Dec.
(1)	(2)	(3)
Mrk 697	243.06233	29.08164
...	243.06107	29.08032
...	243.08600	29.07108
Mrk 499	252.11509	48.70081
...	252.11409	48.69421
...	252.11743	48.70345
...	252.11443	48.70521
...	252.08608	48.72171
IZw 191	265.08991	47.73658
...	265.12002	47.74076
...	265.11510	47.73372
...	265.10300	47.74406
...	265.10791	47.74450
...	265.11151	47.72470
Mrk 512	317.94969	-1.37326
...	317.94969	-1.36754
...	317.94616	-1.38074

Table 7.1 (continued)

Name	R.A.	Dec.
(1)	(2)	(3)
...	317.94616	-1.39263
...	317.94132	-1.38624
IIZw 185	340.35951	23.36940
...	340.36407	23.36434
...	340.34297	23.38766
...	340.34657	23.39427
...	340.36023	23.38590
...	340.36838	23.36082

Col. (1) Primary galaxy name. Cols. (2)-(3) The R.A. and Dec. of the stars presented in decimal hours and degrees as defined by the Sloan Survey. The coordinates are from the J2000 epoch.

Bibliography

[1] Aloisi, A., Tosi, M., & Greggio, L. 1999, AJ, 118, 302

[2] Anders, E. & Grevesse, N., 1989, GeCoA, 53, 197

[3] Arp, H. 1966, ApJS, 14, 1

[4] Barnes, J. 1985, MNRAS, 215, 517

[5] Bastian, N., 2008, Astron. Soc. 390, 759-768

[6] Beck, S.C., Turner, J.L., & Kovo, O., 2000, AJ, 120, 244-259

[7] Bell, E.F., & Kennicutt, C., 2001, ApJ, 548, 681-693

[8] Bessel, 1990, PASP 102, 1181

[9] Biermann, P., Clarke, J.N., & Fricke, K.J., 1979, A&A, 75, 19-25

[10] Boesgaard, A. M., Edwards, S., & Heidmann, J. 1982, ApJ, 252, 487

[11] Bottinellit, L., Gouguenheim, L., Heidmann, J., & Duflot, R., 1975, A&A, 41, 61

[12] Brinks, E. 1990, in Dynamics and Interactions of Galaxies, ed. R. Wielen (Berlin: Springer), 146

[13] Brocca, C., Bettoni, D., & Galletta, G., 1997, A&A, 326, 907B

[14] Bruzual, G., & Charlot, S., 2003, MNRAS, 344, 1000

[15] Buat V., 1992, A&A, 264, 444-54

[16] Buat, V., & Xu C., 1996, A&A, 306, 61-72

[17] Buat, V., Iglesias-Paramo, J., & Seibert, M., et al., 2005, ApJ, 619, L51-L54

[18] Bundy, K., et al., 2006, ApJ, 651, 120

[19] Burstein, D.K & Heiles, C., 1984, ApJS, 54, 33

[20] Cairos, L.M., Vilchez, J.M., Gonzalez Perez, J.N., Iglesias-Paramo, & J., Caon, N., 2001, ApJ, 133, 321-343

[21] Cairos, L.M., 2003, ApJ, 593, 312-332

[22] Cappellaro, E., Evans, R., & Turatto, M., 1999, A&A, 351, 459-466

[23] Casini, C., & Heidmann, J. 1976, A&A, 47, 371

[24] Chapelon, S., Contini, T., & Davoust, E., 1999, A&AA, 345, 81−92

[25] Charmandaris, V., Stacey, G.J., & Gull, G., 2002, ApJ, 571, 282-287

[26] Chatzichristou, E.T., 2002, ApJ, 581, 161-181

[27] Conselice, C.J., et al., 2000, AJ, 114, 79C

[28] Conselice, C.J., et al., 2007, MNRAS, 381,962, (C07)

[29] Contini T., Conside‘re S., & Davoust E., 1998, A&AA 130, 285 (paper III)

[30] Crone, M. M., Schulte-Ladbeck, R. E., Greggio, L., & Hopp, U. 2002, ApJ, 567, 258

[31] K. M. Dasyra, L. Yan, G. Helou, J. Surace, A. Sajina, & J. Colbert, 2008, ApJ, 680, 232245

[32] Davies, J., & Phillipps S., 1988, MNRAS 233, 553

[33] Davoust, E., & Continit, T., 2004, A&A, 416, 515-527

[34] de Jager, C., Nieuwenhuijzen, H., & van der Hucht, K.A., 1988, A&AS, 72, 259

[35] de Vaucouleurs, G., 1948, Ann., d'Astropys., 11, 247

[36] de Vaucouleurs, G., 1959, Handbuch der Physik, 53, 275

[37] Donas, J., Deharveng, J.M., & Laget, M., et al., 1987, A&A, 180, 12-26

[38] Donas, J., et al. 2007. ApJ, 173, 597

[39] Eggen, O.J., Lynden-Bell, D., & Sandage, A.R. 1962, ApJ, 136, 748

[40] Fanelli, M. N., OConnell, R. W., & Burstein, D., &A Wu, C.-C. 1992, ApJS, 82, 197

[41] Focardi, P., Zitelli, V., & Marinoni, S., 2008, A&A, 484, 655-670

[42] Friedli D., & Benz W., 1993, A&A 268, 65

[43] Gallager, J.S., Hunter, Dd.A., 1984, AR, 22, 37-74

[44] Gallagher, J.S., 1990, ASPC, 10, 157G

[45] Garland, C.A., Pisano, D.J., Williams, J.P., Guzman, R., & Castander, F.J., 2004, ApJ, 615, 689-701

[46] Genzel, R., et al., 1998, ApJ, 498, 579

[47] Genzel, R., Tacconi, L. J., Rigopoulou, D., Lutz, D., & Tecza, M. 2001, ApJ, 563, 527

[48] Gerola, H., & Seiden, P. E. 1978, ApJ, 223, 129

[49] Gil De Paz, A., Madore, B.F., & Pevunova, O., 2003, ApJ,147,29-59

[50] Gil De Paz, A., et al., 2007, ApJ, 173, 185

[51] Glazebrook, K. et al., 2004, Nat, 430, 181

[52] Grevesse, N., & Anders, E., 1991, in: Solar Interior and Atmosphere (Tucson: University of Arizona Press), 1227

[53] Grevesse, N., et al., 1991, A&A, 242,488

[54] Grevesse, N., & Noels, A., 1993, in Origin and Evolution of the Elements. eds. N. Prantzos, E. Vangioni-Flam, & M. Casse, (Cambridge: CUP), 14

[55] Guzman,R., Koo, D,C., Faber, S.M., Illingworth, G.D., Takamiya, M., Kron, R., & Breshady, M.A., 1996, ApJ,460,5

[56] Guzman, R., Gallego, J., Koo, D. C., Phillips, A. C., Lowenthal, J. D., Faber, S. M., Illingworth, G. D., & Vogt, N. P. 1997, ApJ, 489, 559

[57] Hammer,F., Gruel, N., Thuan,T.X., Flores, H., & Infante, L., 2001, ApJ, 550, 570

[58] Hannaford, P., Lowe, R.M., Grevesse, N., & Noels, A., 1992, 259, 301

[59] Haro, G., 1956, AJ, 61R, 178H

[60] Hawarden T.G., Huang J.H., & Gu Q.S., 1996, In: Buta R., Crocker D.A.,Elmegreen B.G. (eds.) Barred Galaxies. Proc. IAU Coll. 157, ASP Conference Series, p. 54

[61] Heckman, T.H., Hoopes, C.G., & Seibert, M., 2005, ApJ, 619, L35-L38

[62] Helou, G., 1995, ASP Conf. Series, Vol. 73

[63] Hibbard, J.D., Yun, M.S., 1999, AJ, 118, 162-185

[64] Homeier, N.L., & Gallagher, J.S., 1999, ApJ, 522, 199-208

[65] Hopkins, A.M., Schulte−Ladbeck, R.E., & Drozdovsky, I.O, 2002, 124, 862-876

[66] Hopkins, A.M., Connolly, A.J., Haarsma, D.B., & Cram, L.E., 2001, AJ, 122, 288-296

[67] ESA/Hubble, 2008, http://www.spacetelescope.org/

[68] Huchra, J.P., 1977, 35, 171-195

[69] Hunter, D.A., Elmegreen, B.G., & Ludka, B.C., 2010, AJ, 139, 447-475

[70] Ilbert, O., et al., 2010, ApJ, 709, 644

[71] Jeong, H., et al., 2009, Astron. Soc., 398, 2028

[72] Jester, S., Schneider, D.P., & Richards, G.T., et al., 2005, AJ, 130, 873-895

[73] Kennicutt, R.C., 1983, ApJ, 272, 54-67

[74] Kennicutt, R.C., 1994,Tamblyn, P., & Congdon, C.W., ApJ, 435, 22-36

[75] Kennicutt,R.C., 1998, AR, 36, 189-231

[76] Khachikian, E.Ye., & Movsessian, T.A., 1998, Astrophysics, Vol. 51, No. 4, 543-553

[77] Khachikian, E.E., & Petrosyan, A.R., 1983, Astrophysics, V19, Number 2, 138-141

[78] Klimanov, S.A., & Reshetnikov, V.P., 2001, 378, 428-440

[79] Knapen, J.H., & James, P.A., 2009, ApJ, 698, 1437-1455

[80] Kong X., & Cheng, F.Z., 2002, A$&A, 389, 845-854

[81] Kong, X., Charlot, S., Weiss, A., & Cheng, F.Z., 2003, A&AA, 403, 877-887

[82] Kong, X., 2004, A$&A, 425, 417-427

[83] Koo, D. C., Bershady, M. A., Wirth, G. D., Stanford, S. A., & Majewski, S. R., 1994, ApJ, 427, 9

[84] Koo, D. C., Guzma?n, R., Faber, S. M., Illingworth, G. D., Bershady, M. A., Kron, R. G., & Takamiya, M. 1995, ApJ, 440, L49

[85] Koss, M., Mushotzky, R., Veilleux, S., & Winter, L., 2010, ApJ, 716, 125-130

[86] Kroupa, P., 2002, Science, 295, 85

[87] Kuchinski, L.E., et al. 2000, ApJS, 121, 441

[88] Kuchinski, L.E., Madore, B. F., Freedman, W. L., & Trewhella, M., 2001, AJ, 122, 729

[89] Kunth D., Maurogordato S., & Vigroux L., 1988, A&A, 204.10

[90] Landolt, A.U., 1992, AJ, 104, 340

[91] Lauger, S., Burgarella, D., & Buat, V., 2005, A&A, 434, 77

[92] Lee, J. C., Kennicutt, R. C., Jr., Funes, S. J., J. G., Sakai, S., & Akiyama, S. 2009, ApJ, 692, 1305

[93] Leitherer, C. & Heckman, T., 1995, 96, 9-38

[94] Leitherer, C., Schaerer, D., Goldader, J., et al., 1999, ApJ, 123, 3-40

[95] Lilly, S., et al. 1998, ApJ, 500, 75

[96] Loose, H., H., & Thuan, T.X., 1985, in Star-Forming Dwarf Galaxies and Related Objects, ed. D. Kunth, T.K. Thuan, and J.T.T. Van (Gif-sur-Yvette: Edition Frontieres), 73

[97] Lowenthal, J.D., et al. 1997, ApJ, 481, 673

[98] Mac Low, M., & Ferrara, A., 1999, ApJ, 513, 142

[99] Madau, P., Ferguson, H.C., Dickinson, M.E., Giavalisco, M., Steidel, C.C., & Fruchter, A., 1996, MNRAS, 238, 1388

[100] Mallen-Ornelas, G., Lilly, S. J., Crampton, D., & Schade, D.,1999, ApJ, 518, 83

[101] Marcum, P., O'Connell, R., & Fanelli, M., et al., 2001, ApJ, 522, 183

[102] Marigo, P., & Girardi, L., 2007, A&A, 469, 239

[103] Markarian, B.E., 1967, Afz, 3, 24

[104] Martin, D.C., et al., 2005, ApJ, 619, L1

[105] Martin, D.C., Small, T., & Schiminovich, D., et al. ApJ, 173, 415-431

[106] Masegosa, J., & Marquez, I., 2003, Astrophysics and Space Science, 284, 483-486

[107] Mazzarella, J.M., & Balzano, V.A., 1986, ApJ, 62, 751-819

[108] Mazzarella, J.M., Bothum, G.D., & Boroson T.A., 1991, AJ, 101, 2034

[109] Mendez, D.I., Cairos, L.M., Esteban, C., & Vilchez, J.M., 1999, AJ, 117, 1688-1699

[110] Mollenhoff, C., 1992, A&A, 255, 35

[111] Morrissey, P., Conrow, T., & Barlow, T.A., et al., 2007, ApJS, 173, 682-697

[112] Mueller, W. K., & Arnett, W. D. 1976, ApJ, 210, 670

[113] Neff, S.G., Ulvestad, J.S., & Teng, S.H., 2004, ApJ, 611, 186-199

[114] Noeske, K.G., Papaderos, P., Cairos, L.M., & Fricke, K.J., 2005, A&A, 429, 115-127

[115] Noeske, K.G., Koo, D.C., Phillips, A.C., Willmer, N.A., Melbourne, J., Gil De Paz, A., & Papaderos, P., 2006, ApJ, 640, 143-146

[116] Norman, C., & Scoville, N. 1988, ApJ, 332, 124

[117] OConnell, R., 1997, AIP Conference Series 408: 11-20

[118] Oestlin, G., Bergvall, N., &A Roennback, J. 1998, A&AA, 335, 85

[119] Okamura, S. 1988, Astronomical Society of the Pacific 100, 524-544

[120] Papaderos P., Loose, H.H., Thuan, T.X., & Fricke, K.J., 1996, A&A, 120, 207-228

[121] Papaderos, P., Izotov, Y. I., Thuan, T. X., & Noeske, K. G., et al. 2002,A&AA, 393, 461

[122] Perez-Gallego, J., Guzman, R., Castander, F.J., Garland, C.A., & Pisano, D.J., 2005, ASSL, 329

[123] Perez-Gonzalez, P.G., et al., 2008, ApJ, 675, 234

[124] Phillips, A. C., Guzman, R., Gallego, J., Koo, D. C., Lowenthal, J. D., & Vogt, N. , 1997, ApJ, 489, 543-558

[125] Pisano, D.J., Kobulnicky, H.A., Guzman, R., Gallego, J., Bershady, & M. A., 2001, AJ, 122, 2471

[126] Pisano, D.J., Garland, C.A., Guzman, R., Perez-Gallego, J., Castander, F.J., & Gruel, N., 2008, ASP Conference Series, 396

[127] Prugniel, & Heraudeau, 1998, A&AS, 128, 299

[128] Rujopakarn, W., Rieke, G.H., Eisenstein, D.J., & Juneau, S., 2011, pJ, 726, 93

[129] Ryan, C.J., & De Robertis, M.M., 2010, ApJ, 710, 783-796

[130] Salim, S., et al., 2007, ApJ, 656, 770

[131] Sanders, D. B., Scoville, N. Z., Young, J. S., Soifer, B. T., Schloerb, F. P., Rice, W. L., & Danielson, G. E. 1986, ApJ, 305, L45

[132] Sanders, D., & Mirabel, I. 1996, ARA&A, 34, 749

[133] Sargsyan, L., A., & Weedman, D., W., 2009, ApJ, 701, 1398-1414

[134] Schawinski, K., et al., 2007. ApJ, 173, 512

[135] Schneider, S.E., & Salpeter, E.E., 1992, ApJ, 385, 32

[136] Schwarz M.P., 1984, MNRAS 209, 93

[137] Schlegel, D., J., Finkbeiner, D., P., & Davis, M., 1998, ApJ, 500, 525-553

[138] Searle, L., Sargent, W. L. W., & Bagnuolo, W. G. 1973, ApJ, 179, 427

[139] Smail, I., Ivison, R. J., Blain, A. W., & Kneib, J.-P. 1998, ApJ, 507, 21

[140] Smith, B., Giroux, M., Struck, C., & Hancock, M., 2010, J, 139, 1212-1241

[141] Soto, K.T., & Martin, C.L., 2010, ApJ, 716, 332-340

[142] Stoughton, C., et al., 2002, AJ, 123, 485-548

[143] Struck, C., Galaxy Collisions Dawn of A New Era, in Astrophysics Update 2: Topical and Timely Reviews on Astrophysics, ed. John W. Mason, (Springer-Praxes, Chichester), pp 115-158, 2006

[144] Taylor, C., Brinks, E., & Skilman, E. D. 1993, AJ, 105, 128

[145] Taylor, C., Brinks, E., Grashuis, R. M., & Skilmann, E. D. 1995, ApJS, 99, 427

[146] Taylor, C., Brinks, E., Grashuis, R. M., & Skilmann, E. D. 1995, ApJS, 99, 427

[147] Thuan,T.X., & Martin,G.E., 1981,ApJ,247,823-848

[148] Thuan, T., 1985, ApJ 299, 881

[149] Tielens, A.G.G.M., Peeters, E., Bakes, E.L.O., Spoon, H.W.W., & Hony, S., 2004, ASPC, 323, 135T

[150] Toomre, A. & Toomre, J. 1972, ApJ, 178, 623

[151] Twite, J.W., et al., 2012, Royal Astronomical Society, 420, 1061-1078

[152] Vazquez, G. A., & Leitherer, C., 2005, ApJ, 621, 695

[153] Veilleux, S., Kim, D.C., & Sander, D.B., 2002, ApJS 143, 315

[154] Wada K., & Habe A., 1992, MNRAS 258, 82

[155] Walcher, C.J., Coelho, P., Gallazzi, A., & Charlot, S., 2009, Astron. Soc. L398, 44

[156] Wang, B., & Heckman, T., 1996, ApJ, 457, 645-657

[157] Werk, J.K., Jangren, A., & Salzer, J.J., 2004, ApJ 617, 1004-1016

[158] Westoby, P.B., Mundell, C.G., Naga, N.M., Maciejewski, W., Emsellem, E., Roth, M.M., Gerssen, J., & Baldry, I.K., 2012, ApJS, 199, 1W

[159] Windhorst, R. A., 2002, ApJS, 143, 113

[160] Woods, D.F., Geller, M.J., & Barton, E.J., 2006, AJ, 132, 197-209

[161] Wyder, T. K., et al., 2007, ApJS, 173, 293

[162] Yi, S.K., 2003, ApJ, 582, 202

[163] Yang, M., Greve, T.R., Dowell, C.D., & Borys, C., 2007, ApJ, 660, 1198-1208

[164] Yi, S. Y., e al., 2005, ApJ Lett., 619, L111

[165] Zhao Y., Gu, Q., & Gao, Y., 2011, AJ, 141, 68

[166] Zwicky, I.J., 1964, ApJ, 140, 1467Z

ABSTRACT

LUMINOUS BLUE COMPACT GALAXIES: PROBES OF GALAXY ASSEMBLY

by Cassidy Louann Newton

Thesis or Dissertation Advisors:

Dr. Pamela Marcum, Professor of Physics and Astronomy

Dr. Michael Fanelli

The life cycles of galaxies over cosmic time is yet to be fully understood. How did galaxies evolve from their formative stages to the structures we observe today? This dissertation details the identification and analysis of a sample of Luminous Blue Compact Galaxies (LBCGs), a class of galaxy in the local ($z < 0.05$) universe exhibiting blue colors, high surface brightness, and high star formation rates. These systems appear to be very similar in their global properties to the early evolutionary phases of most galaxies, however their locality permits detailed investigation over a broad range of the electromagnetic spectrum in contrast to the smaller angular sizes and extreme faintness of distant galaxies. We use a combination of optical, ultraviolet, and infrared data to investigate a sample of LBCGs utilizing space and ground-based data.

Vita

Cassidy Louann Newton was born January 6, 1985, in San Angelo, Texas. She is the daughter of Gary and Janice Smith. A 2003 graduate of Central High School, San Angelo, Texas, she received a Bachelor of Science degree with a major in Physics from Angelo State University, San Angelo, in 2007.

In August, 2007, she enrolled in graduate study at Texas Christian University. While working on her doctorate in Physics with a focus on Astrophysics, and MBA option, she held a University Teaching Assistantship during the years 2007-2012. She is a member of the American Astronomical Society, and has presented at 3 of their national level meetings. While at TCU she received 3 Texas Space Grants from the Texas Space Grant Consortium.

She is married to John D. Newton of Ft. Worth